FUNDAMENTAL BEHAVIOUR IN BENDING AND SHEAR OF REINFORCED CONCRETE

A Thesis presented for the degree of Doctor of Philosophy in Civil Engineering at The City University

by
H.P.J. Taylor
1971

ACKNOWLEDGEMENTS

The writer carried out the work described in this Thesis whilst working for the Cement and Concrete Association and would like to thank the Director General of the Association for allowing him to present this work.

The writer would like to thank his supervisors, Dr R.E. Rowe, Director of Research and Development at the Association and Dr P. Roberts, Senior Lecturer at The City University, for the help that they have given.

Many members of the Association's staff have helped with various stages of the experimental work described in this Thesis; of these the writer acknowledges the valuable practical contributions of Mr T. Giles, Mr E. Gray and Mr T. Pearce. The writer would also thank Dr W.B. Cranston for many thought provoking discussions on this subject.

CONTENTS

ABSTRACT

A review of research on the shear strength of reinforced concrete beams is given, indicating that although reliable empirical conclusions can be made about beam behaviour, little is known about the way in which reinforced concrete beams carry shear.

Extensive tests are described in which the distribution of shear force in a beam subjected to combined bending and shear is studied. In the first of the tests, the shear force carried by beam compression zones was investigated and these tests showed that only a quarter of the total shear force is carried by the compression zone. The shear force carried across the cracks in beams was then studied, in two investigations. Firstly the force carried across cracks by the main tension steel acting as a dowel was measured in a series of model and prototype tests. Secondly the forces carried across cracks by interlock of the aggregate were estimated in two separate tests, one on cracked blocks of concrete and one on beams specially designed to eliminate other methods of shear transfer.

The strains and displacements from elastic analysis of the concrete cantilevers between cracks loaded by the measured force in the beams are shown to be consistent with the observed crack patterns in beams.

A mathematical model is then described in which the path of a shear crack and distribution of shear forces was found in beams by considering the equilibrium and compatibility of displacements of the parts of the beams separated by a section through the crack and beam compression zone.

Finally the implication of these theories in explaining the behaviour of beams with stirrups was considered and some experimental evidence is given of the internal distributions of shear forces in beams with stirrups.

NOTATION

a	shear span
b	beam width
c_b	bottom cover to bars
c_i	distance between bars
c_s	side cover to bars
d	beam depth
d_1	beam effective depth
d_n	depth of neutral axis
f_c	compressive strength of 150 x 300 mm concrete cylinder
f_n	normal stress across a crack
f_{nu}	ultimate normal stress across a crack
f_s	shear stress across a crack
f_{su}	ultimate shear stress across a crack
f_t	flexural tensile strength of concrete
f_{ts}	direct tensile strength of concrete
f_y	characteristic strength of reinforcement
f_{yq}	characteristic strength of stirrup reinforcement
h	distance from support to a section through a beam compression zone
h_o	initial crack height
k_a, k_b	contributions to lamella strength - Lorentson
k_1, k_2, k_3	stress block constants - Hognestad, Hanson & McHenry
l	distance from a crack to the nearest stirrup restraining the dowel
l_a	lever arm
m	modular ratio
p	tensile steel ratio in a beam A_{st}/bd_1
q	nominal shear stress in a beam
q_h	horizontal shear stress in a beam at a distance y from neutral axis
r	percentage of shear reinforcement A_{sq}/bs_h
r	reinforcing bar radius
s_h	stirrup spacing in the direction of the longitudinal axis of a beam
s_p	stirrup spacing normal to the plane of a stirrup
t	distance from the line of action of the horizontal interlock force to the longitudinal steel

u_w	characteristic strength of 150 mm concrete cube
v_c	nominal shear stress of a member unreinforced in shear
v_a	ultimate shear stress on a reinforced concrete member
A_{sq}	cross sectional area of a stirrup
C	concrete compression force
H_I	horizontal interlock force
M	bending moment
M_{FL}	ultimate moment carried by a beam, from flexural theory
M_p	plastic moment of a steel section
M_u	ultimate moment carried by a beam
P_s	force carried by the dowel in a reinforced concrete beam
P_{sp}	splitting strength of a dowel
P_{ult}	ultimate strength from a dowel test
T	steel tensile force
V	shear force
V_1	shear force carried by a beam compression zone
V_2	shear force carried by dowel action
V_3	shear force carried by aggregate interlock
α	angle of inclination of concrete compression strut
β	angle of inclination of a stirrup
δ_N	vertical distance from the head of a crack to an interlocking section
δ_H	horizontal distance from the head of a crack to an interlocking section
θ	rotation of a plastic hinge
ϕ	curvature
Δ_H	horizontal displacement across a crack
Δ_N	normal displacement across a crack
Δ_{NU}	ultimate normal displacement across a crack

TITLES OF FIGURES

TITLES OF TABLES

CHAPTER 1

INTRODUCTION

Throughout the eighty years of the use of structural concrete, research has been carried out into the strength of reinforced concrete members subject to combined bending and shear. A number of shear failures of structures in service have occurred and as these are usually abrupt and cause severe structural damage, research work has been instigated continuously on this problem.

So far, inadequacy of design knowledge in this subject has led to failures which affect the safety of structures, rather than their serviceability. Complaints of inadequate performance of structures at their working loads due to the effects of shear forces are almost unknown.

Because of this and because of the difficulty of formulating a reliable mathematical analysis of the behaviour of beams in shear, research has tended to concentrate on predicting the collapse load of such members, usually on an empirical basis. This trend has been accentuated by the increasing use of new materials and by changes in structural form.

Thus the use of high strength deformed steels and the doubling of steel working stresses over the last thirty years has made it essential that test work be constantly carried out. Similarly, the current unpopularity of haunched beams and bent up bars, because of their cost, has also changed the conditions under which earlier work was carried out. At the moment approximately two thousand test results exist in the literature from which reliable design rules have been developed. The rules in the Draft Unified Code of Practice, the ACI-ASCE Code and the C.E.B. Recommendations all lean heavily on these tests.

It is unfortunate that because of the need for this large amount of test work to be carried out, studies of basic behaviour of beams and the way in which they carry shear forces has been neglected. If this understanding was available, the extension of design rules to

cover future changes in practice, for example the increasing use of high strength steel and concretes leading to members of greater slenderness, would be much more simple and would not involve as much test verification.

The intention of the work described in this Thesis was to study the basic way in which beams carry shear and to provide some of this background knowledge.

The most convenient way to describe the various kinds of beam failure mode that exist is to consider the crack patterns and form of failure of a series of beams of constant section and steel percentage, point loaded at the centre of simply supported spans of varying length. As the section of each beam has the same flexural capacity, the only variable within the test series is the shear force to bending moment ratio. Figure 1.1 shows the results of a series of such tests plotted in terms of Mu/Mfl, the actual ultimate moment divided by the calculated flexural ultimate moment and $^{a}/_{d_1}$, the ratio of shear span length to beam effective depth. It may be seen that the presence of the shear force causes a premature failure of the beam if its $^{a}/_{d_1}$ ratio is between 1·5 and 5. Many interaction diagrams of this type have been produced, mainly by Brock[1] and Kani[2], for different steel percentages, loading arrangements and beam types. Apart from the case of beams with steel percentages less than 0·6% all the interaction diagrams have the same basic shape.

Four areas are marked in Figure 1.1 in which different failure modes can be identified. These failure modes have been given a number of different, sometimes conflicting, names in the past and the following summary gives the most common names and definitions. It is dangerous to rely too much on the description of failure and failure modes given in the literature as, for example, a new word for a particular failure mechanism pre-supposes that the mechanism must exist. What is more important is to study the crack pattern of each kind of beam as this gives the best description of its failure. The boundaries between the various zones are not fixed and an infinite variety of failure modes is possible.

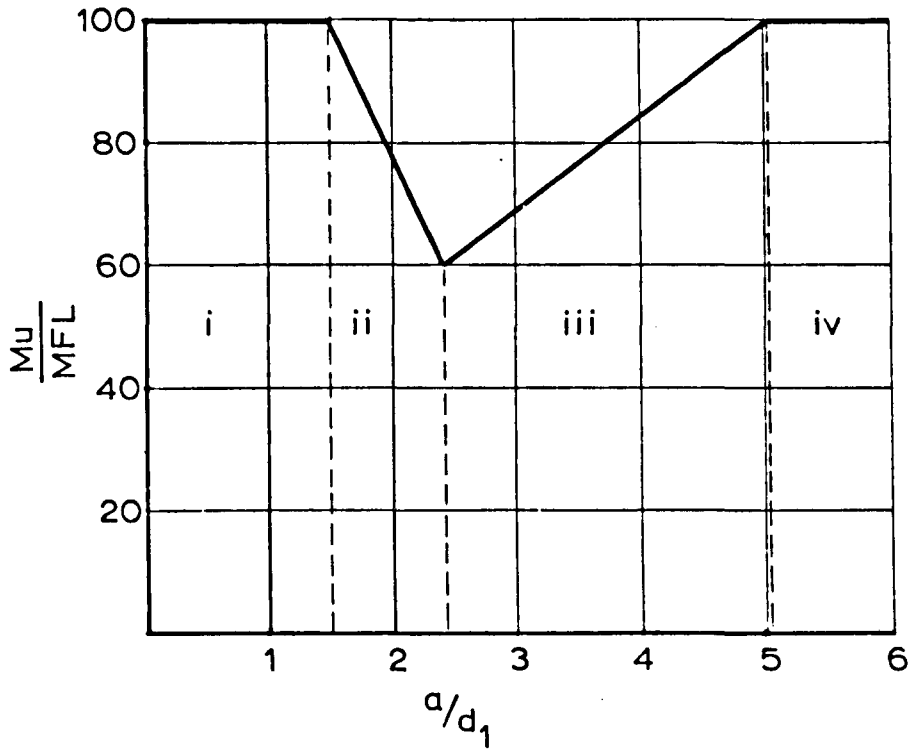

1.1 INTERACTION BETWEEN ULTIMATE MOMENT AND SHEAR SPAN

i Shear Proper

Members of this shape are commonly constructed as pile caps and corbels. Figure 1.2 shows a corbel of this type with its final crack pattern marked in. The strength of this type of member depends largely on the detailing of the steel and the most frequent design approach is to consider the triangle of force shown. Special attention should be given to the anchorage of the tensile reinforcement, both in the column and in the corbel: the provision of a welded transverse anchorage for the steel is sometimes considered. At the same time, a maximum shear force on the member is usually defined so as to prevent failure of the compressive concrete strut in the system. The Draft Unified Code of Practice[10] defines the shape of such members and requires the provision of horizontal stirrups in the upper part of the corbel.

ii Shear Compression

The crack pattern of a beam which has failed in shear compression is shown in Figure 1.3. In this case, a few flexural cracks formed and then, at a moment sometimes considerably less than the flexural capacity of the beam, a shear crack formed through the web of the beam, extending from the load point to the support point in almost a straight line. In some cases, this crack crosses flexural cracks that have previously formed without attempting to follow them but in others the crack forms along the line of an inclined flexural crack. If the inclined crack does not cause an immediate failure then the beam is changed into a tied arch and may eventually collapse either by the steel failing in anchorage, or the concrete crushing at the head of the crack. It is quite possible for an inclined crack to form, stabilize and carry considerably more load before the beam fails.

This failure mode is called Diagonal Tension by some workers.

iii Diagonal Tension

This is a type of shear failure which occurs most frequently in reinforced concrete members. It is intermediate between type ii 'tied arch action' and type iv 'flexural action'. In this case the cracking is characterised by flexural cracks which form vertically

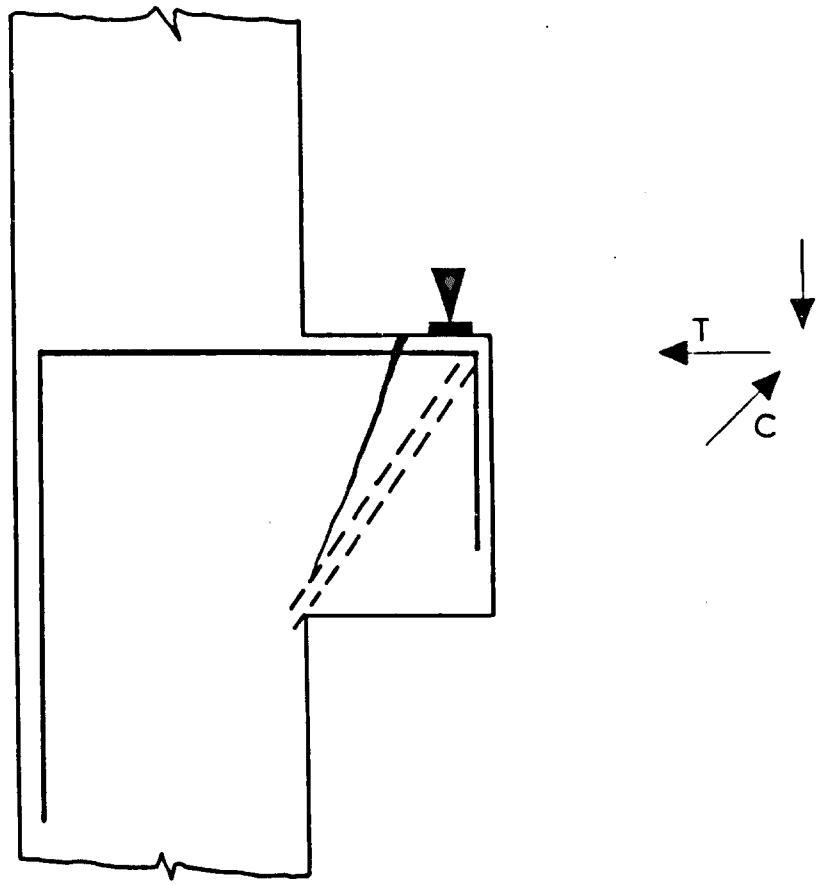

1.2 FAILURE MECHANISM I

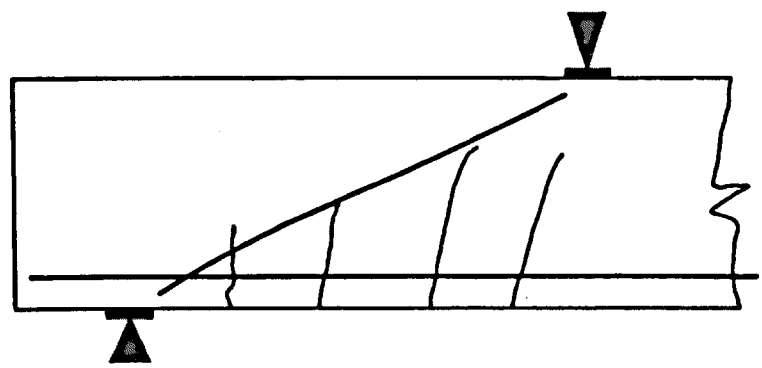

1.3 FAILURE MECHANISM II

and gradually extend and incline towards the load point as more load is applied. Shear failure occurs as one of these cracks, usually the nearest large one to the support suddenly extends both forwards towards the point of load application and backwards, along the level of the steel, to the support. A beam with this form of crack pattern is shown in Figure 1.4. The way in which a beam of this type carries the load is not fully understood and this Thesis describes a study of the internal distribution of load in beams of this type.

The shear force across any particular section of such a beam must be carried by the concrete above the crack, by the steel acting as a dowel across the crack and by mechanical interlock of the aggregate across the crack. The relative magnitude of each of these mechanisms of force transfer can only be decided by experiment as their contribution to ultimate shear capacity of a beam is a complex statically indeterminate problem. In the past it was assumed that all the shear force carried by any section of a beam must be concentrated above the crack and it is only recently that dowel action and aggregate interlock action have been considered to be worth studying.

iv Flexural Failure

Beams within this range fail by the well known bending mechanism. Although the flexural cracks are inclined, the failure of the beam is caused either by yielding of the steel or by crushing of the concrete in the compression zone. In each case, the failure moment may be accurately determined by considering horizontal equilibrium and compatibility across a section and using failure criteria for the steel, its yield point or its ultimate strength including the effects of strain hardening, and for the concrete, either experimentally determined stress blocks or an actual concrete stress-strain curve.

This discussion so far has been concerned solely with beams unreinforced in shear. When a beam has stirrups, its cracking is modified by their presence but the basic modes of failure still apply. A stirrup may have a variety of functions, firstly to carry forces across inclined cracks by acting as a tie or a dowel, secondly in

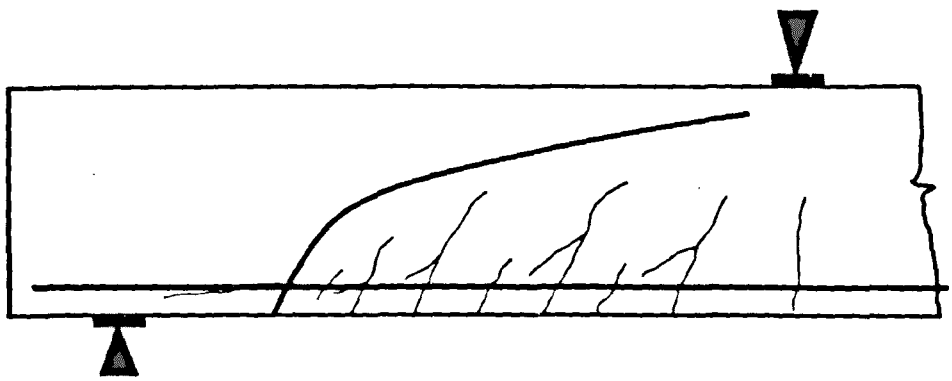

1.4 FAILURE MECHANISM III

strengthening the concrete compression zone by restraining the concrete from bursting and thirdly in increasing dowel action by restraining splitting along the line of the tensile steel.

The crack pattern of beams with stirrups is shown in Figure 1.5. The behaviour of such a beam has often been described in terms of a truss, the steel carrying the tensile forces and the concrete carrying the compressive forces. This truss system may fail not only because the steel tension members of the truss yield or the horizontal compressive members crush causing one of the failure mechanisms described earlier but also by the inclined concrete struts crushing. This kind of behaviour is commonly called web crushing failure.

The two chapters that follow describe some of the more notable research on which our knowledge of the strength of reinforced concrete members is based. The first chapter describes work that is basically empirical, investigating the effect of the various parameters of the problem and producing the test evidence on which our Code rules are based; the second chapter describes work that is generally more recent which studies the way in which beams carry shear forces.

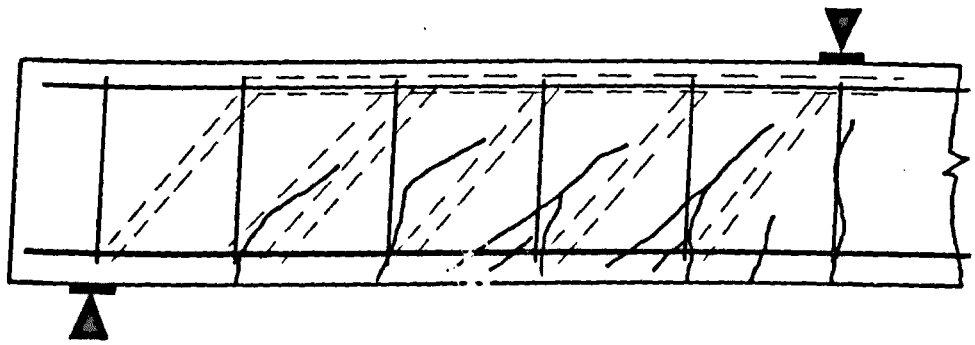

1.5
CRACK PATTERN OF A BEAM WITH STIRRUPS

CHAPTER 2

REVIEW OF PREVIOUS RESEARCH - EMPIRICAL

The earliest pioneers of reinforced concrete design assumed that reinforced concrete behaved in a similar way to the building materials that they were used to, namely steel and timber. Initially the failure of a reinforced concrete beam in shear was assumed to occur because the horizontal shear in the beam was greater than the shear capacity of the concrete, reflecting the design of rivets in the webs of steel members. The most common equation used was of the form

$$q_h = V \frac{A\bar{y}}{Ib}$$

where V = shear force on the section.

q_h = horizontal shear stress at a distance y from the neutral axis.

$A\bar{y}$ = first moment of area about the neutral axis of the section between the extreme fibre and a line distance y from the neutral axis.

I = moment of inertia of the section about the neutral axis.

b = width of the cross section at a distance y from the neutral axis.

In the case of a rectangular section, the equation which comes from the theory of elasticity defines a parabolic distribution of shear stress through the section, assuming it to be uncracked. This equation could give reasonable results for beams unreinforced in shear providing an appropriate limiting stress is defined depending on the strength of the concrete.

When stirrups were needed, this method of design was extended to assume that the stirrups acted as horizontal shear keys or dowels in resisting shear. It was found that the strength of beams with stirrups in shear was seriously underestimated using this approach. The work of Zipkes[3] is typical of the early work on this subject.

At the same time that this method of design was being studied, other pioneers, led by Ritter and Mörsch, proposed the classical

distribution of shear stress across a reinforced concrete section and proposed that stirrups carried tensile forces across cracks and that a cracked beam with stirrups could be analysed as a simple truss.

Figure 2.1 shows a section through a beam carrying shear forces. Considering first the section above the neutral axis, from the Theory of Elasticity

$$\tau_{xy} = \int_{y}^{dn} \frac{\partial \sigma_x}{\partial x} \, dy$$

Taking moments about the steel level

$$\sigma_o = \frac{2M}{b\,(d_1 - d_n/3)\,d_n}$$

where b is beam width

$$\sigma_{(x)y} = \sigma_o \times \frac{y}{d_n}$$

$$\sigma_{(x)y} = \frac{2My}{b\,(d_1 - d_n/3)\,d_n^2}$$

$$\therefore \tau_{xy} = \int_{y}^{dn} \frac{2Vy}{b\,(d_1 - d_n/3)\,d_n^2} \, dy$$

where V is the shear force on the beam

$$\therefore \tau_{xy} = \frac{V\,(d_n^2 - y^2)}{b\,d_n^2\,(d_1 - d_n/3)}$$

at the neutral axis therefore

$$\tau_{na} = \frac{V}{b\,(d_1 - d_n/3)}$$

Assuming that no tensile stresses exist below the neutral axis, no increase or decrease of shear stress is possible and the stress must therefore remain constant until the steel level. The shear stress distribution from this analysis is shown in Figure 2.1. In this case, assuming that the stress block at failure of the beam is triangular, the area of the shear stress block is

$$\tau_{na} \times b \ (d_1 - d_n/3)$$

This must equal the total shear force on the beam and rearranging we obtain the design equation for finding the nominal ultimate shear stress that is used to this day

$$v_c = \frac{Q}{b \ l_a}$$

where v_c = nominal ultimate shear stress
b = beam width
l_a = internal lever arm between centroid of the compression block and steel forces

In its original form the truss analogy made the following assumptions.

1. The compression zone carried longitudinal compression only.
2. The tensile reinforcement carried longitudinal tensile forces only.
3. Shear forces are carried by stirrups or inclined bars.
4. Inclined compression forces are carried by the concrete struts between the cracks.

These assumptions imply that the truss is pin jointed and that all the members of the truss are separated from each other so that there is no shear transfer between them.

The following equations may be derived from this model, illustrated in Figure 2.1.

Consider the shear force carried across section A-A

$$V = A_{sq} \ f_{yq} \ \text{Sin} \ \beta \times \text{No. of stirrups crossing A-A}$$

where A_{sq} total are of one stirrup
f_{yq} yield stress force stirrup

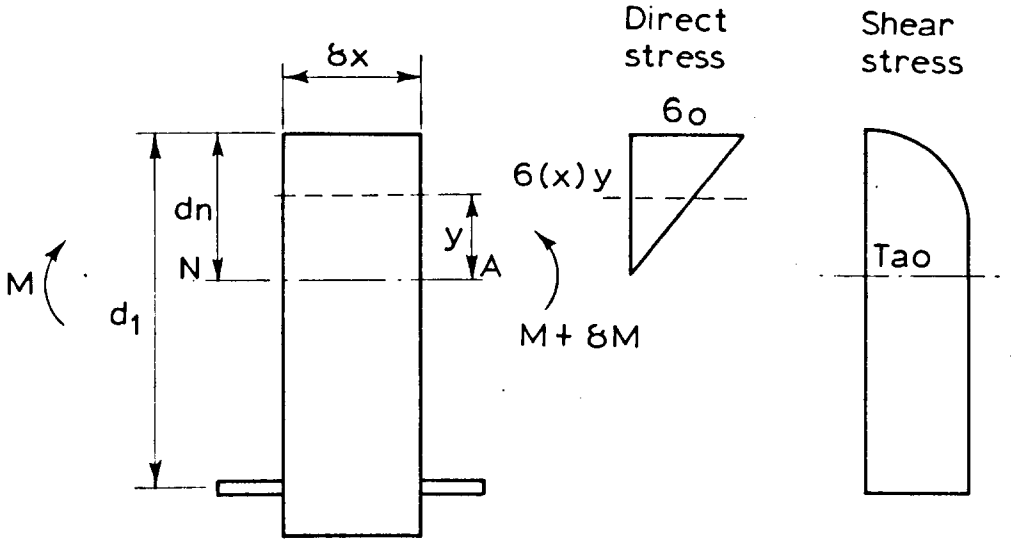

2.1 CLASSICAL SHEAR STRESS DISTRIBUTION IN A BEAM

$$\therefore V = A_{sq} f_{yq} \text{Sin } \beta \, (\text{Cot } \alpha + \text{Cot } \beta) \frac{l_a}{S_h}$$

$$= A_{sq} f_{yq} \, (\text{Cos } \beta + \text{Sin } \beta \text{ Cot } \alpha) \frac{l_a}{S_h}$$

if the inclined compression struts are assumed to be at 45° to the longitudinal axis of the beam,

$$V = A_{sq} f_{yq} \, (\text{Cos } \beta + \text{Sin } \beta) \frac{l_a}{S_h}$$

In his paper, Ritter made the simplification that the stirrups are always vertical and that the stirrup spacing is the same as the internal lever arm.

Then

$$V = A_{sq} f_{yq}$$

Ritter said that if the stirrup spacing were increased then the stress in the stirrups would increase and said that he designed in this way in the centre of a beam where the shear forces are low. In his 1899 paper he said that he did this by eye but proposed that in future, calculations should be carried out to compute the wider spacing necessary.

Talbot[6] reported in a series of papers a number of shear tests on reinforced concrete beams. A number of important variables were studied including the effect of shear span and steel percentage but one of the most important things that he pointed out was that the truss analogy was conservative. Talbot said that at failure of a beam the stirrups carry $^2/_3$ of the total shear force and the concrete in the compression zone carried $^1/_3$ of the shear force. This recommendation was accepted in America and figured in the ACI report in 1916 but this report was never accepted as a code of practice.

Another important contribution to this subject was made in 1927 by Richart, also of the University of Illinois[7]. Richart

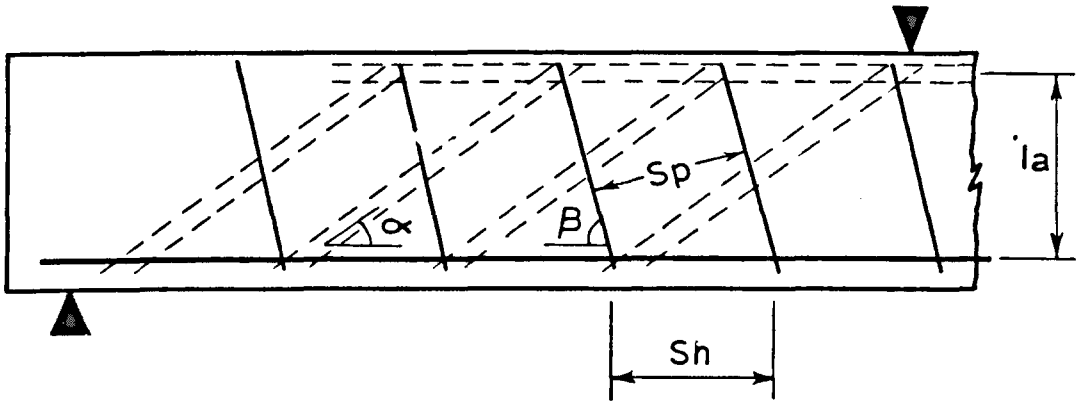

2.2
TRUSS MECHANISM IN A SHEAR SPAN

re-stated the fact that the ultimate shear capacity of a beam with stirrups was greater than that accounted for by the strength of the stirrups alone and attributed this to the load carrying capacity of the uncracked compression zone. He said that the two common design formulae in use were

$$v_u = \frac{V}{b\, l_a} = A + r f_{yq}$$

and

$$\frac{V}{b\, l_a} = B\, r f_{yq}$$

where

$$r = \frac{A_{sq}}{b\, S_h}$$

S_h = stirrup spacing

These equations imply two approaches to design, the first that the proportion of the load carried by the stirrups is not fixed, in fact A varied in his test between 0·6 and 1·4 N/mm^2 and secondly that a fixed proportion of the total shear force must be carried by the stirrups and as previously stated, a commonly used value of B is $^2/_3$. Richart stated that he was not in favour of the 'fixed proportion' method of design.

In 1945, Moretto[8] as well as drawing attention to the difference between previous work which was concerned with relating stirrup stress to shear capacity and his own which was concerned with ultimate strength introduced another of the now acknowledged important variables into a design equation.

Moretto suggested the equation, at the ultimate load.

$$v_u = \frac{V}{b\, l_a} = A\, r f_{yq} + 0{\cdot}10\, f_c + 5000\, p \qquad \text{(in Imperial units)}$$

where A = (Sin β + Cos β) from truss analogy.

f_c = strength of a 12" x 6" dia. concrete cylinder in compression.

r = ratio of web reinforcement A_{sq}/bd_1.

p = ratio of tensile reinforcement, A_{sq}/bd_1.

The important variable p was therefore introduced into a formula for the first time.

In 1951, Clark[9] derived a similar formula and this time included the effect of the shear span variable, which, for simply supported beams, is $^{a}/_{d_1}$. Clark's formula was of the form:-

$$v_u = 7000p + 0{\cdot}012\, f_c' \frac{d_1}{a} + 2500\sqrt{p}$$

Clark was careful to point out that this formula was not for general use but this work, with that of the other empirical approaches before it had had an important influence on the ACI-ASCE Code design method which remains to this day. The ACI formula, for the ultimate shear stress in beams without shear reinforcement is:-

$$v_c = 1{\cdot}9\sqrt{f_c'} + 2500p\frac{Vd_1}{M} \qquad \text{in Imperial units.}$$

where v_c = nominal ultimate shear stress of a member unreinforced in shear.

$\frac{V}{M}$ = the ratio of shear to moment at the section considered.

In the case of simply supported beams, $\frac{Vd_1}{M} = \frac{1}{a/d_1}$.

Thus the ACI formula which is essentially empirical states that the nominal shear stress v_c increases (a) As the square root of the concrete strength

(b) With increase of steel percentage.

(c) With a decrease of $^{a}/_{d_1}$.

In the Committee Report there is no account of why these parameters have the effect that they do but despite this the formula does provide a safe design approach for beams carrying shear, providing that experimental work is continuously carried out to up-date it when changes in design practice go outside the range of the experimental evidence on which it is based.

For the design of members with stirrups, the ACI Code relied on the formula by Richart,

$$V_u = A + \rho f_{yq}$$

and proposed the version

$$V_u = V_c + (\text{Sin}\,\beta + \text{Cos}\,\beta)\,\rho\, f_{yq}$$

where V_c comes from the previous equation and $(\text{Sin}\,\beta + \text{Cos}\,\beta)$ comes from the truss analogy.

The new Draft British Code[10] is similar to the ACI Code except that the nominal ultimate shear stress for beams without stirrups is dependent on concrete strength and tensile steel percentage only. The stresses have been derived from an amalgam of various workers opinions and are therefore presented in tabular form. When stirrups are added, an equation of the following form is used.

$$V_u = V_c + \frac{0{\cdot}8}{\sin\beta}\,\rho\, f_{yq}$$

The factor 0·8 was included as it was found that the factor of safety of certain members was too low without it and the factor $1/\text{Sin}\,\beta$ was provided as a simplification of $(\text{Sin}\,\beta + \text{Cos}\,\beta)$ and is slightly conservative.

The British Code encourages the use of nominal stirrups in most major design situations.

One problem that has concerned experimentalists in recent years is that in some of the experimental work there has been a confusion between the load to cause diagonal cracking and the load to cause failure in a beam. In some tests these are coincidental, in others they are not. This confusion as to exactly what constitutes beam failure is probably responsible for some of the large scatter of the results of shear tests and is an unfortunate legacy of too much reliance on tests.

A different approach which was intended to resolve this problem was produced by Laupa[11] and Moody[12] in 1955. In this case, failure of a beam was assumed to be by the crushing of the compression zone at the head of an inclined crack. The compression zone at this time

was not as deep as the zone in a beam carrying the same moment in pure flexure as the presence of the shear force raised the neutral axis. This description of beam failure obviously caters for the beams in which the presence of inclined cracking occurs some time before the beam fails, the failure mode that is commonly called Shear Compression. Laupa said that the only difference between a beam failing in shear compression and one failing in compression in flexure is that the neutral axis is higher in the shear compression case. A number of theoretical approaches to the problem have started from this proposition.

In 1960, Brock[1] published details of tests of a number of plaster model beams in which the effect of the basic parameters of the shear problem, steel percentage, concrete strength and moment to shear ratio were studied systematically. This work and that of Kani[2] published six years later gives a clear account of the interaction of the three parameters. The tests by Brock were on model beams using gypsum plaster with threaded brass rod as tensile reinforcement. This paper therefore not only puts the problem of shear in perspective but demonstrates the value of model testing as a design technique. The results of Brock's tests are shown in a very simplified form in Figure 1.1 and his complete generalised design chart for ultimate moment capacity is shown in Figure 2.3. In this figure, the zone of shear failures for beams with $^{a}/_{d_1}$ ratios less than 5 can be seen together with the effect of steel percentage. The relationship p/p_o is the ratio of the steel percentage to the steel percentage causing a balanced failure in flexure. Brock used the term Shear Bond to describe one of the failure mechanisms and illustrated the various types of failure in the manner shown in Figure 2.4. It must be remembered that the beams were of reinforced plaster and not of reinforced concrete but there are great similarities between the crack patterns in Figure 2.4 and Figures 1.3 & 1.4.

In his tests Kani tried to produce a similar series of interaction diagrams to those produced by Brock, this time using reinforced concrete beams. Kani looked through the literature and found that no suitable tests were reported that covered the full range of the variables f_c, $^{A_{st}}/_{bd_1}$ and $^{a}/_{d_1}$ that he was interested in. Kani therefore found it necessary to test a further 133 beams before

he could draw his interaction diagram. The results of these tests are shown in three dimensional form in Figure 2.5.

One of the conclusions of a report of extensive work carried out by Leonhardt and Walther[13] which has also been corroborated by Kani[14] is that there is some scale effect on the shear strength of beams. Tests have shown that large beams are significantly weaker in shear than the scaled up results of tests on small beams would suggest. At the moment very little evidence is available and it is not clear whether this is a scale effect or an effect of shape; for example, do deep narrow beams show the same loss of strength as deep slabs? This subject is important as most of the tests on which our design rules are based are on shallow beams, less than 500 mm deep, thus by relying on tests another important parameter may have been missed.

After seventy years of test work we now have the 'Basic facts of shear failure'.

1. Shear failures occur in simply supported point loaded beams with a/d_1 ratios less than 6. For beams with distributed loading the parameter $\frac{M}{Vd_1}$ may be used instead of a/d_1.

2. The problem of shear failure is slightly less acute in beams with distributed loading.

3. Beams with high steel percentages carry greater shear forces before failure than beams with low steel percentages but their failure may occur at a lower percentage of their ultimate flexural moment.

4. Beams with high concrete strengths carry slightly greater shear forces before failure than beams with low concrete strengths.

5. When beams are designed with stirrups, the method of the truss analogy may be used but this is generally conservative.

6. The provision of nominal stirrups to beams in which the shear stresses are not high greatly increases their safety.

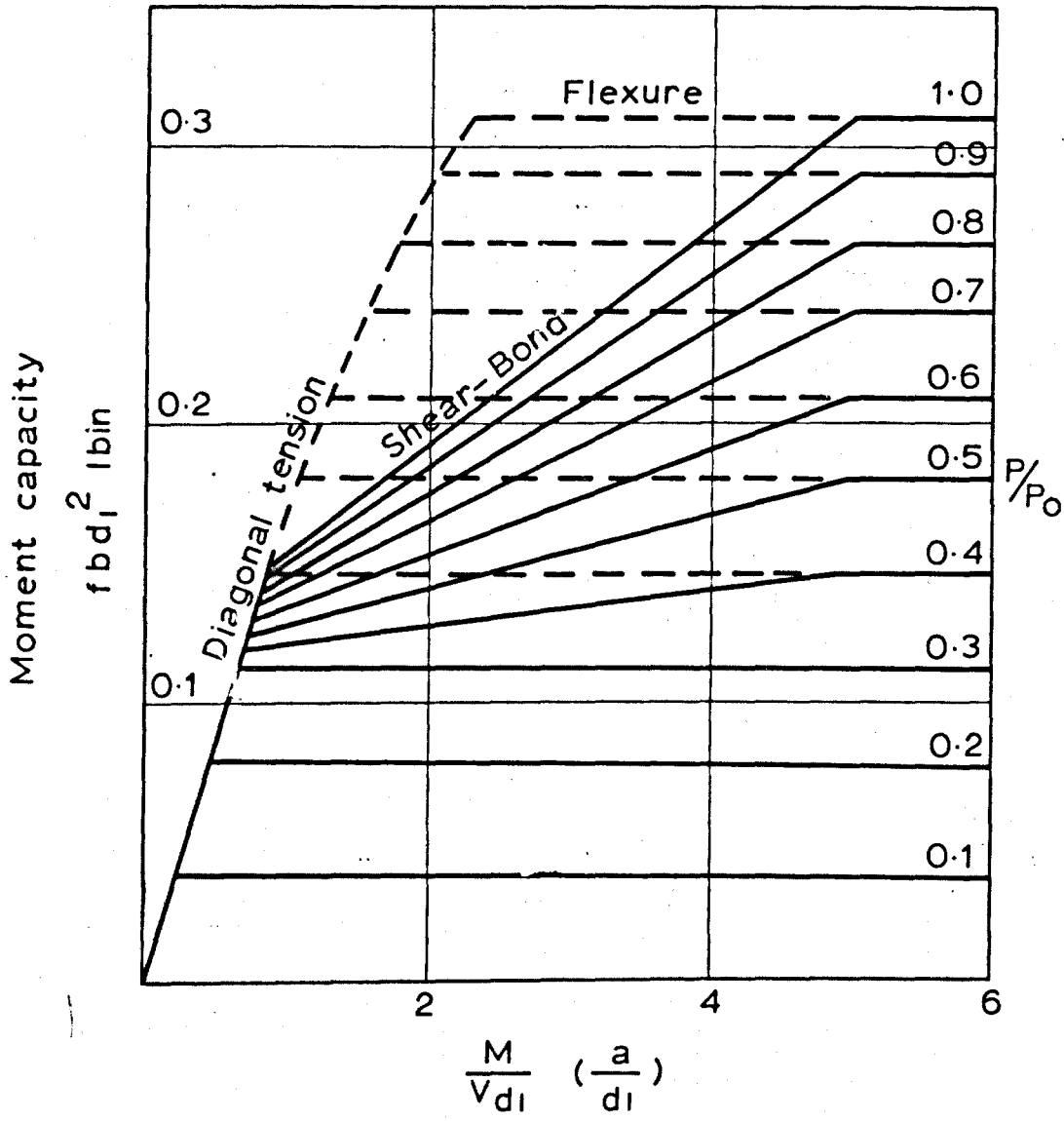

P/P_o ratio of steel percentage to balanced steel percentage

f crushing strength of lin plaster cube

b beam width

d_1 beam effective depth

a shear span

2.3.
INTERACTION BETWEEN MOMENT CAPACITY AND SHEAR SPAN FROM TESTS BY BROCK

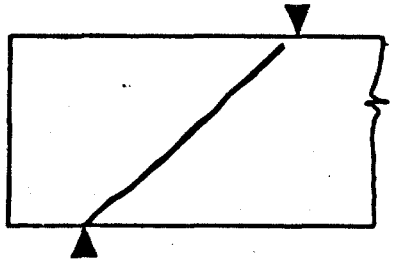

Diagonal tension

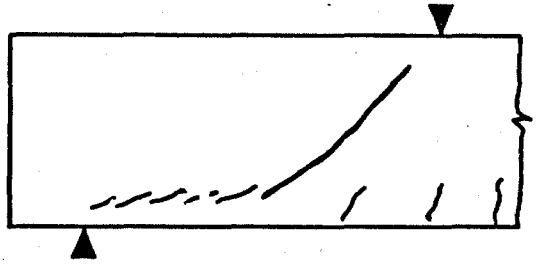

Shear bond

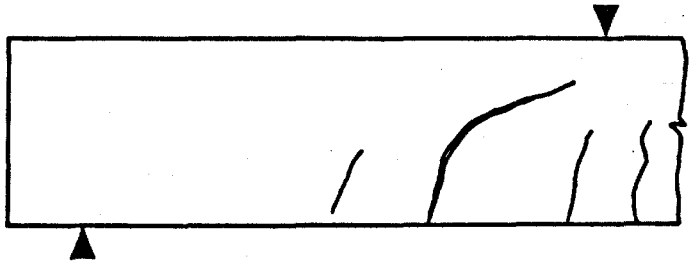

Flexure

2.4. FAILURE MECHANISMS PROPOSED BY BROCK

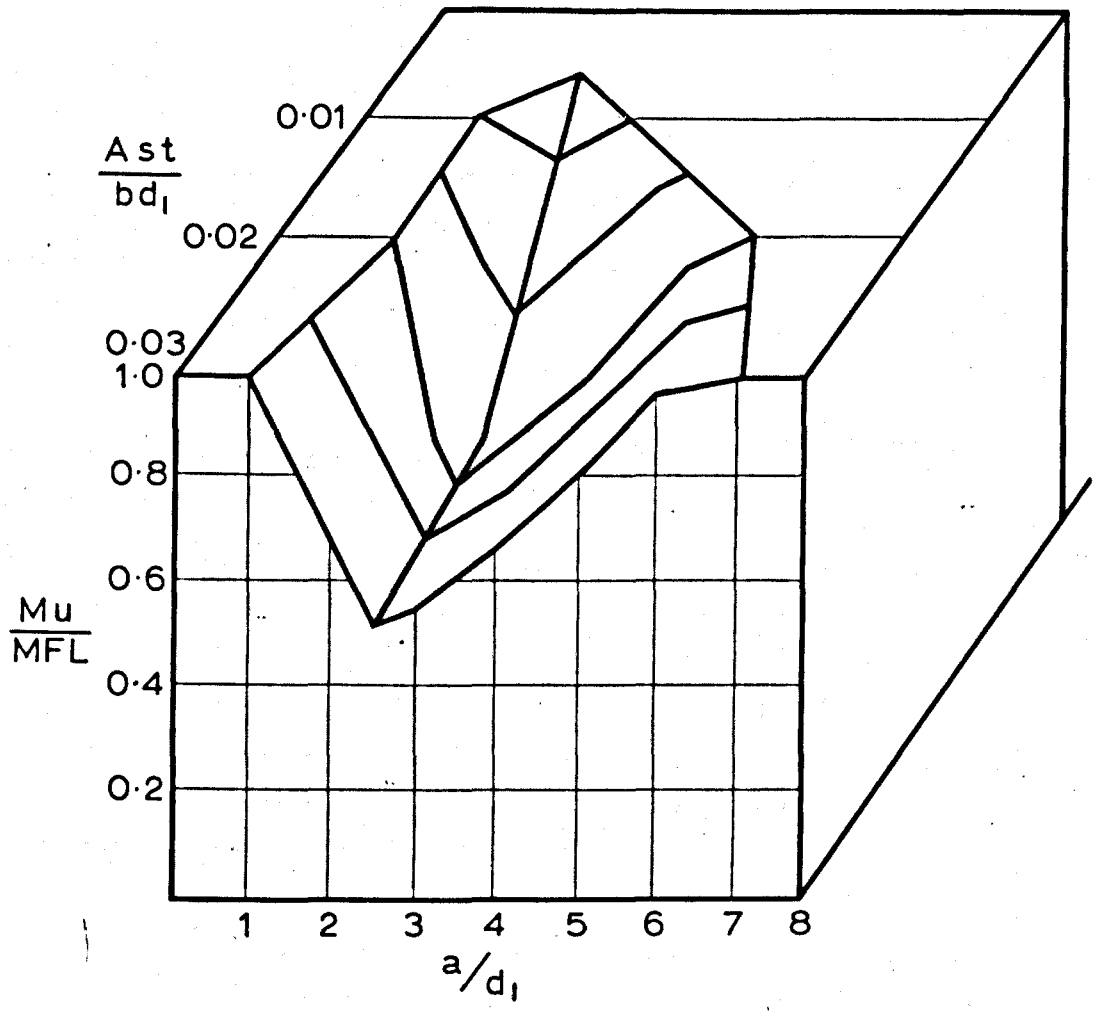

$\frac{Mu}{MFL}$ ratio of bending moment from test divided by the flexural capacity of the sections

2.5
INTERACTION BETWEEN MOMENT CAPACITY AND SHEAR SPAN FROM TESTS BY KANI

CHAPTER 3

REVIEW OF PREVIOUS RESEARCH - BEHAVIOURAL

A very common technique in the analysis of indeterminate structures is to cut sections through the structure to make it statically determinate and postulate force systems that must act across the sections in order to hold the parts of the structure in equilibrium. The correct forces must obey a further law that when they are acting on each part of the structure they must cause deformations across the sections such that the parts of the structure, or free bodies, will still fit together. Thus the forces on the free bodies must ensure equilibrium and compatibility of displacements.

This method of analysis has been used in the study of the shear strength of beams on many occasions, a number of internal force systems of varying degrees of complexity have been proposed and attempts have been made to measure the forces, In some cases, forces that could occur have not been considered or have been neglected for quite arbitrary reasons and workers have then had to rely on empirical terms in their analyses. Attempts to reconcile these simplified force systems with the displacements they impose on the structure have naturally not been very successful.

The earliest workers on shear made drastic assumptions that have gradually been refined as our knowledge of shear built up. This may be seen by comparing a free body diagram with a rigorous system of forces acting on it with the more simplified versions that have been proposed.

Figure 3.1 shows such a free body diagram of a reinforced concrete beam unreinforced in shear with the forces marked in. A basic and reasonable assumption has already been made, that the three dimensional reinforced concrete beam can be so represented in two dimensions. A three dimensional study of rectangular beams with external forces applied in two dimensions is not likely to add any basic knowledge to the way in which beams carry shear forces.

Forces may be transmitted at each point on section A - A and these have been integrated to sets of forces in three main areas of

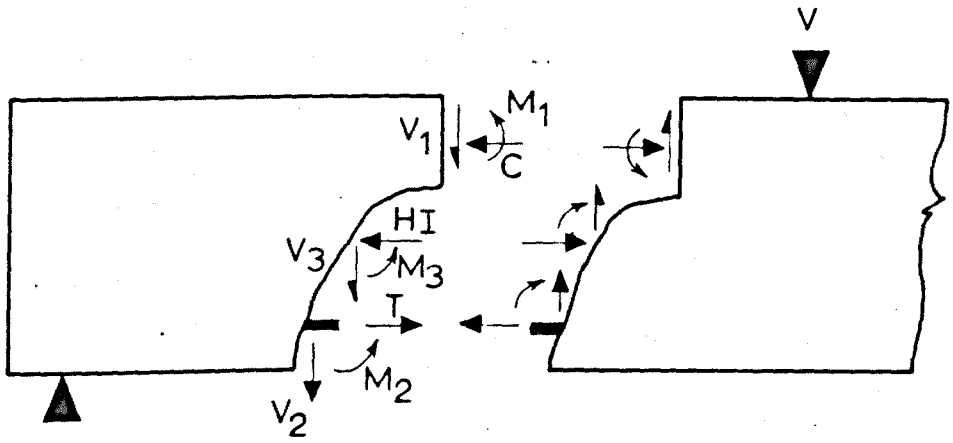

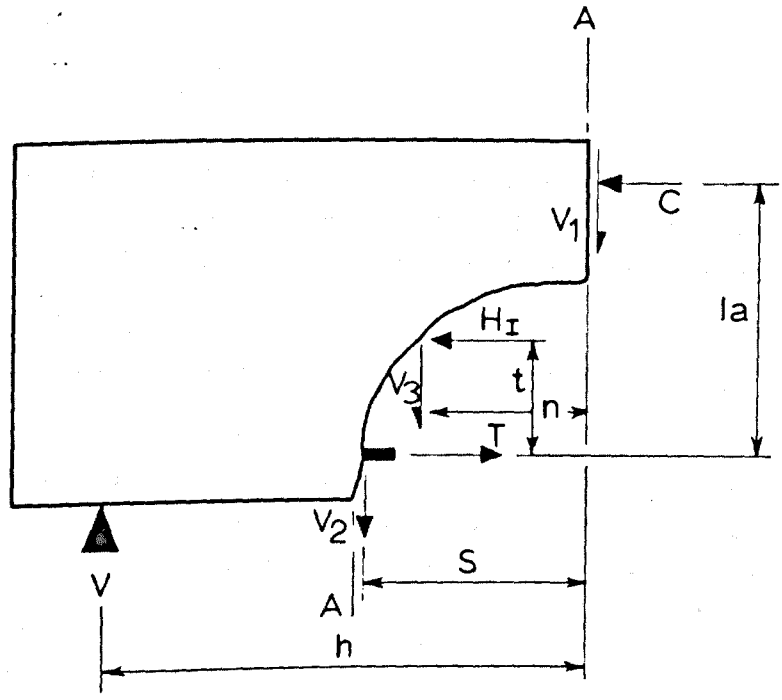

3.1
FREE BODY DIAGRAMS

the beam, the forces in the compression zone above the crack, the forces acting on the sides of the crack and the force carried by the tensile steel. If there are stirrups crossing such a section then these too may carry direct and possibly dowel forces and give terms that may be added to each of the equations. Thus three types of shear force transfer across section A - A are possible and may be significant, forces in the compression zone, aggregate interlock forces and dowel forces carried by the main steel. Most of the work on assessing these forces has been carried out within the last fifteen years although some of the pioneers in their description of tests mentioned these forces.

Considering the equilibrium of the free bodies the following equations may be derived.

$$C - T + H_I = 0 \qquad 3.1$$

$$V - V_1 - V_2 - V_3 = 0 \qquad 3.2$$

$$Vh - V_2 S - V_3 n - H_I t - T l_a = 0 \qquad 3.3$$

In his early work, Talbot[6] described the shear failure of some reinforced concrete beams in detail and gave some clues as to the existence of dowel forces although he did not mention them specifically. In a description of the horizontal cracks which formed along the level of the tensile reinforcing bars he said

"The condition of the beam at failure showed that the horizontal crack was due to vertical tension and that horizontal shear or slip did not take place until after this crack has formed. The indentations in the concrete formed by the corrugations of the bars were left in perfect condition and there was no crushing or tearing at the edges of these indentations. The bar had simply been pulled down and out of the place in which it had rested".

This statement gives a clear description of dowel failure but the possibility that the force which caused the cracking may be significant was not considered until much later.

In his book written in 1924, Faber[15] described his theory of the behaviour of a reinforced concrete beam in shear and proposed a

design method. His theory which he called a Diagonal Compression Theory, assumes that the shear force in a beam is carried by the beam acting as a truss, even when unreinforced in shear. He postulated that inclined compression forces exist between the point of application of the load and the support and act as a truss or arch in conjunction with the tensile steel. Figure 3.2 shows the force system proposed. This mechanism has been proposed since by a number of workers to describe the forces in a beam with a low a/d_1 ratio in which the inclined crack has formed but has not immediately caused failure and the force system has changed from that of a beam to that of a tied arch. From the figure it may be seen that near the support at A - A small tensile strains on the top of the beam are proposed whereas at the point of load application, B - B, the upper face of the beam is in compression.

This apparent reversal of strain in the compression zone was measured and reported by Watstein and Mathey[16] in 1958 and a free body type of analysis in which the dowel force was calculated was also presented.

Watstein and Mathey tested four short beams and on one of them measured strains on the tensile steel and on three sections down the beams. The layout of the beams is shown in Figure 3.3. Strains were measured at four levels on each of the sections I, II and III as indicated and at two places on the tensile steel. On the other beams, which were even shorter than the one shown, with an a/d_1 ratio of 2, they only measured strains on the steel. Also on Figure 3.3 the crack pattern has been drawn with the extent of the crack marked at various stages of the test. The numbers marked on the crack mark its extent and the shear force on the beam in kN at that time.

Some of the results of the strain measurement may be seen in Figure 3.4 & 3.5. The strains were measured on lines I and III on the test beams at five values of the shear forces, 34, 56, 78, 100 and 122 kN. The beam failed in flexure when the shear force was 133 kN. It may be seen that initially the strain profile at low values of the shear force was linear and the maximum compressive strain was on the extreme upper fibre of the beam. At a shear force of 78 kN for Section I and 100 kN for Section II the strain profile

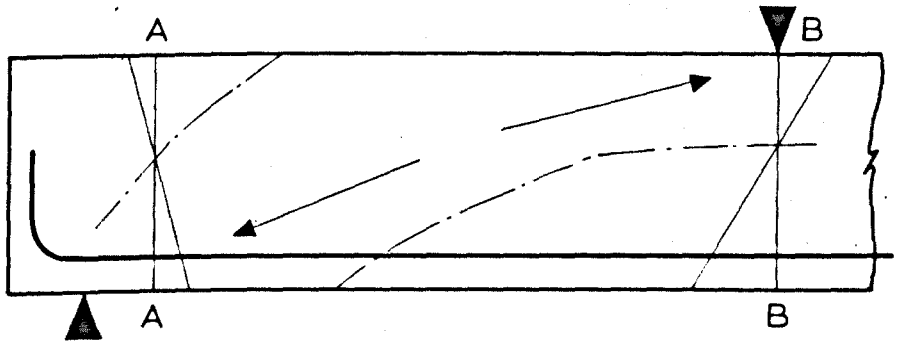

3.2 DIAGONAL COMPRESSION MECHANISM PROPOSED BY FABER

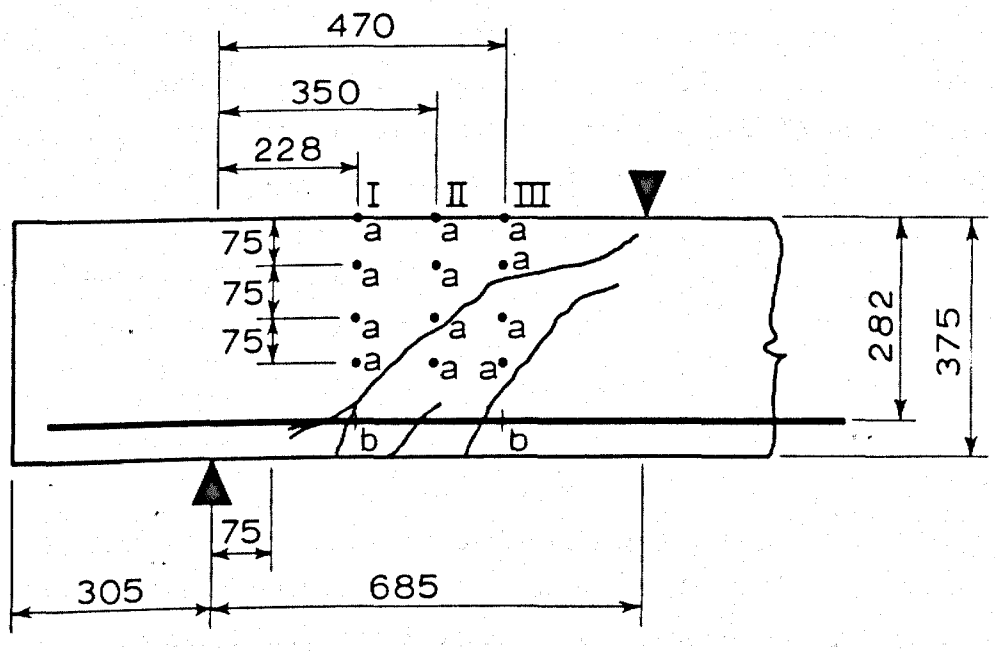

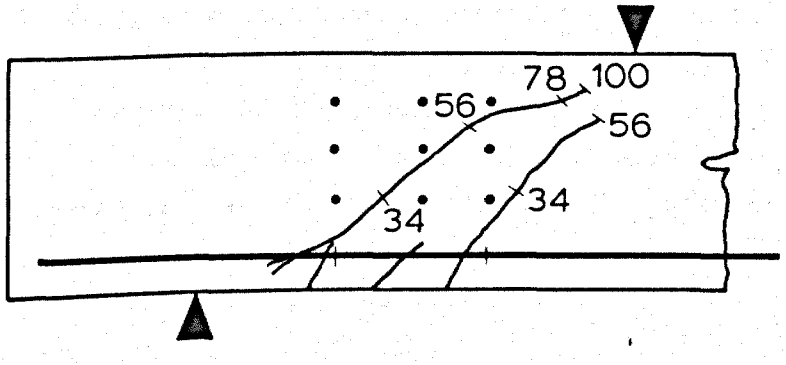

3.3 LAYOUT OF TEST BEAMS – WATSTEIN AND MATHEY

reversed and the maximum was just above the inclined crack in the beam. In the case of Section I, the extreme fibre of the beam went into tension, agreeing with the fact that in beam tests, cracks can sometimes be seen in this area. The section of the beam on the support side of the diagonal crack had therefore initially acted as a beam but as the diagonal crack formed the beam transformed itself into a tied arch and the strain profiles at Section I reversed. This change of behaviour is illustrated in Figure 3.6. The forces that are shown acting on the block are those that were assumed by Watstein and Mathey: the possibility of aggregate interlock forces was not considered. Finally Watstein and Mathey calculated the dowel forces in the beam using the equation:-

$$V_2 = \frac{Vh - Tl_a}{S}$$

which is a simplification of equation 3.3.

At low values of load on the beam, ranging from 42 - 46% of the ultimate loads they found that between 38 and 74% of the shear force must be carried by the longitudinal reinforcement at the base of the crack. At higher loads on the beam the shear carried in this way decreased continuously. Thus when the compressive stress was at its maximum at the upper face of the beam and the member was acting in a beam-like manner, dowel action and aggregate interlock must be carrying a significant shear force. When the action of the beam was like that of a tied arch, little shear was transferred across the crack. If the possibility of aggregate interlock occurring across the crack is considered, this conclusion still stands but the significance of shear forces being carried across the crack is even greater. For example if 50% of the force V_2 was in fact carried by aggregate interlock the point through which the net force acts would be nearer to the load point than that shown in Figure 3.6. Thus S would be smaller and V_2 would be larger.

This work by Watstein and Mathey was of particular importance as it was among the first investigations that studied force systems within beams experimentally and it came to conclusions about the forces carried across inclined cracks that are accepted today.

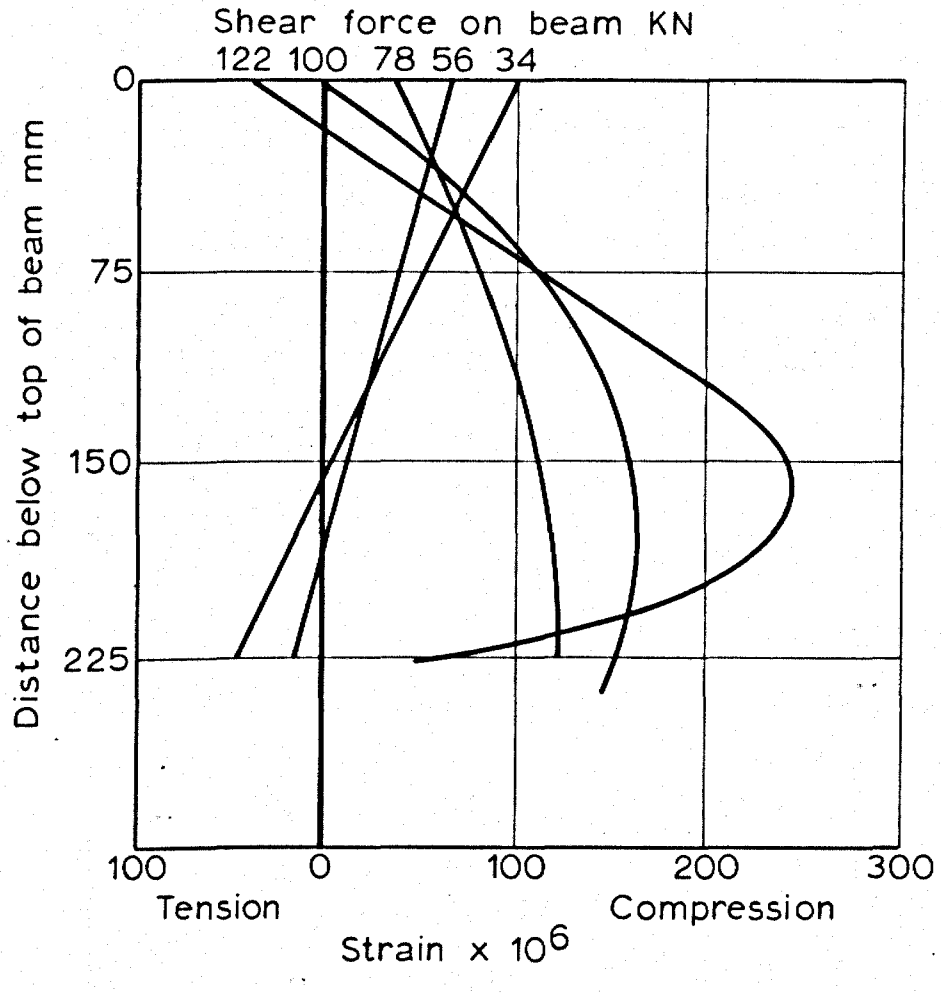

3.4 TEST RESULTS - WATSTEIN AND MATHEY

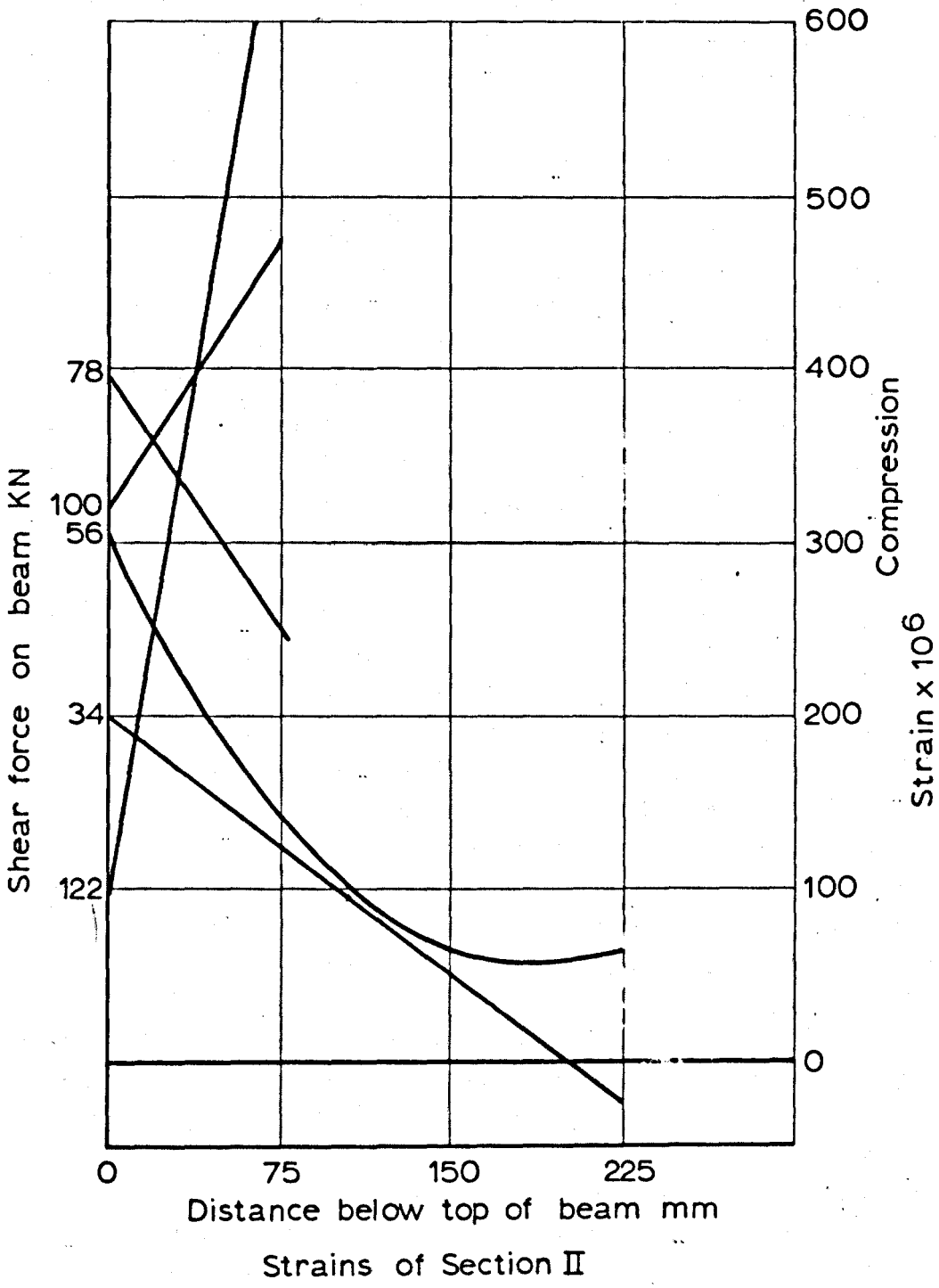

Strains of Section II

3.5 TEST RESULTS - WATSTEIN AND MATHEY

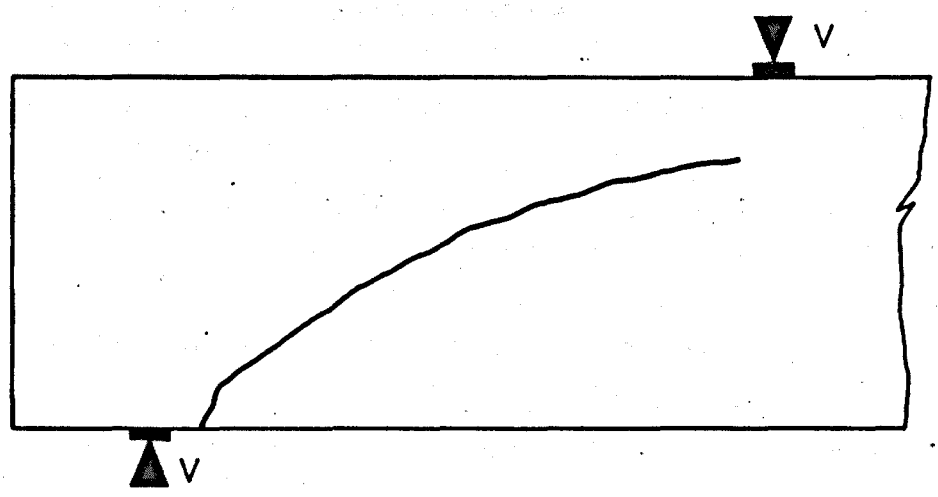

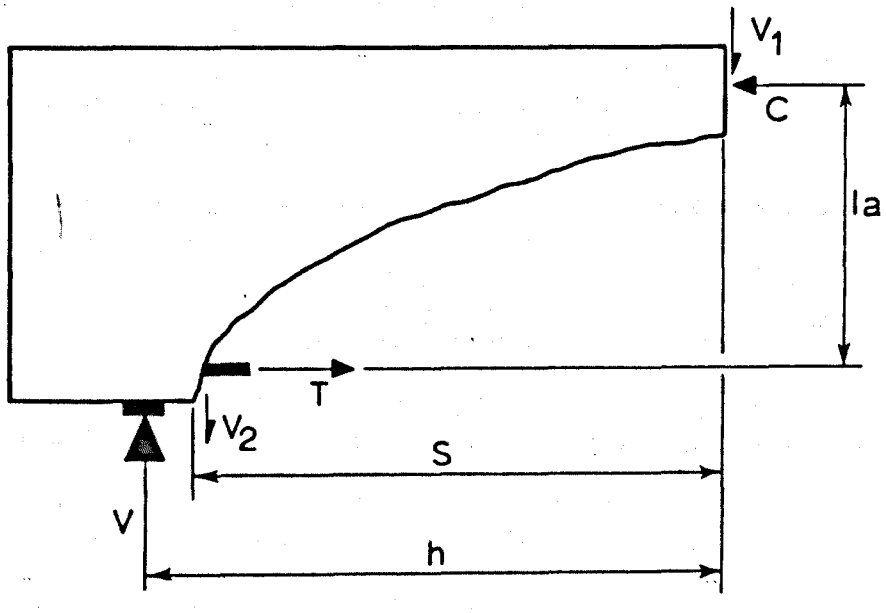

3.6 FREE BODY DIAGRAM ANALYSED BY WATSTEIN AND MATHEY

Another early paper about experimental work on dowel action was one by Royston Jones[17]. In this paper Jones describes tests on three beams with very wide pre-formed cracks.

The layout of the test beams is shown in Figure 3.7 together with a drawing of the shear device which was cast into the beam at the crack in place of the compression zone and carried compressive and shear forces across the crack. The device was instrumented with electrical resistance strain gauges so that the compressive and shear forces could be measured. Strain gauges were also fixed to the compressive and tensile reinforcement and to the shear reinforcement where it crossed the crack so that it was possible to measure the dowel forces carried by the tensile and compressive steel. These tests had the disadvantage that the deformations across the crack were not beam-like, the width of the crack would make the dowel stiffness much less than a dowel in a real beam. The tests have no value in estimating the contribution of a dowel force to the shear capacity of a beam and only show that dowel forces may be significant.

Acharya and Kemp[18] produced a paper which by inference showed that shear force transfer across cracks must be significant and gave a good assessment of its magnitude. The analysis that they used did not include aggregate interlock forces so that, as in Watstein and Mathey's work, they can be considered as an unknown component of the dowel force.

The free body considered by Acharya and Kemp is shown in Figure 3.8, section 1 - 1 is the face of the applied load on the beam and section 2 - 2 is at the base of an inclined crack. Using first the assumption that the dowel force is not zero the following equations may be derived.

$$V_1 = V - V_2 \qquad 3.4$$

$$M = Cl_a = Vh - V_2S \qquad 3.5$$

Secondly, assuming that the dowel force is zero the equations may be simplified to

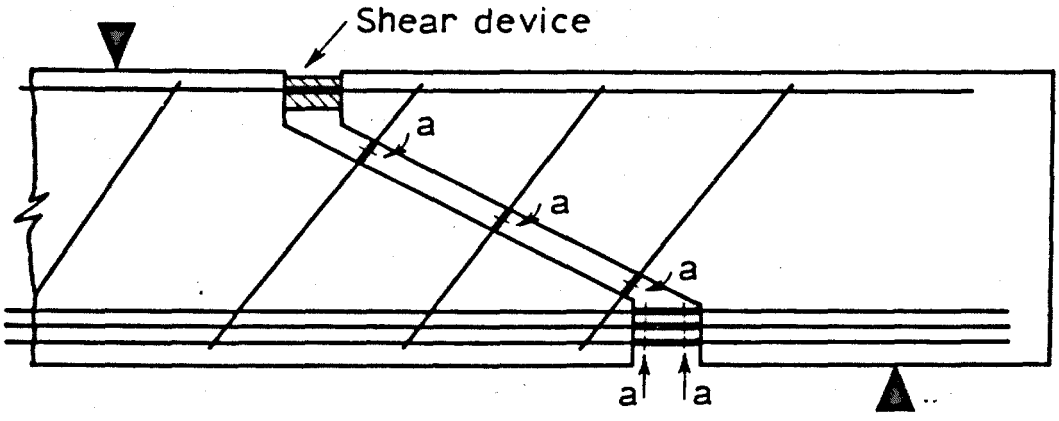

Test beam

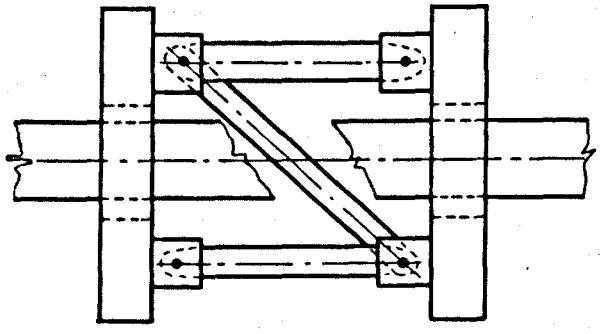

Shear device

3.7 LAYOUT OF TEST BEAM – ROYSTON JONES

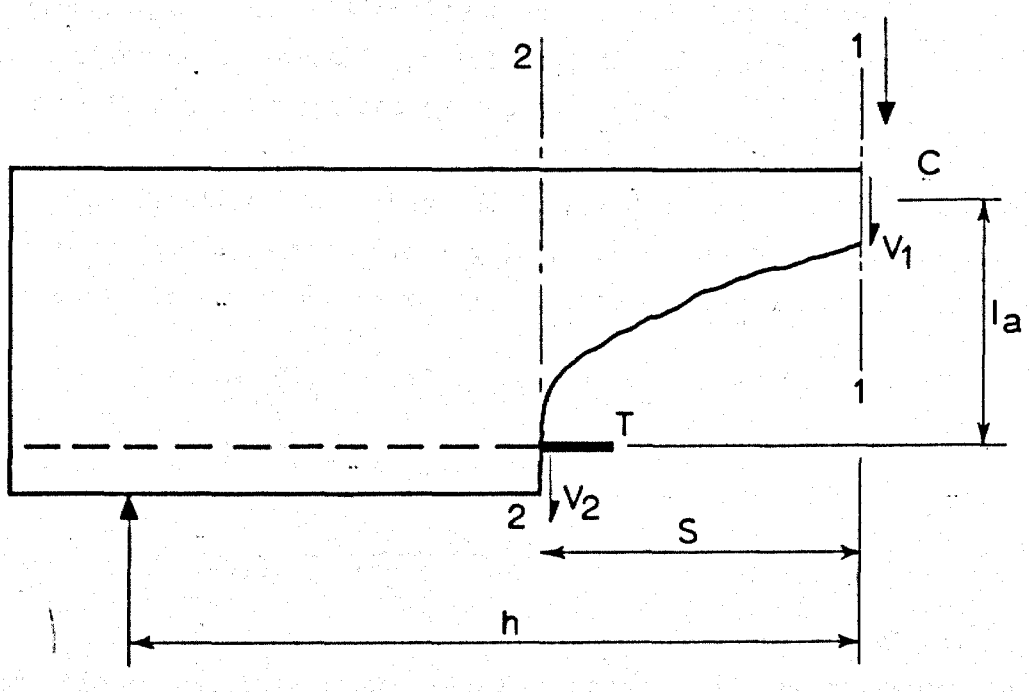

3.8 FREE BODY DIAGRAM ANALYSED BY ACHARYA AND KEMP

$$V_1 = V \qquad 3.6$$

$$M = Cl_a = Vh \qquad 3.7$$

Acharya and Kemp carried out a series of beam tests and, from strains measured in the compression zone, found the depth of the neutral axis of the beams at section 1 - 1 at the last load stage. They reported that the strain profiles that they measured were linear.

Using the experimentally measured neutral axis depths Acharya and Kemp calculated the maximum compressive and shear stresses in the compression zone at section 1 - 1 and showed that unless a significant dowel force is postulated, the stresses are so high that they could not be sustained by the concrete.

The first analysis they made assumed zero dowel force and therefore used equations 3.6 and 3.7. Using the measured neutral axis depth it was possible to re-write equation 3.7 as

$$Vh = Cl_a = \sigma_{x(ave)}\, b\, d_n\, l_a$$

where $l_a = d_1 - k_2\, d_n$

$$\therefore \quad \sigma_{x(ave)} = \frac{Vh}{bd_n\,(d_1 - k_2\, d_n)}$$

$\sigma_{x(ave)}$ is the average compressive stress in the stress block. From this the maximum stress was obtained by dividing by k_1 and this was made nondimensional by dividing by f_c'.

Thus

$$\frac{\sigma_{x(max)}}{f_c'} = \frac{Vh}{k_1\, f_c'\, bd_n\,(d_1 - k_2\, d_n)}$$

where k_2 and k_1 come from the work of Hognestad, Hanson and McHenry[19].

Unfortunately Acharya and Kemp also divided by k_3, the factor which relates 300 x 150 cylinder compressive strength to the maximum stress found in the stress block and this had the effect of making the compressive stresses that they calculated about 5% too high but

this does not affect the conclusions that they drew.

The shear stress in the compression zone was calculated from equation 3.6 assuming that the shear force is distributed evenly down the section

$$T = \frac{V}{bd_n}$$

Acharya and Kemp estimated the vertical stresses at the section 1 - 1 by dividing the failure load on the beam by the area of the loading plate on the beam.

Finally they compared these stresses with a biaxial failure criterion which stated that for values of the ratio of the minor principal stress to the cylinder strength of less than 0·3, failure occurs when

$$\frac{\sigma_2}{f_c} > (1 + 4\frac{\sigma_1}{f_c})$$

where σ_1 minor principal stress
σ_2 major principal stress

Acharya and Kemp found that the stresses that they had computed, on the basis of zero dowel force were so high that this failure criterion predicted failure well before the beams actually did fail.

They then repeated the calculations, this time using equations 3.4 and 3.5 and the assumption that the dowel force is 60% of the total shear force i.e.

$$V_2 = 0{\cdot}6\ V$$

and $$V_1 = 0{\cdot}4\ V$$

In this case the stresses were considerably less than the case from the previous calculations. Where the original beam failure was reported as being in shear compression, that is failure where the compression zone crushed sometime after inclined cracking, the principal stresses were unsafe. When the failure was reported as being by diagonal tension, the principal stresses were just unsafe.

The major conclusion of their work therefore was that shear forces carried across cracks are significant and must be of equal magnitude to the compressive zone shear forces in order that the failure criterion is satisfied.

In the discussion of this paper, Gopalakrishnan[20] pointed out that aggregate interlock had not been considered and probably was significant and he cited as a reason the fact that the strength of beams increase with increasing width whereas dowel strength must approach a maximum value and cannot always be 60% of the shear capacity of the beam.

Krefeld and Thurston[21] carried out tests to study dowel forces on two types of beams. In the first test, the tension zone at the centre of the span was completely separated from the compression zone by a pre-formed crack, the two parts of the beam only being connected by the tensile steel. The tension zone was pulled down during the test and the dowel force was therefore found when the beam split along the line of the tensile steel. This test specimen is illustrated in the upper part of Figure 3.9. The results of these tests indicated that dowels were capable of carrying significant shear forces in beams unreinforced in shear. In a typical test the dowel carried a shear force of 7·5 kN equivalent to a shear stress of 0·19 N/mm^2 on the beam. This is approximately 20% of what would be a normal ultimate shear stress of 1 N/mm^2 for such a beam. The dowel tests by Krefeld and Thurston are considered in more detail later in this Thesis.

The second type of test specimen, on which only one test was conducted is illustrated in the lower half of Figure 3.9. In this case, a wide pre-formed crack was made in the tension zone of the beam and strain gauges were applied to the tensile steel and the compression zone so that the direct and shear forces could be measured in each area. The strains in the compression zone were measured with electrical resistance gauges in two delta rosettes. The compressive force and the shear force in the concrete were calculated using the assumption that the stresses estimated from the rosette strains were constant through the depth of the compression zone. The dowel force was calculated from the displacement of the bar across the crack,

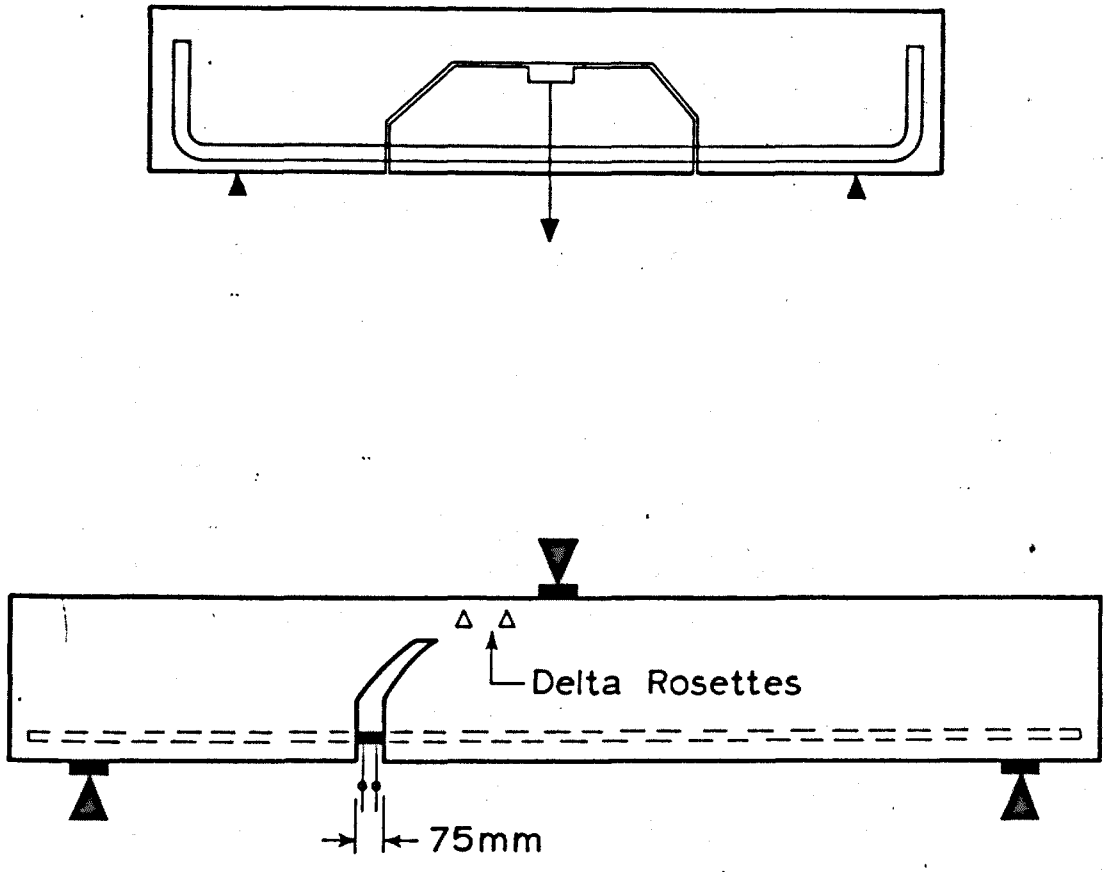

3.9 LAYOUT OF TEST BEAMS – KREFELD AND THURSTON

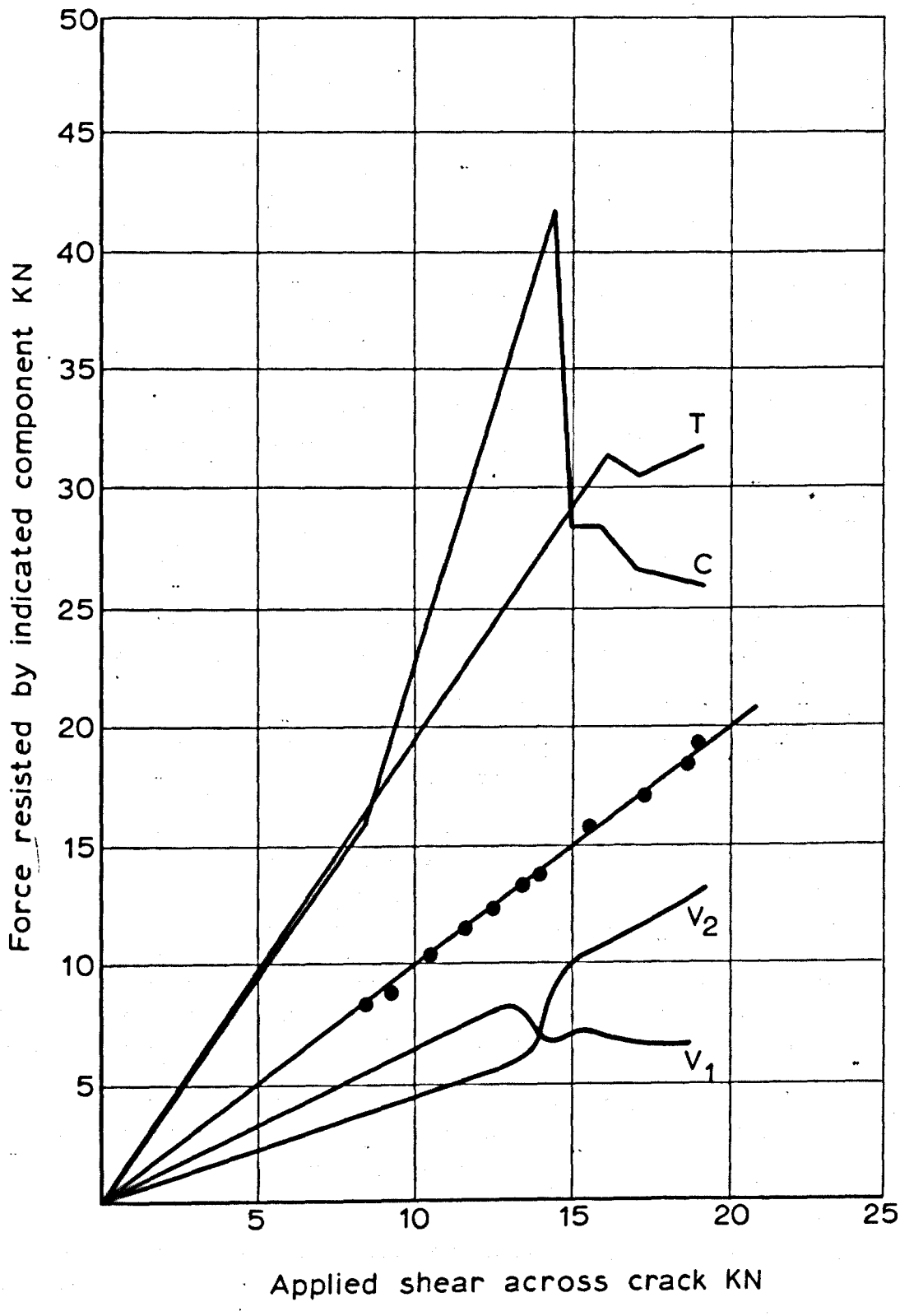

3.10 TEST RESULTS - KREFELD AND THURSTON

measured by a pair of dial gauges bearing on the bar, one at each side of the crack. This test beam had a tensile steel percentage of 3·3%.

The results of this test are illustrated in Figure 3·10. It can be seen that reasonable agreement is obtained between the concrete compressive force C and the steel tensile force T except at high loads, this discrepancy possibly being due to the fact that the method of calculating the force C was in error. The two contributions to the shear force on the beam, V_1 the compression zone shear and V_2 the dowel shear add up to the total shear force and are of approximately equal magnitude. At failure, the dowel force is 69% of the shear force and the compression zone force 31%. The ultimate strength of this beam was low, the average shear stress on the beam, computed from

$$q = \frac{Q}{bd_1}$$

being 0·5 N/mm^2. Krefeld and Thurston suggested that this was because of 'the exaggerated conditions imposed'. This is of course correct, the stiffness of the test beam in the direction parallel to the shear force is much less than in a normal beam, a beam with a narrow crack is likely to be much stronger. This same argument applies to the tests carried out by Royston Jones. Another and even more important difference between the behaviour of this test specimen and the behaviour of a normal beam is that the preformed crack completely excludes the possibility of aggregate interlocking across the crack. A normal beam, with the tensile steel percentage of the test specimen would be expected to have an average shear stress at failure of at least 1 N/mm^2, twice that found by Krefeld and Thurston with their divided beam. Thus aggregate interlock forces possibly give a very significant contribution to the shear capacity of reinforced concrete beams.

Once there was an accumulation of evidence that consistently pointed to the fact that significant forces could be carried across cracks by dowel action, workers naturally turned to study the sections of beams between cracks to see if they could sustain the forces that were proposed. This led to a number of papers in which an

idealisation was made of a beam as having two sections, one at the support which was uncracked and behaved as an arch and the other, nearer to the applied load which had a comb like structure. This idealisation is illustrated in Figure 3.11.

One of the earliest published papers which postulated a theory based on this form of beam action was one by Lorentson[22]. Lorentson assumed that the forces on a single section of a beam between two cracks and a vertical section above them to the compression face are as shown in Figure 3.12 and also made the further assumption that the sides of the crack are vertical.

By assuming that the teeth between the cracks were infinitely narrow he produced a function for $\frac{dT}{ds}$, the rate of change of tensile force along the beam, at which the teeth would fail. The theory led to an equation that stated that the shear strength of a beam is related to the strength of the laminae between cracks, the lamina strength being the sum of two components, k_a, the shear force carried by the reinforcement by dowel action and k_b, the force carried by the compression zone. Thus:-

$$k = k_a + k_b$$

Lorentson then carried out a limited series of dowel tests to determine k_a and some splitting tests on, and analyses of, concrete plates to find k_b.

Although this work was an interesting attempt to consider the strength of the laminae between cracks it had the following disadvantages.

Firstly the functions that were used in the analysis were considered to be continuous for the cracked area of the beam and had a discontinuity at the first crack from the support. In practice the steel stress and neutral axis depth are not simple functions of the distance along the beam.

Secondly, the stress analysis of the laminae between cracks, which had vertical sides, only considered an inclined thrust in the compression zone and ignored aggregate interlock forces.

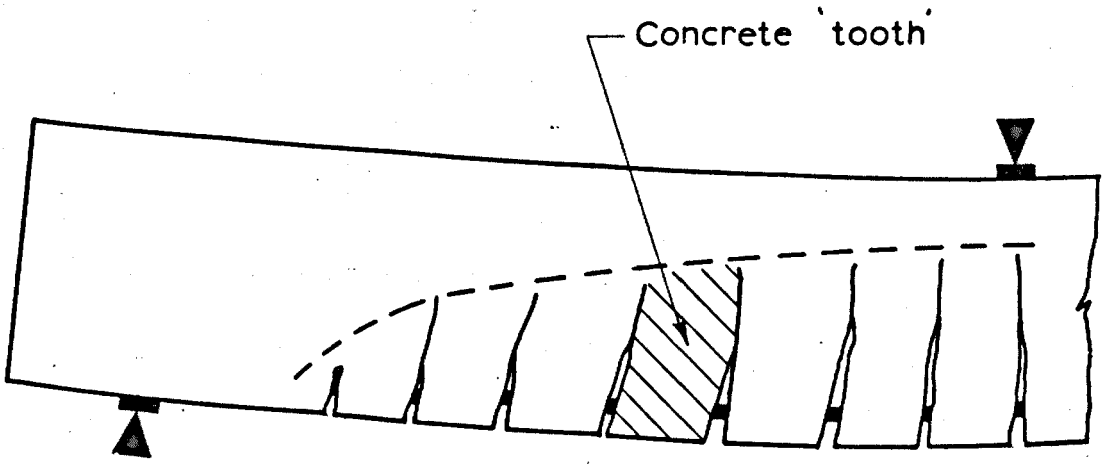

3.11 CONCRETE TOOTH IN A SHEAR SPAN ANALYSED BY LORENTSON

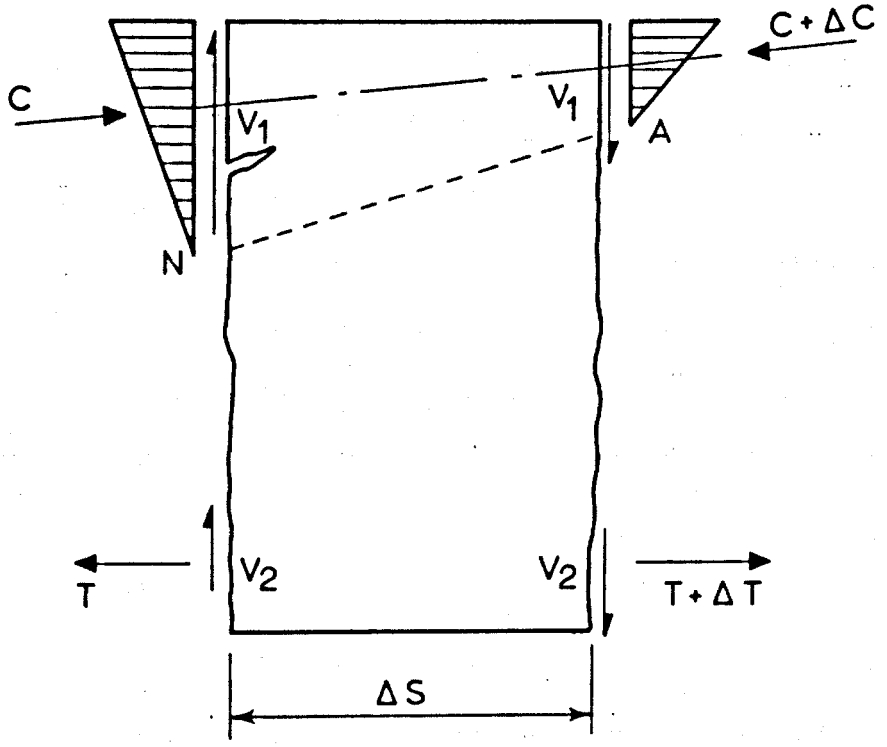

3.12 CONCRETE TOOTH WITH FORCES ACTING ON IT

The dowel tests were carried out on beams reinforced with prestressing wire as Lorentson's work was on the shear strength of prestressed concrete and not on reinforced concrete. These tests are considered in more detail later in this Thesis.

Finally, the assumption that two contributions to the lamina strength are additive, without considering any compatibility of displacements is questionable.

Another paper in which the strength of the concrete teeth between cracks was considered was one by Kani[23].

Kani said that under load a reinforced concrete beam cracked and transformed itself into a comb like structure with the tension cracks forming almost vertical concrete teeth held together by the compression zone which acts like the backbone of a comb. If the strength of the teeth is exceeded and they break off, a short beam is still capable of carrying load by acting as an arch but a long beam will fail immediately. Kani produced two relations which showed that shear strength interacted with shear span in the manner shown by tests. The results of this analysis are shown in Figure 3.13. The line for the strength of the concrete teeth came from the assumption that the steel stress varied uniformly along the shear span and that the only force acting on the teeth was the tensile steel force. Aggregate interlock and dowel forces were not considered in the theory. The arch strength line came from a geometrical consideration that the beam strength was a function of the size of the compression thrust block of concrete beneath the load point. The ratio of the arch strength to the beam flexural strength was therefore $\frac{y}{y_o}$, as illustrated in Figure 3.14 and thus was a function of a/d_1, the shear span to effective depth ratio.

It is interesting to consider how it is possible to ignore the presence of shear forces on the concrete teeth and still get the theoretical results in Figure 3.13 which compare favourably with the test results summarised in Figure 1.1. The analysis used by Kani was derived from consideration of a tooth of the general shape shown in the upper half of Figure 3.15. From the Figure, considering the

3.13 INTERACTION DIAGRAM BETWEEN MOMENT AND SHEAR SPAN SHOWING WHEN ARCH AND TOOTH MECHANISMS ARE CRITICAL - KANI

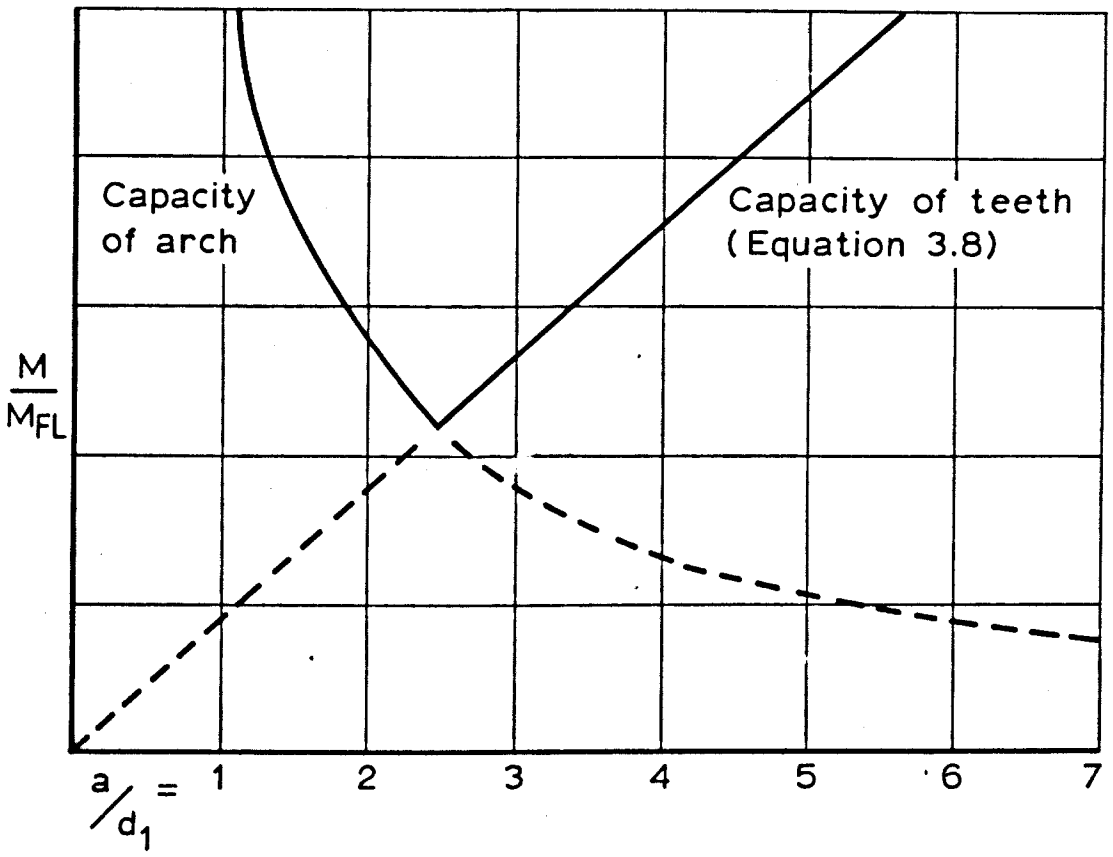

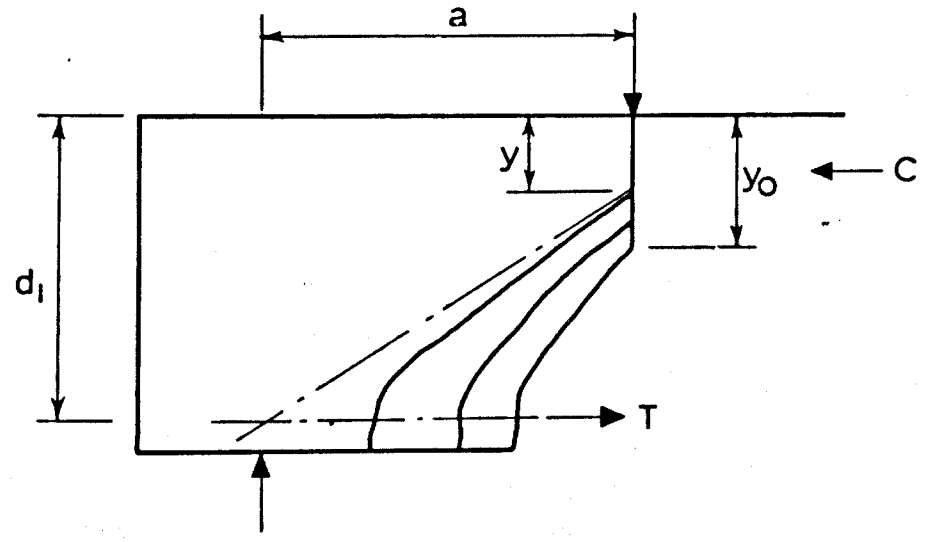

3.14 ARCH ANALYSED BY KANI

tensile stress at the root of the cantilever, the following relationship may be derived,

$$f_t = \frac{M}{Z} = \frac{\Delta T \, h_c}{b \Delta S^2/6}$$

where Z = section modulus of tooth.

When the tensile strength of the concrete is reached.

$$\frac{\Delta T}{\Delta S} = \frac{f_t}{6} \cdot \frac{\Delta S}{h_c} \cdot b$$

where f_t = tensile strength of concrete.

If $\frac{\Delta T}{\Delta S}$, the rate of change of the steel force along the beam is assumed to be $\frac{T}{a}$, i.e. the steel stress increases linearly from support to load point, a relationship for the ultimate moment for the beam may be derived

$$\frac{T}{a} = \frac{f_t}{6} \cdot \frac{\Delta S}{h_c} \cdot b$$

assuming that the lever arm is $^7/_8 \, d_1$

$$M = \frac{f_t}{6} \, {}^7/_8 \, b \, d_1^2 \cdot \frac{\Delta S}{h_c} \cdot \frac{a}{d_1} \qquad 3.8$$

The ultimate moment of the beam is therefore a function of the concrete strength and beam size, the shape of the tooth, $\frac{\Delta S}{h_c}$, and the $^a/_{d_1}$ ratio. For a particular value of $\frac{\Delta S}{h_c}$ taken from tests Kani plotted equation 3.8 in the form shown on Figure 3.13. The theory therefore ignored the strengthening effect of dowel and aggregate interlock shears on the tooth shown dashed in the upper part of Figure 3.15. If these forces are significant they would increase the shear force carried by the beam when the tooth fails and make the line from equation 3.2 much steeper and give a poor fit to the test results. The answer to this enigma lies in the fact that the tooth that was considered when equation 3.8 was plotted was not as shown in the upper part of Figure 3.15 but the tooth section that is shaded in the lower part of the Figure. The value of $\frac{\Delta S}{h_c}$ used was 1·9. Kani said that only the part of the tooth with vertical sides

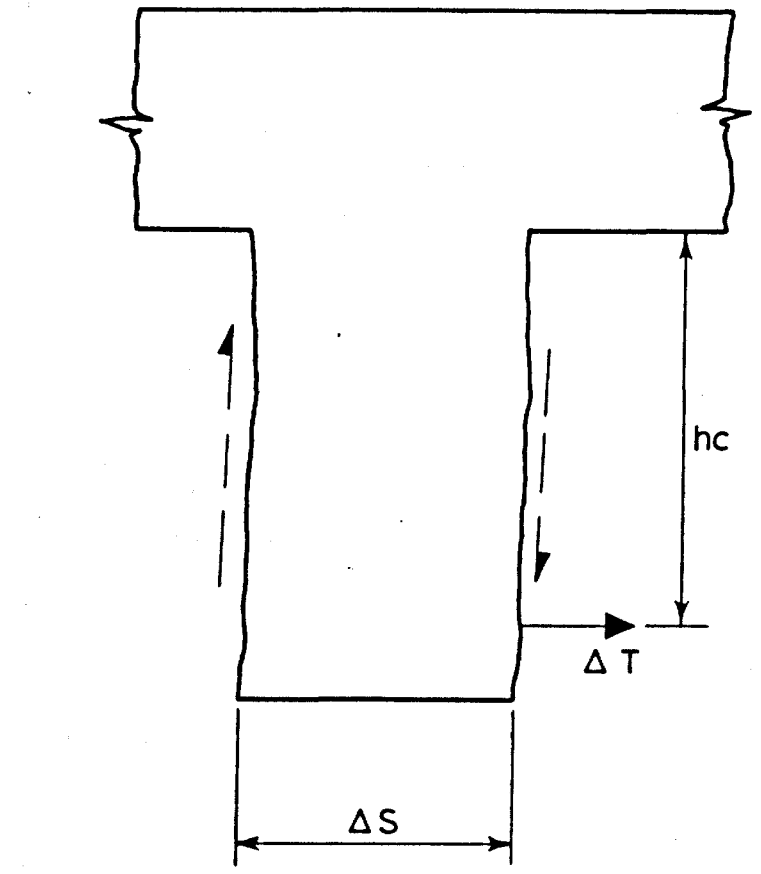

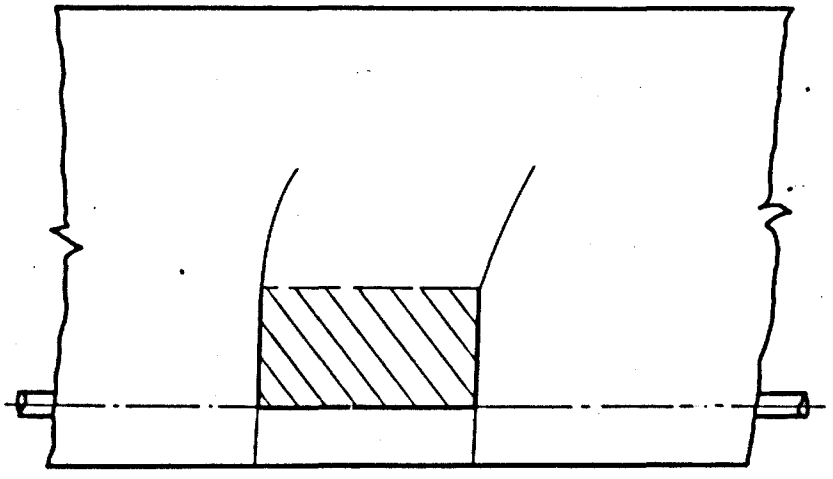

3.15 TOOTH ANALYSED BY KANI

should be considered in the analysis as the crack became inclined when arch action was starting; yet, according to Figure 3.13 the shear capacity of the arch was much less than the capacity of the teeth when $a/d_1 > 3$ and failure would occur immediately when the teeth failed. In practice it is extremely difficult to justify the whole concept of tooth failure from the crack patterns that are observed in tests. A further objection to the theory is that the relationship

$$f_t = \frac{M}{Z}$$

certainly does not apply to a cantilever with the length to breadth ratio of 1·9.

Fenwick[24] has written an excellent description of how beams without stirrups behave in shear. Like Kani he said that beams carry shear forces in two ways, long beams by beam action and short beams by arch action. He realised that as the concrete teeth between cracks do not necessarily break off as the beam fails and as they are much stronger than the Kani teeth illustrated in the upper part of Figure 3.15 then the teeth must have significant shear forces on them. By studying the section of a beam between two cracks illustrated in Figure 3.16 he estimated the relative magnitude of the shear forces carried across the crack, V_3 and V_2.

At the same time Fenwick carried out a series of dowel tests to find the magnitude of the force V_2 and a small series of aggregate interlock tests from which he estimated the magnitude of the force V_3. Neither of these tests were on beams but were carried out on small test specimens in which the specific method of shear transfer was isolated.

The dowel tests were carried out by casting a bar into a block of concrete and then by pulling the bar sideways the dowel force was measured as the concrete cover to the bar split. The aggregate interlock tests were carried out by measuring the shear force that could be carried across a crack in a block of unreinforced concrete. These tests will be described in more detail later in this Thesis.

Fenwick carried out eight tests on beams, some of which had

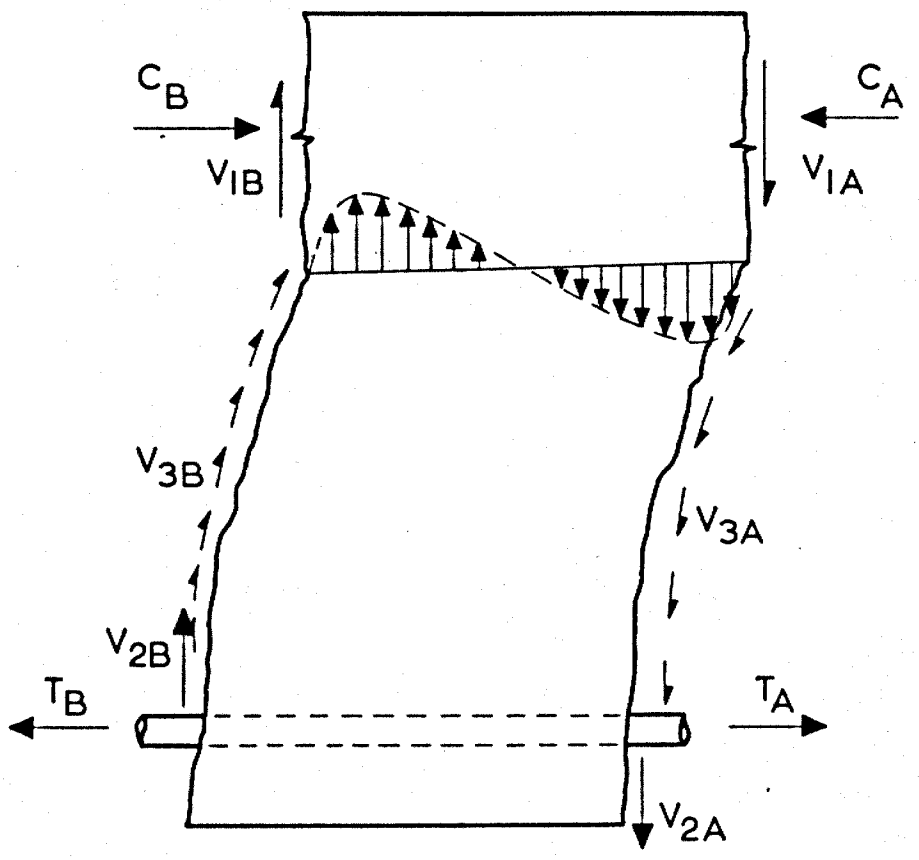

3.16
TOOTH WITH FO:'CES ACTING ON IT ANALYSED BY FENWICK

smooth preformed cracks to eliminate aggregate interlock action and some had foam rubber wrapped round the main tensile steel to eliminate dowel action. From these tests and from the measurements he made of the displacements across cracks Fenwick was able to estimate the relative significance of the various ways in which beams carry shear and more particularly how the concrete teeth between cracks carry the bond force moment. In the conclusion of his thesis he said that in typical rectangular beams without web reinforcement it was found that the bond force moment acting on the concrete blocks between the flexural cracks could be resisted in approximately the following proportions

i 20 percent by the flexural resistance of the concrete at the head of the tooth.

ii 60 percent or more by aggregate interlock action.

iii 20 percent or less by dowel action of the reinforcement.

CHAPTER 4

SHEAR FORCES CARRIED BY BEAM COMPRESSION ZONES

The survey of previous research in chapter 3 of this Thesis indicates that a complete study of the distribution of the internal forces in beams carrying shear has not yet been made. Only Fenwick has attempted to measure interlock and dowel forces in one investigation but his work was limited because, of the eight beams that he tested, only one was complete and was without any form of device to reduce or eliminate dowel or aggregate interlock forces.

Although the technique of eliminating internal forces in beams by, for example, preforming smooth sided cracks, is very useful in determining their significance it is important to realise that in doing this the stiffness of the beam and therefore the way in which it carries forces is also altered.

The next three chapters of this Thesis describe a series of experiments in which the distribution of internal forces in beams was studied. Wherever possible in this work the tests were carried out on complete beams or on specially designed rigs that simulated the displacements measured in beam tests.

This chapter describes the tests which were carried out to estimate the shear forces carried in beam compression zones. Two series of tests were carried out and the compression zone shears were found on a total of ten beams. The shear stresses were computed from strain measurements that were taken in the compression zones of the beams at various stages from first cracking to failure of the beams. Although measurements taken on a number of strain gauges in a rosette are the easiest way to find shear strains in a material, this method was not used in the tests as rosettes require a large number of strain measurements to be taken and are too large for shear strains to be measured at a number of points on one section of a beam.

TEST PROGRAMME SERIES I

Details of test beams

Six beams were tested in this programme. All the beams were 5·18 m long and 400 x 200 mm in cross-section. Five of the beams had two 20 mm diameter bars of GK 60 steel as tension reinforcement; one beam had three bars. All the beams had 25 mm of cover to the main bars. The steel percentages calculated from the expression

$$100\,\frac{A_{st}}{bd_1}$$ were therefore 1·03 and 1·55.

The beams were cast in pairs in wooden moulds and were cured under polythene for three weeks before being taken into the laboratory for instrumentation and testing. The concrete had a 9·5 mm maximum size aggregate so that small gauge lengths could be used on the surface. The details of the concrete are

Aggregate 9·5 - 4·75 mm	60%	by weight
Sand	40%	by weight
Aggregate/cement ratio	4·5	by weight
Compaction factor	0·88	

Twelve 150 mm cubes and six 150 x 300 mm cylinders were cast. The latter were tested to determine the modulus of elasticity of the concrete in compression. Details of the test beams and rig are shown in Table 4.1 and Figure 4.1.

TABLE 4.1
Details of test beams 1 - 6

Beam	a (mm)	a/d_1	Number of 22 mm diameter bars	Steel (%)	U_w (N/mm²)	E_c N/mm² x 10^3
1	1120	3·02	2	1·03	36·6	28·3
2	1120	3·02	3	1·55	42·1	27·6
3	1120	3·02	2	1·03	40·0	25·9
4	1470	3·99	2	1·03	44·8	25·9
5	915	2·48	2	1·03	37·9	23·6
6	1295	3·51	2	1·03	35·2	23·6

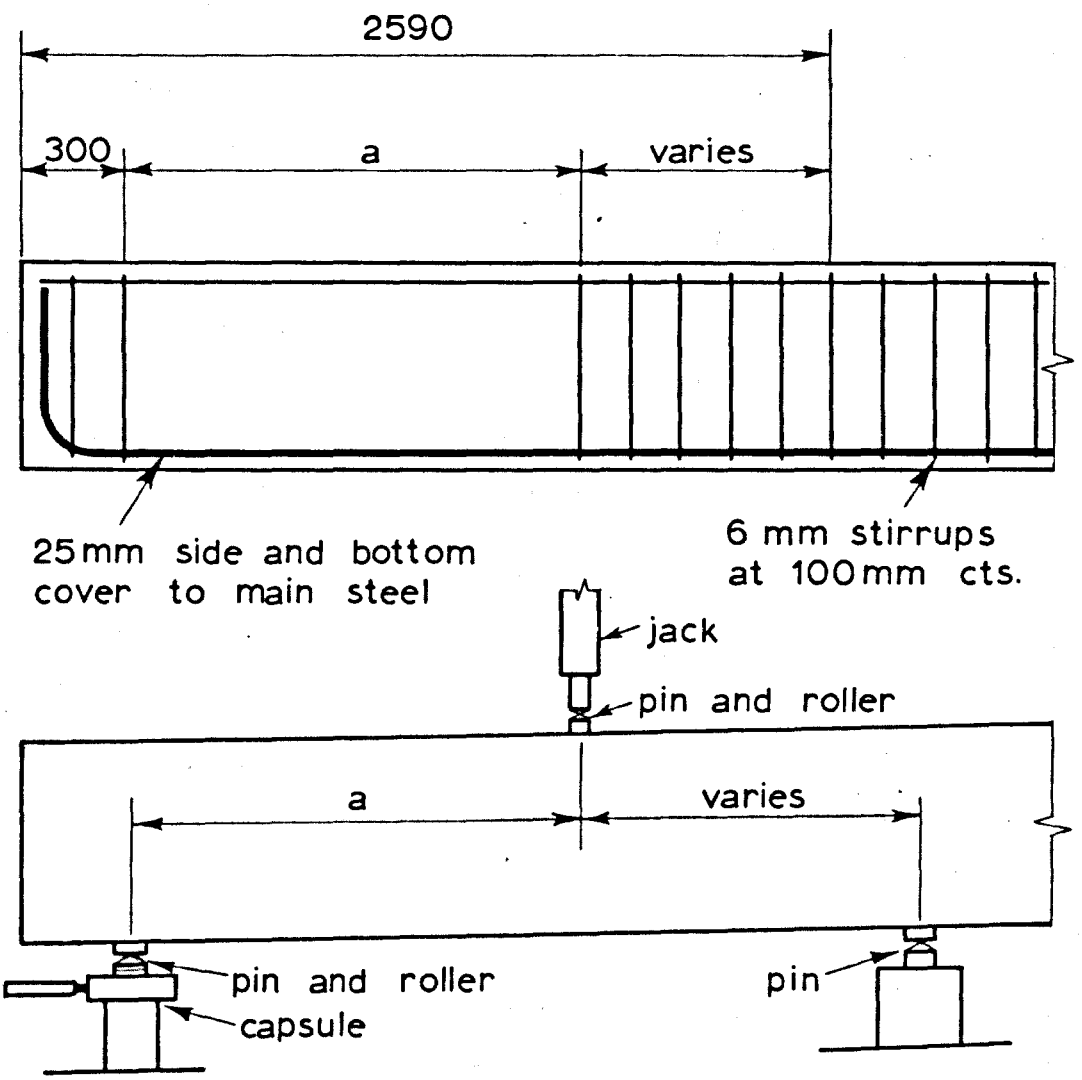

Main steel 22 mm GK 60
Top steel 6 mm GK 60
All dimensions in mm

FIG 4.1 LAYOUT OF TEST BEAMS – SERIES I

Test method

The beams were tested in the rig, one end at a time. The first end was tested a day before the second so that the instrumentation could be put on for the second test after the crack pattern produced by the first test had been inspected.

For the test of the first end, the load was increased until flexural cracks appeared. These were studied under magnifying glasses, marked in and photographed. The load was increased slightly and the cracks were then re-marked and photographed. The marking and photographing were carried out on both sides of the beam at all load stages. There were usually eight load stages before failure. The crack pattern at failure was then examined so that locations could be chosen for the lines of gauge positions for the test of the second end. The test method for the second end of the beam was the same as that used in the first test with the addition that strain readings were taken at each load stage.

Beam 3 was tested differently and the result of this test will be discussed later.

The modulus of elasticity of the concrete was determined from tests on 150 x 300 mm cylinders and this value was used in calculations. For the first two beams, the modulus of elasticity was determined by short-term tests, carried out immediately after the main tests on the beams. These short-term tests produced rather large values of the modulus of elasticity and, in order to arrive at a value of the modulus representative of the conditions of the beam test, a cylinder was put in the testing machine at the start of the beam test and was loaded to produce strain increments similar to the maximum strain increments found in the beam. While the measurements on the beam were being taken, the load on the cylinder was held constant ready to be increased at the next load stage. This gave slightly lower values of the modulus of elasticity for the concrete. Table 4.1 shows the values of the modulus that were used. For both the beam and the cylinder test, strain measurements were made just before the load was increased.

Theory

It is possible to calculate the state of stress at any point in an elastic material by solving the three equilibrium equations from the theory of elasticity.

$$\frac{\partial \sigma_x}{\partial x} + \frac{\partial \tau_{xy}}{\partial y} + \frac{\partial \tau_{xZ}}{\partial Z} + X = 0$$

$$\frac{\partial \sigma_y}{\partial y} + \frac{\partial \tau_{yx}}{\partial x} + \frac{\partial \tau_{yZ}}{\partial Z} + Y = 0$$

$$\frac{\partial \sigma_Z}{\partial Z} + \frac{\partial \tau_{Zx}}{\partial x} + \frac{\partial \tau_{Zy}}{\partial y} + Z = 0$$

where σ_x, σ_y and σ_Z are the direct stresses acting in three orthogonal directions on the member; τ_{ab} is a shear stress acting on a plane perpendicular to axis a and parallel with axis b on the member;

X, Y and Z are body forces per unit area at a point.

In the case of a beam with its length along axis x and depth along axis y, the shears in the Z directions may be neglected. By also neglecting the body forces, the first equation may be simplfied to

$$\frac{\partial \sigma_x}{\partial x} + \frac{\partial \tau_{xy}}{\partial y} = 0$$

This may further be re-written to give the expression

$$\tau_{xy} = \int_0^y \frac{\partial \sigma_x}{\partial x}\, dy \qquad 4.1$$

This expression may be more simply derived by considering a section of a beam δx long (Figure 4.2). The shear stress τ_{xy} may be found by integrating the shear stress required to keep all the elements y wide in equilibrium from the top of the beam to the section considered thus

$$\tau_{xy} = \int_0^y \frac{\partial \sigma_x}{\partial x}\, dy$$

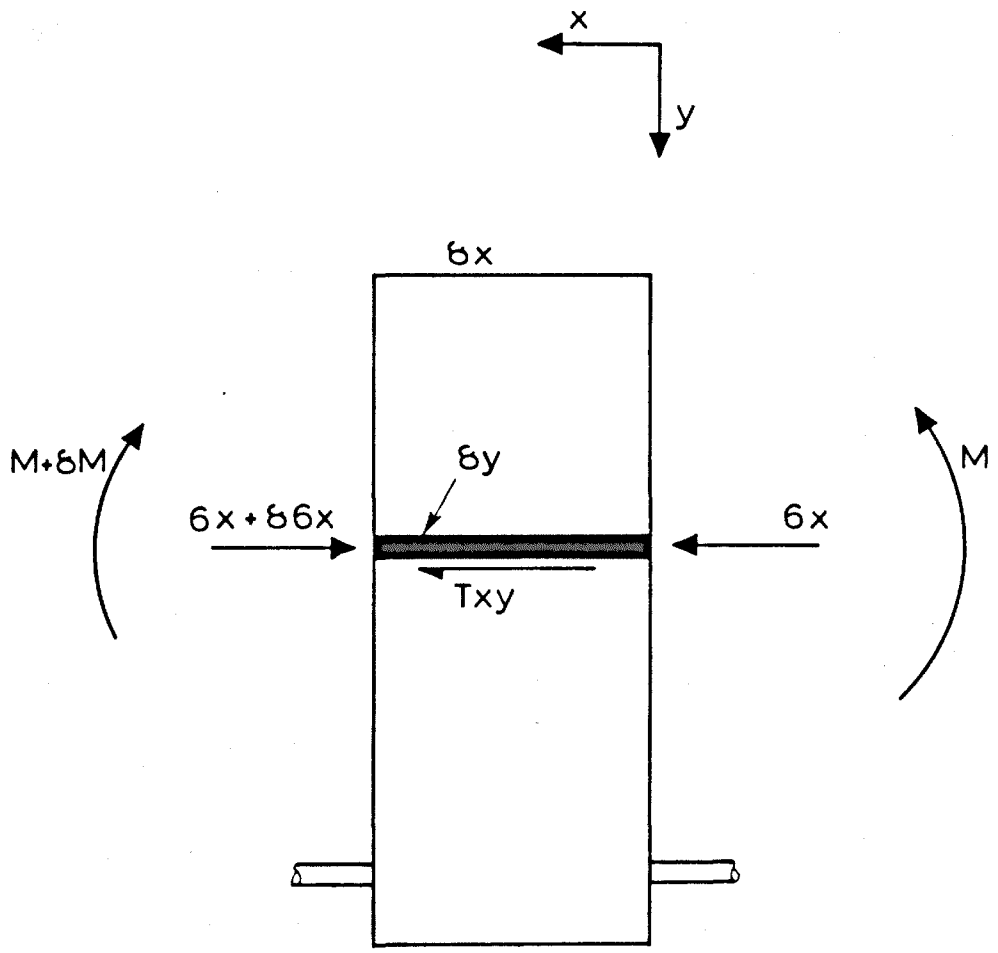

FIG 4.2 DERIVATION OF SHEAR STRESSES

Although expression 4.1 is suitable for an analytical treatment of the problem, its assessment numerically would involve a considerable amount of strain gauge instrumentation. Many rows of closely spaced gauge points would be required in the beam compression zone. A number of longitudinal strain gauge readings would be required in a row along one level of the beam to find $\frac{\partial \sigma_x}{\partial x}$ at the point where the row crosses the line where shear stress is to be calculated. Many rows of gauges would also be required to find $\frac{\partial \sigma_x}{\partial x}$ at more than one level on the line where shear stress is to be calculated. Readings on all the gauges would be required at each load stage at which shear stresses were required.

It is possible to re-write expression 4.1 so that the readings of longitudinal strain taken at various levels down a line in a beam compression zone can be used to find the shear stress distributions in that line. Figure 4.2 shows a typical line of strain gauge positions on a test beam. Expression 4.1 may be re-written as

$$\tau_{xy} = \int_0^y \frac{\partial \sigma_x}{\partial M} \frac{\partial M}{\partial x} \, dy \qquad 4.2$$

This expression now requires longitudinal strain readings taken across only one vertical line in the compression zone but the readings must be taken at more than one load stage.

In the tests, therefore, lines of longitudinal strain gauge points were fixed on the beam compression zone in the manner shown in Figure 4.3 at critical sections of the beam. The longitudinal strain readings were taken with a Demec gauge with a 50 mm gauge length. In each line, the first gauge length was 12·5 mm below the compression face of the beam and succeeding gauge lengths were 25 mm apart.

The steps in the calculation of τ_{xy} are given below.

1. For a gauge length, plot ϵ_c against M and calculate the slope of the plot

$$\frac{\partial \epsilon_c}{\partial M} \qquad 4.3$$

for each value of M.

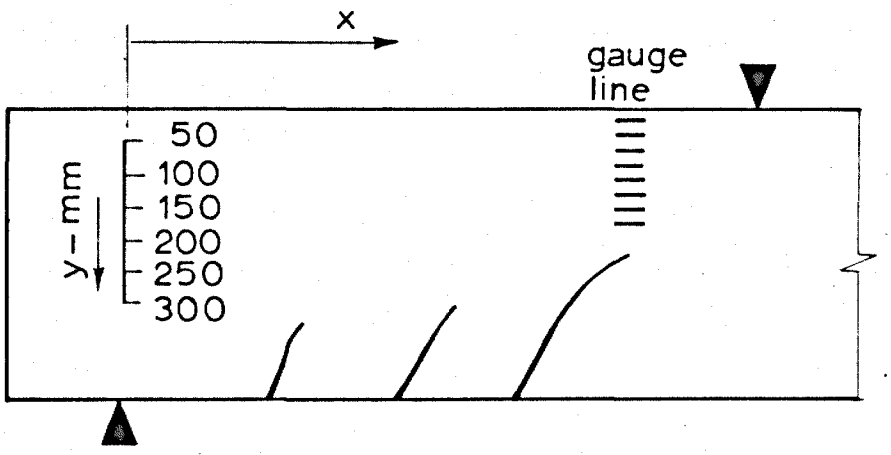

FIG. 4.3 LAYOUT OF STRAIN GAUGES ON A TEST BEAM

In this thesis the slope used in calculations was assumed to be constant with respect to M.

2. Calculate the value of

$$\frac{\partial M}{\partial x} \qquad 4.4$$

for the load stage. This is constant at a load stage for all levels and is the total shear force.

3. Multiply expressions 4.3 and 4.4 and convert the result to

$$\frac{\partial \varepsilon_x}{\partial M} \quad \frac{\partial M}{\partial x} \qquad 4.5$$

by multiplying by the modulus of elasticity of the concrete.

4. Integrate expression 4.5 from the compression face of the beam down to each gauge level. This is the shear stress at the gauge length.

5. Plot shear stress down the beam and find the area of this plot from the compression face of the beam to the neutral axis. This is the shear force carried by the compression zone.

Figure 4.4 shows a typical compressive and shear stress-block from the analysis.

The calculations to find the shear stresses from strain readings were first carried out by hand but, as such a large amount of computation was required, a computer program was written which, from the strain increments, gave the shear stress at each gauge location and the shear force carried in the concrete, at each load stage. Figure 4.5 shows the flow diagram of the program.

Results of tests

Table 4.2 gives the shear forces carried by the beams at failure; two values are shown for each beam as each end of the beams was tested separately. From the results, the typical reduction in ultimate moment of shear tests on beams with low a/d ratios and no web reinforcement is seen.

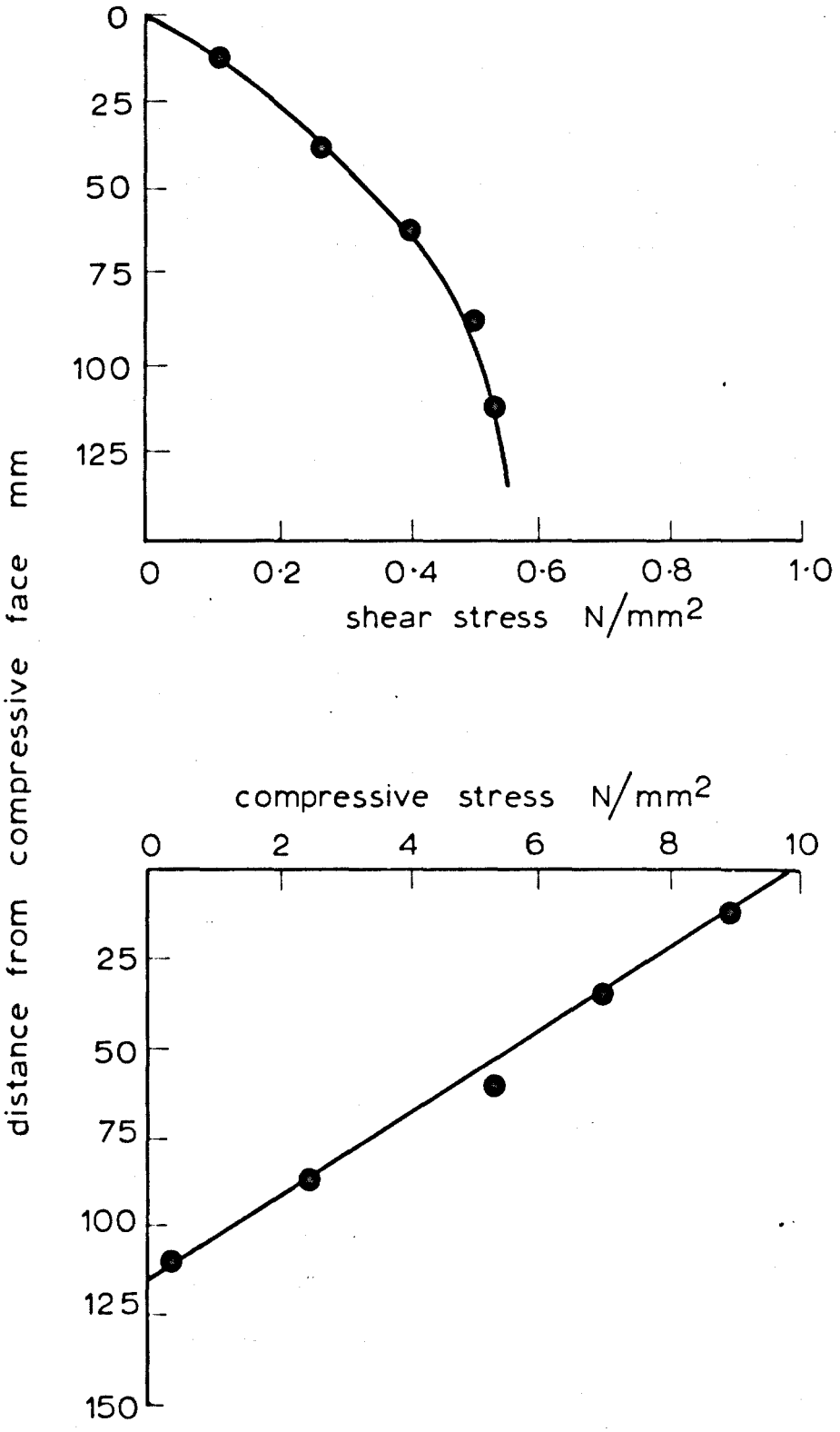

FIG. 4.4 TYPICAL STRESS BLOCKS FROM ANALYSIS

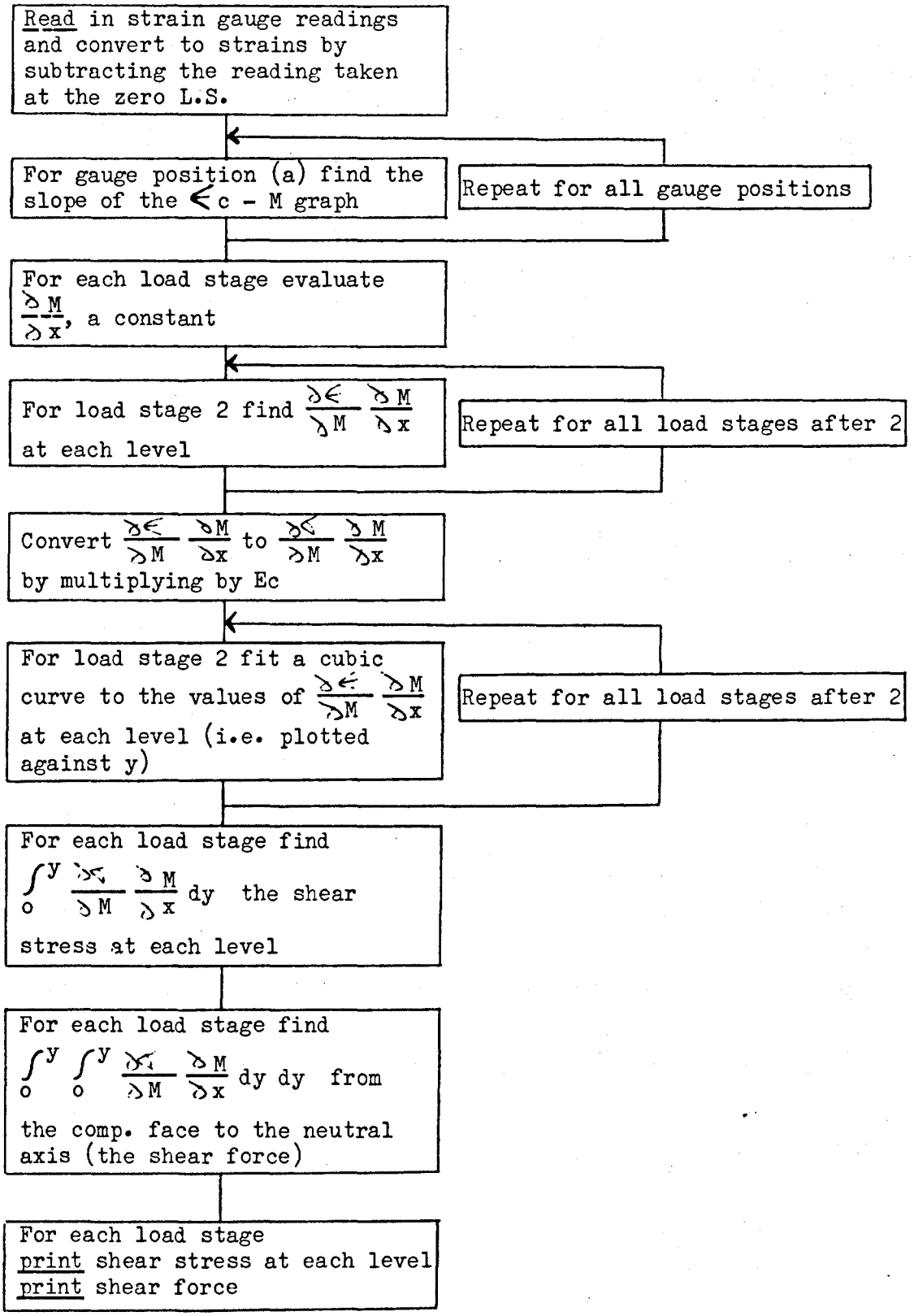

Figure 4.5 Flow diagram of program for calculating σ_{xy}.

TABLE 4.2

Results of tests 1 - 6

Beam	End	V_{ult} kN	M_{ult}/M_{flex}	a/d_1
1	A	61·7	0·61	3·02
	B	75·5	0·75	3·02
2	A	88·9	0·89	3·02
	B	100·5	0·93	3·02
3	A	107·5	-	3·02
	B	76·0	0·51	3·02
4	A	91·5	1·17	3·99
	B	86·6	1·13	3·99
5	A	80·5	0·65	2·48
	B	80·5	0·65	2·48
6	A	86·6	0·99	3·51
	B	77·8	0·89	3·51

In Table 4.2, V_{ult} is the shear force in the beam at failure, M_{ult} is the bending moment under the jack at failure of the beam and M_{flex} is the ultimate flexural strength of the beam calculated from a strain compatibility analysis using the stress-block reported by Hognestad, Hansen and McHenry[19].

Figures 4.5 to 4.11 are photographs of the crack patterns of each end of the beams at failure and they demonstrate that, apart from beam 5, the diagonal crack which caused failure had a similar trajectory on each end of a beam. In beam 5, the dowel splitting began much nearer the centre of the beam in the test of the second end of the beam than in that of the first end, although the shear force carried by each end of the beam at failure was the same.

After the test on the first end of each beam, the crack pattern was inspected before lines of gauge points were stuck on the second end. The positions of the lines were selected so that, if the crack pattern was the same at each end, the lines would go down the beam from the compression face to the heads of inclined cracks. Three or four lines of gauge points were fixed to each beam but not all of these ended at an inclined crack as the crack patterns of the two ends of a beam were never identical. The strain readings from

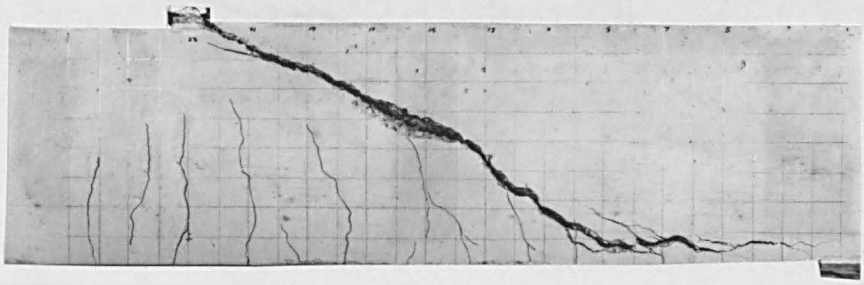

First test

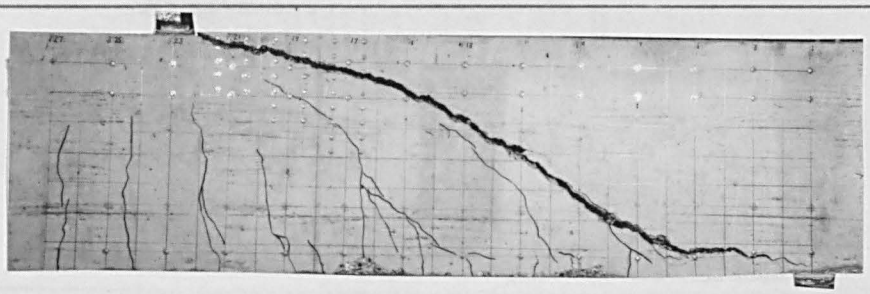

Fig 4.6 Crack patterns at failure Second test
Beam 1

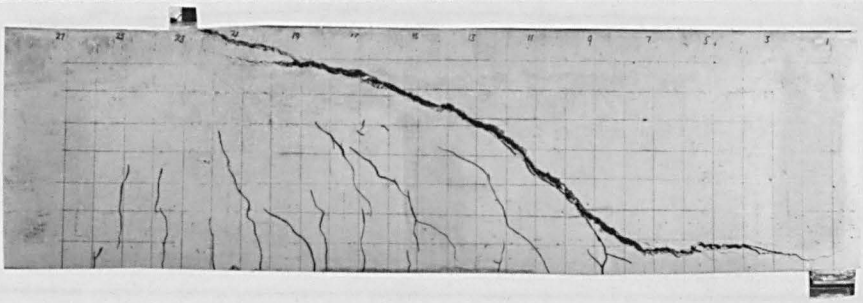

First test

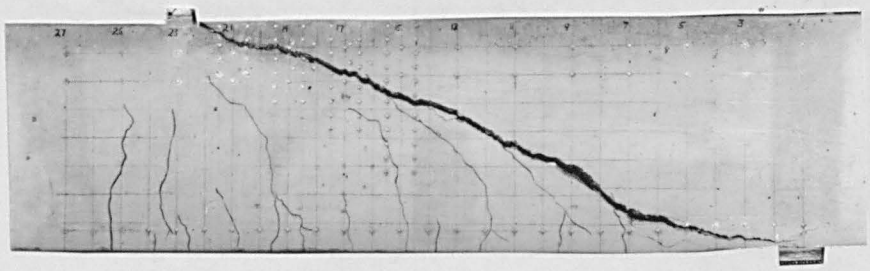

Fig 4.7 Crack patterns at failure Second test
Beam 2

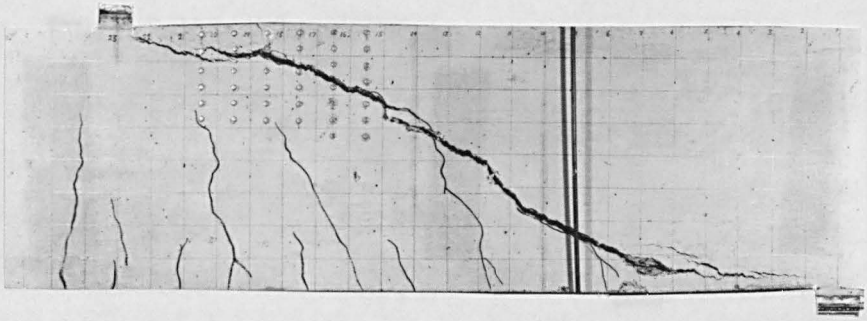

First test

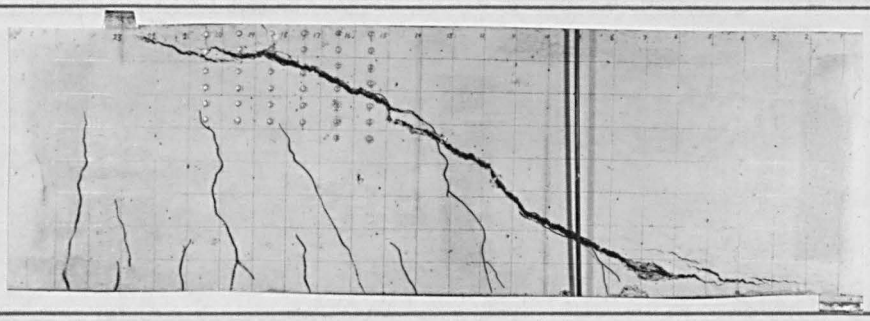

Fig. 4.8 Crack patterns at failure Second test

Beam 3

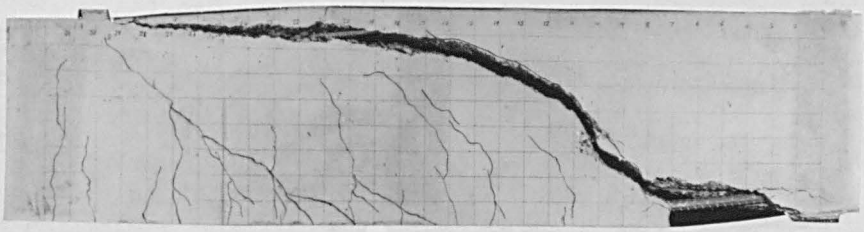

First test

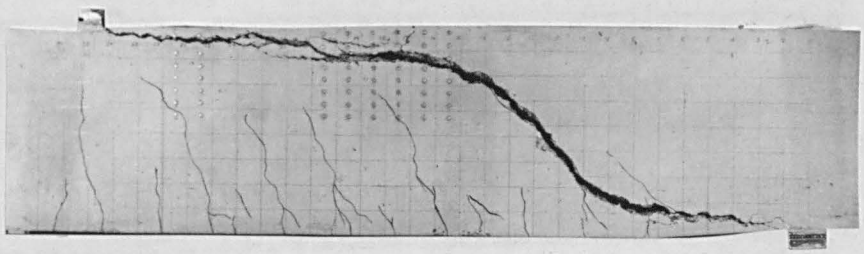

Fig. 4.9 Crack patterns at failure Second test

Beam 4

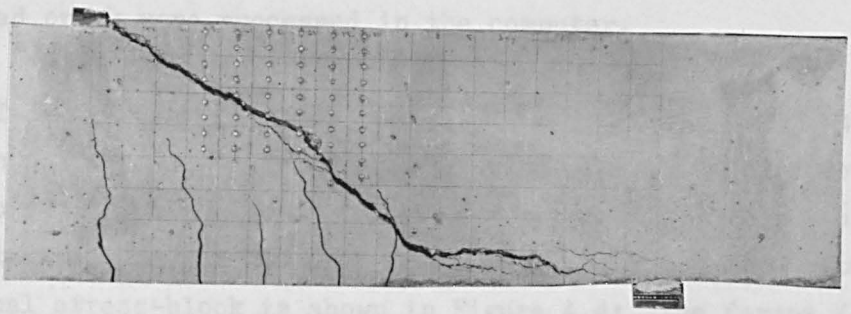

First test

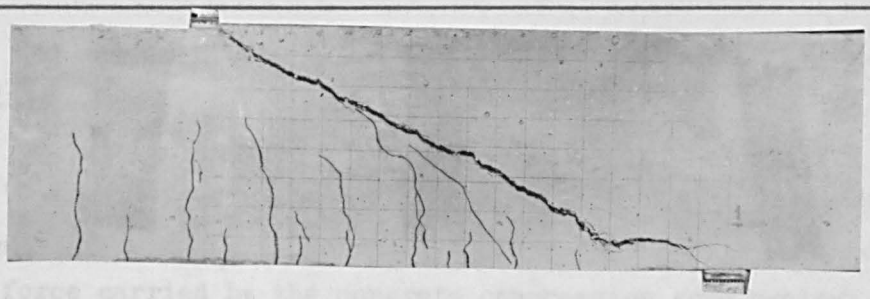

Fig 4.10 Crack patterns at failure Second test
Beam 5

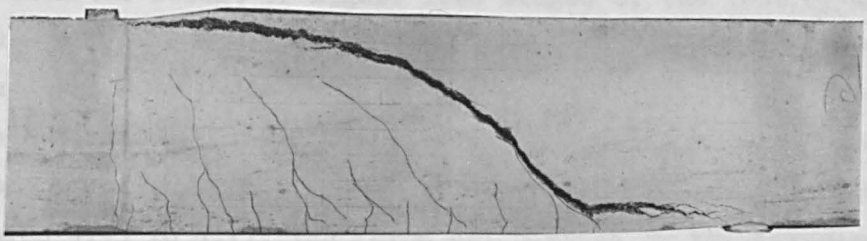

First test

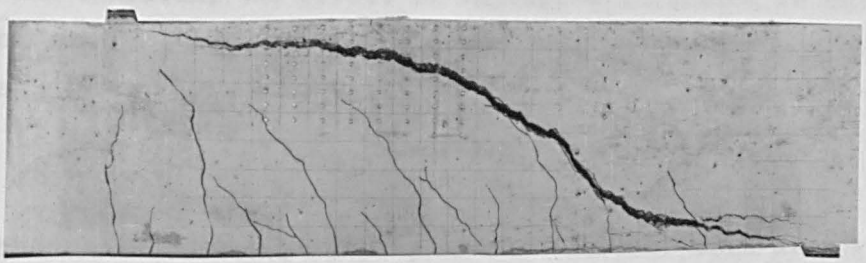

Fig 4.11 Crack patterns at failure Second test
Beam 6

the lines that terminated at the neutral axis between cracks were discarded and only the results of the lines that terminated at an inclined crack were processed in the computer.

The results of the computer work are shown in Tables 4.3 to 4.8 in each of which the shear force carried by the beam and the shear force carried by the concrete compression block are given for each load stage. The shear stress-block ordinates are not reported but a typical stress-block is shown in Figure 4.4; the forces V and V_1 are acting in the positions given in Figure 3.1.

For beam 3, the forces recorded were measured in the test of the first end of the beam and not on the second end.

The shear forces given in Tables 4.3 to 4.8 are plotted in Figures 4.12 to 4.17. The lower part of each Figure is a plot of the shear force carried by the concrete compression zone against the total shear force in the beam. The straight line is the line that would occur if all the shear were carried by the concrete. It can be seen that the concrete carried about 30% of the total shear, which agrees with the result of higher load stages of the test by Krefeld and Thurston shown in Figure 3.10. It is evident that, in Krefeld and Thurston's test, the proportion of the total force carried by the concrete decreased as the test progressed until the concrete was carrying only about 30% of the total shear on the beam. At the top of Figures 4.13 to 4.17, the force not carried by the compression zone has been plotted as a percentage of the total force on the beam. If in this case, in order to give a comparison with the work by Krefeld and Thurston, the effect of aggregate interlock is not represented in the equilibrium equations and the dowel force is found from the vertical equilibrium equation,

$$V = V_1 + V_2 \qquad 4.6$$

and is therefore the total shear less the shear carried by the concrete.

TABLE 4.3

Shear force carried in compression zone

Beam 1

Load Stage	Reaction at support, V kN	Gauge line 813 mm from support V_1 kN	Gauge line 915 mm from support V_1 kN
1	0	0	0
2	31·4	15·4	9·5
3	37·9	17·9	11·4
4	44·5	16·8	11·9
5	45·8	17·2	13·1
6	53·5	17·8	13·3
7	56·6	18·9	9·6
8	59·7	19·9	9·35
9	69·2	23·0	10·7

TABLE 4.4

Shear force carried in compression zone

Beam 2

Load Stage	Reaction at support, V kN	Gauge line 710 mm from support V_1 kN
1	0	0
2	36·8	11·5
3	46·8	12·8
4	56·9	13·0
5	66·6	15·25
6	76·7	17·5
7	86·9	19·7
8	89·4	20·8

TABLE 4.5

Shear force carried in compression zone

Beam 3

Load Stage	Reaction at Support, V kN	Gauge line 760 mm from support V_1 kN	Gauge line 860 mm from support V_1 kN	Stirrup load kN
1	0	0	0	0
2	53·6	8·94	8·5	0
3	63·6	7·6	8·1	0
4	73·8	9·0	8·3	0
5	83·8	11·5	10·6	20
6	93·8	13·0	11·4	40
7	103·8	-	13·0	60

TABLE 4.6

Shear force carried in compression zone

Beam 4

Load Stage	Reaction at support, V kN	Gauge line 1270 mm from support V_1 kN
1	0	0
2	36·9	6·8
3	46·8	8·6
4	56·8	10·8
5	66·8	13·1

TABLE 4.7

Shear force carried in compression zone

Beam 5

Load Stage	Reaction at support V kN	Gauge line 510 mm from support V_1 kN	Gauge line 610 mm from support V_1 kN
1	0	0	0
2	-	-	-
3	51·6	19·8	18·2
4	56·8	20·9	20·4
5	61·6	22·7	20·8
6	66·6	26·0	19·2
7	71·6	29·0	21·4
8	76·6	28·8	20·2

TABLE 4.8

Shear force carried in compression zone

Beam 6

Load Stage	Reaction at support V kN	Gauge line 813 mm from support V_1 kN	Gauge line 915 mm from support V_1 kN	Gauge line 1020 mm from support V_1 kN
1	0	0	0	0
2	36·8	10·1	9·6	8·0
3	46·6	11·7	10·4	9·7
4	56·8	15·3	11·3	11·8
5	61·6	15·4	11·9	13·7
6	71·6	18·3	13·3	15·0

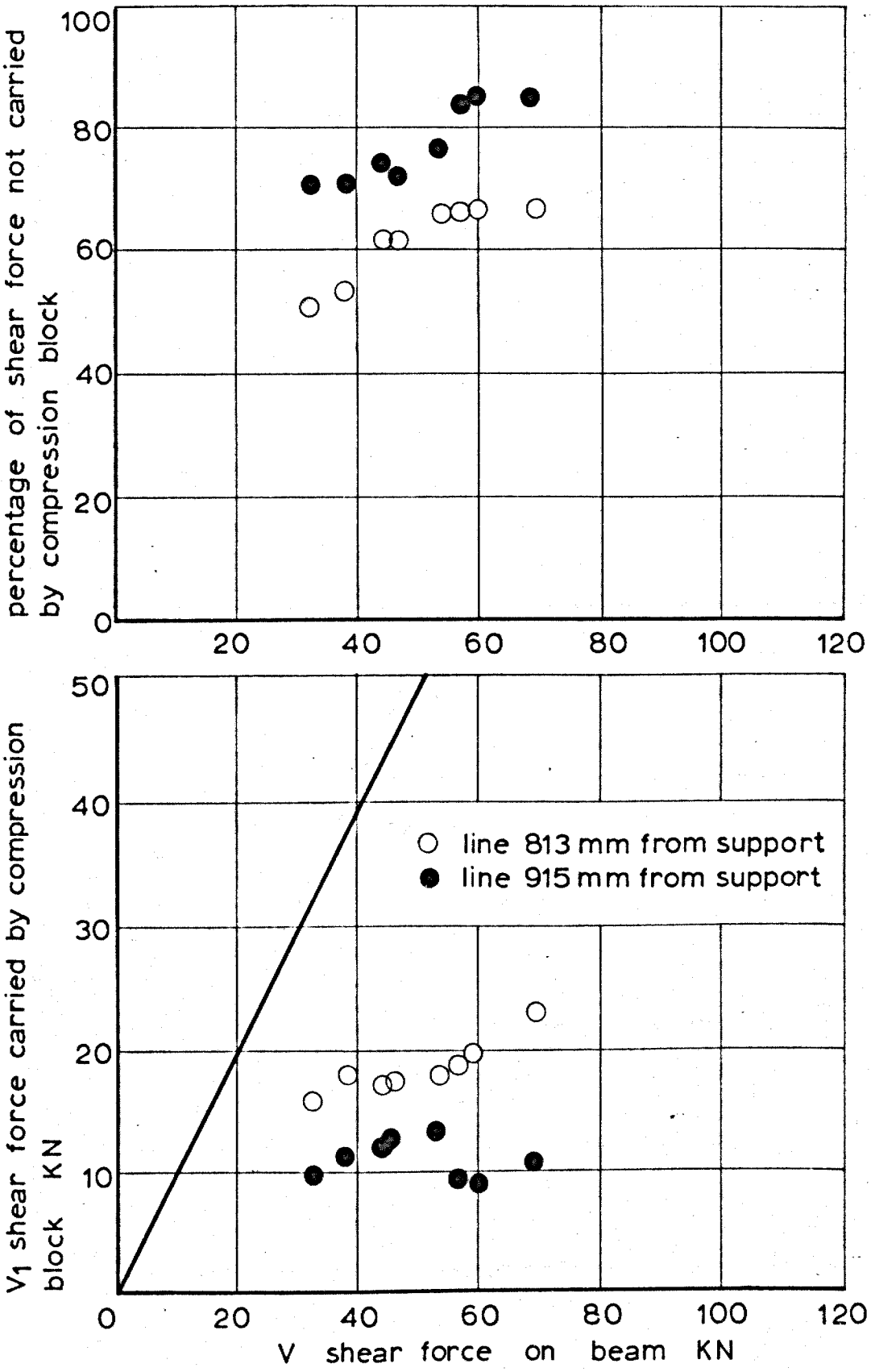

FIG 4.12 TEST RESULTS — BEAM I

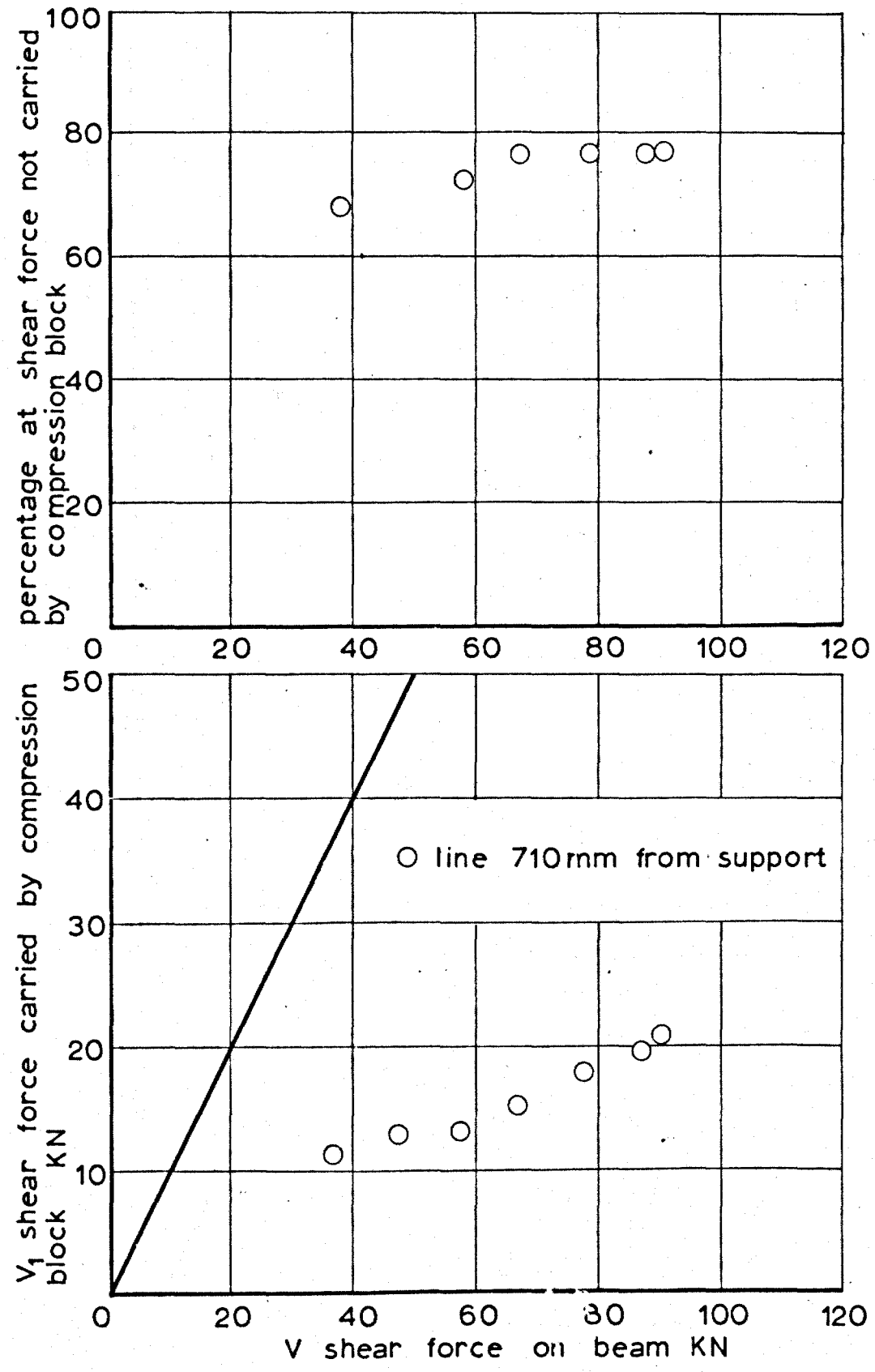

FIG 4.13 TEST RESULTS BEAM 2

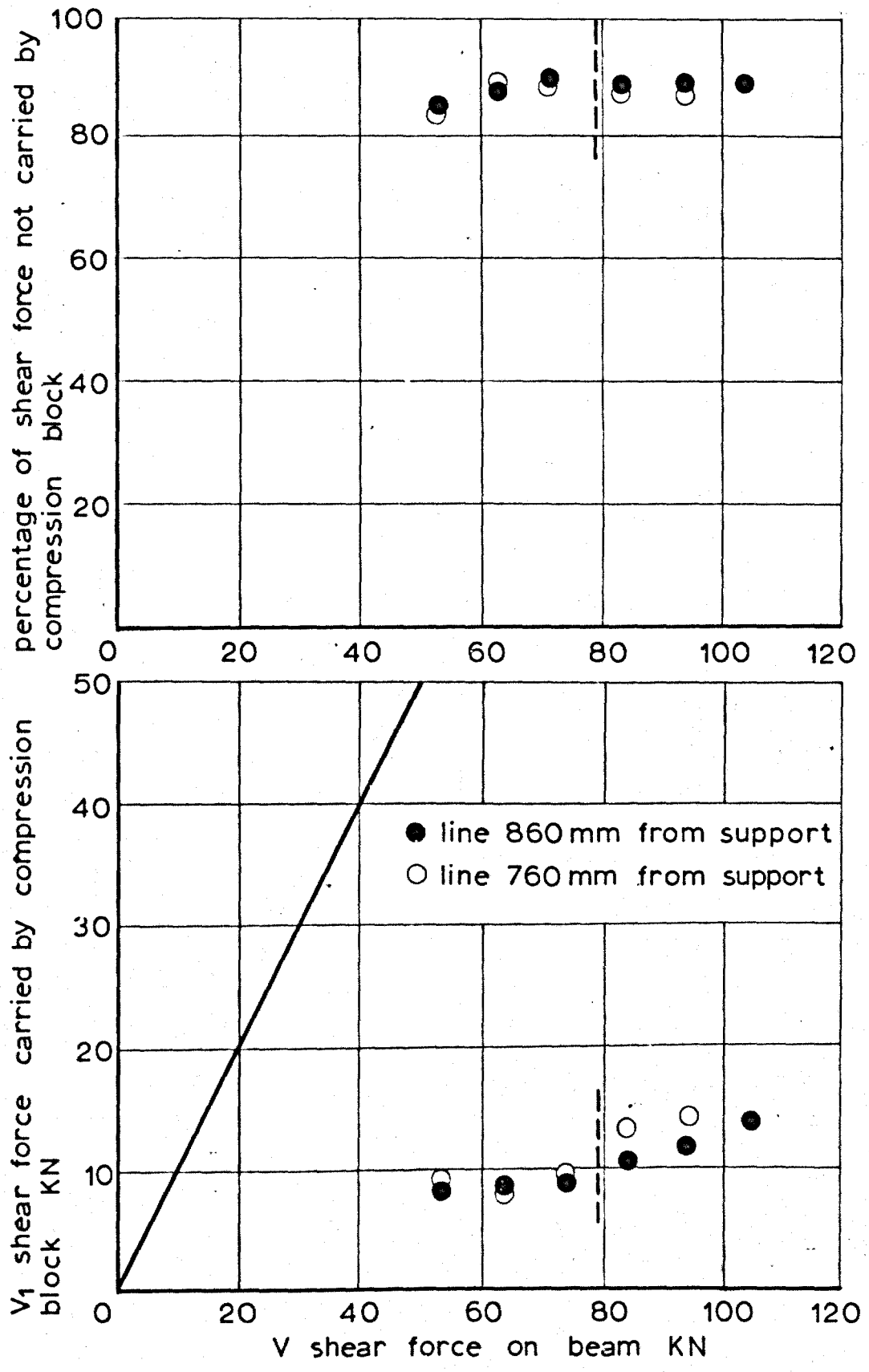

FIG. 4.14 TEST RESULTS BEAM 3

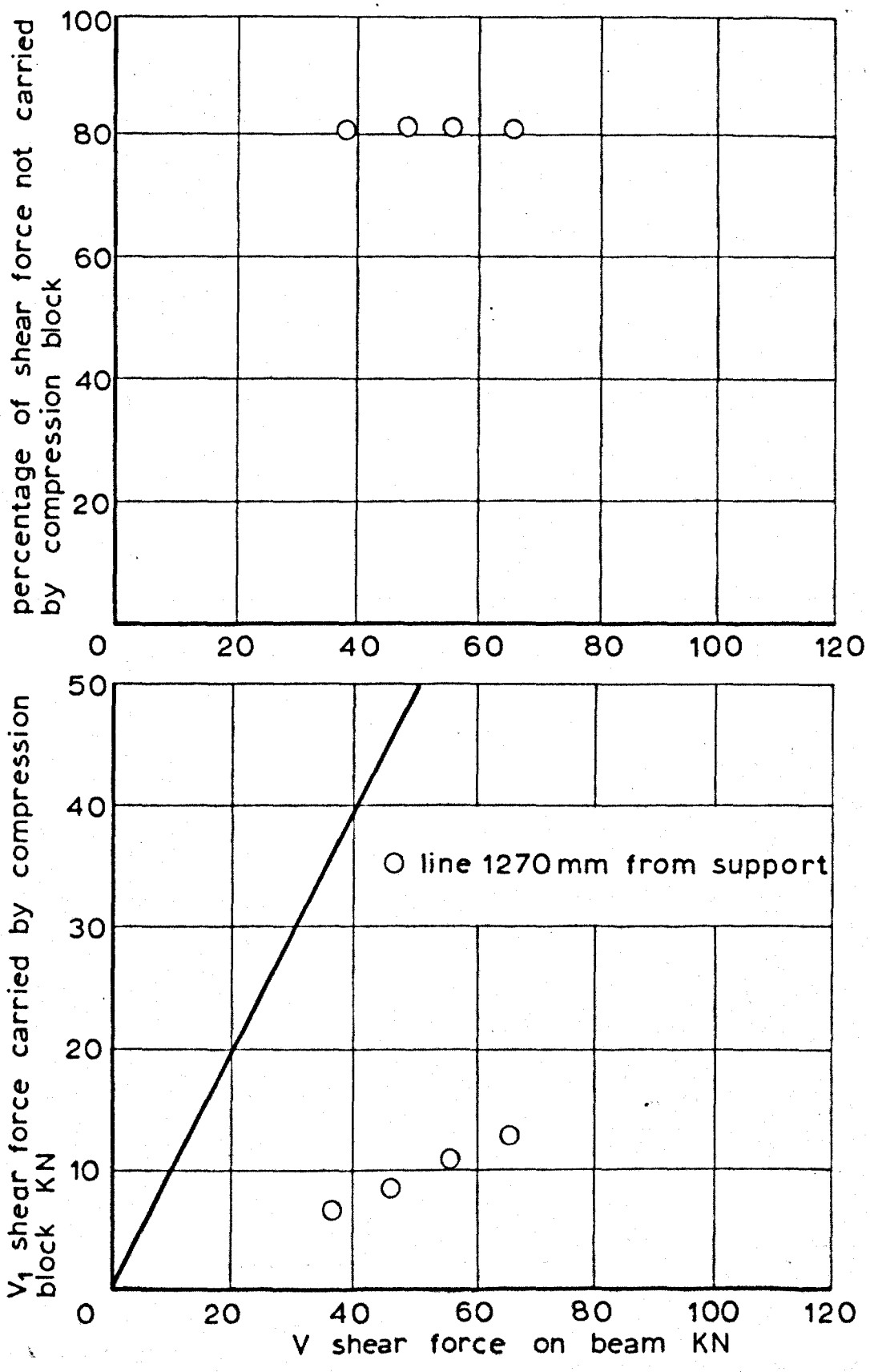

FIG. 4.15 TEST RESULTS BEAM 4

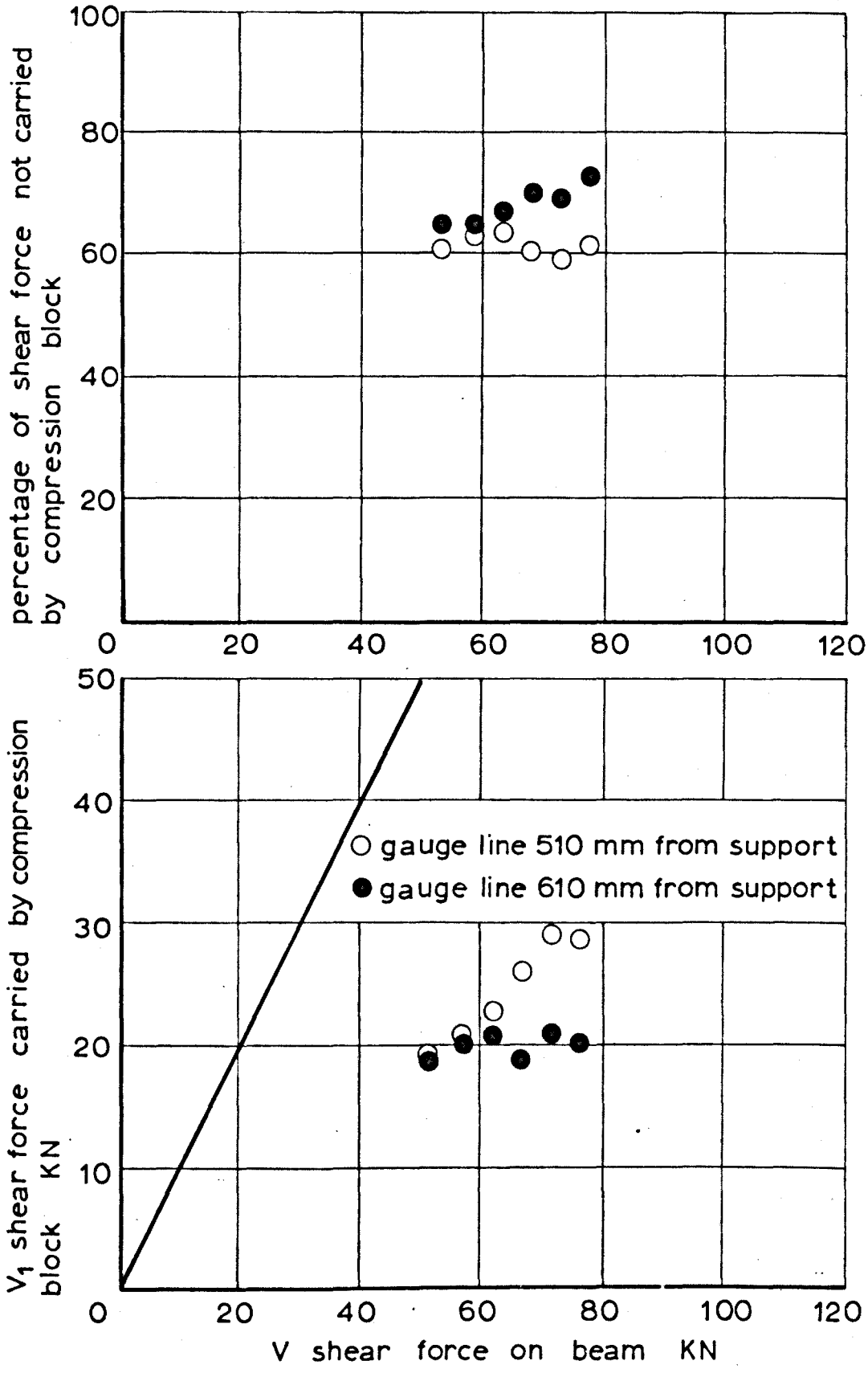

FIG. 4.16 TEST RESULTS BEAM 5

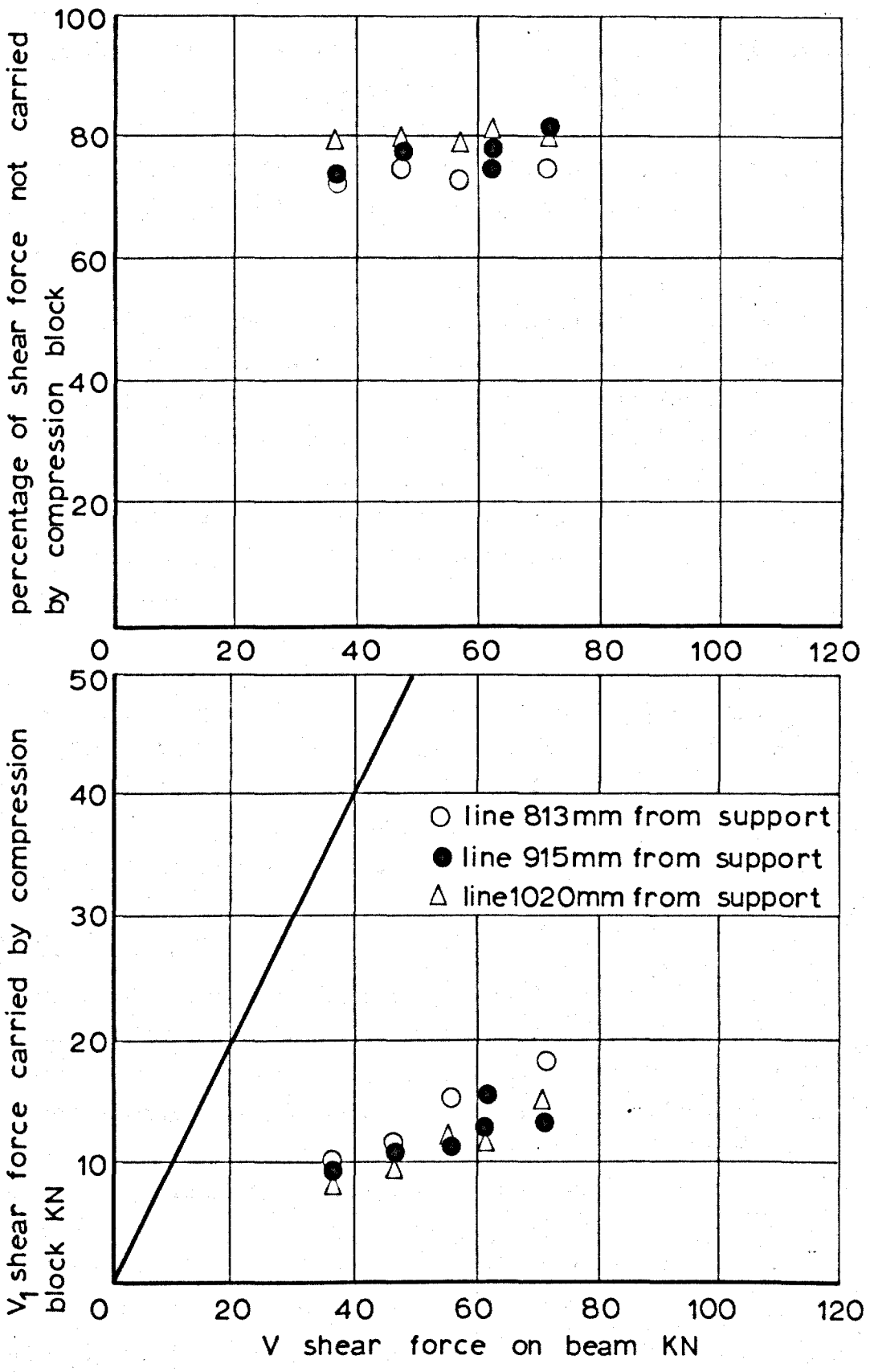

FIG. 4.17 TEST RESULTS BEAM 6

TEST PROGRAMME SERIES II

As the results of the Series I tests were favourable, it was decided to carry out more tests in which the compression zone was instrumented for strain measurement and this time to measure displacements across the cracks in the beams so that eventually the forces due to dowel action and aggregate interlock could be estimated.

The original strain measurements in Series I were taken with a 50 mm demec gauge and as such a large number of strain measurements had to be taken it was decided to use a data logger for the measurement and to use electrical resistance gauges in the Series II tests. As 9·5 mm maximum sized aggregate was used in the mix, the minimum sized strain gauge that was likely to give satisfactory results was 25 mm, the minimum being at least twice the maximum aggregate size.

The data logging equipment was capable of reading 100 strain gauges in one run and two of the beams had nearly this number of gauges in a block on the compression zone so that the computational method could be studied and compared with the ideal method of measuring the rate of change of longitudinal strain in the beams with the shear force on the beam held constant.

DETAILS OF TEST SPECIMENS

A total of six tests was carried out, one on each end of three beams. Two of these tests were exploratory and are not reported in detail. The other four tests, 7, 8, 9 and 10, are reported here. The exploratory tests, labelled 9A and 10A, were made with the same shear span as was used for tests 9 and 10. The numbering system therefore continues from tests 1 to 6 in Series I.

Two beams without pre-formed cracks, for tests 7, 8, 9 and 9A were cast at the same time; a third beam with pre-formed cracks, for tests 10 and 10A, was cast later.

All the beams were cast in wooden moulds, the mix design and beam layout was the same as in Series I. After casting, they were

cured for two weeks under damp sacking before being taken to the laboratory and were then allowed to dry out for one month before the strain gauges were installed. Details of the test beam are given in Table 4.9.

TABLE 4.9
Details of tests 7 - 10

Beam	Shear span, a (mm)	a/d_1	Steel (%)	150 mm cube strength (N/mm^2)	300 x 150 mm cylinder strength (N/mm^2)
7	860	2·32	1·03	57·5	46
8	1170	3·16	1·03	57·5	46
9	1470	3·99	1·03	60	52
10†	1470	3·99	1·03	49·5	43·5
9A*	1470	3·99	1·03	60	52
10A*†	1470	3·99	1·03	49·5	43·5

* Exploratory beam

† Beam with pre-formed cracks

The beams were marked out with a grid of approximately 50 mm (2 in.) between load and support. This enabled the positions of strain gauges and cracks marked on the beams to be plotted from photographs taken during the tests. The surfaces of the beams were gently rubbed down and any small blow holes that occurred in areas where gauges were to be applied were filled with strain-gauge cement. The first gauge down the beam was then fixed 12·5 mm from the compressive face and subsequent gauges were fixed down the compression zone at 25 mm centres. Small tag strips, separate from the gauges, were stuck on to the beams, one for each gauge, and these were wired to the gauge at one end and to the data logger at the other end. The tag strips added considerably to the robustness of the instrumentation and enabled a considerable number of gauges to be re-used, after the first two tests, as dummy gauges for the later tests. Initially, gauges on beams to be tested later were used as dummies for the first tests. Figure 4.18 shows a set of gauges on one of the beams before the test was started.

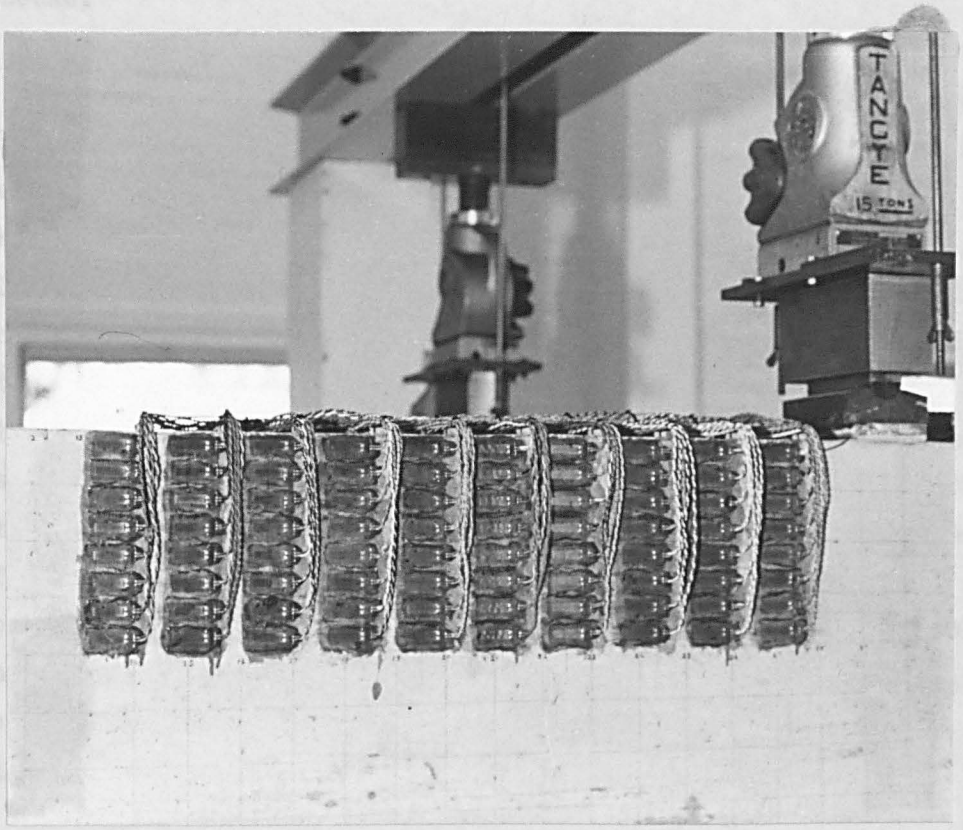

FIG. 4.18 Strain gauges on test beam 9

The layout of the gauges on beam 7 is shown in Figure 4.19. Seven columns of eight gauges were used on one side of the beam and three columns, B', D', and F', were repeated on the back of the beam to provide a check on the results. The gauge layout on beams 8 and 9 is also shown in the Figure. For these tests, ten columns of eight gauges were used, two columns, B' and H', being repeated as checks.

Cracks were pre-formed on beams 10 and 10A by slotting aluminium alloy crack formers, 0·5 mm thick, into the sides of the moulds before casting. Two 30 mm square holes were cut in the crack former through which the tensile steel was threaded. The holes were slightly larger than the steel as it was only intended to destroy interlock action across the crack and not to affect dowel action. It was considered that, by leaving the concrete round the bar in place, the dowel action across the pre-formed crack was as realistic as possible. The layout of the crack formers is shown in Figure 4.19. It was found that these formers became loose on the second load stage of the test and transmitted no interlock forces from then on. Four rows of eight gauges were used on beam 10 and these are also shown in the Figure. As beams 9 and 10 had the same span, a comparison between these tests was expected to give an indication of the significance of interlock forces.

Beam 9A was identical to beam 9 but no instrumentation was used during the test. This test was performed so that the crack pattern could be inspected and a trial run-through of the test method could be carried out before any measurements were taken. Beam 10A was identical to beam 10, with pre-formed cracks but without gauges, and was tested to assess the value of carrying out the test on beam 10 with gauges added.

The test rig was constructed so that two beams could be in position at one time, one due to be tested and one, unloaded, provided dummies for the test. The beams were tested with single point loads and the centre section of the beam provided a shear span for the tests on the two ends; it was therefore heavily reinforced in shear to ensure that it did not crack excessively and could be re-used in the second test.

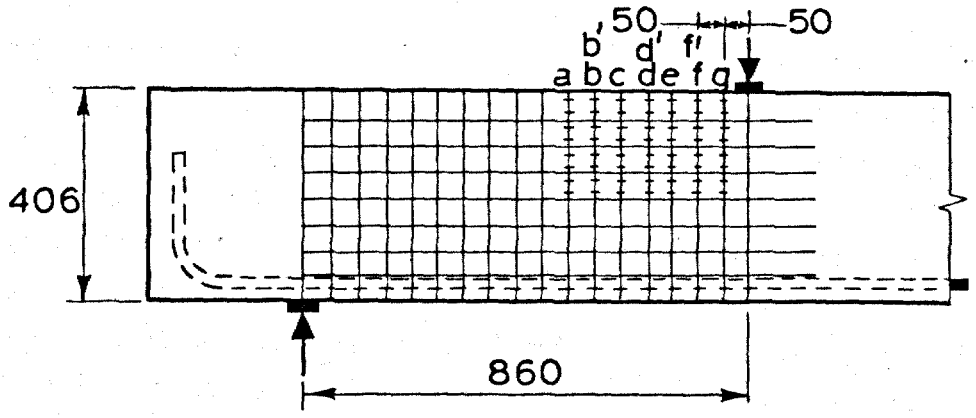

Beam 7 (dimensions in mm) the 50 mm grid is shown

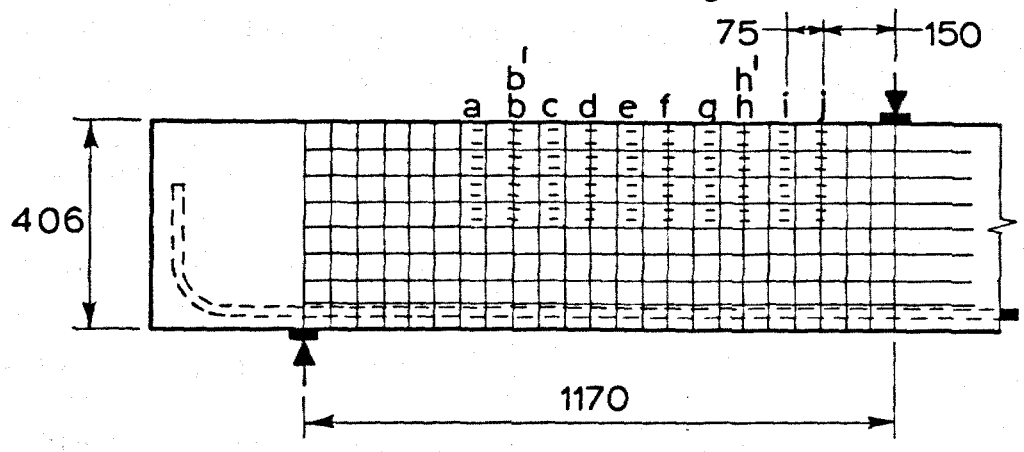

Beam 8

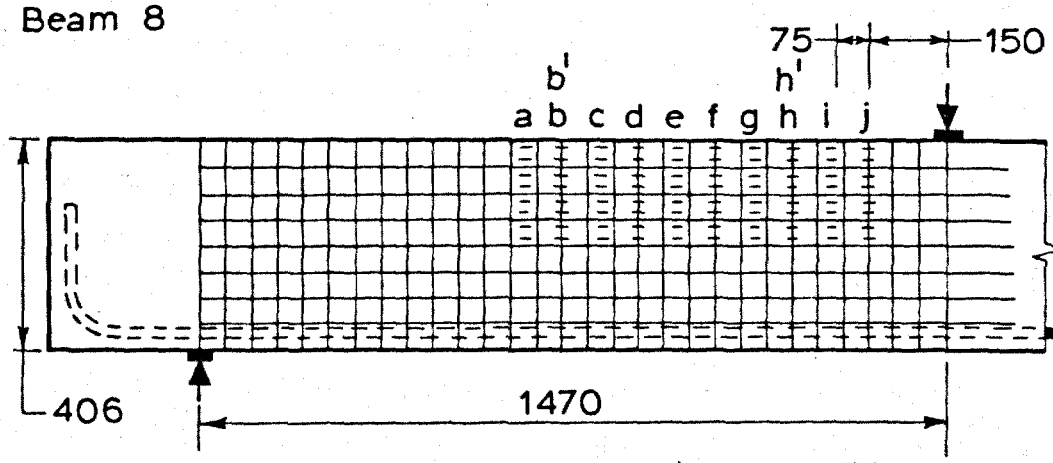

Beam 9

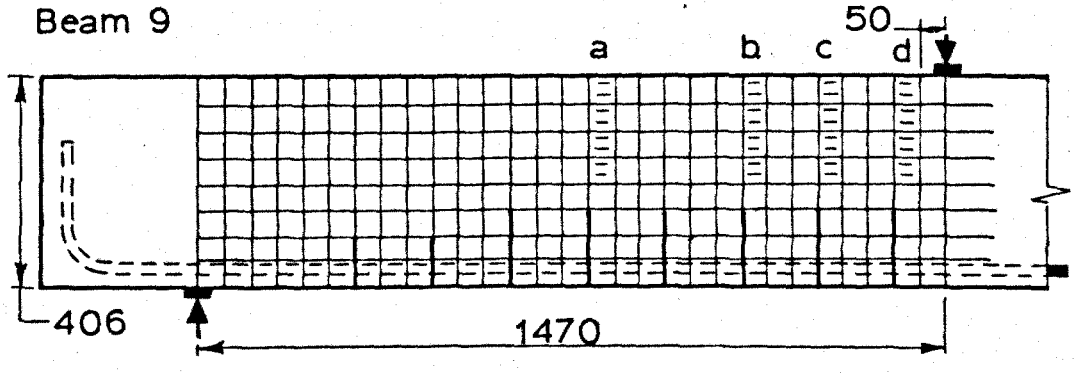

Beam 10 showing crack formers

FIG 4.19 LAYOUT OF TEST BEAMS 7 TO 10

TEST PROCEDURE

The first test to be carried out was that on beam 9A. Ten equal load stages up to failure of the beam, which occurred when the steel yielded, were carried out and the crack pattern was plotted. Trials on delta gauge rosettes, used to measure displacements across the cracks, were also carried out at this stage. The rosettes consisted of three 'Demec' points at the corners of an equilateral triangle of 50 mm side length. The rosettes were put on to the beams across the cracks at a level of 50 mm or 100 mm above the tensile face of the beam as soon as the crack had formed. At each load stage after the points were applied, strains on the three sides of the triangle were measured. This information and the inclination of the sides of the triangle were sufficient to enable the relative movements of the three corners to be computed. The results of these calculations were initially compared with measurements of crack width taken with a crack microscope having a graduated scale, and agreement was found.

The test procedure that was finally used at each load stage for the instrumented beams was as follows. First, the electrical resistance gauges were read by the logger, and then the tape was immediately printed so that all the strain readings could be checked. The first channel on the data logger contained an internal reference resistance enabling a rapid check on the correct functioning of the logger to be made.

A series of 'Demec' measurements was then taken using the 200 mm 'Demec' gauge on two lines of gauges on the beam, near to the compressive and tensile faces of the beam. These gauge readings were then used as a further check on the electrical resistance readings.

The cracks were then plotted and marked in and crack width measurements were taken on all the cracks at each of the 50 mm spaced grid lines on the beam.

Finally the 50 mm 'Demec' gauge rosettes were measured and further rosettes were stuck on if existing cracks had extended or new cracks had formed. The time taken for each load stage was

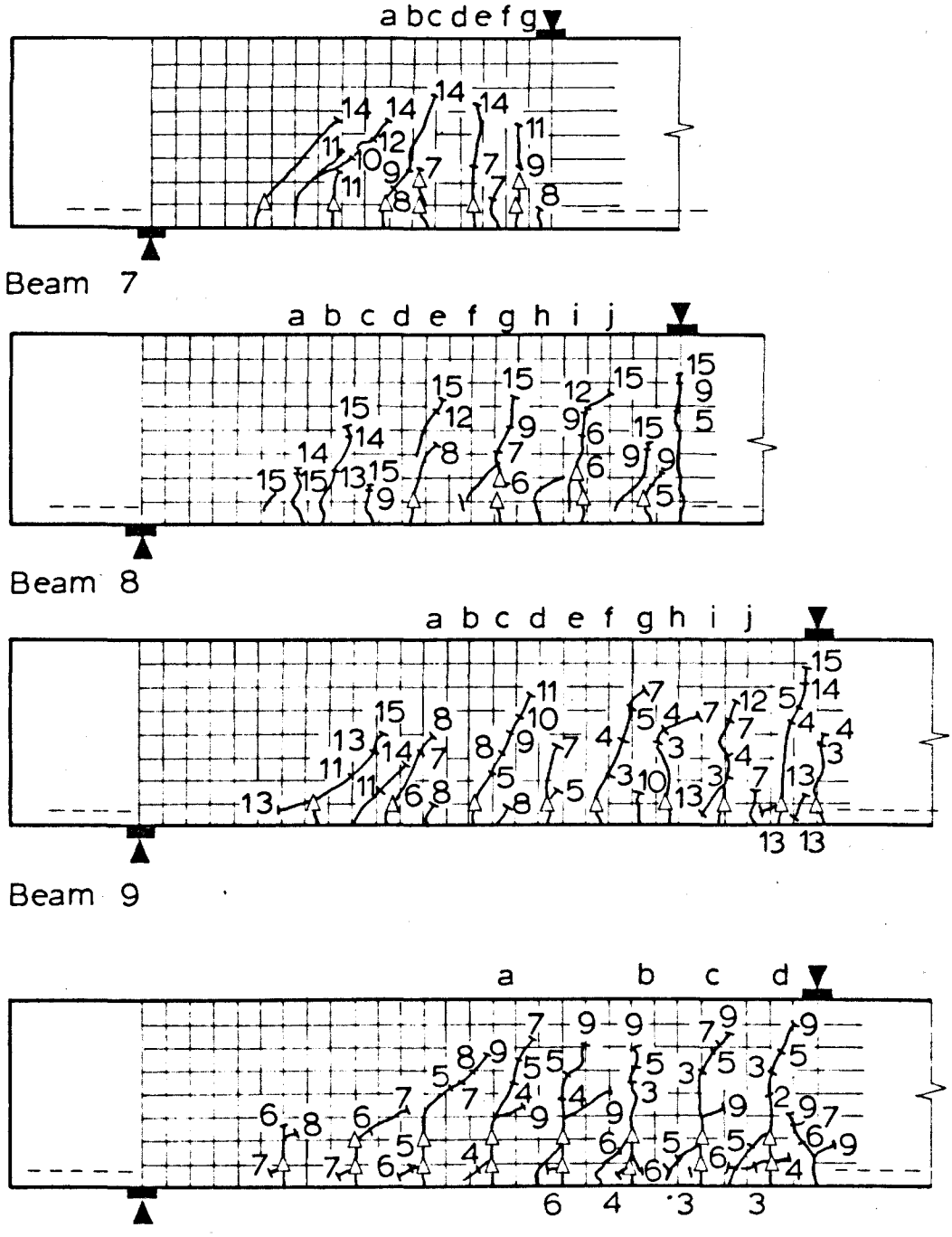

crack pattern and rosette layout. Numbers denote the load stage reached

FIG. 4.20 CRACK PATTERNS BEAMS 7 - 10

approximately one hour and, for a complete test, two or three days. Figure 4.20 shows the crack patterns and rosette positions on the beams after the test.

TEST RESULTS

The computational method already described involved the solution of the equation

$$\tau_{xy} = \int_0^y \frac{\partial \sigma_x}{\partial x} \qquad 4.1$$

This may ideally be carried out in one way, by holding the force on the beam constant and measuring the longitudinal strain in the beam at varying distances from the support point. Thus the rate of change of strain and therefore stress with distance along the beam may be found.

This was not attempted in the Series I tests as a very large number of strains would have to be measured in order to carry out the calculations and a 50 mm demec gauge is not ideal for measuring strains for this purpose.

The simple moment transform

$$\tau_{xy} = \int_0^y \frac{\partial \sigma_x}{\partial M} \frac{\partial M}{\partial x} \qquad 4.2$$

was therefore used. This implies that the rate of change of strain at any point in the compression zone with increasing moment, holding x constant and varying the load is similar to the rate of change of strain with moment, holding the load constant and varying x. This is not rigorous as the strain in the beam is a function of other effects, the main one being the neutral axis depth, as well as the load distance from the support.

In the latter case for example

$$\epsilon_x = f(M\, d_n) \qquad 4.6$$

$$\frac{\partial \epsilon_x}{\partial x} = \frac{\partial f}{\partial M} \frac{\partial M}{\partial x} + \frac{\partial f}{\partial d_n} \frac{\partial d_n}{\partial x}$$

As electrical resistance gauges were used in the Series II tests and two regular grids of gauges were used in the tests carried out on beams 8 & 9 it was possible to study the strains that were measured, see what perturbations were observed and whether significant changes of strain could be found near to the head of cracks. If the neutral axis depth is a significant variable in equation 4.6 the strains in the compression zone should increase considerably as a crack tip is approached from the support side and then decrease away from it.

Figure 4.21 shows a plot of the measured strains taken during the test on beam 9, load stage 11. Strains were measured on the beam on an orthogonal grid, at ten positions along the beam, 50 mm apart, lettered A to J, and at eight levels down the beam, 25 mm apart. The layout of the grid is illustrated in Figure 4.19 and the gauges in Figure 4.18. In Figure 4.21 the strains are plotted as ordinates vertically above the grid, which is drawn obliquely. The upper surface is therefore a surface of longitudinal strain on the beam and the slope of this surface in the x direction is a function of the shear stress. The positions of the cracks that were present at this load stage are marked. If the local changes in the surface are due to the cracks, the calculations will be in error. At first sight it appears that there are two hollows in this surface, one 100 mm before the crack at line D and one 100 mm before the crack at line J. The highest point along the surface is between lines D and G. These local changes are changes in strain and not necessarily in stress. If the material properties change from place to place, a steadily increasing stress will give local changes in strain. Two other observations support the fact that the local changes in strain in Figure 4.21 are a function of the material and not of the cracks.

Figure 4.22 shows a second plot of strains measured in the test on beam 9, this time for load stage 2, before the cracks had formed. The scale of this Figure is five times that of Figure 4.21 so that local variations in level can be compared. The general shape of the surface is similar to that of Figure 4.21, showing that the local variations were not caused by the cracks but, possibly, by material

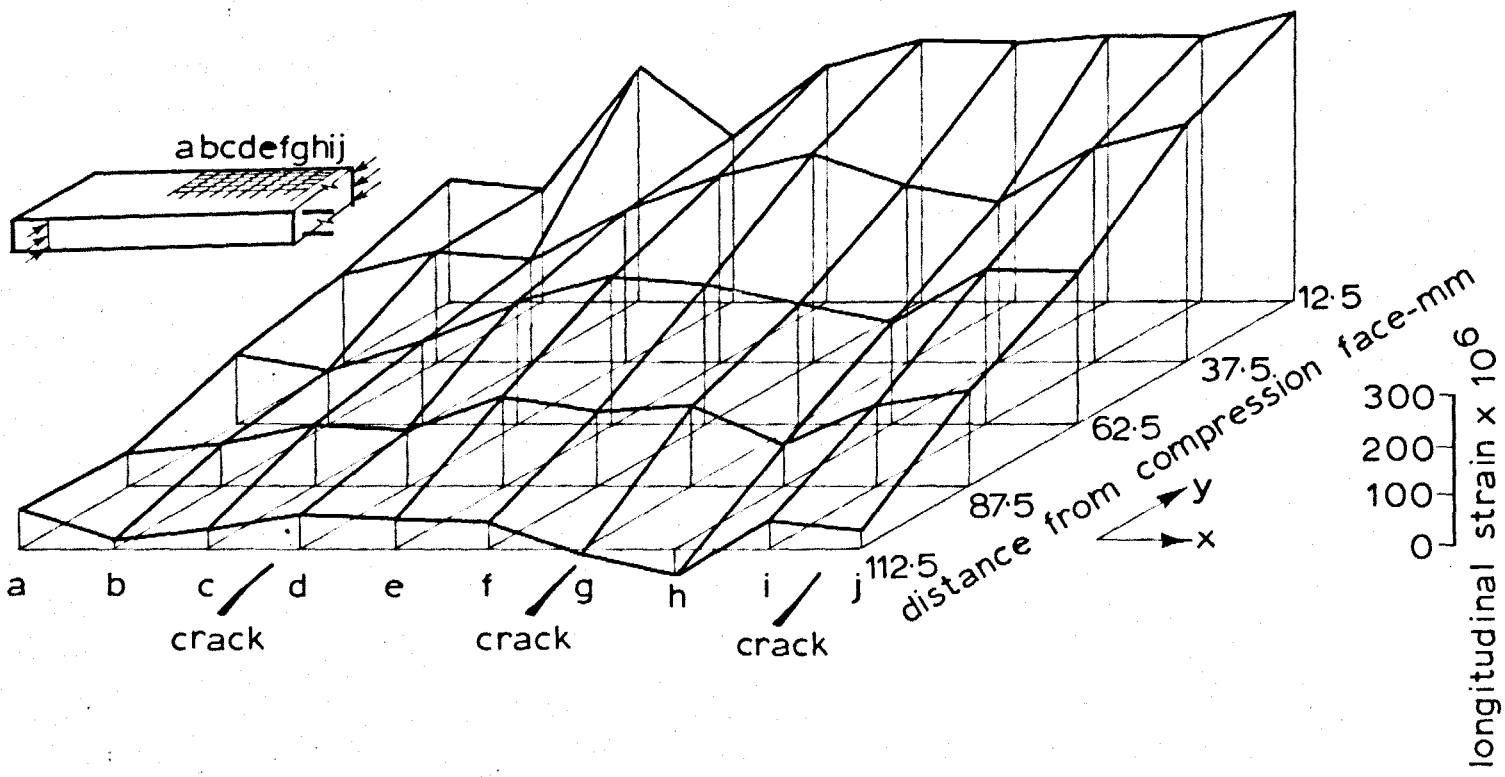

FIG 4.21 MEASURED STRAINS ON BEAM 9 AT LOAD STAGE 11

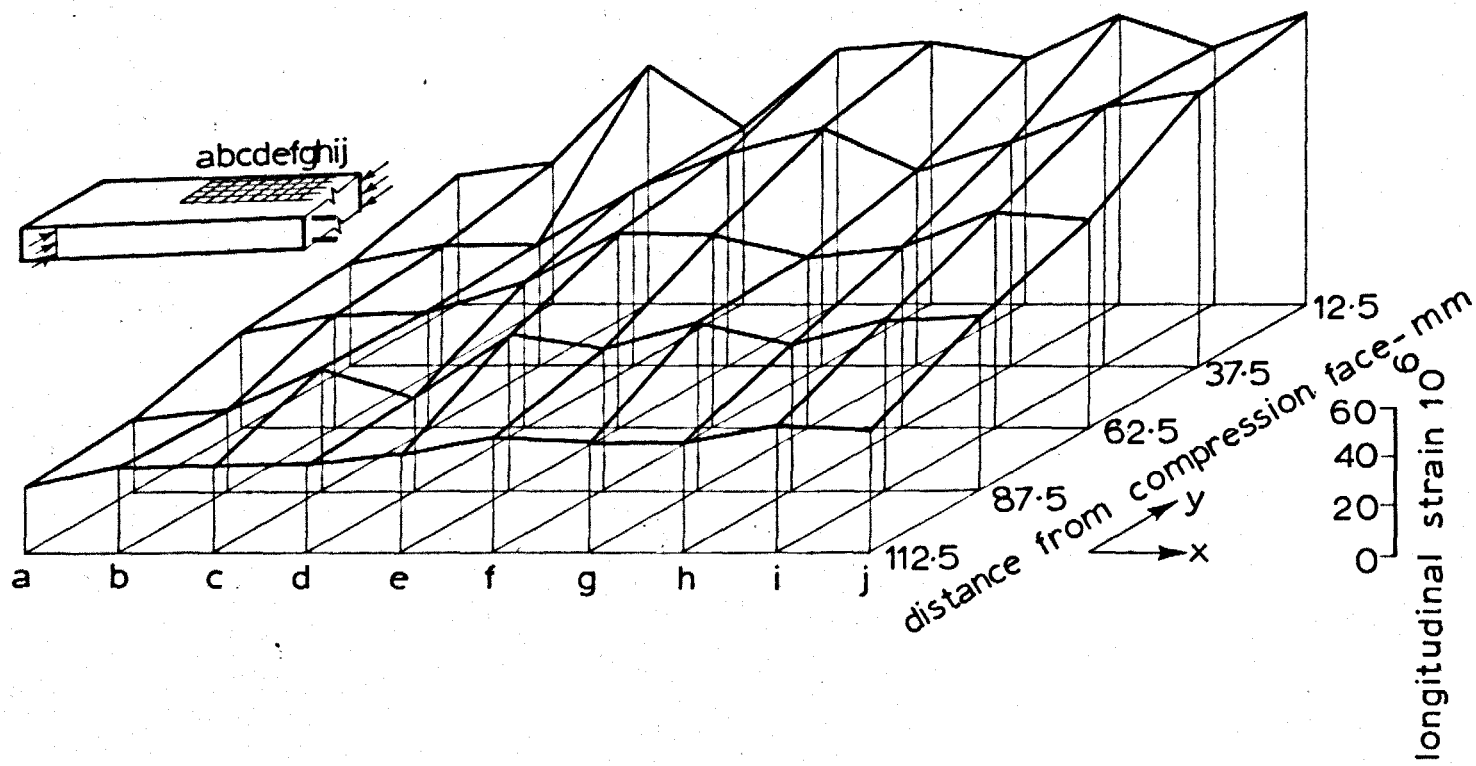

FIG. 4.22 MEASURED STRAINS ON BEAM 9 AT LOAD STAGE 2

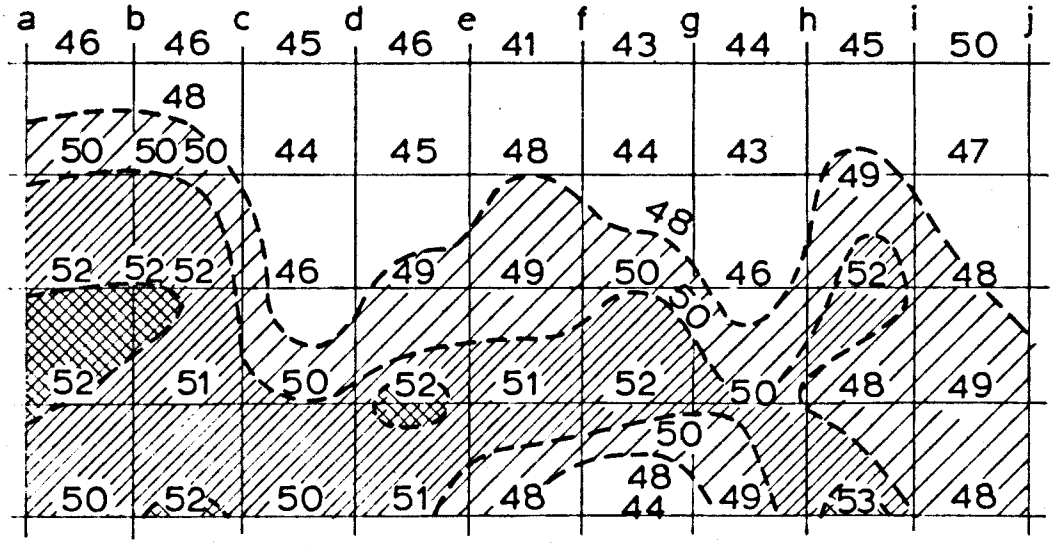

FIG. 4.23 RESULTS OF SCHMIDT HAMMER TESTS ON BEAM 9

variation in the concrete. It is possible, though, that the cracks form in areas of weak concrete, or areas of high strain, during the tests and that the cracks are features of the hollows in the surface and not the converse.

A survey of the area covered by this grid was carried out, using a Schmidt hammer, to test whether the material was stronger in the areas where there are hollows in the surfaces. The results of this survey, with contours of equal hammer scaling, are shown in Figure 4.23. It was not possible to carry out more tests on this beam since the beam, with its gauges left intact, was saved for use as a dummy block in later tests, but Figure 4.23 gives an indication of the material variations that can occur. The accuracy of the hammer at this strength level is $\pm$ 5 divisions. This leads to the conclusion that the shear stress in the compression zone of a beam does not vary significantly between and over cracks and the computational method is likely to give good results.

A similar result is found when the strain readings taken on beam 8 are studied. Figure 4.25 shows the strains taken on beam 8, load stage 4, before the cracks had formed and Figure 4.24 shows the strains on the same area of the beam at load stage 18, the penultimate load stage of the test. In this case, the surfaces are also of similar shape to each other and the cracks that formed between load stages 4 and 18 appear to have little local effect on the strains.

These measurements still do not show that there are no high local changes of strain close to the head of cracks and therefore that no local high shear stresses are produced although large changes in strain appear to be unlikely. The state of stress on the area of concrete between the heads of cracks, the roots of the 'concrete teeth' will be studied further later in this Thesis.

A record of the load stages taken in the tests with shear force at each load stage is shown in Table 4.10. The complete set of compression zone forces calculated by the method used with the Series I test results is shown in Tables 4.11 to 4.14.

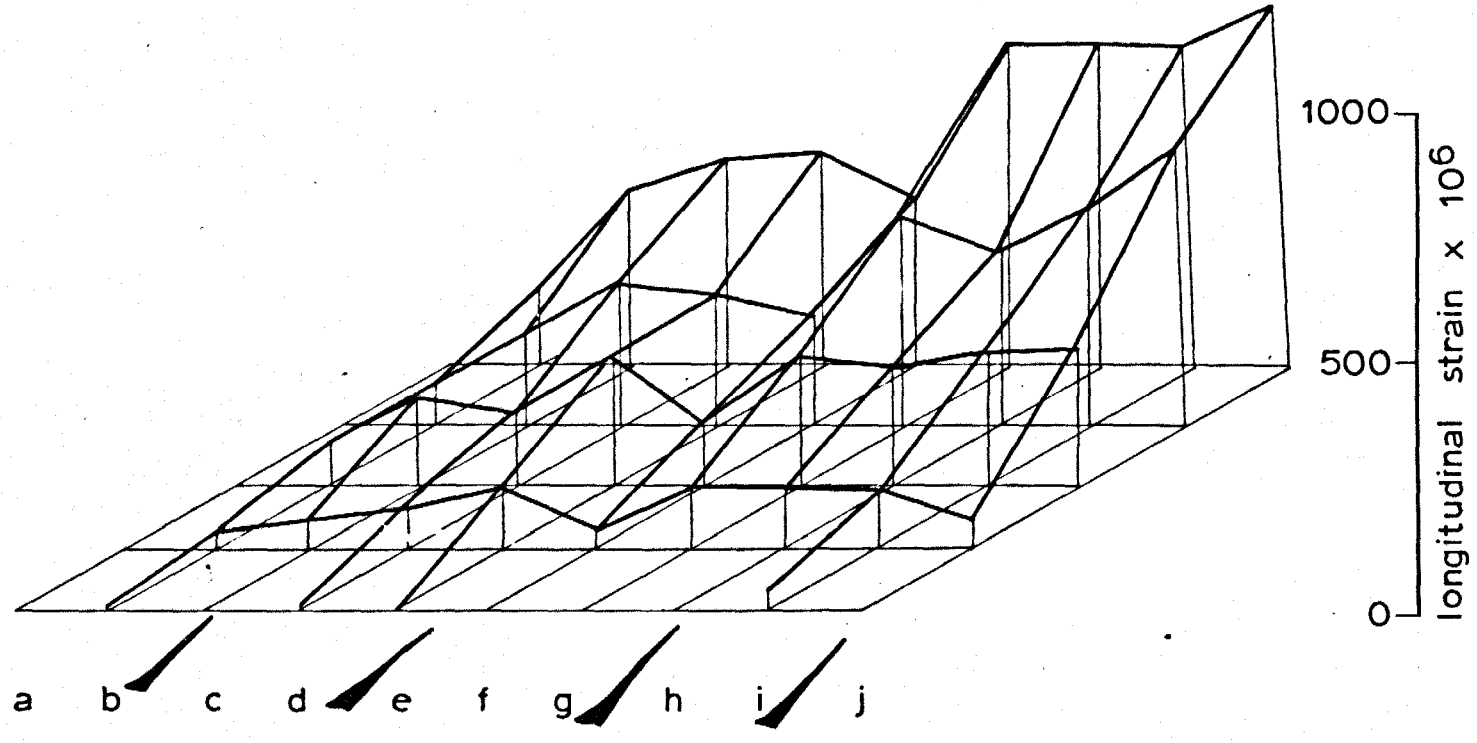

FIG. 4. 24 MEASURED STRAINS ON BEAM 8 AT LOAD STAGE 18

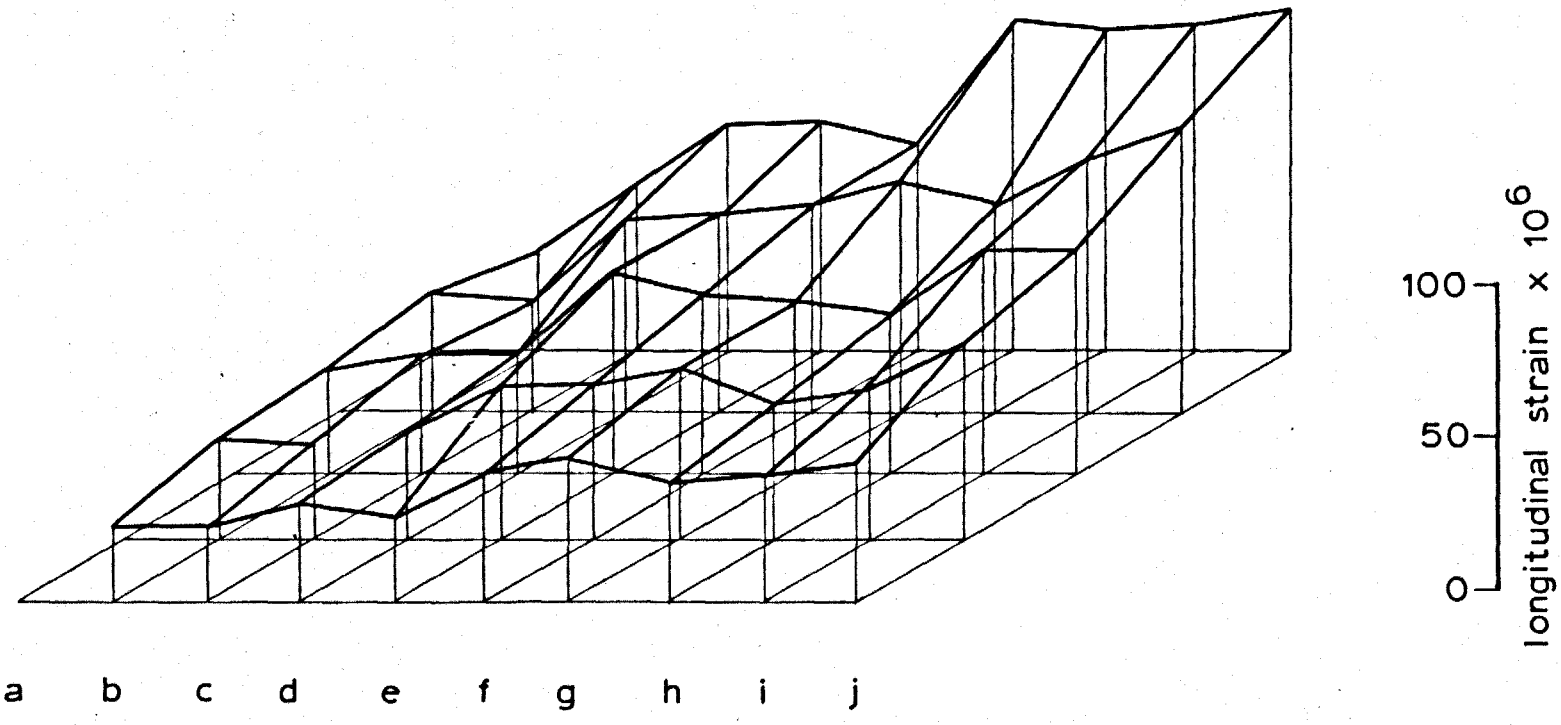

FIG. 4.25 MEASURED STRAINS ON BEAM 8 AT LOAD STAGE 4

In the case of beam 7, the calculations only go as far as load stage 8 as trouble was experienced with the data logger at this stage and the remaining results had to be discarded. It was eventually discovered that the logger was not capable of giving satisfactory results if one of the gauges was broken during the test. If a crack formed through a gauge, the gauge would break causing it to change the load on the rest of the gauges in the logger and make these gauges unreliable. This could immediately be spotted during the tests as the reference resistance changed when any gauge was broken. The procedure that was adopted to stop this occurring was to take the broken gauge out of the circuit and replace it by a sound dummy gauge. This would make the reference resistance return to its correct value and allow the test to continue.

The tests on Beams 8 and 9 produce more load stages than could be handled by the computer and the results were therefore computed using two runs of the program. For Beam 8 the runs used load stages 5, 7, 9, 11, 14, 16 & 18 and then 4, 6, 8, 10, 12, 15, 17 & 19. For Beam 9 the load stages were 2, 3, 4, 6, 8, 10, 12 & 14 and then 5, 7, 9, 11, 13 & 14.

As a set of strain gauges was put on Beam 9 in a regular grid it was possible to calculate the shear forces in the beam compression zone from equation 4.1 directly. In this case, the strains from all the gauges at one load stage were taken and $\frac{\partial \epsilon}{\partial x}$ was calculated for each horizontal row of gauges on the beam.

A straight line was fitted to the ϵ_x - x curve so that $\frac{\partial \epsilon_x}{\partial x}$ was constant for each row. The value of $\frac{\partial \epsilon_x}{\partial x}$ was converted to $\frac{\partial \sigma_x}{\partial x}$ by multiplying by the modulus of elasticity of the concrete, $27{\cdot}5 \times 10^3$ N/mm^2 for these tests, and integrated twice down the beam to the neutral axis to find the shear force in the compression zone.

The results of the calculation, for Beam 9 load stage 11 are shown in Table 4.15. These compare reasonably well with the results in Table 4.13 and give a further idea as to the reliability of the computation method.

TABLE 4.10

Shear force on test beams 7 - 10 (kN).

Load Stage	Beam number			
	7	8	9	10
1	0	0	0	0
2	9·0	8·9	22·3	17·8
3	17·7	17·8	30·0	22·1
4	26·7	26·7	40·0	31·0
5	35·5	35·5	44·5	40·0
6	44·4	44·4	49·0	53·5
7	53·2	49·0	53·5	62·0
8	62·7	57·7	57·8	66·6
9	67·4	62·3	62·3	71·0
10	72·0	66·7	66·8	71·0
11	75·6	71·0	71·2	
12	80·0	75·5	75·6	
13	84·5	80·0	80·0	
14	89·0	84·5	84·5	
15	93·2	89·0	89·0	
16		93·2		
17		97·8		
18		100·0		
19		106·8		
failure	99·0	114·0	-	72·5

TABLE 4.11

Shear force carried in compression zone Beam 7

Load Stage	Total shear force, V kN	Gauge line						
		A	B	B^1	C	D	E	F
2	9·0	2·84	2·4	5·9	2·5	3·1	2·0	2·6
3	17·7	6·6	4·3	7·6	6·8	6·8	6·7	6·7
4	26·7	10·3	6·5	14·2	9·3	9·4	9·5	8·2
5	35·4	12·6	7·4	18·0	11·5	11·1	10·4	9·1
6	44·4	15·3	8·2	18·2	12·5	12·7	11·3	10·1
7	53·2	14·5	8·8	21·0	12·9	12·6	11·7	11·0
8	62·7	15·7	8·6	23·2	13·1	13·6	11·7	12·0

TABLE 4.12

Shear force in compression zone Beam 8

Load Stage	Total shear force, V kN	Gauge line											
		A	B	B'	C	D	E	F	G	H	H'	I	J
3	17·8												
4	26·7		10·1	8·6	11·3	9·9	9·2	10·1	10·7	7·9	7·1	7·5	8·1
5	35·5		7·8	8·9	13·1	12·5	11·9	8·0	12·1	9·6	7·5	9·3	9·7
6	44·4		15·5	10·5	16·5	15·4	13·5	13·0	13·3	10·6	9·3	10·5	10·4
7	49·0		10·0	9·2	16·8	16·6	15·0	9·4	15·4	11·1	8·8	11·0	11·5
8	57·7		17·8	11·7	18·6	18·8	16·5	13·8	14·6	12·0	11·0	11·9	11·3
9	62·3		11·0	9·2	17·0	16·6	15·5	9·9	13·9	12·8	9·2	12·1	12·2
10	66·7		14·9	9·4	14·7	15·7	15·1	13·0	14·1	11·5	10·5	12·0	12·0
11	71·0		11·0	9·4	15·8	16·6	15·8	10·2	14·8	12·3	10·0	12·6	12·8
12	75·5		17·5	10·7	16·6	17·0	16·5	16·3	15·8	12·8	11·7	13·7	13·2
14	84·5		11·0	9·7	15·6	16·5	15·8	11·4	15·2	14·0	10·0	14·1	13·5
16	93·2		11·2	10·3	16·8	17·4	17·0	12·4	16·7	13·6	12·3	15·5	14·4
17	97·8		16·6	11·3	16·8	18·1	18·0	17·7	17·8	14·3	12·8	16·5	14·5
18	100·0		11·0	11·4	15·5	17·9	18·3	9·8	18·3	15·0	12·2	16·6	14·9
19	106·8		18·3	13·5	15·2	18·7	19·2	19·2	19·7	15·7	14·4	15·9	15·2

TABLE 4.13

Shear force carried in compression zone Beam 9

Load Stage	Total shear force, V kN	Gauge line											
		A	B	B'	C	D	E	F	G	H	H'	I	J
2	22·3	10·2	11·1	6·8	6·3	8·6	10·5	9·8	8·7	8·1	4·9	9·5	8·4
3	30·0	13·1	14·3	8·9	8·2	11·2	13·1	11·9	10·5	8·9	5·5	9·8	8·7
4	40·0	15·3	16·8	9·9	10·2	12·7	14·5	13·1	11·5	9·9	6·1	11·4	10·6
5	44·5	14·2	14·2	6·3	11·9	9·9	14·5	12·4	10·8	9·8	5·9	11·0	9·5
6	49·0	16·2	16·5	10·5	8·7	16·5	17·0	14·2	12·1	11·2	6·9	12·6	11·9
7	53·5	15·6	15·3	7·7	14·2	16·0	17·8	14·3	12·4	11·7	7·0	13·2	11·6
8	57·8	17·7	18·1	12·1	11·6	17·5	18·8	16·0	14·2	13·0	7·9	14·5	12·8
9	62·3	12·7	17·5	7·9	14·6	18·3	19·9	16·7	14·5	13·7	7·9	15·4	13·6
10	66·8	13·4	18·0	12·5	11·9	20·0	21·8	18·4	16·1	15·0	8·1	16·6	14·5
11	71·2	12·2	15·9	7·7	14·7	17·5	19·9	17·2	15·0	14·8	7·8	16·2	14·3
12	75·6	13·0	17·2	12·1	6·7	18·6	21·8	19·7	16·4	16·2	8·5	17·6	16·6
13	80·0	11·6	16·1	8·2	16·0	18·0	21·6	19·7	16·3	16·5	8·3	18·0	15·4
14	84·5	11·3	15·3	10·4	12·7	18·7	22·8	21·4	17·1	17·6	9·1	19·1	15·9
15	89·0	-	-	-	14·0	17·5	21·9	21·3	16·6	17·4	8·7	18·7	14·8

TABLE 4.14

Shear force carried in compression zone Beam 10

Load Stage	Total shear force, V kN	Gauge line			
		A	B	B^1	C
3	22·1	4·8	5·0	5·4	5·9
4	31·0	6·8	6·1	7·1	7·8
5	40·0	7·6	3·0	6·7	8·7
6	53·5	11·7	10·0	9·8	12·2
7	62·0	12·5	11·0	10·5	13·2
8	66·6	13·9	11·9	11·2	14·1
9	71·0	15·7	12·4	11·7	13·4

TABLE 4.15

Beam 9 Shear force, V_1, in the compression zone
Load Stage 11, calculated by direct method

Line	Shear force kN
A	13·2
B	13·8
C	11·4
D	15·8
E	15·3
F	13·8
G	13·2
H	10·7
I	14·2
J	13·6

The results of the rosette measurements are shown in Figures 4.26 to 4.28. $\triangle_H$ is the horizontal displacement across the crack and $\triangle_V$ is the vertical displacement. Not all the rosette results are reported. The rosettes were put on the beam as soon as the first sign of a flexural crack was observed. In some cases, the cracks did not extend and other flexural cracks were formed later which stopped the first cracks extending. The rosettes on beam 7, 570 mm from the support, are an example of this. In other cases, particularly near the load points, the cracks are not inclined and therefore do not show any shear displacement from the rosette measurements. At the beginning of each line, the load stage at which the displacement was first measured is recorded and the other points on the lines are at the subsequent load stages.

DISCUSSION OF RESULTS SERIES I

Two important questions arise from these results. Firstly, are the forces produced by this analysis reasonable? Do they satisfy the equilibrium equations? Secondly, are the stresses produced by the analysis reasonable? Do they, when compared with a failure criterion, show that the compression zone of the beam is sound before the final diagonal crack forms and that the beam compression zone would fail if the diagonal crack formed at high load stages?

The equilibrium equations are

$$C - T + H_I = 0 \qquad 3.1$$

$$V - V_1 - V_2 - V_3 = 0 \qquad 3.2$$

$$Vh - V_2S - V_3n - H_It - Tl_a = 0 \qquad 3.3$$

The first of these cannot be used as no attempt was made in the tests to measure steel strains. The instrumentation that is required to do this would affect the bond strength of the bars and probably their dowel strength. The second equilibrium equation has already been used, when comparing the work to that done by Krefeld & Thurston, to find the force not carried by the compression zone. The equation that remains, once more adding the effects of the dowel and interlock forces together and ignoring the horizontal interlock force, written in the form

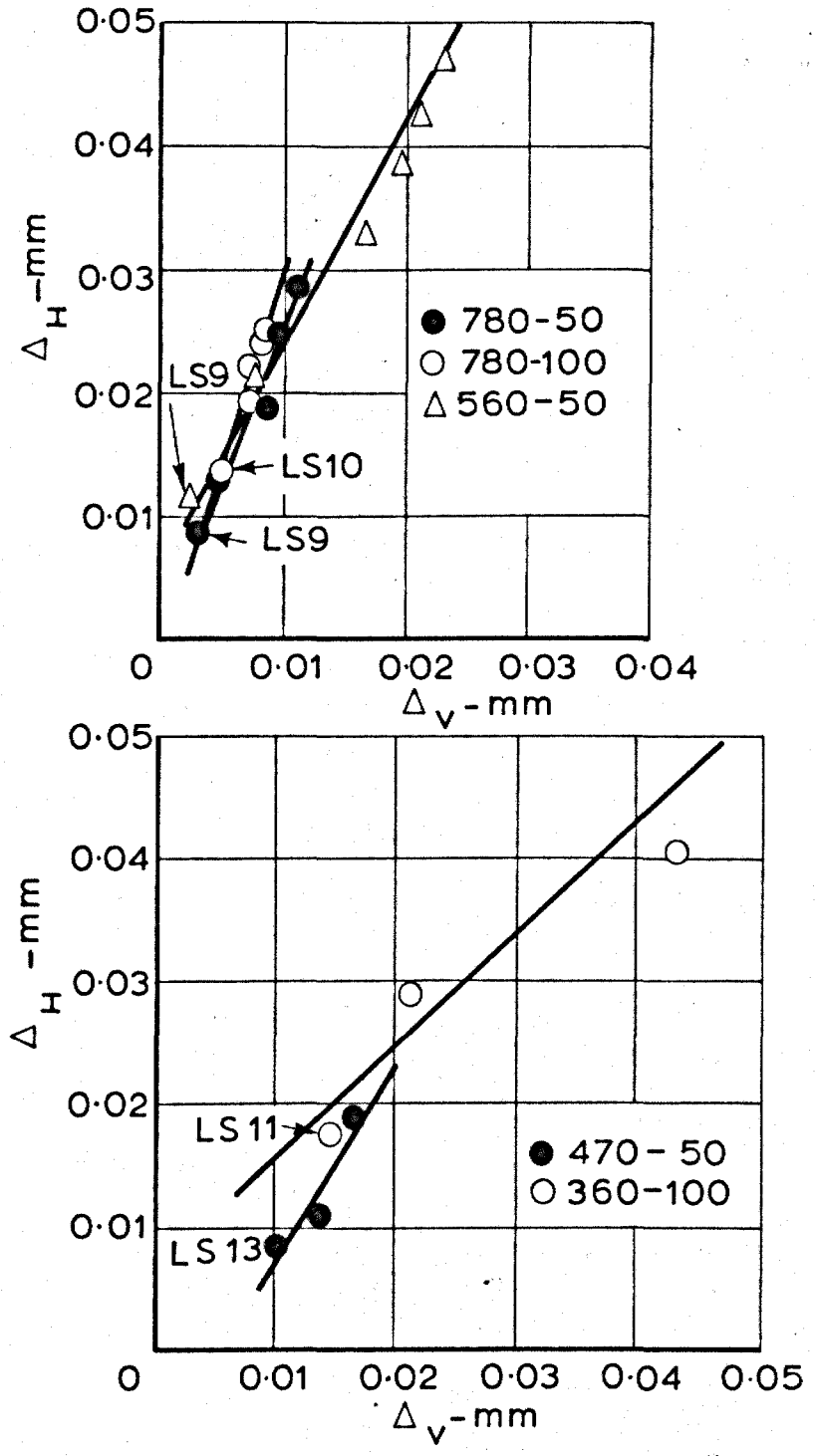

FIG. 4.26 ROSETTE RESULTS FOR BEAM 7

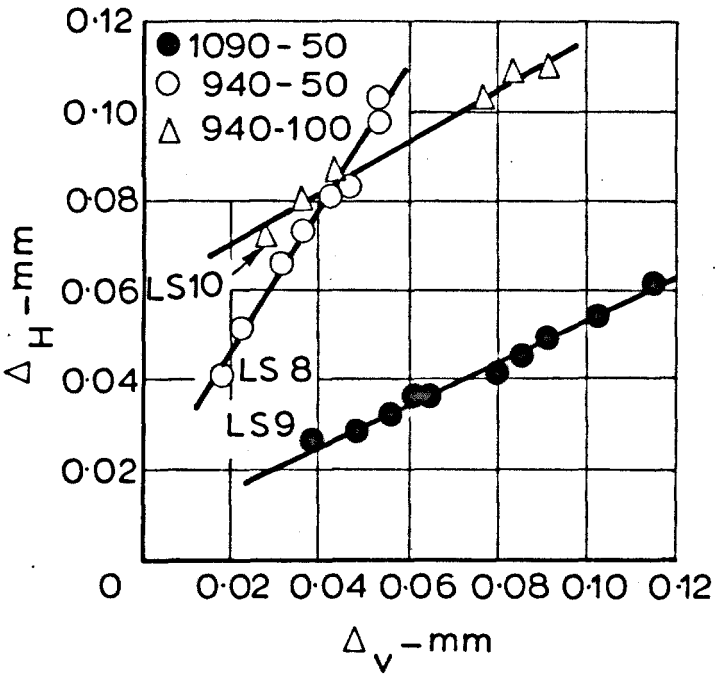

beam 8

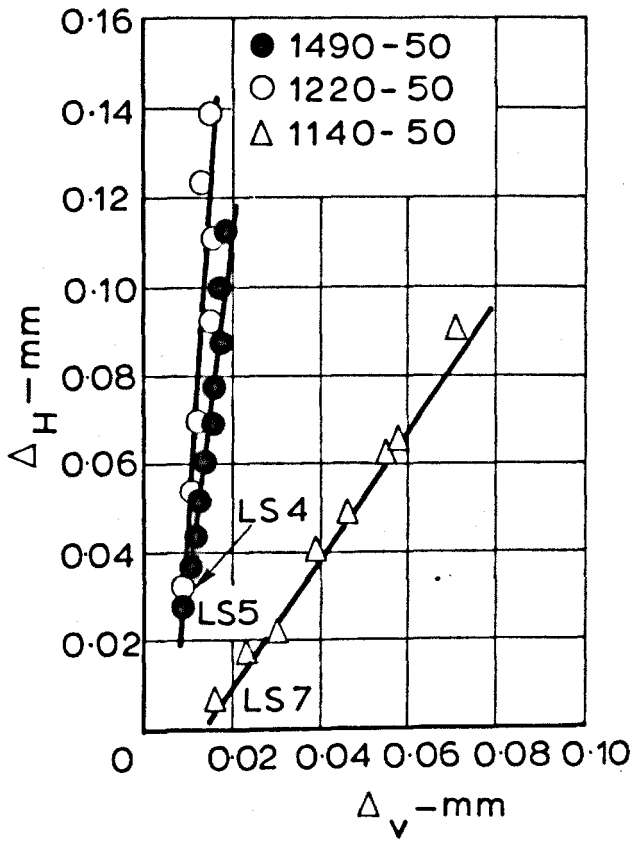

beam 9

FIG. 4.27 ROSETTE RESULTS FOR BEAMS 8 AND 9

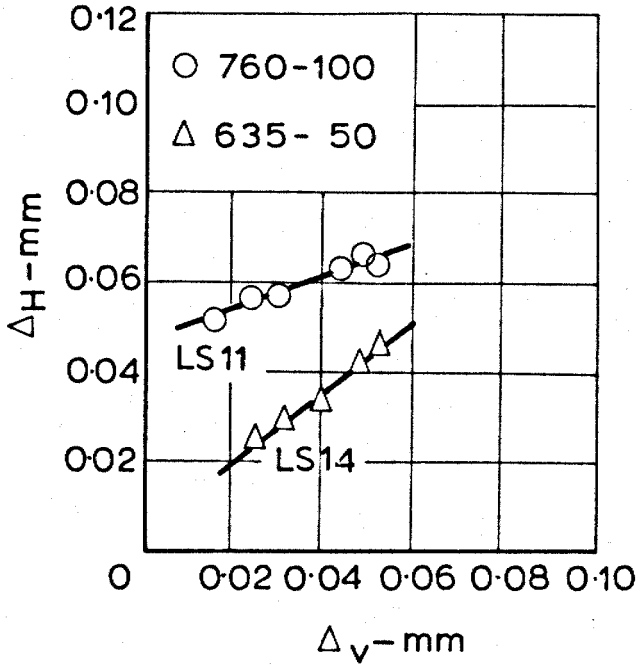

beam 8

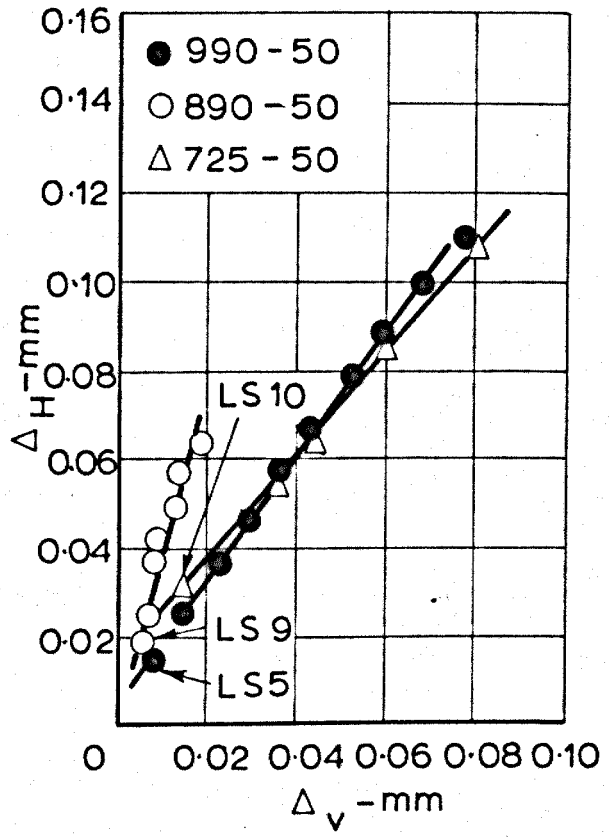

beam 9

FIG. 4.27 ROSETTE RESULTS FOR BEAMS 8 AND 9

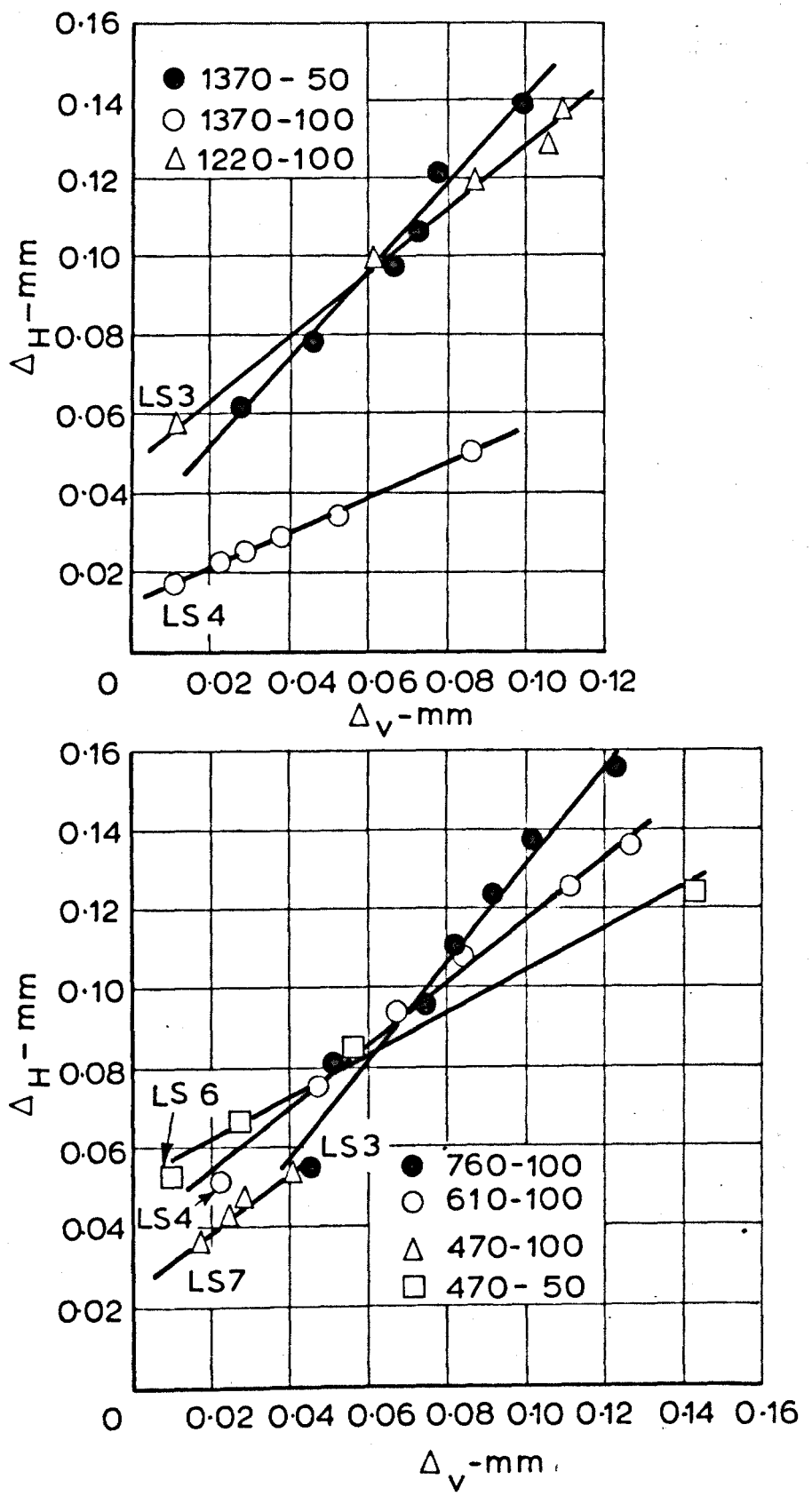

FIG. 4.28 ROSETTE RESULTS FOR BEAM 10

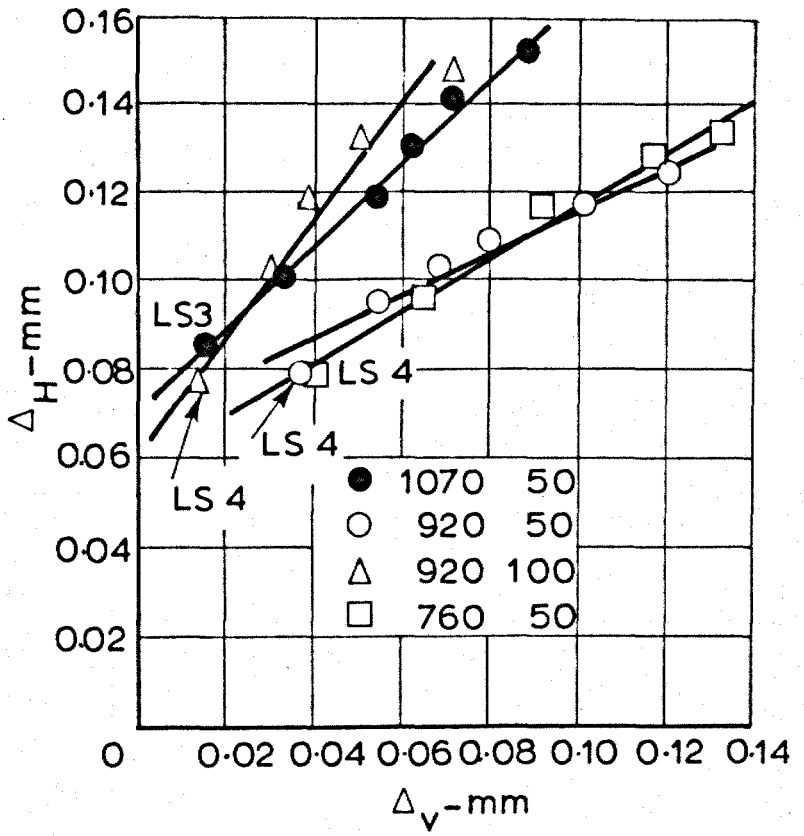

FIG. 4.28 ROSETTE RESULTS FOR BEAM 10

$$Vh = V_2S + Cl_a \qquad 4.7$$

can be used to check the forces that have been measured.

Equation 4.7 was evaluated for all the cases where lines of gauge readings were reported and the result of this analysis is shown in Table 4.16. The calculations for Table 4.16 were carried out on the measurements taken on the last load stage of the test on a beam, as this was the stage of the test nearest to failure. (This is the point where most of the theorists say that the compression zone is carrying most of the shear force.) The moment produced by the compression block about the steel level was evaluated by assuming a triangular strain profile in the compression zone of the beam, the modulus of elasticity for the concrete being measured from cylinder tests. The strain profile was determined by fitting a straight line to the strain readings taken in the tests. A study of the shape of the compression block strain profiles showed that this was a reasonable assumption. The force V_2 was calculated from the vertical equilibrium equation and the distance s was measured from the crack patterns before failure.

TABLE 4.16

Solution of equilibrium equation at final load stage, Beams 1 - 6

Beam and line	Cl_a kNm	V_2S kNm	$Cl_a + V_2S$ kNm	$\frac{Cl_a + V_2S}{Vh}$	$\frac{Cl_a}{Vh}$
1-813	76·6	9·36	86·1	1·52	1·36
1-915	53·6	19·1	73·0	1·15	0·85
2-710	74·0	12·5	86·5	1·33	1·14
3-760	50·5	24·5	75·0	1·05	0·71
3-860	66·6	13·8	80·5	0·90	0·74
4-1270	61·2	5·4	66·6	0·79	0·72
5-510	33·2	3·6	36·8	0·95	0·85
5-610	40·3	5·8	46·0	0·98	0·86
6-813	44·6	8·1	52·6	0·91	0·77
6·915	56·5	14·8	71·4	1·09	0·86
6-1020	55·0	5·8	60·5	0·83	0·75

Equation 4.7 may be re-written in the form

$$\frac{V_2S + Cl_a}{Vh} = 1$$

If the force not carried by the compression zone at the last load stage is held to be negligible (i.e. $V_2 = 0$), then the equation becomes

$$\frac{Cl_a}{Vh} = 1$$

The ratios $\frac{V_2S + Cl_a}{Vh}$ and $\frac{Cl_a}{Vh}$ are given in Table 4.16. The average value of $\frac{V_2S + Cl_a}{Vh}$ is 1·04 and the average value of $\frac{Cl_a}{Vh}$ is 0·87. This indicates that, at the last load stage, the force not carried by the compression zone has to be put into equation 3 in order to satisfy equilibrium conditions.

Beams 3, 4, 5 and 6 gave results which indicate that the forces measured fit the equilibrium equation. The values of internal moment produced by beams 1 and 2 are high because high values of the modulus of elasticity of the concrete from short-term tests were used. Where the modulus was measured at the same rate as the beam was tested, as in the case of the other beams, the equation was satisfied. All the calculations were carried out again, this time with a modulus of 24·8 x 10^3 N/mm^2 and this gave values of $\frac{V_2S + Cl_a}{Vh}$ of 1·37, 1·05 and 1·22 for lines 813 and 915 on beam 1 and line 710 on beam 2 respectively. (Lines are numbered by their distance in mm from the support: i.e. line 813 is 813 mm from the support.) A change in the value of the modulus of elasticity of the concrete has more effect on the calculation of Cl_a than on the calculation of V_2. For example, for beam 1 line 915, a change from 2·3 to 3·2 x 10^3 N/mm^2 increased the value of V_1 by 38% at the last load stage but this was only 4·5% of the total shear on the section and so the effect of a change in the modulus of elasticity of the concrete on the value of the force not carried by the compression zone is very small.

Before a study of the stresses derived from the experimental results can begin, a failure criterion is required. The stress conditions from the test results can then be compared with the failure criterion to see whether they predict failure of the concrete at high load stages.

Failure criterion

The failure criterion used in this chapter was produced by plotting results reported by research workers who have carried out tests to produce a shear-compression interaction diagram on concrete under stress states similar to those in the beam tests.

The test results used for the interaction diagram were those of Bresler & Pister[25] and Reeves[26]. These tests were carried out on thin-walled hollow cylinders which were loaded in compression and torsion. The stress conditions in the cylinder were those of uniform compressive and shear stress. Figure 4.29 shows the results plotted in terms of shear stress and compressive stress at failure divided by the 150 x 300 mm compressive cylinder stress f_c'. In this way, concretes of different strengths may be compared on the same diagram. Two curves are drawn on the diagram which enclose 95% of the test results. For the purpose of this chapter, it is proposed that any concrete with its stresses represented by a point under the lower line is sound. Any concrete between the lines may or may not be sound whilst any concrete with stress conditions above the top line may be said to have failed. This assumption recognizes that there is considerable scatter in the test results from which the diagram was prepared and that the test specimens were under uniform compressive and shear stress whereas, in beam compression zones, both these stresses vary through the section.

The line of gauges that was compared with the failure criterion had to be the most critical one: it should be at the head of a critical crack at the penultimate load stage. The beam would then fail without the crack extending when the load was increased and so the stresses would be from the most critical part of the beam. For this reason, line 915 on beam 6 was chosen (see Figure 4.11). The compressive and shear stress-blocks for load stages 5 and 6 (the

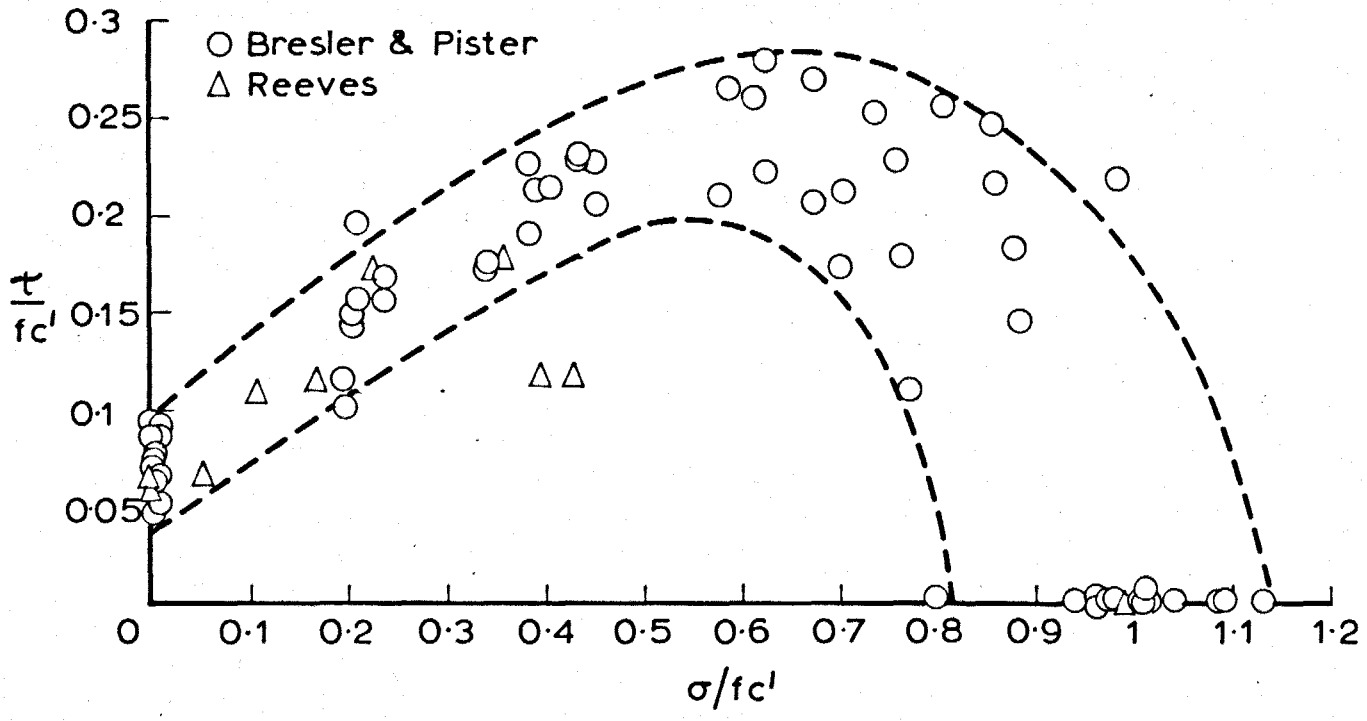

FIG. 4. 29 FAILURE OF CONCRETE UNDER COMPRESSIVE AND SHEAR STRESS

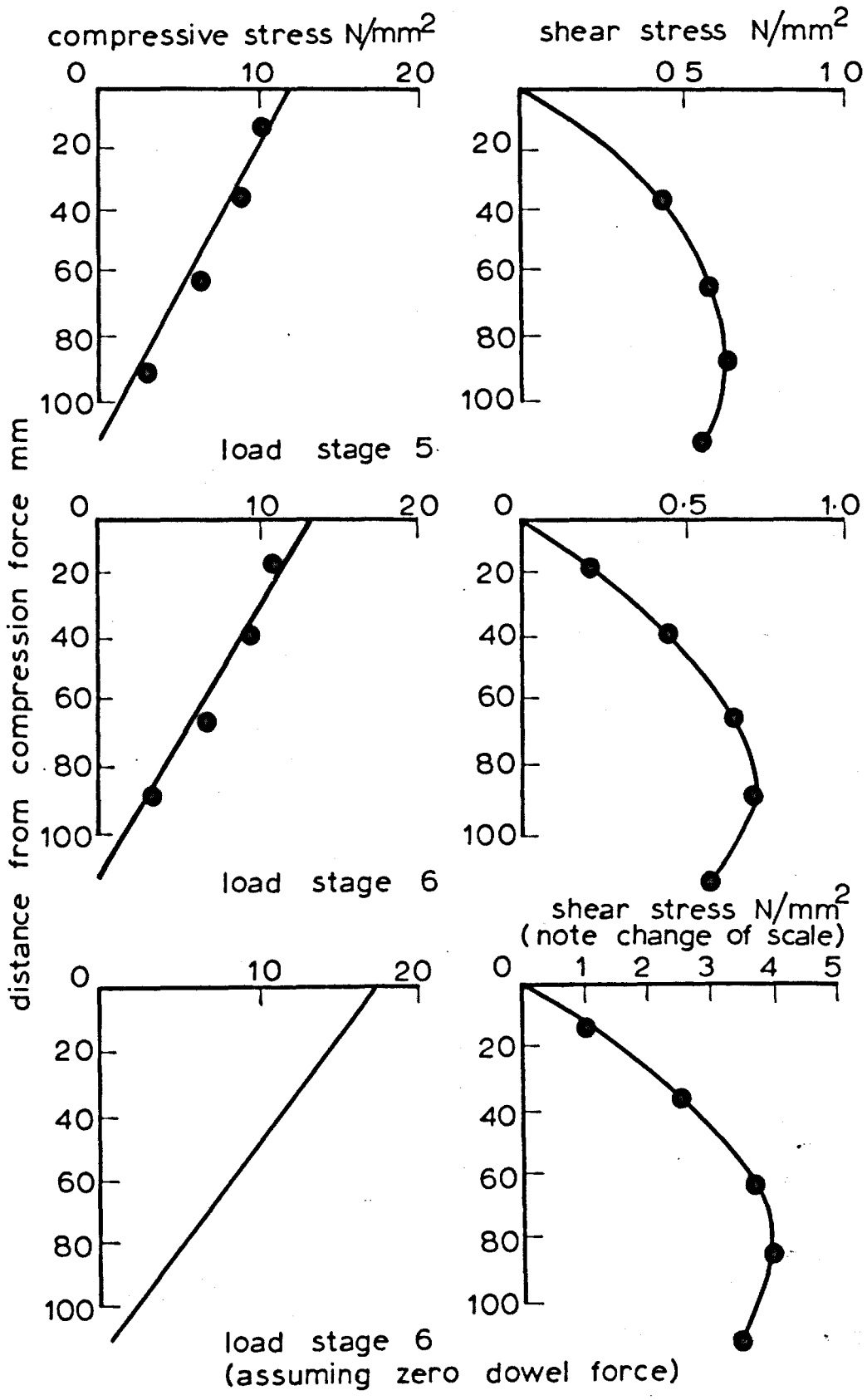

FIG. 4·30 STRESS BLOCKS FROM TEST ON BEAM 6

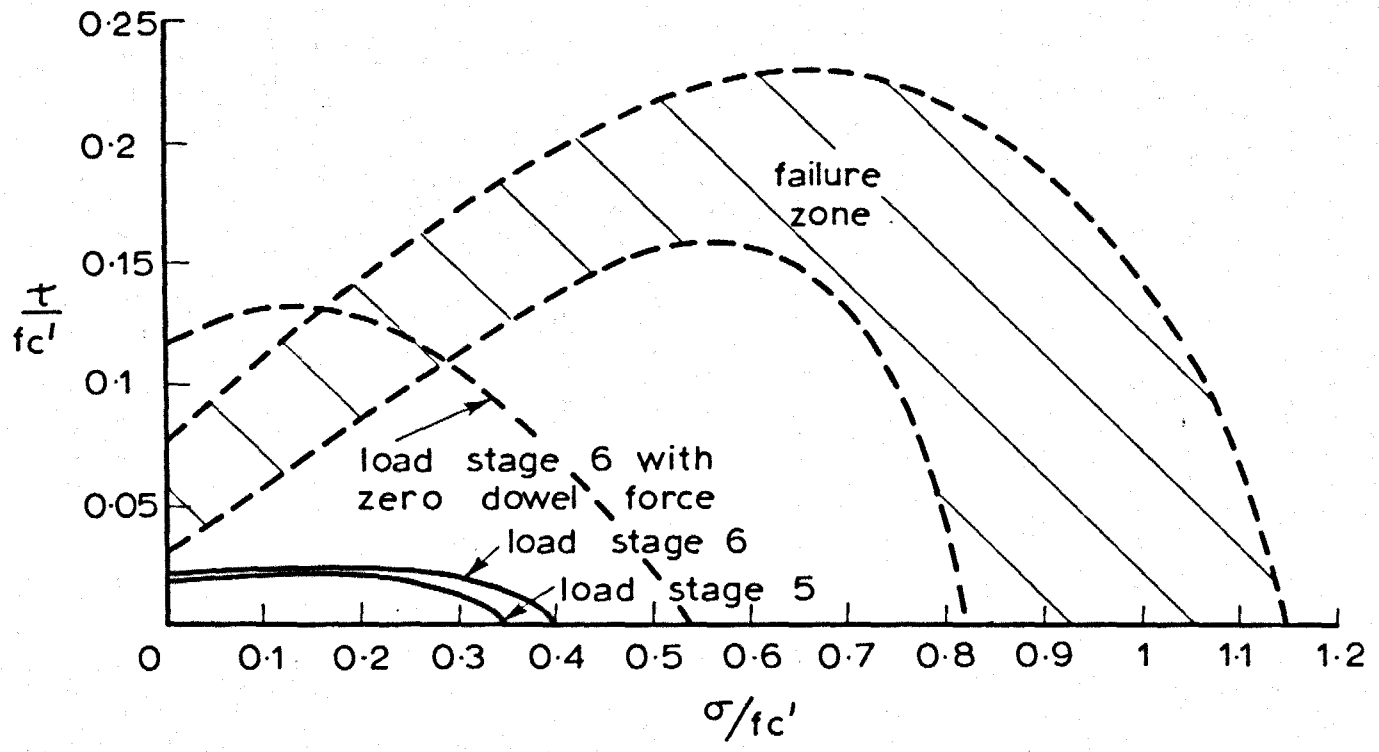

FIG. 4.31 STRESS BLOCKS FOR BEAM 6, LINE 915MM FROM SUPPORT COMPARED WITH THE FAILURE CRITERION

penultimate one) are shown on Figure 4.30. At each level of the stress-block, compressive and shear stress may be read off, divided by f_c' and plotted as on Figure 4.31 which shows the failure zones from the failure criterion. The complete stress-blocks therefore define lines on Figure 4.31. The two lines produced by plotting the stress-blocks for load stages 5 and 6 are also shown on the Figure. It can be seen that the line for load stage 6 is slightly higher than that for load stage 5 but both of these are well on the safe side of the failure zone. It is reasonable to assume that, if the next increment had been similar to previous ones and the dowel had still carried the same proportion of the shear as before, then the stress-block line would be only slightly higher than that for load stage 6 and would still be safe.

It is possible, however, to predict the state of stress on line 915 if the dowel and interlock force was lost at load stage 6. If the assumption is used that the neutral axis depth remains the same, i.e. at the crack, then the equilibrium equation 3.3 may be used with V_2 & V_3 = 0 to calculate C. The stress-block which fits the formula is shown in Figure 4.30. The concrete is now carrying all the shear on line 915. Provided that the shape of the shear stress-block remains the same, it is very much larger than when the dowel and interlock force was present. These two stress blocks now define the broken line on the failure criterion in Figure 4.31. It can be seen that this is well outside the safe area of the Figure at the neutral axis level and is only very safe at the top of the stress-block. This will be critical for diagonal tension failure where the shear crack spreads upwards from the centre of the beam to cause a very rapid failure. If the dowel had split or the interlock failed at load stage 6 then the beam would have failed in diagonal tension. In fact the dowel failure did occur with a shear force of 77·8 kN on the beam, only 6·2 kN higher than the shear force present at load stage 6.

The test on beam 3 was slightly different from the tests on the other beams and gave more information on the nature of the stresses in the concrete compression zone. The test was started in the usual way but an external stirrup was applied to the beam at the fifth

load stage to restrain splitting. The stirrup consisted of three cross-heads, one above and two below the beam, connected by prestressing wire, the centre cross-head being a sliding fit on the wire. A small hydraulic jack was fixed between the lower cross-heads so that a vertical prestress could be applied to the beam.

Before the test on the first end of beam 3, lines of strain gauges were fixed to the beam, the positions of which were dictated by the results of the test on beam 1 which had the same a/d_1 ratio and steel percentage. Four rosettes for the 50 mm Demec gauge were also stuck on the same end of the beam. The rosettes were on the opposite side of the beam from the lines of gauges but at the same distances from the support. The rosettes consisted of a circle of twelve gauge points at 15° intervals with one gauge length in the vertical position. This arrangement is preferable to the usual three-gauge rosettes as one faulty reading does not invalidate all the rosette data.

The test on beam 3 was started in the usual way but, before the beam was loaded to load stage 5, the external stirrup was applied to the beam and loaded to 20 kN. The test was then continued, the stirrup being loaded by a further 10 kN between each load stage. When the shear force on the beam was 103·8 kN, the beam had reached its theoretical ultimate strength according to strain compatibility analysis in pure flexure[19]. The load on the stirrup was then released slowly to see whether the dowel could sustain the extra shear force. When the load on the stirrup had dropped to 10 kN the beam failed in shear. The load on the capsule under the support just before failure was 94 kN. The concrete compression zone was therefore able to sustain higher stresses than those obtained just before the dowel failure, provided that the dowel was held together. Some shear stress redistribution is inevitable in this type of test but this does demonstrate that, as long as the dowel is held together and its failure is averted, beam compression zones can carry far more severe stress states than those which exist just before diagonal tension failure.

The other end of the beam was similarly tested but failed

before the stirrup was first tensioned. However, the failure of the compression zone was not complete (see Figure 4.8) and when the stirrup was tensioned after the dowel failure, the beam was able to carry another 26 kN before failure. The shear force on the beam was 103 kN, a load similar to that carried by the first end that was tested.

The readings taken on the strain gauge rosettes on one side of the first end of the beam also gave evidence that the stresses in the concrete compression zone calculated from the longitudinal strain measurements on the other side of the beam are reasonable.

Figures 4.32 and 4.33 (upper parts) show the stress-blocks from the computer analysis of the longitudinal strain readings taken on one side of the beam for load stage 4. The broken line across the stress-blocks gives the ordinates of stress at the level of the rosette on the back of the beam. The Figures also give (lower parts) a plot of the rosette strain measurements for the same load stage. The peaks of this curve give the direction of maximum compressive strain from measurements on the beam itself. From a principal stress analysis of the compressive and shear stress-block ordinates at the rosette level, it is possible to calculate the direction of maximum compressive strain. This direction is shown on the plot of the rosette results as a broken line. It can be seen that the directions of principal strain calculated from the stress-blocks are in close agreement with the peaks of the rosette curve. The principal stress analysis from the stress blocks is not very sensitive to changes in shear stress but the results of this test, together with the comparison of stresses with the failure criterion, show that the stresses predicted by the computer program are consistent with two other independently measured effects - the direction of principal strain and the failure criterion. This indicates that the concrete stress-blocks in the beams were not near failure before the dowel split and that the dowel breakdown is probably the trigger for the rapid shear failure of the beams.

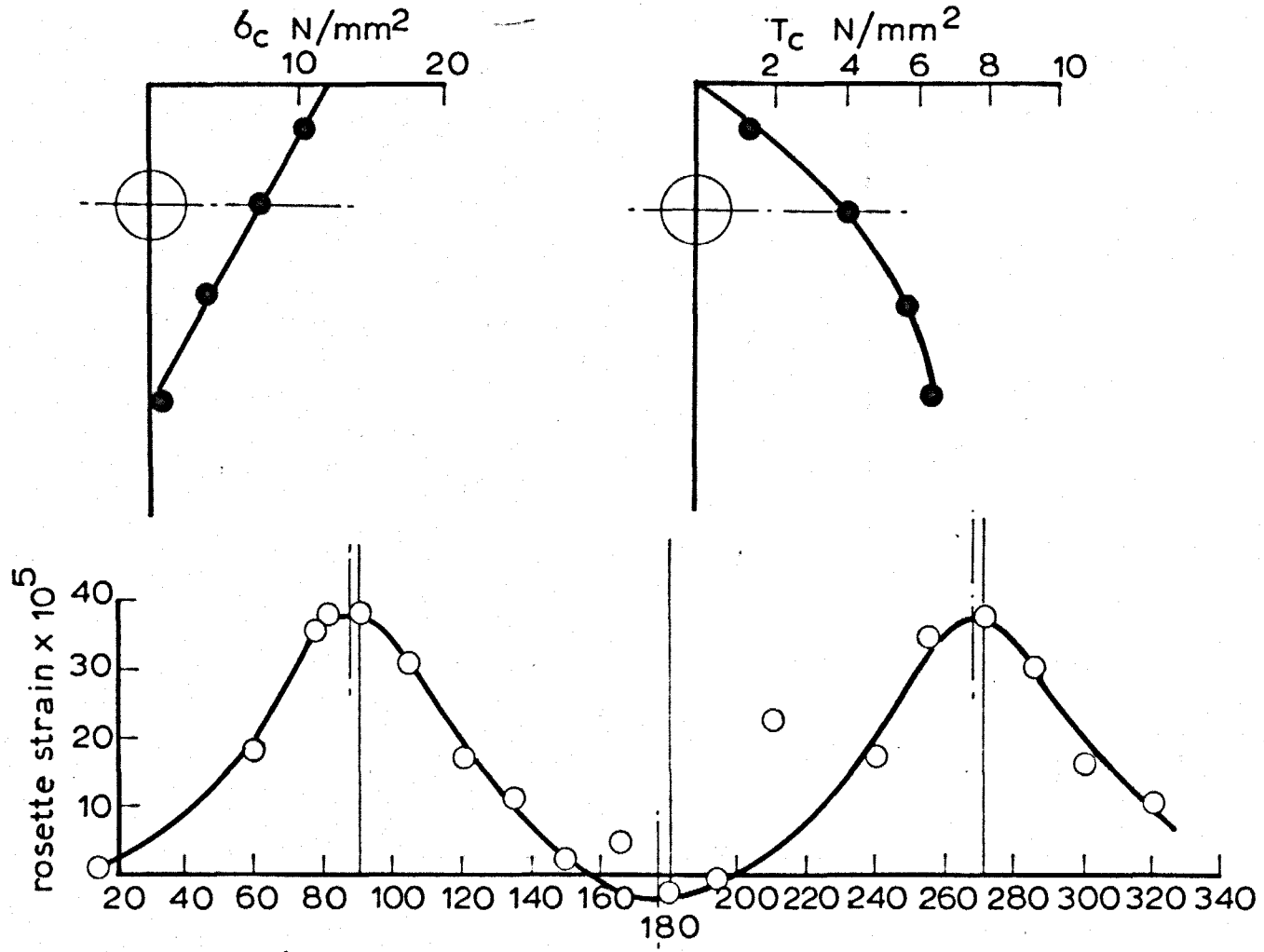

FIG.4.32 RESULT OF ROSETTE MEASUREMENTS BEAM 3 LINE 860

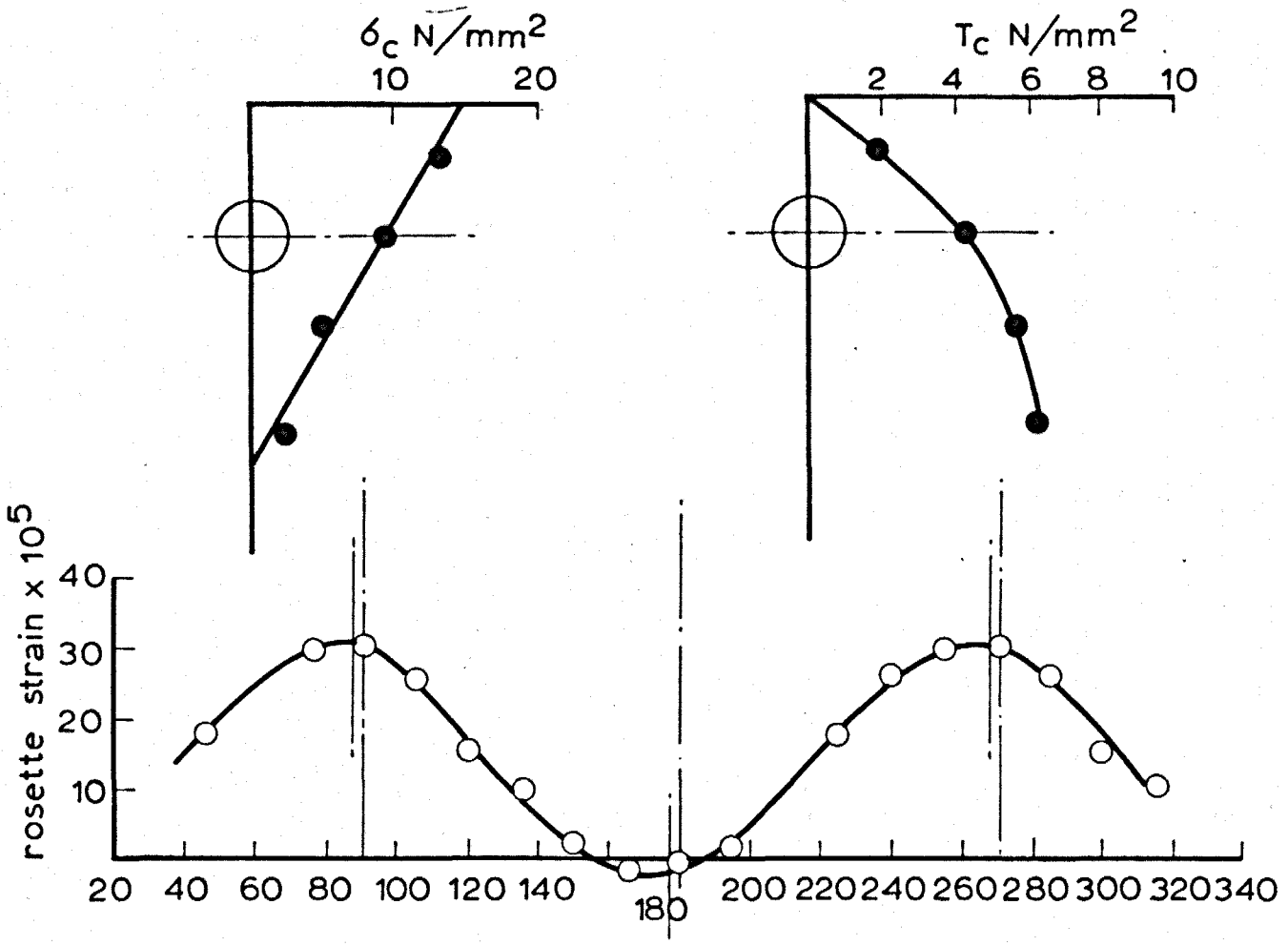

FIG. 4.33 RESULT OF ROSETTE MEASUREMENTS BEAM 3 LINE 940

DISCUSSION OF RESULTS SERIES II

Shear Forces

The shear forces shown in Tables 4.11 to 4.14 are similar in magnitude to those found in the Series I tests and the same conclusions from Series I still apply. At no stage in the tests was the compression zone found to be over stressed, when compared with the simple failure criterion.

The shear forces in the compression zone of beam 10, the beam with pre-formed cracks are similar to those found in beam 9, which had the same layout, apart from the pre-formed cracks.

The failure mode of this beam was interesting. The beam had pre-formed cracks, 150 mm deep, at 150 mm centres. As the beam was loaded flexural cracks formed at the head of the pre-formed cracks and then small cracks formed at the level of the steel as the dowel forces across the cracks became excessive. Finally a new set of cracks, starting at the head of the pre-formed cracks, occurred at the penultimate load stage and these joined to form a horizontal crack along the beam as the beam failed.

Figure 4.34 shows the final crack pattern of test 10A, the trial test of the beam with pre-formed cracks. Both forms of flexural cracking can clearly be seen in this Figure. This illustrates exactly the cracking predicted by the Kani theory described in Chapter 3 and shows that, as the secondary cracking when the 'teeth' break off is never present in normal beams, his theory, in neglecting force transfer across cracks, does not predict the true behaviour of beams in shear.

Displacement across cracks

The results of the analysis of the displacement rosette measurements were found to be extremely variable. In most cases, the amount of shear displacement was proportional to the horizontal displacement across the crack since all the sets of data shown in Figures 4.26 to 4.28 are linear.

Fig. 4.34 Beam 10 at failure

It would be extremely useful if a method of predicting the shear displacement across a crack were produced as this could be used as a compatibility condition in the development of a theory to describe shear failure. So far only very tentative conclusions of this type may be drawn from the rosette data, but it seems logical that the shear displacement should be a function of the moment-to-shear ratio on the beam and the geometry of the crack.

Table 4.17 and Figure 4.35 give a record of the slope of the rosette plots Δ_H/Δ_V and, for each rosette, the relation δ_V/δ_H, where:

Δ_V is the vertical displacement at the crack;
Δ_H is the horizontal displacement at the crack;
δ_V is the vertical distance from rosette to crack tip;
δ_H is the horizontal distance from rosette to crack tip.

The relation δ_V/δ_H is the ratio between the vertically and horizontally projected distances from the rosette to the head of the crack and is illustrated in Figure 4.35. This ratio may be measured from the drawings of the crack patterns on the beams.

Beams 7, 8 and 9 are typical reinforced concrete beams without pre-formed cracks and may therefore be considered together. The results of the rosette measurement on beam 10 are not typical of beam behaviour and may be used only for assessing the forces carried in that beam by interlock and dowel action.

Some of the cracks near the point of maximum moment on the beam are not inclined as they were influenced by the stress conditions local to the loaded area and by the fact that any inclination would make them pass under the loaded area into an area of decreasing moment. Shear failure of beams does not appear to be influenced by these cracks and they may therefore be said to be non-typical of inclined cracks. These cracks have therefore been excluded from this consideration of compatibility conditions.

In the test on beams 8 and 9, some of the inclined cracks extended downwards, past the flexural cracks that they started from,

TABLE 4.17

Rosette data results

Beam number	Position*	$\frac{\Delta H}{\Delta V}$	$\frac{\delta V}{\delta H}$
7	780-50	2·32	∞ †
	780-100	2·78	∞ †
	560-100	1·82	4·7
	470-50	1·67	2·3
	360-50	0·94	1·25
8	1090-50	0·46	3 †
	940-50	1·59	3·2 #
	940-100	0·58	2·5 #
	760-100	0·37	4 #
	635-50	0·76	2·3
9	1490-50	7·15	∞
	1220-50	12·5	4 †
	1140-50	1·43	2·3
	990-50	1·37	3
	890-50	4·0	4
	725-50	1·15	1·57
10	1370-50	0·79	5·5
	1370-100	0·44	4·5
	1220-50	0·78	4·2
	1070-50	0·93	9·0
	920-50	0·49	4·7
	920-100	1·33	3·7
	760-50	0·58	3·2
	760-100	1·22	2·5
	610-100	0·78	1·56
	470-100	1·38	1·0
	470-50	1·96	1·66

* Example: '780-50' denotes that the rosette was 780 mm from the support and 50 mm from the tension face.

† Crack too near support

\# Inclined cracking affected the result

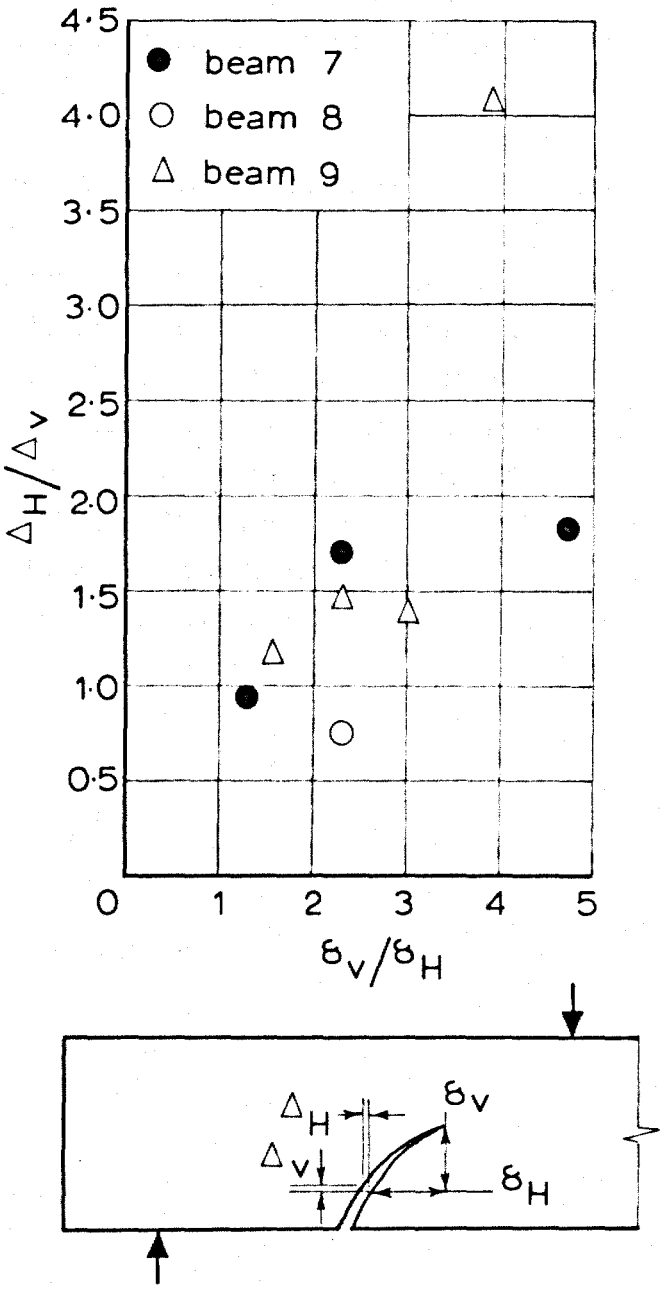

FIG. 4.35. RELATION BETWEEN CRACK DISPLACEMENTS AND CRACK GEOMETRY

towards the tension face of the beam. These cracks are presumably associated with the loss of dowel and aggregate-interlock action in the area. In some cases these cracks affected the rosette measurements, either by cutting across the rosettes or by starting above the rosettes and extending past them so that the rosettes no longer measured the correct displacements. These results also are not considered.

The remaining eight results have been plotted on Figure 4·35.

These conclusions are very tentative but illustrate that a simple compatibility condition based on crack geometry may be possible. If this is so, then, since reliable formulae for predicting Δ_H already exist, it is only necessary to postulate a crack trajectory in order to work out Δ_V for any value of the steel stress in the beam. Tests on other beams with different depths, steel percentages and crack spacings would also have to be carried out before a general compatibility condition of this type could be obtained.

CHAPTER 5

SHEAR FORCE CARRIED BY DOWEL ACTION

REVIEW OF PREVIOUS WORK ON DOWEL ACTION

Dowel tests have been carried out and reported by at least six workers in the last few years; Krefeld and Thurston[21], Fenwick[24], Lorentson[22], Baumann[27] and Arroyo[28].

Krefeld and Thurston carried out nine tests on divided beams in which the tension zone was cast separately from the compressive zone and was secured to it only by the main steel. The beam is illustrated in Figure 5.1. The dowel was tested by pulling the centre section of the beam downwards until a crack formed and rapidly propogated at the steel level. The force acting on the specimen when the crack formed is called, in this Thesis, the dowel splitting force. This test has the advantage that it is beam-like in layout, the main steel being in tension throughout the test. The dowel shear force and the tensile steel stress are related to each other by the geometry of the test specimen. Krefeld and Thurston carried out tests with a slight difference in the dimension a but, even so, the tensile stresses in the bars at failure were always low, 77 N/mm^2 being the highest.

Fenwick carried out tests on short dowels and long dowels; the short dowel was intended to model the conditions in a beam between cracks and the long dowel to model the conditions at the end of the beam beyond the last crack. These are illustrated in Figure 5.2. The tests have the disadvantage that the steel is not in tension and cannot therefore exactly model the behaviour of dowels in beams and these tests therefore gave lower values for dowel-splitting load than those of Krefeld and Thurston. The effect of tension on the bar could be to unbond it on each side of the crack for some distance, allowing it to move both horizontally and very slightly vertically and thus transfer dowel force further back into the concrete.

Lorentson carried out nine dowel tests with a divided beam (Figure 5.3). The vertical division was formed by a 1 mm wide oiled

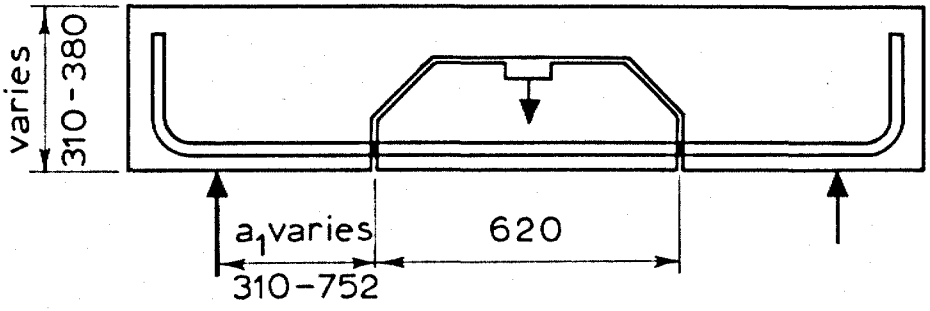

FIG. 5.1. DOWEL TEST SPECIMENS KREFELD & THURSTON

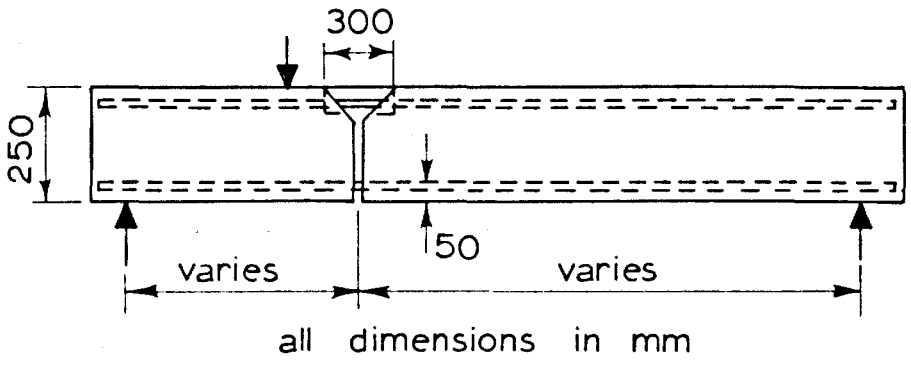

FIG. 5.3 DOWEL TEST SPECIMENS LORENTSON

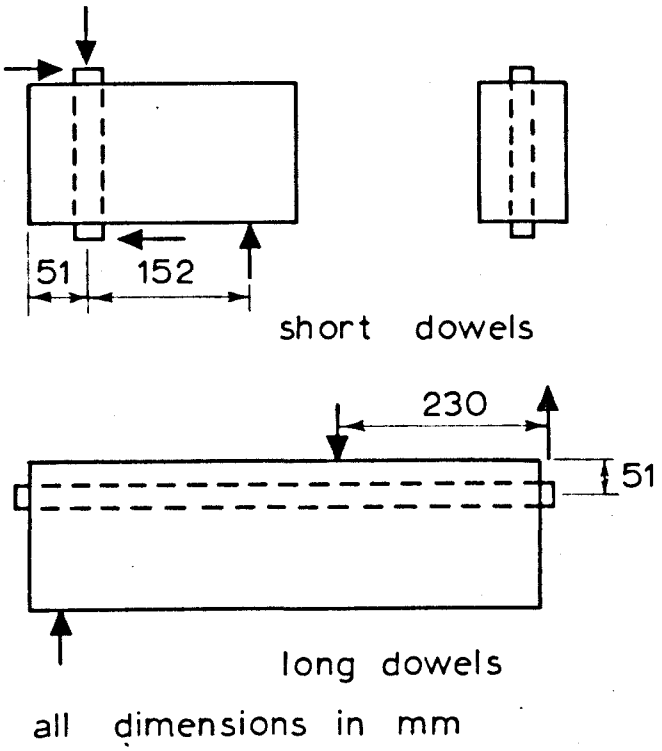

FIG. 5.2 DOWEL TEST SPECIMENS FENWICK

plate, removed after casting. Only two of the tests were of reinforced concrete, the test beams having either eighty or forty-seven 2 mm wires as main reinforcement.

In the compression zone of the beams the concrete was cut away leaving either two 25 mm bars or one 32 mm bar acting over a 300 mm length of the compression zone.

The splitting strength of the dowels was greater than that found by Krefeld and Thurston, probably because the beams had substantial bottom cover to the bars.

The load-displacement relationship measured by Lorentsen was almost elastic-plastic and therefore markedly different from the relationships found elsewhere. The bars in the compression zone would effectively act as encastré beams and carry load throughout the dowel test, possibly modifying the load-displacement relationships. Krefeld and Thurston's test method gives a less plastic curve than Lorentsen because the only member carrying shear across the crack is the tensile reinforcement.

Baumann, in a report published after the test work described in this chapter was carried out, gives the results of 26 tests on specimens of similar shape to those tested by Krefeld and Thurston. One of the major variables in this programme was the diameter of the tension reinforcing steel, sixteen tests had 20 mm bars, three had 16 mm bars and five had 26 mm bars. Bar diameter was found to be a significant variable, and the splitting strength of the dowel varied linearly with bar diameter. Only four of the tests carried out by Baumann were without stirrups.

In another recently published report, Arroyo gives the results of ten tests on beams with a pre-formed crack. The layout of the beams was similar to the tests by Lorentsen with the pre-formed crack passing right through the section. In this case, a pair of inclined pre-formed cracks was employed, one on either side of a central point load in the test beam. This test had the same disadvantage as the test by Lorentsen: the displacements across the crack were not truly beam-like and the shear force carried by the

compression reinforcement which passed through the inclined crack had to be estimated.

As well as carrying out three tests on divided beams to isolate the effects of dowel action, R. Jones[17] developed an expression for the dowel force which causes cracking by considering the bar embedded in the beam as a point-loaded cantilever on an elastic foundation. This model is illustrated in Figure 5.4. Parmelee[29] suggested a slightly more complicated model in which the bar is embedded on each side of a crack in an elastic material, this model being illustrated in Figure 5.5. In each case, the model is far from ideal. The effect of crack width was neglected by Jones, who was only studying dowel strength, and the effect of change of crack width and embedment length cannot be accurately included in the second model owing to our incomplete knowledge of these subjects. It can be seen, however, that the behaviour of a dowel must be more like the second model than the first. It is also clearly impractical to rely purely on a mathematical model at this stage as the unknown effects of bond and local cracking can only be dealt with practically. For this reason it was decided to carry out tests similar to those by Krefeld and Thurston as they are the closest to the true beam environment in which dowels work. The bar forming the dowel is put in tension during the test and is bonded on each side of the crack in a zone of varying moment. The stresses in the main steel at the dowel failure are of the order of 70 N/mm^2, consistent with a dowel near to a support or with a point of zero moment in a beam. It is this type of dowel that commonly fails in beam tests.

The tests were carried out in two stages. Firstly, a series of model beams was tested to find the effect of the major variables on ultimate dowel strength and stiffness, and secondly a few full-scale tests were carried out to verify the validity of scaling on stiffness.

MODEL TESTS

The scale for these tests was selected so that a 6 mm GK60 bar would model a 22 mm bar. In Imperial units, to which the bars were made, this gives a scale of exactly 2/7. The 22 mm bar was the size

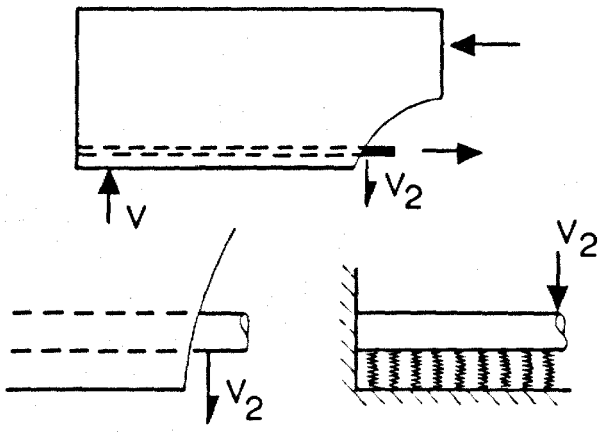

FIG. 5.4 MATHEMATICAL MODEL OF DOWEL ACTION
JONES

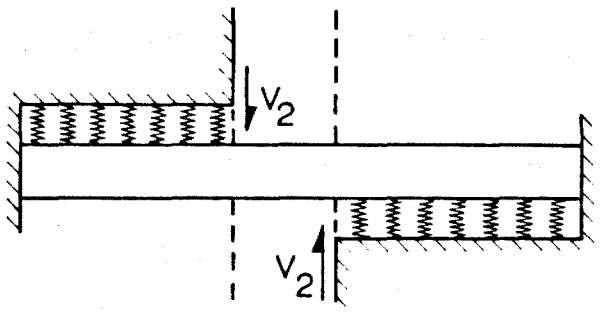

FIG. 5.5 MATHEMATICAL MODEL OF DOWEL ACTION PARMELEE

used by Krefeld and Thurston and the 6 mm bar is the smallest diameter deformed reinforcing bar available. The layout of the test specimen to this scale is shown in Figure 5.6.

Mix design

Two mixes were used in the tests: a strong micro-concrete mix for the centre section of the beam and a 2/7 scale mix of a normal structural concrete for the beam itself. The mix for the centre section was designed to be strong enough to permit the elimination of stirrup reinforcement, so simplifying the casting process.

The mix that was selected is detailed below (by weight).

Aggregate	2·4 - 1·2 mm	58%
	1·2 - 0·6 mm	20%
	0·6 - 0·3 mm	15%
	0·3 - 0·15 mm	7%

Aggregate/cement ratio 4·5
Water/cement ratio 0·4

This mix proved to be satisfactory and the centre section of the dowel beams did not fail in any of the tests.

As the mix used by Krefeld and Thurston was not reported, the mix for the outer section of the beam was designed to be a 2/7 mix of a normal structural concrete. The mix details were as follows (all by weight).

Aggregate	4·75 - 2·4 mm	40%
	2·4 - 1·2 mm	15%
	1·2 - 0·6 mm	10%
	0·6 - 0·3 mm	15%
	0·3 - 0·15 mm	20%

Aggregate/cement ratio 5·3
Water/cement ratio 0·65

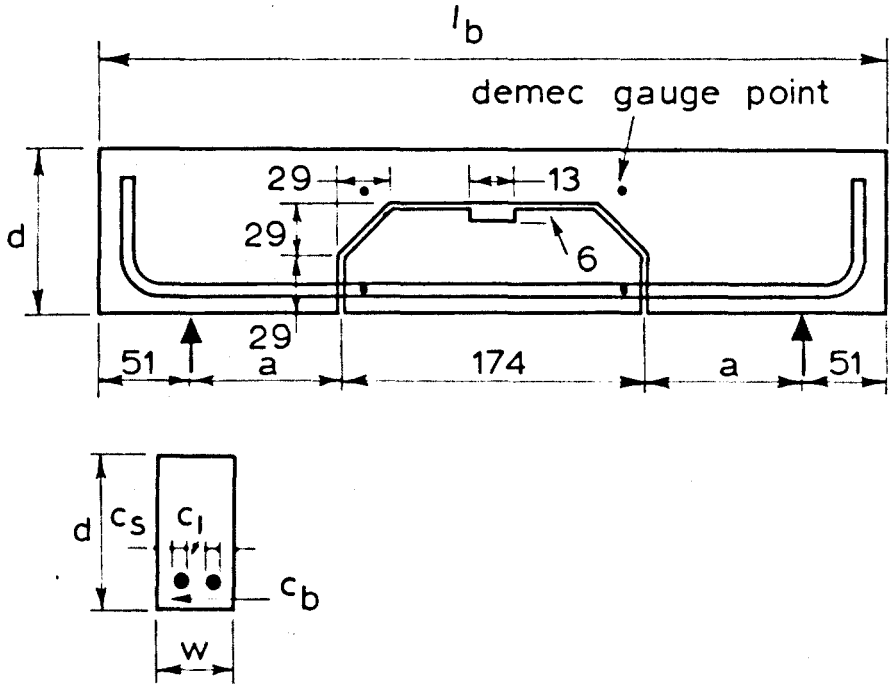

all dimensions in mm

FIG. 5.6 MODEL DOWEL TEST SPECIMEN

This mix produced a compressive strength on 112 x 56 mm diameter cylinders of 48 N/mm^2 at 14 days. The mix, like other micro-concrete mixes, produced a tensile strength which was high when compared with the compressive strength. Johnson[30] reported that the splitting strength of $^1/_4$ scale mixes, at this water/cement ratio, was 11% of the compressive strength, both tests being carried out on 150 mm cylinders; if 70 mm cylinders were used, the figure was 12%. As the tensile strength of the concrete was an important parameter in the problem, twelve 112 x 56 mm test cylinders were made whenever a beam was cast. These were tested at the same age as the beam, some in compression and some in splitting. A plot of these results can be seen in Figure 5.7. The line for the relation $f_{ts} = f_c/7$ is included in this Figure and fits the results reasonably well. When comparisons between model results, the prototype tests and the tests by Krefeld and Thurston were made, a tensile strength of one-tenth of the 300 x 150 mm cylinder strength was used for the prototype tests. A considerable amount of experimental work has been carried out on the relation between compressive and indirect tensile strength of concrete cylinders. The results show a lot of scatter but the figure of 1/10 is a reasonable fit to the results.

Manufacture

The centre section of the specimens was cast first in a steel mould, the strong micro-concrete mix being used. The sections were stripped after 24 hours and then cured under damp sacking for 7 days. They were then cleaned and stored in the laboratory for one month to gain strength before they were prepared for the second casting.

Before the second casting, the centre sections of the dowel beams were covered with a sheet of expanded polystyrene 1·5 mm thick, and the beams were then fixed in a second steel mould. This was finally filled with the 2/7 scale mix to form the complete beam. The beams were stripped after 24 hours and then the expanded polystyrene was dissolved with trichloroethylene to form the crack and the beams were then washed thoroughly with water. Curing was for 7 days under damp sacking after which the beams were stored dry for a further 7 days until they were tested.

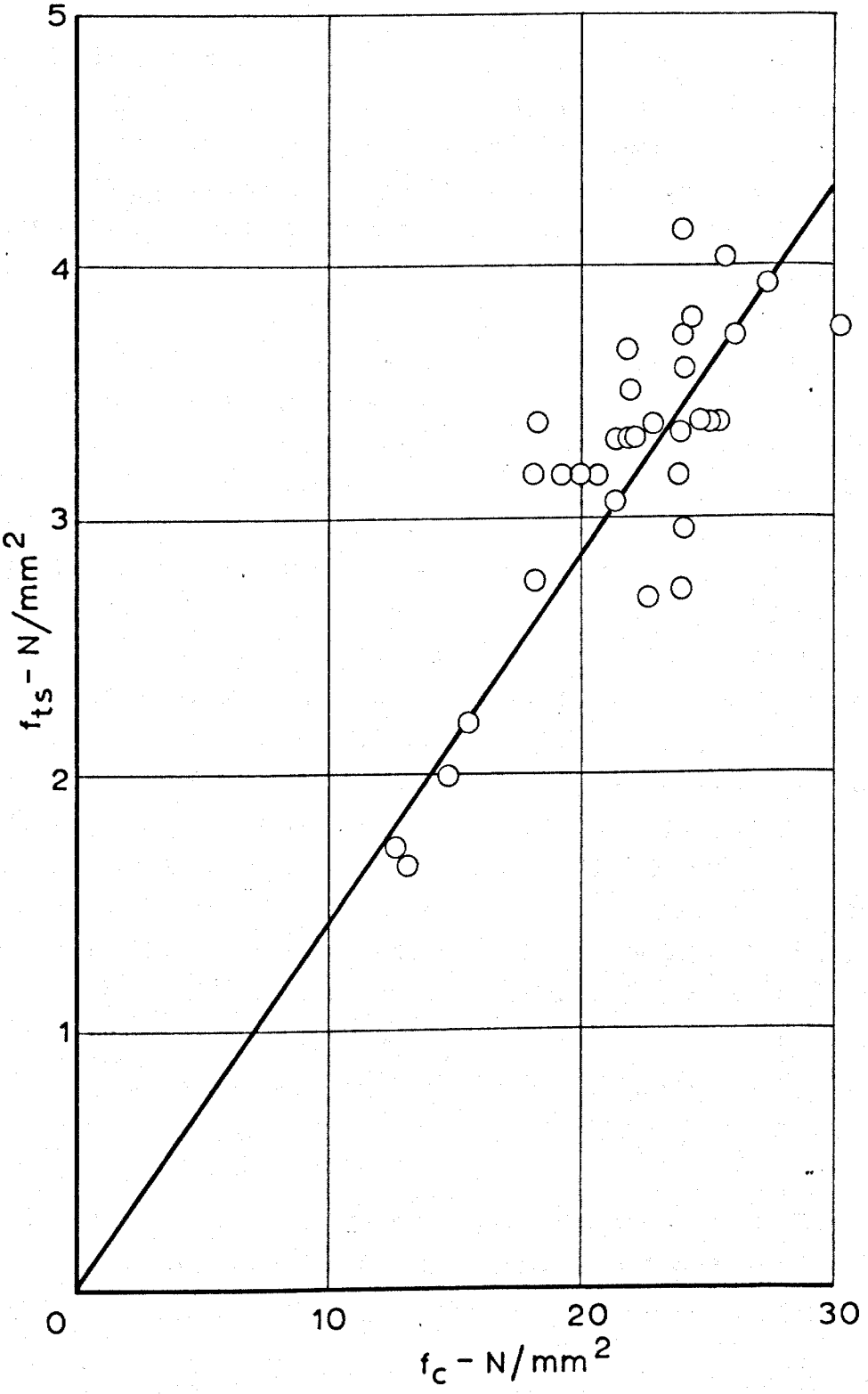

FIG. 5.7 RELATION BETWEEN COMPRESSIVE AND TENSILE STRENGTH OF MICRO-CONCRETE

Testing

The type of load-displacement relationship expected was a straight line with some change of slope as failure was approached and the curve reached its maximum value. After this, an initially steep falling branch was expected, possibly levelling out at large displacements. The test rig should therefore be very stiff or be constructed in such a way that this type of curve could be measured if it exists.

The dowel beams were tested in a rig, diagrammatically shown in Figure 5.8, which applied the load to the centre section of the beam through a lever system. The beam was connected to a lever by a threaded rod which passed through the lever and had a load cell, thrust washer and screw below it. Load was applied by tightening the screw which tilted the lever against an upper stop. The lever was then balanced by adding lead shot to a bucket suspended at its outer end. If the dowel split, the bucket dropped and pulled the lever onto a lower stop, releasing the dowel load and restraining the splitting. In order to follow the falling branch, a fixed displacement could be given to the dowel and the bucket load could be adjusted until the lever floated between the stops. Displacements were measured by using a Demec gauge with a 50 mm gauge length only when the lever was in the floating position. The gauge positions are shown in Figure 5.6 and the test rig in Figure 5.9. This rig did not prove to be completely successful in following falling branches because of the flexibility of the lever systems, but falling branches were observed in some cases and these are discussed later.

DETAILS OF TEST SERIES

Altogether 34 model beams were tested and these can be divided into 8 series which explore the main variables that were considered to affect the problem. Details of the beams are given in Table 5.1.

Series 1 (8 specimens)

This series was carried out first for two reasons. The beams are direct scale-models of Krefeld and Thurston's beams; No. 1 is a model of DA-2 and No. 2 models DA-1. Four specimens of each type

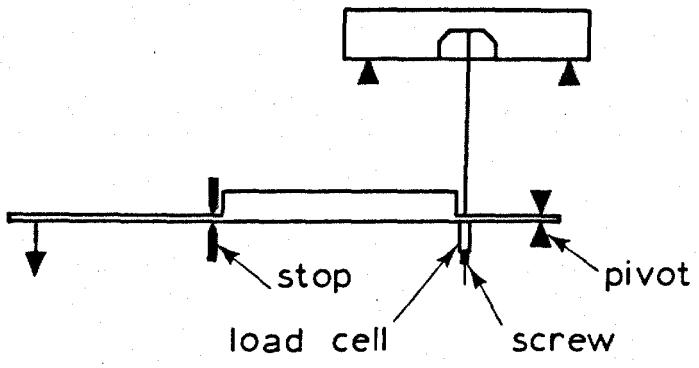

FIG. 5.8 DIAGRAM OF MODEL TEST RIG

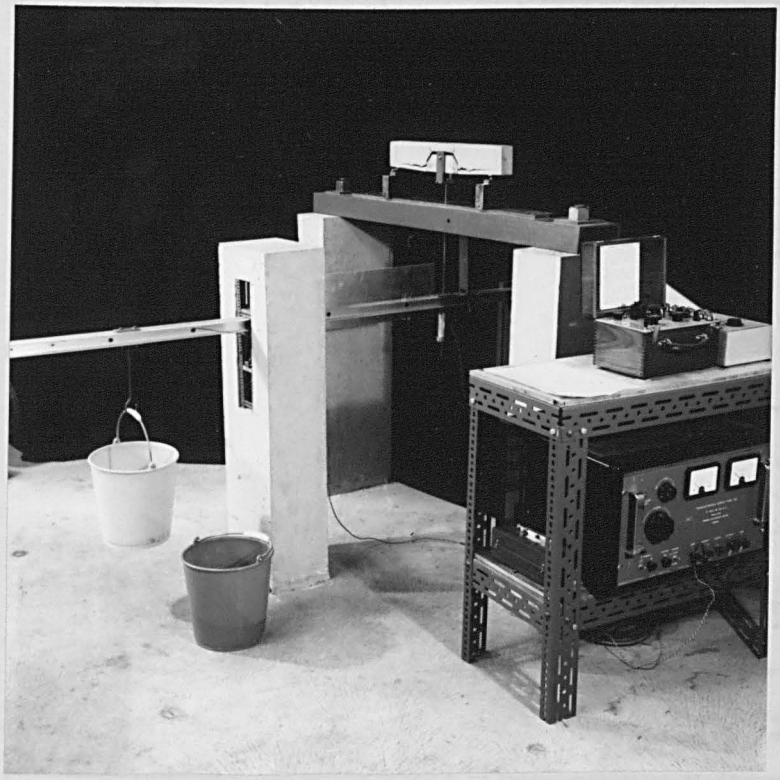

Fig. 5. 9 Model test rig

TABLE 5.1

Details of dowel test beams

No.	Series	Variable	b (mm)	d (mm)	w (mm)	a (mm)	Number of bars	c_s (mm)	c_b (mm)	c_i (mm)	f_c (N/mm²)
1. 1-4 2. 1-4	1	scale	450 625	87	44	87 174	2	7·6	7·6	15·8	20
3 4 5 6	2	f_c	625	87	44	174	2	7·6	7·6	15·8	15 20 27 35
7 8 9 10	3	a	535 625 710 800	87	44	130 174 218 263	2	7·6	7·6	15·8	20
11 12 13	4	c_s	625	87	44	174	2	2·5 7·6 12·7	7·6	25·9 15·8 5·7	20
14 15 16	5	c_b	625	87	44	174	2	7·6	2·5 7·6 12·7	15·8	20
17 18 19	6	number of bars	625	87	44	174	1 2 3	18·5 7·6 6·1	7·6	0 15·8 6·1	20
20 21 22	7	number of bars	625	87	49 54 59	174	2	10·2	7·6	15·8 20·8 25·9	20

Continued /...

TABLE 5.1

Details of dowel test beams Continued /...

23 24	8	bar layers	625	87	44	174	4	10•2	7•6	15•8	20
25 26 27 28	9	f_c	625	87	44	174	2	7•6	7•6	15•8	15

The symbols are defined in Figure 5.6.

were tested. The effects of scale and of repeating tests with similar beams were therefore studied in this one series.

Series 2 and 9 (8 specimens)

The effect of concrete strength was studied in this group. Series 2 had four tests with concrete tensile strengths of 3·3 to 4·8 N/mm^2. These were higher than those of Krefeld and Thurston but nearer to normal structural concrete grades; series 9 was therefore carried out with material tensile strengths of 1·6 to 2·2 N/mm^2 to give a better comparison with the prototypes of Krefeld and Thurston.

Series 3 (4 specimens)

This series was included because the shear span, a, which is an important variable in the problem of shear, had been considered by other workers to affect dowel strength.

Series 4, 5, 6 and 7 (3 specimens in each series)

The layout of the tensile steel was considered to have a significant effect on both strength and stiffness and, as this had previously not been studied by other workers, a considerable amount of care was devoted to this parameter.

The effect of side cover to the steel and the distance between the bars, c_s and c_i, were studied in various ways. Varying c_s in beams of constant width was achieved by moving the bars together, thus altering c_i (series 4); c_i was also varied in beams of different width, keeping c_s constant (series 7), and both c_s and c_i were varied by testing beams with varying numbers of tensile bars (series 6). The effect of bottom cover to the bars was studied in series 5 with three tests.

Series 8

This series was included as the use of two layers of steel had not been studied before and it was suspected that these tests would be different in character from the others.

Whenever possible, each series of beams contained one beam with the same layout as dowel beam 2, which enlarged the population of these beams and gave a check on the rest of the beams in the series. In fact, 16 beams of this type were tested - Nos. 2.1, 2.2, 2.3, 2.4, 3, 4, 5, 6, 8, 12, 15, 18, 25, 26, 27 and 28.

The effect of bar diameter was not studied for two reasons: firstly, because these dowel tests were carried out to provide information on dowel layouts that had been used in previous tests which only used one bar size and, secondly, because of the difficulty in modelling other sizes of deformed bar.

RESULTS

Ultimate strength

The test results from all the model tests are recorded in Table 5.2. The values of f_c and f_t are the crushing and splitting tensile strengths respectively of the 112 x 56 mm model cylinders. The value of splitting load, P_{ult}, is the maximum load that the beam centre section carried during the test and this corresponds to the rapid propagation of the crack at the steel level. P_{ult} is therefore the strength of two dowels, one at each end of the centre section.

The strength of the dowel specimens was found to vary directly with the splitting tensile strength of the concrete forming the outer part of the beams.

Figure 5.10 shows the splitting strength (P_{ult}) of all 16 of the beams which had similar layout plotted against the splitting tensile strength of the concrete. Although there is a considerable amount of scatter it can be seen that a linear relationship may be assumed from a tensile strength of 1·6 N/mm^2 to 4·8 N/mm^2. An idea of the repeatability of these tests may be gained by studying the width of the band which contains them. All the model results are within $\pm$ 15% of the mean line.

Except for beam 17, the failure surface in all the beams, after cracking, was at the steel level with a width of $\sum(c_s + c_i)$. This expression is therefore used as the most convenient way of assessing

TABLE 5.2

Dowel test results

No.	Series	f_c (N/mm²)	f_{ts} (N/mm²)	P_{ult} (kN)
1.1	1	18·2	2·76	2·21
1.2		24·0	3·17	1·99
1.3		21·9	3·31	2·12
1·4		21·9	3·66	2·38
2.1		21·4	3·07	2·14
2.2		24·1	4·14	2·53
2.3		19·3	3·17	2·31
2·4		20·7	3·17	2·23
3	2	18·3	3·38	2·18
4		22·1	3·31	2·33
5		18·2	3·17	1·88
6		38·9	4·33	2·53
7	3	22·9	3·37	1·91
8		27·5	3·93	2·12
9		24·2	3·58	2·12
10		24·5	3·79	2·10
11	4	21·4	3·31	2·01
12		25·8	4·03	2·19
13		22·1	3·51	2·16
14	5	24·1	3·34	1·78
15		26·2	3·72	2·19
16		24·1	2·72	2·12
17	6	24·1	2·96	1·98
18		20·0	3·17	2·19
19		24·1	3·72	2·02
20	7	24·8	3·38	2·72
21		22·7	2·69	2·36
22		25·2	3·38	3·13
23	8	25·5	3·38	3·06
24		30·4	3·75	3·03
25	9	13·1	1·65	1·88
26		14·8	2·00	1·91
27		15·5	2·20	1·91
28		12·7	1·72	1·91

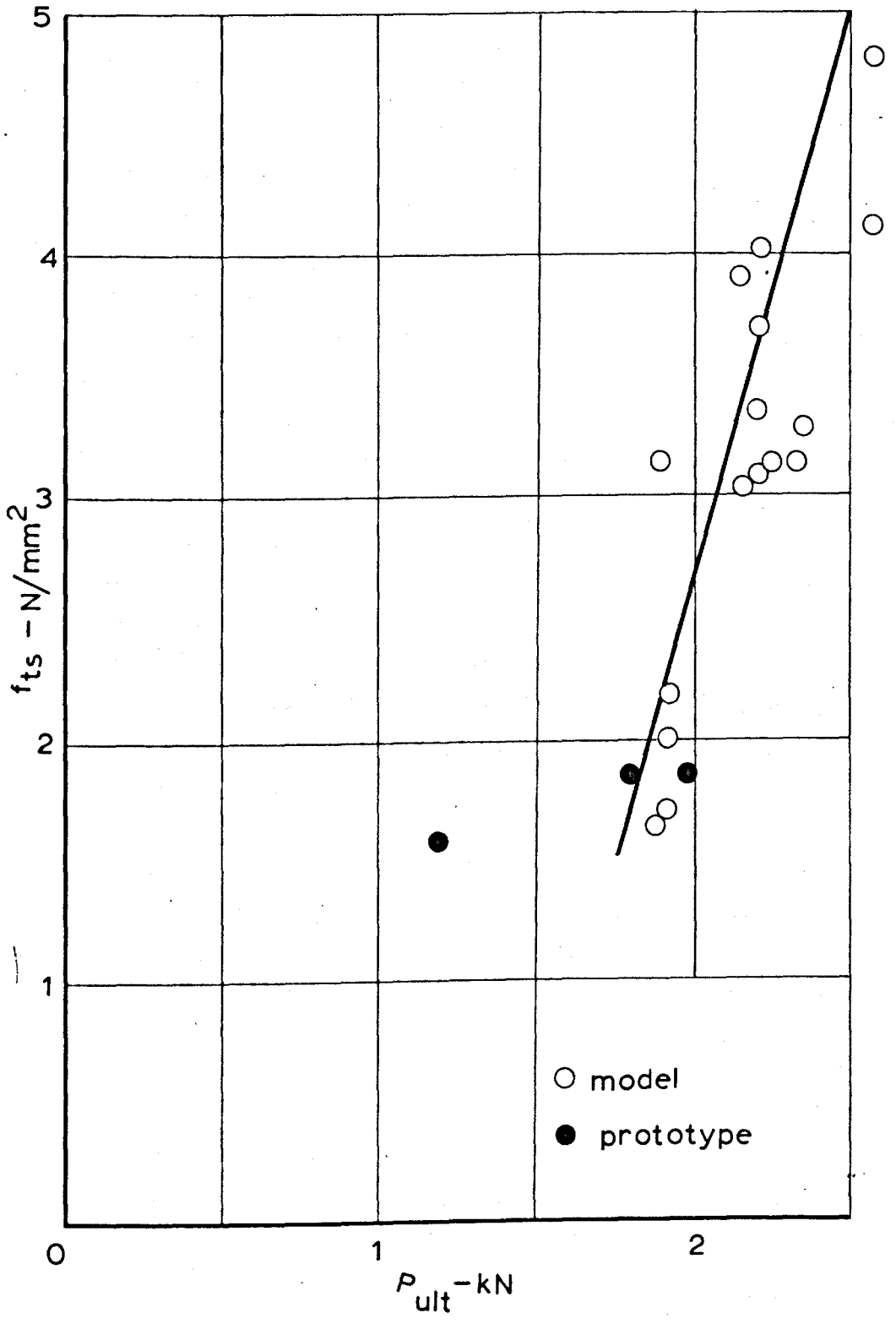

FIG. 5.10 EFFECT OF f_t ON THE SPLITTING STRENGTH OF DOWEL

the effect of the layout of the tensile steel reinforcement. In beam 17, in the cross-section the crack sloped slightly upwards from the outside of the beam to the steel in the middle of the section but, as this made only a slight difference to the failure surface width, $\sum(c_s + c_i)$ has still been used. Figure 5.11 shows the results of the nine beams in these series and a relationship between $\sum(c_s + c_i)$ and P_{ult} may exist. Even though only a few tests have been carried out, a linear relationship may be assumed, provided that the failure surface is horizontal, which is so with beams with normal reinforcement layouts.

The results of the tests that were carried out to study the effect of bottom cover to the bars were less conclusive, although a slight trend towards higher dowel-splitting strength with greater bottom cover is indicated in Figure 5.12 particularly when the material strengths of the beams are taken into account. It would appear that a larger variation of bottom cover is required for the stiffness of the concrete below the bar to alter dowel strength significantly. A variation as large as this would have little significance in practical design.

The results of the two tests of beams with two layers of reinforcement indicate that the splitting strength, P_{ult}, is approximately 40% greater than that with only two bars of the same type. The load-displacement relationship is of a similar shape to that of the two-bar dowel tests.

Four tests were carried out to study the effect of the dimension a, the distance from the crack to the support, on the dowel-splitting strength, as Krefeld and Thurston reported that this affected dowel strength in their tests. A study of the results of these tests, beams 7, 8, 9 and 10 in Table 5.2, does not show a significant change with varying a.

Stiffness

Measurements of displacement across the dowel were taken throughout each test enabling load-displacement curves to be drawn. The test rig was constructed in such a way that controlled displacement

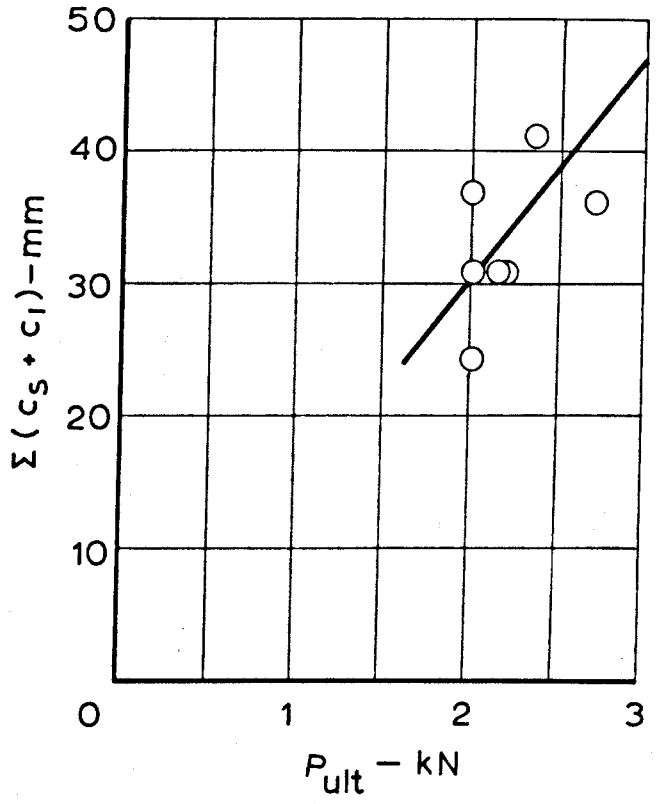

FIG. 5.11 EFFECT OF WIDTH OF FAILURE SURFACE ON SPLITTING STRENGTH

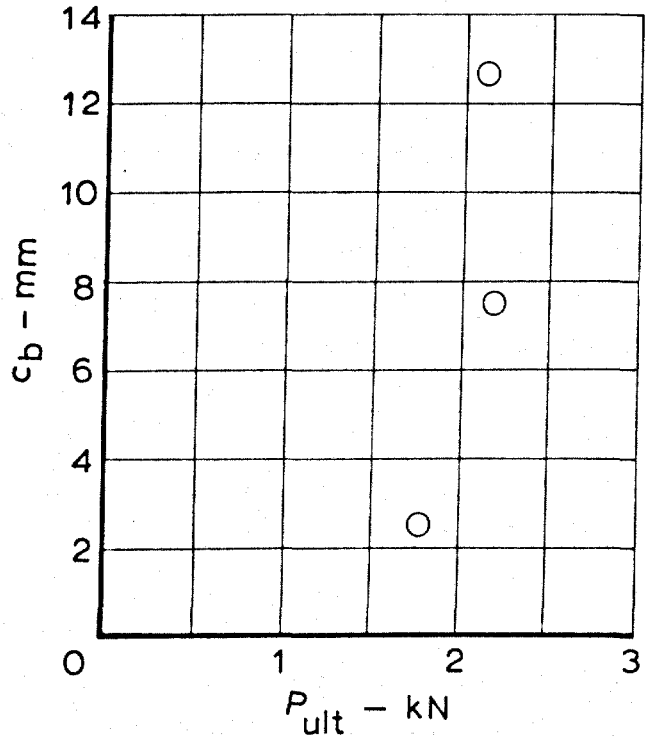

FIG. 5.12 EFFECT OF BOTTOM COVER TO BARS ON SPLITTING STRENGTH

tests could be carried out to investigate the behaviour of the falling branch of the curve. The sudden loss of stiffness after dowel cracking was such, however, that the rig was not always capable of producing a complete load-displacement curve. Figure 5.13 shows a typical curve (for beam 2.2). It can be seen that this is an initially straight line curving over until the dowel-splitting load is reached. The initial part of this curve, drawn to a larger scale, is shown in Figure 5.14. Two symbols are used in plotting Figure 5.14, one for each end of the beam, as displacements were measured across each end of the pre-formed crack in the tests.

PROTOTYPE TESTS

The technique of carrying out model tests of dowel behaviour is new and, before the results of these tests can be said to be generally applicable, comparisons with tests of previous workers have to be made. For this reason, the model tests were chosen as models of Krefeld and Thurston's tests in order to cut down the amount of prototype work needed. The scale of the models was 2/7 of Krefeld and Thurston's tests using similar materials to the prototype.

Thus,

model displacements = 2/7 prototype displacements

model splitting force = 4/49 prototype splitting force

Krefeld and Thurston carried out three tests that can be compared with the models and the results of these are shown to the model scale in Figure 5.10. The three tests had different shear spans (which the model tests showed not to be a variable) and have all been included in the comparisons. In order to study the load-displacement relationship more closely, particularly the initial slope of the curve, four prototype tests were carried out. The test specimens were slightly larger than the specimens of Krefeld and Thurston as they were made to the same size and steel layout as the beams which were studied to find forces in the compression zone and reported in the last chapter. The specimens were therefore 400 x 200 mm in cross-section with two 22 mm bars as main reinforcement. Side and bottom cover to the bars was 25 mm.

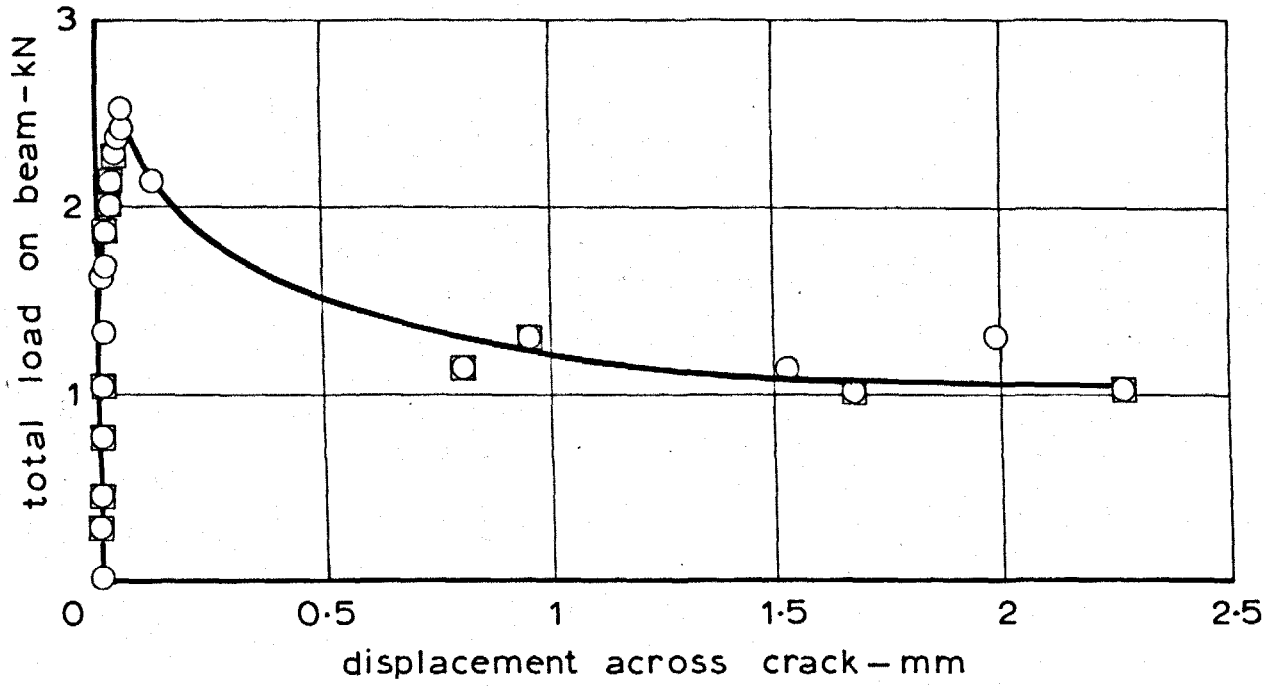

FIG. 5.13 LOAD-DISPLACEMENT PLOT FOR BEAM 2.2.

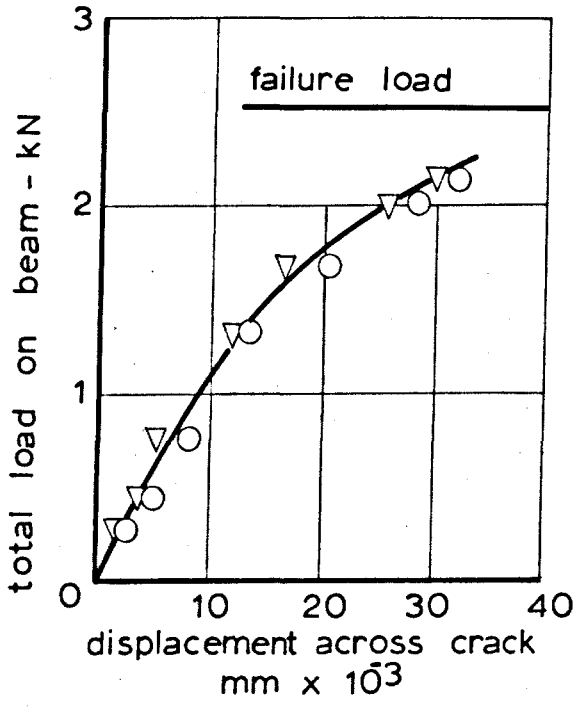

FIG. 5.14 LOAD DISPLACEMENT PLOT FOR BEAM 2.2

The concrete used in the tests had 19 mm aggregate and was to the following mix design (by weight).

Aggregate	19 - 9·5 mm	25%
	9·5 - 4·75 mm	38%
Sand		37%
Aggregate/cement ratio		5·5
Compacting factor		0·9

Details of the prototype specimens and tests are given in Table 5.3.

TABLE 5.3
Details of prototypes

Beam	f_t (N/mm^2)	P_{ult} (kN)	Crack width (mm)
P1	3·86	27·2	1·5
P2	3·7	28·0	1·5
P3	3·75	31·5	5·0
P4	3·65	28·9	0·2

Beams P1 and P2 were constructed with pre-formed cracks of the same width as the cracks in the model beams. The stiffness of the dowel, the initial slope of the load-displacement curve, was less in the model than in the prototype. As the only dimension that had not been scaled correctly was the crack width, beam P3 was made with a scaled crack width much greater than that in P1 and P2. The crack width of beam P3 was 5·0 mm, much nearer to the true scale from the model of 7·0 mm which corresponds to the model width multiplied by 400/87. This dowel was much less stiff than the dowel in the previous two prototype tests and corresponds more to the model tests.

The crack widths found in beams in practice are between 0·02 and 0·3 mm and, at failure, are between 0·1 and 0·3 mm; beam P4 was therefore constructed with a crack width of 0·2 mm to conform with this. The crack was formed by filling the surface voids in the centre part of the specimen with cement grout to give a good finish; three

coats of paint and one coat of grease were then applied before the rest of the beam was cast.

The dowel in this case was stiffer than that in beam P3 and of similar stiffness to that of beams P1 and P2. Some wedging of the concrete across the crack occurred at high loads, so that the test was not satisfactory apart from giving a dowel stiffness for small crack width and confirming that a limiting width of 1·5 mm in dowel tests is satisfactory from both a strength and a stiffness point of view.

Figure 5.15 shows the initial part of the load-displacement curve for beams P1, P3, P4 and a typical model result (beam 1.2).

Idealized load-displacement curve

A study of the dowel strength of tensile steel in reinforced concrete is not complete if only the ultimate strength of the dowel can be predicted. It is important also to be able to assess the displacements that occur in order that the contribution of the shear force in the dowel to the shear strength of the beam may be assessed. If the failure of beams in bending and shear is not triggered by dowel failure, then the ultimate strength of a dowel has little significance.

After a study of both the model and prototype test results, it was decided that the most appropriate way of defining the load-displacement relationship of a dowel was to produce an idealized curve, defined by the parameters of the problem. The form of the curve that was selected is shown to the prototype scale in Figure 5.16. This is a curve up to the splitting strength of the dowel, P_{sp}, followed by an abrupt 50% loss of force and then a long line of constant dowel force for increasing displacements.

The initial slope of the curve (2,000 kN/mm) came from a survey of the prototype results with the minimum crack width, namely P1, P2 and P4.

The shape of the curve up to the splitting strength was found to fit the equation

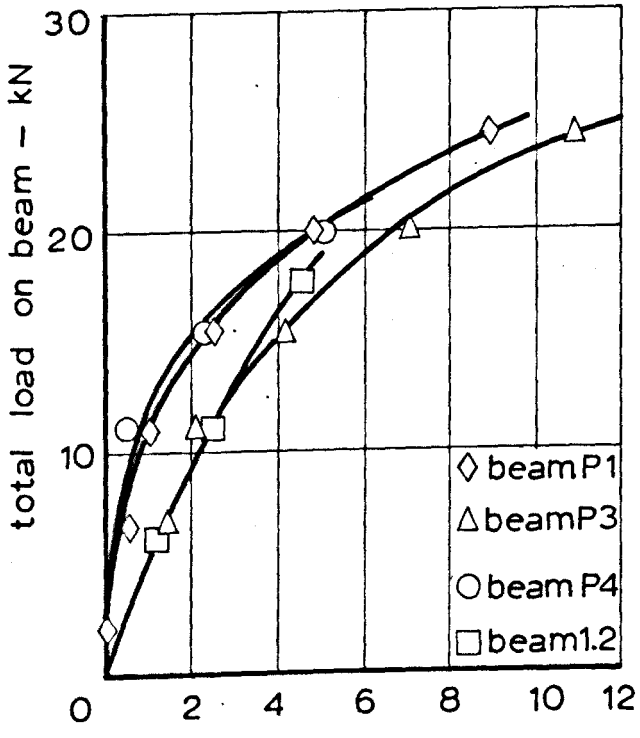

FIG. 5.15 LOAD DISPLACEMENT PLOT FOR PROTOTYPES AND MODEL

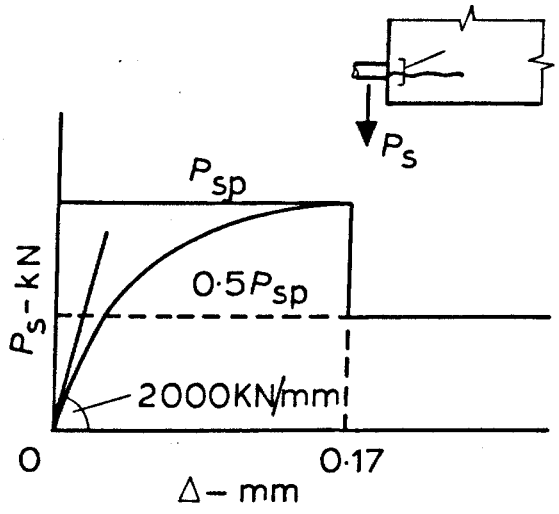

FIG. 5.16 IDEALIZED LOAD-DISPLACEMENT PLOT

$$P_s = 1{\cdot}55\, P_{sp}\, \triangle^{0{\cdot}25} \text{ kN} \qquad 5.1$$

where $\triangle$ is the shear displacement across the flexural crack in mm.

This equation is applicable for the bar diameter and two-bar layout tested.

The displacement at which dowels split was fixed at 0·17 mm, a figure derived from a survey of all the prototype and model beams and found not to vary with any of the beam parameters that were studied.

From a study of all the model test results in which post-splitting behaviour was measured, the residual section of the curve after the dowel had split has the ordinate 0·5 P_{sp}. About 75% of the model results gave information for this analysis, which showed considerable variation within the beams; the figure of 0·5 was selected as a lower bound to the test results. The complete falling branch of model beam 2.2 is shown in Figure 5.13 and is typical of the results that were obtained.

Finally, P_{sp} is defined from a study of the model and prototype test results and the results of Krefeld & Thurston and Baumann.

The model tests were scaled up to the prototype size and the results from the other tests were collected. The variables that were considered to be significant and were used in the analysis were

f_{ts} splitting tensile strength of the beam concrete (N/mm^2)

$\sum(c_s + c_i)$ failure surface width (mm)

c_b bottom cover the bars (mm)

a shear span (mm)

ϕ bar diameter (mm)

The data used in the analysis is shown in Table 5.4.

From a consideration of the way in which dowels fail, a set of transformations of this data were selected and, using regression analysis, a number of equations were produced. The equation for dowel splitting strength that was finally selected, in slightly simplified form, was:-

$$P_{sp} = 4{\cdot}95 + 0{\cdot}001 \sum (c_s + c_i) f_{ts} \phi \qquad 5.2$$

Although one of Arroyo's conclusions was that the splitting strength increased with bottom cover to the bars this variable was not found to be significant with this data, probably because the bottom cover was not varied greatly within the tests, although the variation within these tests covered the practical range.

A list of the beams, the measured P_{sp} and the percentage error produced by the regression analysis are given in Table 5.5.

This equation was selected as it is in variables that have physical significance.

The units of $\sum (c_s + c_i) f_{ts} \phi$ are kN which is the same as the units of P_{sp}. An equation of the form of the regression equation may be derived from a consideration of the failure of the dowels. Figure 5.17 shows a section of a reinforced concrete beam with the dowel just starting to split and the initial failure surface drawn in.

The force transmitted across the failure surface may be written as

$$P_{sp} = f_{ts} \sum (c_s + c_i) n$$

where n is the length of the initial splitting along the beam. If $K\phi$ is submitted for n where K is a constant then this equation is very similar to equation 5.2.

TABLE 5.4

Dowel test results

	P_{sp}	f_{ts}	$\sum(c_s + c_i)$	ϕ	a	c_b
	Model tests					
1.1	13·5	2·76	108	22	305	26·6
1.2	12·2	3·14	108	22	305	26·6
1.3	13·0	3·31	108	22	305	26·6
1.4	14·5	3·66	108	22	305	26·6
2.1	13·1	3·07	108	22	610	26·6
2.2	15·5	4·14	108	22	610	26·6
2.3	14·1	3·17	108	22	610	26·6
2.4	13·3	3·17	108	22	610	26·6
3	13·6	3·38	108	22	610	26·6
4	14·3	3·31	108	22	610	26·6
5	11·5	3·17	108	22	610	26·6
6	15·5	4·83	108	22	610	26·6
7	11·7	3·37	108	22	455	26·6
8	13·0	3·93	108	22	610	26·6
9	13·0	3·58	108	22	763	26·6
10	12·8	3·79	108	22	305	26·6
11	12·3	3·31	108	22	610	26·6
12	13·4	4·03	108	22	610	26·6
13	13·0	3·51	108	22	610	26·6
14	10·9	3·34	108	22	610	8·70
15	13·4	3·72	108	22	610	26·6
16	13·0	2·72	108	22	610	44·5
17	12·1	2·96	130	22	610	26·6
18	13·4	3·17	108	22	610	26·6
19	12·4	3·72	85	22	610	26·6
20	16·6	3·38	127	22	610	26·6
21	14·4	2·69	144	22	610	26·6
22	19·1	3·38	162	22	610	26·6
25	11·5	1·65	108	22	610	26·6
26	11·7	2·00	108	22	610	26·6
27	11·7	2·20	108	22	610	26·6
28	11·7	1·72	108	22	610	26·6

Continued /....

TABLE 5.4 Continued /....

Prototype tests						
P1	13·6	3·86	156	22	610	25
P2	14·0	3·7	156	22	610	25
P3	15·7	3·75	156	22	610	25
P4	14·4	3·65	156	22	610	25
Baumann						
1	7·0	3·14	70	20	450	30
2	9·0	2·84	70	20	450	30
3	9·0	2·84	70	20	450	30
4	7·0	2·97	70	20	450	30
5	7·0	2·97	70	20	450	30
6	11·5	3·01	118	16	450	30
7	6·0	3·14	78	16	450	30
8	6·5	2·96	78	16	410	30
9	11·5	3·01	98	26	450	30
10	7·5	3·14	58	26	450	30
11	6·5	2·96	58	26	460	30
12	17·0	2·93	160	20	450	30
13	8·5	3·00	70	20	450	40
14	9·0	3·05	70	20	450	30
15	6·0	2·34	70	20	450	30
16	6·5	2·34	70	20	450	61
17	7·5	2·75	70	20	300	30
18	7·5	2·75	70	20	600	30
21	7·0	3·05	70	20	450	30
25	11·0	3·16	84	26	450	30
29	5·5	1·16	70	20	450	30
30	7·0	2·52	70	20	450	30
31	9·5	3·98	70	20	450	30
Krefeld and Thurston						
DA-2	15·9	2·95	108	22	305	19
DA-3	14·0	2·95	111	22	456	19
DA-1	8·9	2·55	108	22	610	19

Continued /....

TABLE 5.4 Continued /....

DA-6	14•5	2•91	159	22	305	19
DA-7	12•2	2•90	162	22	700	19
DA-9	20•0	2•66	108	22	305	19
DA-8	15•5	2•66	108	22	610	19
DA-5	16•0	3•08	102	29	305	28
DA-4	13•1	3•08	95	29	610	28

TABLE 5.5

Comparison of tests with regression equation

Test	P_{sp} (kN)	Error %
Model tests		
1•1	13•5	15•5
1•2	12•2	0•1
1•3	13•0	3•2
1•4	14•5	7•5
2•1	13•1	8•1
2•2	15•5	6•5
2•3	14•1	13•0
2•4	13•3	7•8
3	13•6	6•3
4	14•3	12•0
5	11•5	-6•5
6	15•5	-3•7
7	11•7	-8•6
8	13•0	-7•7
9	13•0	-1•5
10	12•8	-6•8
11	12•3	-2•2
12	13•4	-6•2
13	13•0	-2•7
14	10•9	-1•5
15	13•4	-0•89
16	13•0	13•7
17	12•1	-8•7
18	13•4	8•6
19	12•4	5•7
20	16•6	15•1
21	14•4	8•2
22	19•1	12•9
25	11•5	24•0
26	11•7	12•3
27	11•7	14•4
28	11•7	24•0

Continued /....

TABLE 5.5 Continued/....

Prototype tests		
P1	13·6	-30·8
P2	14·0	-23·3
P3	15·7	-11·0
P4	14·4	-18·7
Baumann		
1	7·0	-31·6
2	9·0	2·2
3	9·0	2·2
4	7·0	-28·2
5	7·0	-28·2
6	11·5	9·1
7	6·0	-14·7
8	6·5	-31·2
9	11·5	-7·1
10	7·5	-27·2
11	6·5	42·7
12	17·0	17·5
13	8·5	-6·1
14	9·0	-0·9
15	6·0	-35·4
16	6·5	-24·9
17	7·5	-15·7
18	7·5	-15·7
21	7·0	-29·8
25	11·0	-5·8
29	5·5	-18·6
30	7·0	-19·6
31	9·5	-8·9
Krefeld & Thurston		
DA-2	15·9	26·2
DA-3	14·0	14·8
DA-1	8·9	-21·6
DA-6	14·5	-2·2

Continued /....

TABLE 5.5 Continued /....

DA-7	12•2	-22•7
DA-9	20•0	44•7
DA-8	15•5	28•6
DA-5	16•0	13•9
DA-4	13•1	-0•5

TABLE 5.6

Prototypes with stirrups

Beam	l (mm)	Stirrup diameter (mm)	f_t (N/mm²)
P.1	25	6	4•36
P.2	75	6	4•70
P.3	125	6	4•25
P.4	175	6	4•46
P.5	25	10	4•51
P.6	75	10	3•80
P.7	125	10	3•71
P.8	175	10	3•71

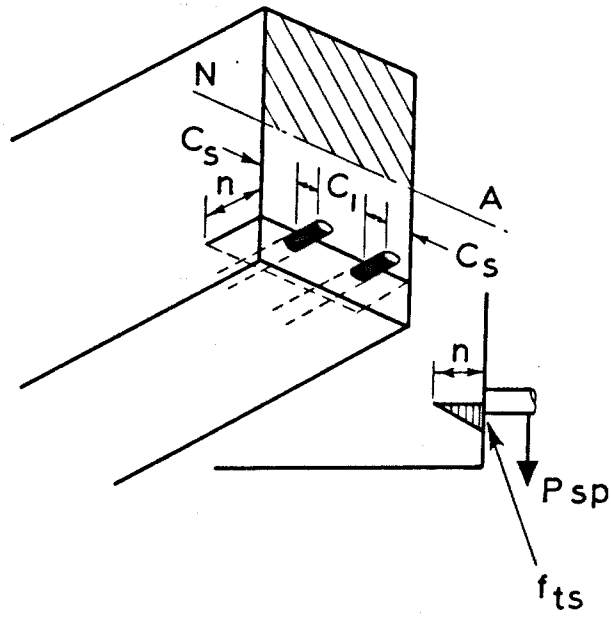

FIG. 5.17 LIMIT ANALYSIS OF DOWEL FAILURE

The dowel load-displacement relationship is now completely defined and is summarized below.

(a) Dowel-splitting strength is calculated from the equation

$$P_{sp} = 4{\cdot}95 + 0{\cdot}001 \sum (c_s + c_i) f_{ts} \phi \text{ kN} \qquad 5.2$$

and occurs at a displacement of 0·17 mm.

(b) The curve up to P_{sp} is of the form

$$P_s = 1{\cdot}55 P_{sp} \triangle^{0{\cdot}25} \text{ kN} \qquad 5.1$$

These equations are applicable to the two-bar layout that was tested.

(c) After P_{sp} is reached, the force carried by the dowel drops to 0·5 P_{sp} and remains at this level for all sensible displacements.

Figure 5.18 shows the idealised curve plotted on the result of the test on prototype 1.

PROTOTYPE TESTS WITH STIRRUPS

Two series of four dowel specimens were tested to investigate the effect of the presence of stirrups on dowel strength and stiffness. The test specimens had the same layout as the specimens previously tested with the addition of single stirrups near to the pre-formed crack. The specimen was the same size as the other prototype beams and is illustrated in Figure 5.19. The dimension l was varied from 25 to 175 mm in 50 mm steps. The maximum distance of 175 mm was intended to correspond to 0·5 d_1. This length would correspond to the crack in a beam just coming on the support side of a stirrup leaving a long unsupported dowel length to the next stirrup.

Details of the test specimens are given in Table 5.6.

A similar series of tests with 10 mm diameter stirrups was also carried out (beams P5.5 to P5.8) and the results of these tests are also shown in Figure 5.20.

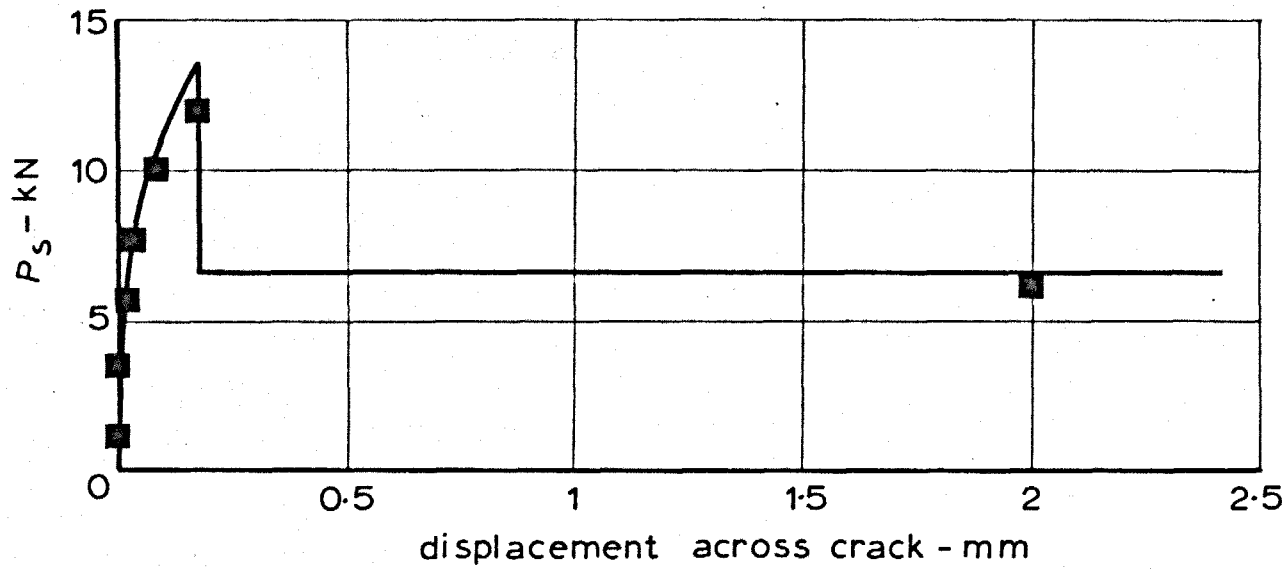

FIG. 5.18 LOAD-DISPLACEMENT PLOT OF BEAM P1 WITH IDEALIZED CURVE

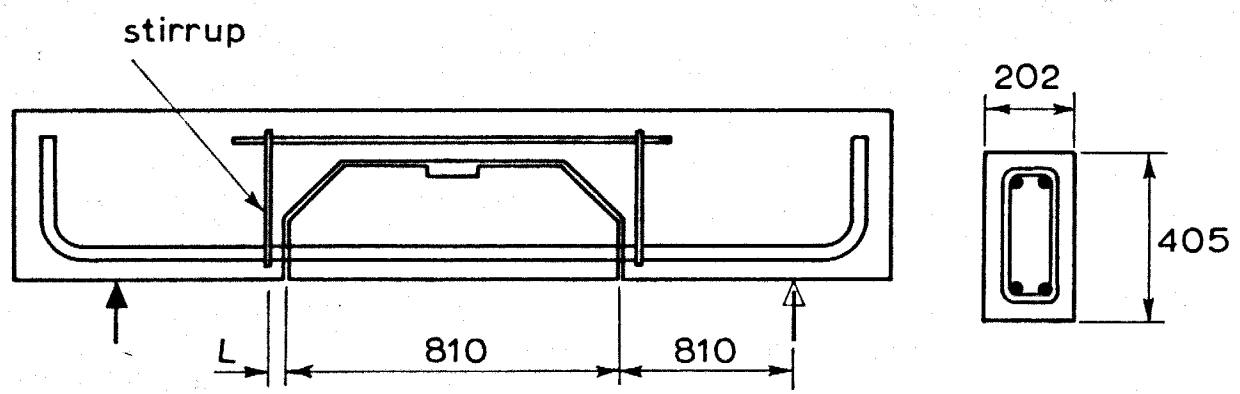

FIG. 5.19 DOWEL SPECIMEN WITH STIRRUP

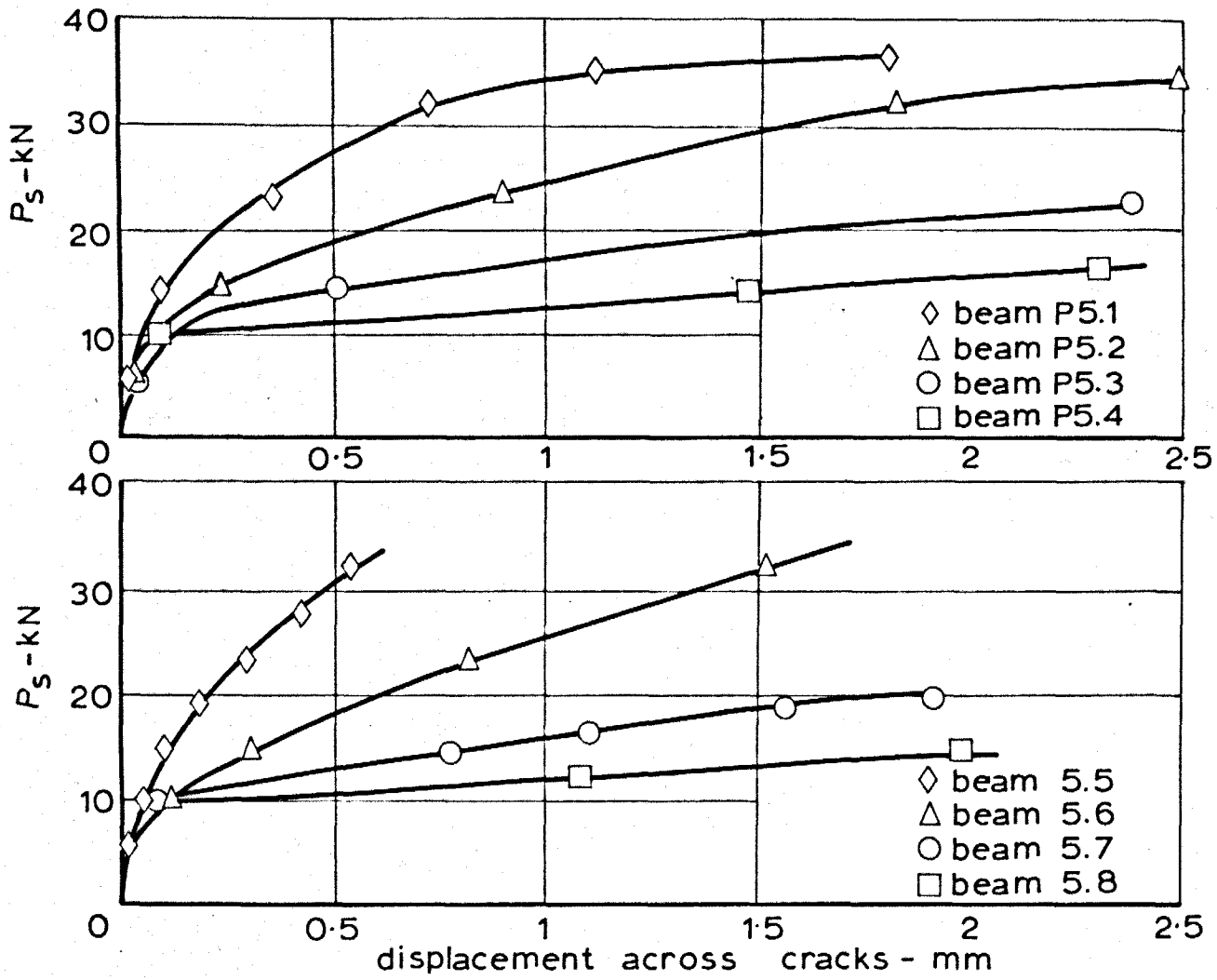

FIG. 5.20 LOAD-DISPLACEMENT PLOT FOR SPECIMENS WITH STIRRUPS

The steel 'encastré beam' strength may be easily calculated.

Assuming that plastic hinges will form at the stirrup and at the pre-formed crack, the following relationship applies.

$$P\,\delta = 2\,M_p\theta \qquad \text{(see Figure 5.21)}$$

$$= 4\,M_p\,\theta \text{ for 2 bars}$$

$$\delta = \theta\, l$$

$$P = \frac{4\,M_p}{l}$$

$$M_p = \frac{2\pi r^2}{2} \times 0{\cdot}424 \times r \times f_y$$

$$= 750 \text{ kN mm}$$

$$P = \frac{4 \times 750}{175}$$

$$= \underline{17 \text{ kN}}$$

where

δ = displacement across dowel

M_p = plastic moment of one bar

r = bar radius

θ = plastic hinge rotation

l = distance from pre-formed crack to stirrups - 150 mm in the case of beam P5.4

f_y = yield stress in reinforcing bar

This figure is higher than the 'beam yield' point of 10 kN from Figure 5.20. This is presumably because the analysis ignores the tensile force in the bar and makes assumptions as to the hinge positions. It is possible to calculate the value of M_p for a given value of T_p, the plastic tensile force in a bar, and to produce an interaction diagram between them, for a circular section.

Figure 5.22 shows a circular section in the plastic state with both moment and direct force upon it.

The following relations apply

$$\frac{T_p}{r^2 f_y} = \pi - \theta + \sin\theta$$

$$\frac{M_p}{r^2 f_y} = \frac{4}{3}\sin^3(\theta/2)$$

These are plotted in Figure 5.23.

A small amount of tensile force will therefore decrease the plastic moment slightly.

From the force at splitting and the geometry of the section it is possible to calculate the steel tensile force and therefore the reduced value of M_p. For beam P5.4 the tensile force in the bar at splitting was 0·1 T_p. From Figure 5.23 the correct value of M_p is therefore 0·98 of the full M_p. The discrepancy between the measured and calculated values of M_p is presumably therefore due to under-estimation of the length of bar 1.

The presence of a stirrup near to a crack can therefore affect the dowel load-displacement relationship in three ways.

(1) If the stirrup is very close to the crack, the dowel strength after splitting is the strength of the stirrup.

(2) When the stirrup is far from the crack, the 'beam strength' may be less than the splitting strength and the stirrup will have no effect on the dowel action.

(3) When the stirrup is at some intermediate position, the dowel strength after splitting is increased to the 'beam strength' of the tension steel.

The change of behaviour between the stirrup being mobilized and the steel acting as a beam can be put in general form by carrying out the previous calculation with the stirrup strength equal to the

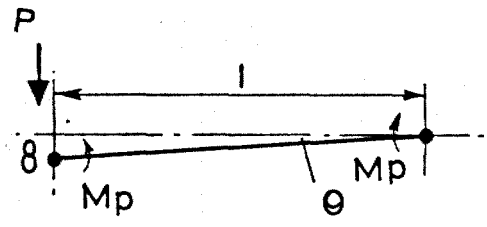

FIG. 5.21 LENGTH OF MAIN STEEL ACTING AS AN ENCASTRÉ BEAM

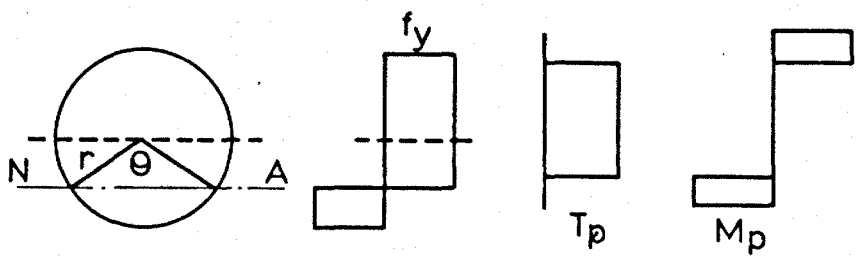

FIG. 5.22 PLASTIC ANALYSIS OF A CIRCULAR BAR

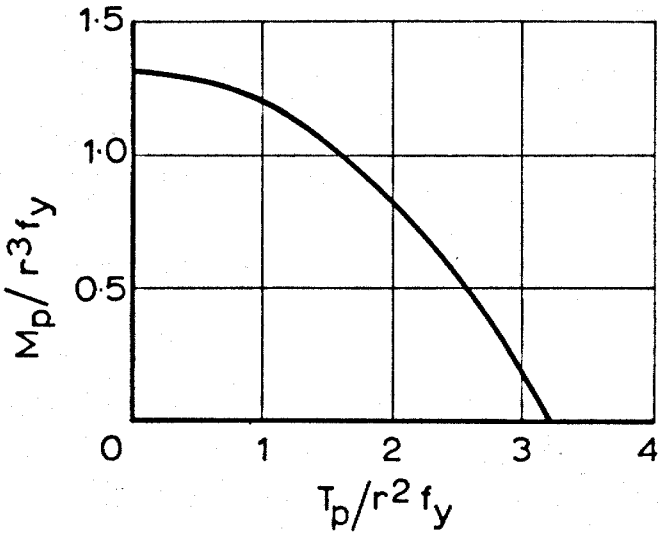

FIG. 5.23 RELATIONSHIP BETWEEN M_p AND T_p

beam strength of the main steel. Figure 5.24 shows the results of this calculation in the form of a graph. The distance l in terms of bar diameters of the main tensile steel may be plotted for the most common ranges of d/d_s, the ratio of the diameters of main steel and stirrup, and f_y/f_s, the ratio of the characteristic strengths of main and stirrup steel.

Thus

$$P = \frac{4M_p}{l} = 2 A_s f_s$$

$l = kr$ $\qquad$ d_s = stirrup diameter

A_s = stirrup area $\qquad$ r_s = stirrup radius

Hence, for a two-bar dowel held by two legs of a stirrup,

$$\frac{4\pi r^2 \, 0{\cdot}424 \, r \, f_y}{kr} = 2\pi r_s^2 \, f_s$$

$$k = 0{\cdot}848 \left(\frac{r}{r_s}\right)^2 \frac{f_y}{f_s}$$

This relation is plotted in Figure 5.24, which shows that close stirrup spacing has to be used if dowel capacity is to be increased to that of the stirrup. This result is therefore of interest in the design of binding reinforcement in plastic hinges carrying heavy shear forces if all the load-carrying capacity is to be realized. The values of k will further be modified by the presence of tensile force in the bar. This may be calculated by referring to Figure 5.23.

It is more difficult to give a general rule as to the transition between stirrup spacings that will achieve the main steel 'beam' strength and those in which the splitting strength is greater, since so many variables are involved.

It is possible in particular cases, however, to calculate quickly this transition from the splitting strength equation and the main steel 'beam' analysis.

This discussion pre-supposes that for a given stirrup spacing

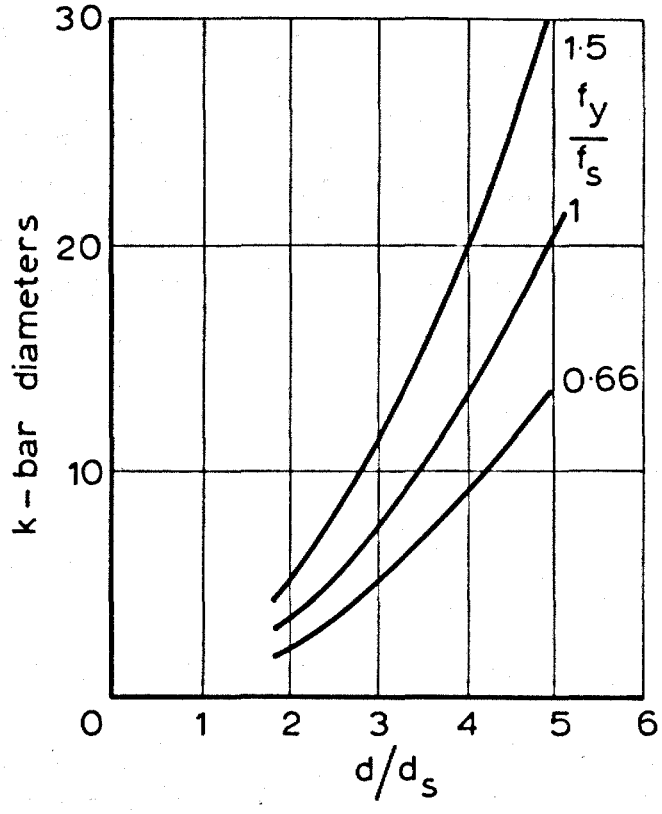

FIG. 5.24 RELATIONSHIP BETWEEN DOWEL LENGTH AND STRENGTH OF ENCASTRÉ BEAM

the flexural-shear cracks will form over the stirrups and that the dowel length to the next stirrup will therefore be the full spacing. In beam tests this happens very often but not always, so that the calculations are only for the most extreme cases that can arise.

It is important also to remember that this discussion concerns only one aspect of stirrup behaviour and not the major effects of the forces carried across inclined cracks and the confinement of the concrete in the compression zone.

Discussion of Results

The significance of the dowel forces measured in these tests are discussed at the end of the next chapter, together with a discussion of the forces carried across cracks by mechanical interlocking of the aggregate.

CHAPTER 6

SHEAR FORCE CARRIED BY AGGREGATE INTERLOCK ACTION

REVIEW OF PREVIOUS WORK

The results of the tests described in the last two Chapters show that the shear force on a beam is distributed over the whole of its section. For a typical case, Beam 9, the shear force in the compression zone of the beam at failure was about 20% of the total shear force and the ultimate dowel capacity of the reinforcement layout was 15 kN, 17% of the total shear force. These percentages are in general agreement with Fenwick's conclusions stated at the end of Chapter 3. The rest of the shear force in a beam must therefore be carried by interlocking of the aggregate. The average value of the interlock shear stress may be found by dividing the shear force not carried by the compression zone and by dowel action by the area of the crack. In the case of beam 9, the stress is 0·85 N/mm^2.

A reinforced concrete beam carrying bending and shear is shown in Figure 6.1. The lower part of the Figure shows a small section of one of the cracks. In the tests on beams described in Chapter 3 it was possible to measure the displacements across the cracks and these show that displacements in the vertical direction, parallel to the cracks (Δ_v in Figure 6.1) do occur and that they are of sufficient magnitude for the opposite sides of the cracks to touch at some points. Figure 6.2 shows a close-up photograph of a shear crack at a late stage in a test on a beam. The interlocking of aggregate particles can clearly be seen and, in the centre of the picture, some spalling of the concrete is visible over the interlocking particles. This kind of behaviour is characteristic of inclined cracks in beams carrying loads near to their ultimate strength; it is never seen in vertical cracks in areas of constant moment and zero shear.

Two tests have been carried out by Gergely[31], one of which corroborates these findings about the magnitude of the interlock force. Gergely cast two beams of the type shown in Figure 6.3. In one shear span, an inclined crack was pre-formed by casting a 1·6 mm wide oiled plate into the beam and removing this plate after the

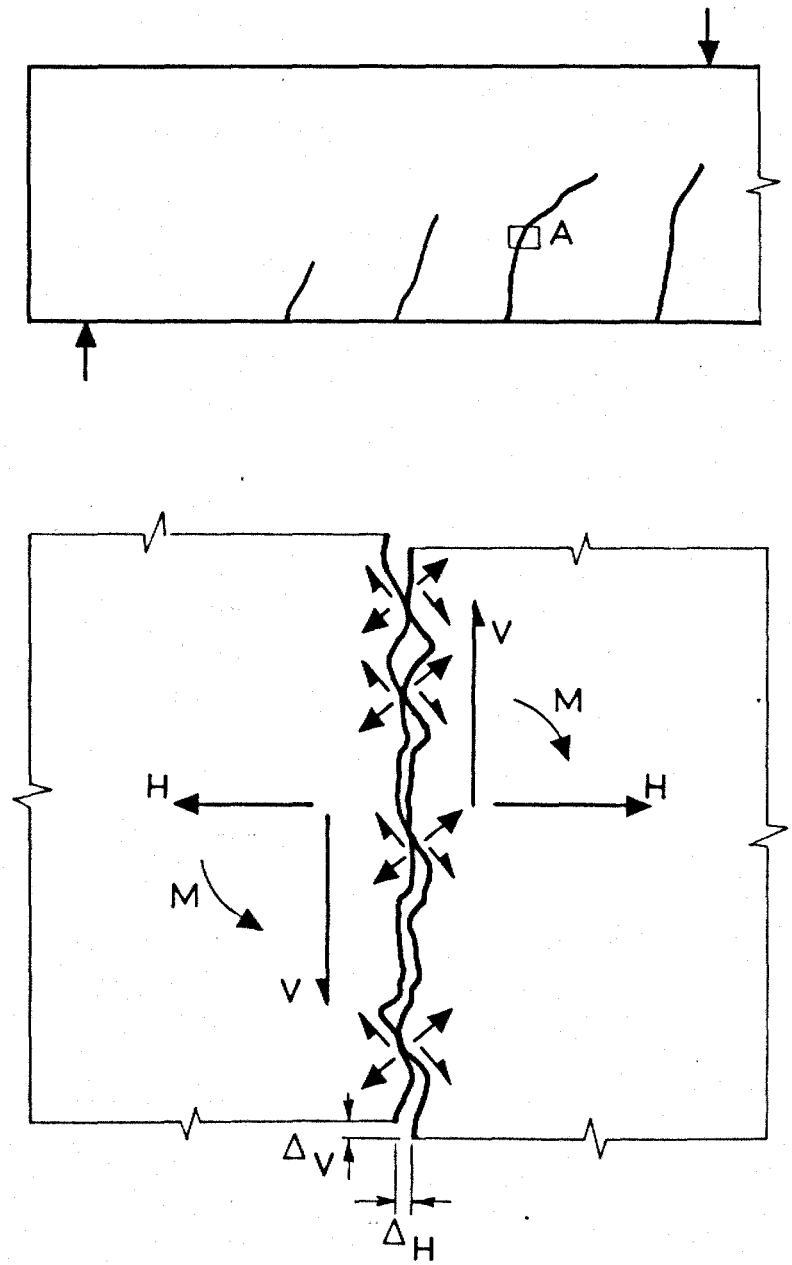

enlarged view of section A

FIG. 6.1 SCHEMATIC ILLUSTRATION OF AGGREGATE INTERLOCK

Fig. 6.2 Shear crack showing interlocking aggregate only

concrete had set. The other end of the same beam was cast without a pre-formed crack. Thus a comparison between the ends of the beam shows the effect of eliminating aggregate interlock over the area of the pre-formed crack.

These beams were made to the same dimensions as the beams reported on in Chapter 4 and may therefore be compared with the results of those tests. Gergely's test can only show whether or not aggregate interlock forces are significant and cannot be used quantitatively as the stiffnesses of the two ends of the beam are not the same. In order to estimate the shear force carried in the compression zone of the beam, Gergely used the first method of analysis in Chapter 4. The results of Gergely's test on one beam, with a ratio of shear span to effective depth. a/d_1, of 3·02 and with a tensile steel percentage of 1·03, may therefore be compared with the test results for beam 1 in Chapter 4.

The test results are shown in Table 6.1. The two results for beam 1 are from opposite ends of the beam. The concrete strengths are the cube strengths taken when each end of the beam was tested. These compare directly with Gergely's test (a) which was on the end of his beam without a pre-formed crack. A range of concrete strengths is given for Gergely's test as he did not report the exact strength but stated that he used the same mix as that used in his dowel test series. The upper three test results in Table 6.1 therefore give the scatter that can be expected from identical shear tests.

TABLE 6.1
Comparison between tests by Gergely[31] and those in Chapter 4.

Test	Ultimate shear strength (kN)	150 mm cube strength (N/mm^2)
beam 1	65	36·5
	79·5	42·0
Gergely (a)	71	24·2 to 37·0
Gergely (b)	33·5	24·2 to 37·0

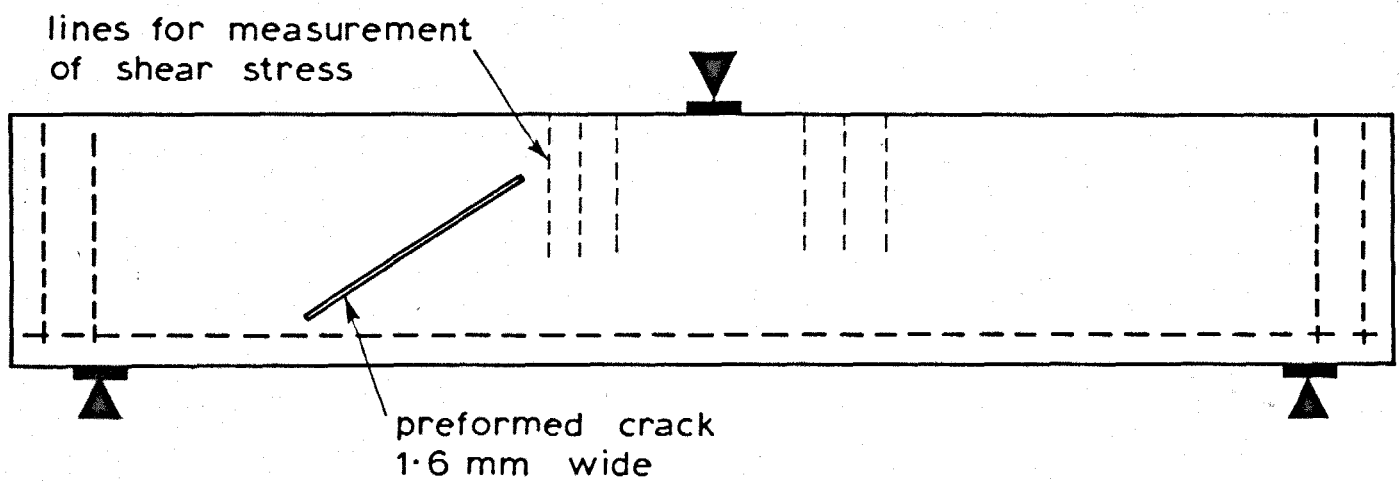

FIG. 6.3 TEST SPECIMEN USED BY GERGELY

The result of Gergely's test (b), the test on the end with the pre-formed crack, is significantly lower than the others. Allowing for the differences in the shear carried by the compression zone and by dowel action in each test, Gergely estimated that 45% of the total shear force of end (a) was being carried by aggregate interlock.

In his second test Gergely carried out the same procedure with a beam which had an a/d_1 ratio of 2·48. In this case, although the end without the pre-formed crack behaved satisfactorily and the shear forces in the compression zone were calculated, the other end of the beam behaved as a tied arch and was as strong as the sound end. This behaviour is analogous to that found by Leonhardt and Walther[13] when they tested beams with good steel anchorage and poor bond. In this case, also, tied arch action occurred and the beams had an increase of shear strength over the beams with good bond. This second test by Gergely, as Gergely himself pointed out, does not therefore provide a valid comparison to determine the significance of aggregate interlock as interlock was not involved in the behaviour of the beam.

The tests described so far, although they provide evidence of the significance of aggregate interlock forces, do not provide any reliable quantitative information.

A series of tests has been carried out by Fenwick[24] in which aggregate interlock forces were assessed from tests on concrete plates. In this case, the tests were not on beams and should therefore have included displacements to simulate those that occur in beams. The test rig used is illustrated in Figure 6.4. A large number of 50 mm x 50 mm x 350 mm concrete blocks were cast with a groove across the centre of each block. This groove was used to initiate a crack which passed right through the specimen. The shear transfer across this crack was then studied by securing the block to the test rig and shearing one end relative to the other. A series of tests was carried out for various values of crack width and concrete strength. Each test was carried out with a constant crack width, the crack width being adjusted after each application of shear force by applying a normal force across the crack. The results of these tests

are summarized in Figures 6.5 and 6.6. Each of the lines on these Figures comes from the combined results of six tests; the scatter of the six results about one typical line is shown in Figure 6.6. It can be seen that large stresses are possible, particularly with small crack widths. The value of average shear stress mentioned previously, 0·85 N/mm^2, is clearly possible and is in fact low compared with the ultimate stresses shown here. Unfortunately, the displacement pattern selected by Fenwick is not the same as that found in beams. In beams the cracks open and shear simultaneously, i.e. they do not shear with constant crack width. The additional normal forces applied in these tests must have had the effect of considerably enhancing the interlock stresses.

Ideally, an aggregate interlock test should be carried out either on a beam, in conditions where displacements can be controlled and all the forces measured, or in a separate test rig where the beam displacements can be simulated. Both types of test have been used and the results of this work are given later in this chapter.

TEST PROGRAMME

Two types of test were carried out in this investigation. The first was a displacement-controlled test on an unreinforced concrete block and the second was a test on a beam with a pre-formed crack and with sufficient instrumentation to enable the interlock forces to be calculated.

BLOCK TESTS

In order that the measured displacements across shear cracks in beams could be modelled the interlock tests were conducted in a rig in which the ratio of normal to shear displacement could be changed between tests but was constant during the test. The rig that was designed is shown in diagrammatic form in Figure 6.8. The test specimen, with a pre-cracked section 127 mm long and 140 mm wide, is bolted to a pair of linked crossheads. The lower crosshead is bolted to a test frame and the upper crosshead pulled horizontally. The linkage system ensures that vertical and horizontal displacements are induced. By casting the test blocks with the crosshead-fixing grooves at varying spacings, it is possible to set up the specimen

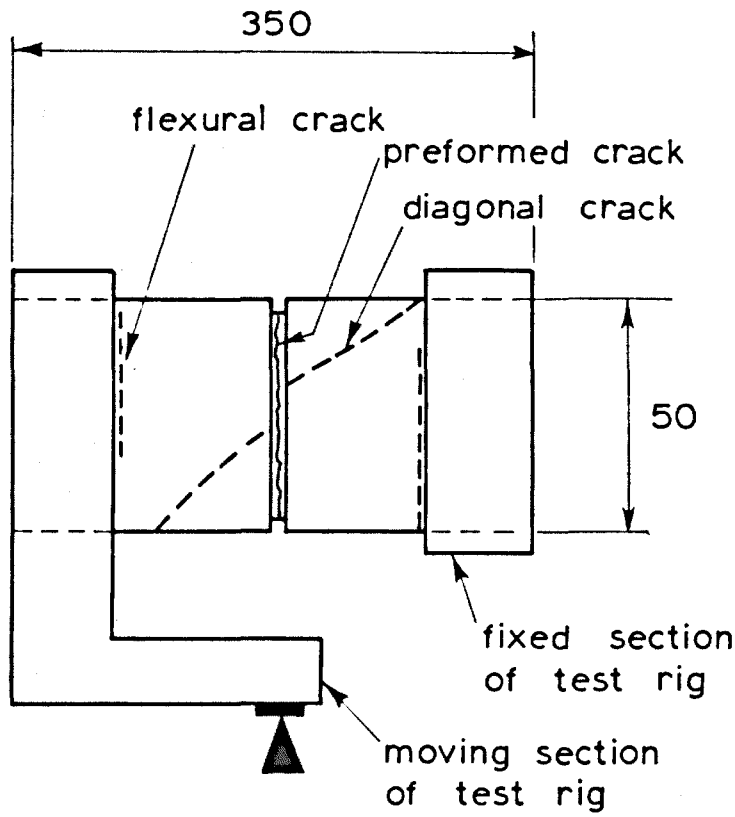

FIG. 6.4 TEST METHOD USED BY FENWICK

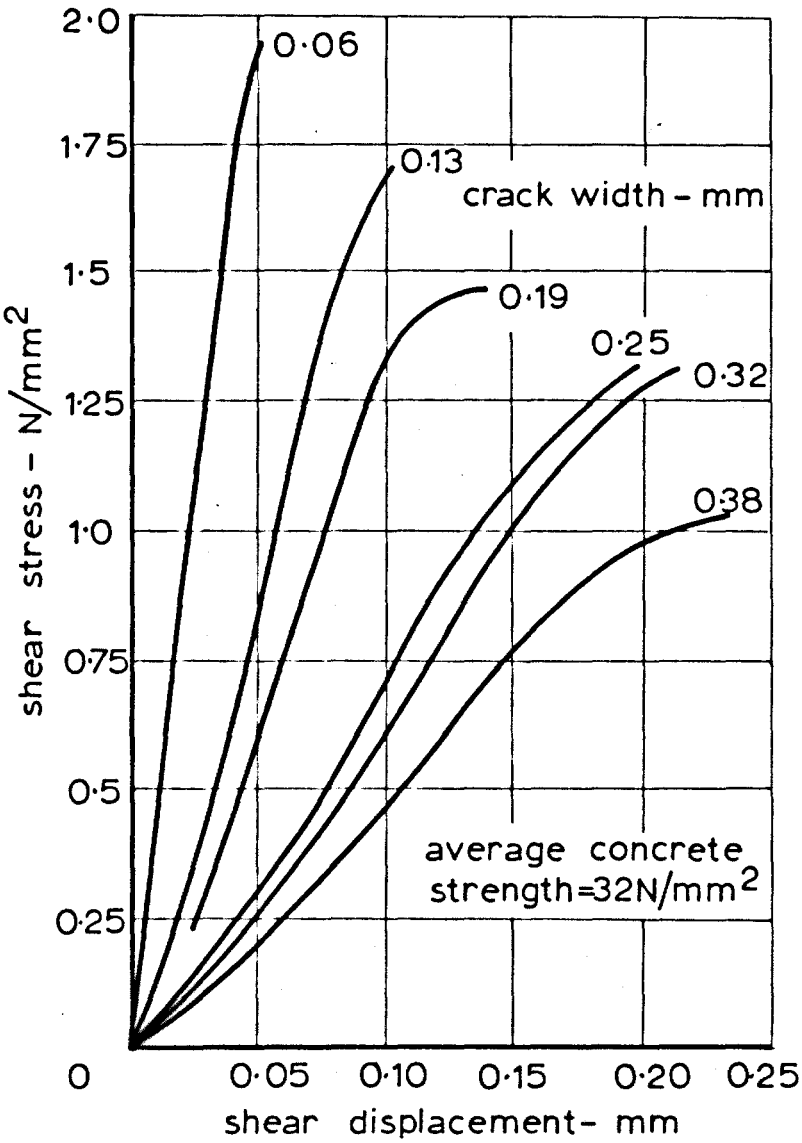

FIG. 6.5 TEST RESULTS – FENWICK

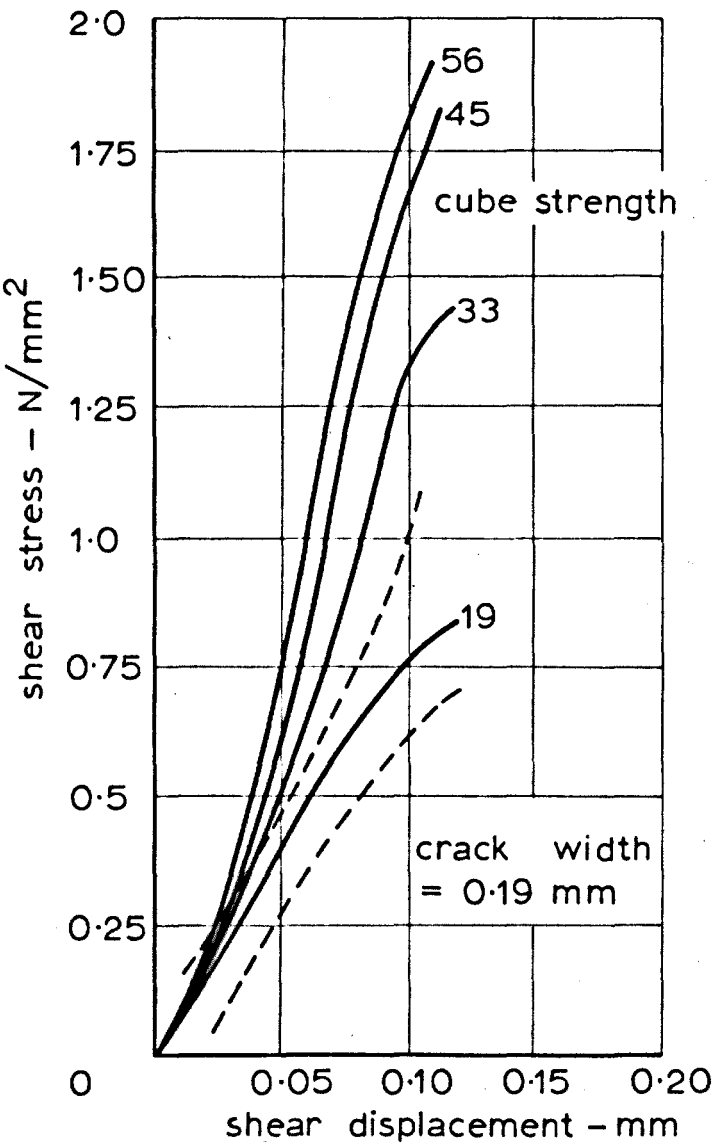

FIG. 6.6 TEST RESULTS – FENWICK

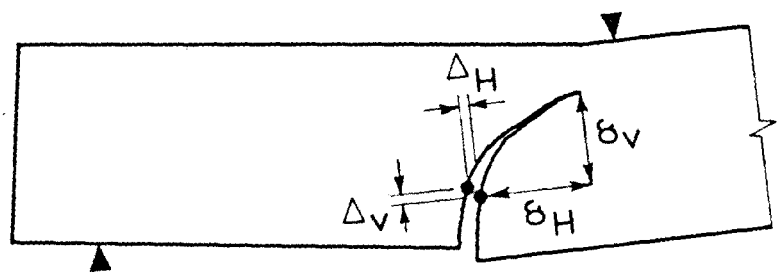

FIG. 6.7 DISPLACEMENT PARAMETERS

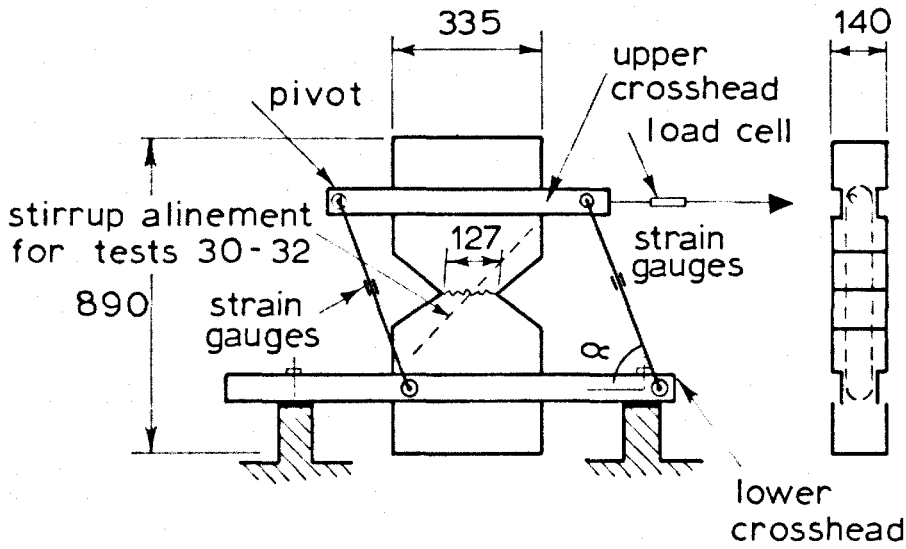

FIG. 6.8 SCHEMATIC ILLUSTRATION OF AGGREGATE INTERLOCK TEST

with varying values of the angle α ; each value, for the small displacements used in the test, defines a different value of the ratio of normal to shear displacement.

Displacements across cracks in beams were measured in the vertical and horizontal directions, giving the ratio Δ_V/Δ_H. These displacements may be converted to the normal and shear displacements across the crack once the slope of the crack at that point is known. In the interlock tests, the displacements were measured in the latter form and in this chapter have been denoted Δ_N and Δ_S respectively. Thus Δ_N/Δ_S is defined as $\cot\alpha$. The forces in the system were measured by a load cell in the pulling system and by strain gauges fixed to the freely pivoting ties between the crossheads. Tests were carried out initially on the rig which indicated that the friction in the pivoting arms of the system was small and was not significant in comparison with the other forces that were to be measured.

Test series

The major variables that were considered to affect the problem were:

displacement ratio Δ_N/Δ_S;
concrete strength;
aggregate size;
aggregate type.

The effect of these variables was studied in a total of 35 tests. The complete test programme is summarized in Table 6.2.

Series 1: 6 tests. This series was carried out to investigate the scatter of results from the test method and rig.

Series 2: 8 tests. These tests were carried out to investigate the effect of the displacement ratio and aggregate size. The displacement ratio was varied between 2.145 and 0.268, the range that was found in the beam tests. The values of Δ_N/Δ_S that were used, 2.145, 1.0, 0.466 and 0.268, correspond to α values of 25°, 45°, 65° and 75°.

Series 3: 6 tests. These tests were carried out to determine the effect of concrete strength on the interlock force.

Series 4: 12 tests. These tests were carried out to study the effect of using different types of aggregate. Thames Valley gravel, rounded gravel, limestone and lightweight aggregate were used.

Series 5: 3 tests. These tests were carried out to find out whether the test rig could be used to find the effect of stirrups on interlock.

Test procedure

The test blocks were cast, three at a time, in timber moulds. The formwork was stripped after one day and the specimens were then cured under damp sacking and polythene for seven days.

The following mix designs were used.

Mix with 9 mm aggregate

9 mm aggregate	60%
sand	40% by weight
aggregate/cement ratio	4·5
compacting factors as in Table 6.2	

Mix with 19 mm aggregate

19 mm aggregate	25%
9 mm aggregate	38%
sand	37% by weight
aggregate/cement ratio	5·5
compacting factors as in Table 6.2	

Lightweight aggregate (Lytag)

Lytag medium	58%
Lytag fine	42% by weight
aggregate/cement ratio	3·25
water/cement ratio	0·92
dry density at 28 days	1680 kg/m^3

TABLE 6.2

Details of block test specimens

Series	No.	$\frac{\Delta_N}{\Delta_S}$	Aggregate size		Compacting factor	Aggregate type			
			19 mm	9 mm		gravel	rounded gravel	limestone	lightweight
1	1	1·0	*		0·9	*			
	1R	1·0	*		0·9	*			
	2	1·0	*		0·9	*			
	2R	1·0	*		0·9	*			
	3	1·0	*		0·9	*			
	3R	1·0	*		0·9	*			
2	4	2·145	*		0·9	*			
	5	1·0	*		0·9	*			
	6	0·466	*		0·9	*			
	7	0·268	*		0·9	*			
	8	2·145		*	0·9	*			
	9	1·0		*	0·9	*			
	10	0·466		*	0·9	*			
	11	0·268		*	0·9	*			

Continued /....

TABLE 6.2 Continued /....

3	12	1·0	*		0·85	*			
	13	1·0	*		0·85	*			
	14	1·0	*		0·89	*			
	15	1·0	*		0·89	*			
	16	1·0	*		0·94	*			
	17	1·0	*		0·94	*			
4	18	1·0	*		0·91		*		
	19	1·0	*		0·91		*		
	20	1·0	*		0·91		*		
	21	1·0	*		0·91			*	
	22	1·0	*		0·91			*	
	23	1·0	*		0·91			*	
	24	1·0	*		0·91				*
	25	1·0	*		0·91				*
	26	1·0	*		0·91				*
	27	1·0	*		0·91			*	
	28	1·0	*		0·91			*	
	29	1·0	*		0·91			*	
5**	30	1·0		*	0·91	*			
	31	1·0		*	0·91	*			
	32	1·0		*	0·91	*			

** Series 5 - all blocks had 6 mm stirrups across the crack.

After the blocks were cured, they were brought into the laboratory and were dried for two weeks before being tested. The blocks were pre-cracked before they were set up in the test rig, by first applying a slight prestress normal to the grooved section in the block and then bending the block by means of a jack as shown in Figure 6.9, to form a flexural crack right across the groove. The crack was formed flexurally, rather than in direct tension, as the cracking in beams that the rig simulates is formed in flexure. The maximum width of the crack just after its formation was 0·1 mm; under the action of the prestress, this closed immediately the block was taken out of the cracking rig.

After cracking, the linked crossheads were bolted round the block and the lower crossheads were secured by filling any small gaps left in the fixing grooves with building plaster. The upper crossheads were only loosely bolted at this stage. The block with its crossheads was then lifted onto the rest of the test rig and the prestress on the block was released. Any gaps between the lower crossheads and the test frames were filled with steel shims and the crossheads were securely bolted to the frame. In some cases the pre-formed crack opened slightly at this stage; when this occurred, the crosshead was released and more shims were packed under it. This enabled the lower crosshead to be secured in the rig without any opening of the crack in all but a few cases where distortions of the block made some opening inevitable, Finally, the upper crossheads were bolted firmly and the gaps around them were plastered. The rig, with a specimen in it, is shown in Figure 6.10.

The specimens were tested by applying small increments of load to the jack which pulled the top of the specimen horizontally. The forces in the ties linking the crossheads and in the load cell in the pulling mechanism were measured, and the displacement across the crack, in the vertical direction only, was measured with a Demec gauge of 50 mm gauge length. At later load stages attempts were made to apply increments of displacement rather than increments of load to the blocks.

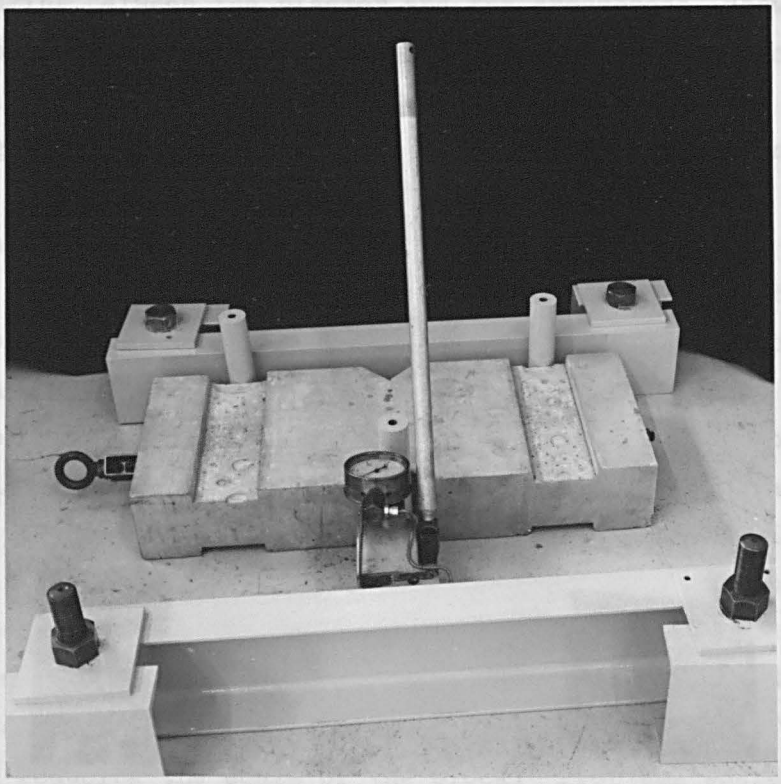

Fig. 6.9 Test block cracking rig

In the initial trial tests, which are not reported, and in the first tests of Series 1, the crack did not open uniformly, the front tending to bind while the rear part opened. This was accompanied by cracking between the plaster and the crossheads, showing that some rotation of the block was occurring. Finally, failure occurred by an inclined crack forming half-way along the pre-formed crack and running to the point where the crosshead joined the front of the block. This kind of failure is analogous to that found by Fenwick as illustrated in Figure 6.4. This problem was finally overcome by adding extra restraints to the blocks to prevent the rotation from developing. The arrangement of these additional bolts can be seen in Figure 6.11. (The block shown in this Figure is one with a stirrup across the crack and the failure mechanism is not typical of the behaviour of the unreinforced blocks.) The modification of the rig helped considerably in keeping the crack parallel-sided as it opened, but the initial binding of the front of the crack still occurred in some cases. Because of the very small displacements involved, it would be almost impossible to force the sides of the crack to remain parallel without increasing the scale of the test rig and reducing the scale of the block. Problems would then arise in designing load-measuring devices on the rig to work with adequate sensitivity.

Test results

A typical test result, for block 20, is shown in Figure 6.12. The upper curve is the relation between shear stress and displacement and the lower curve the relation between normal stress and displacement; a positive normal stress denotes compression across the crack. The horizontal line denoted by f_{Su} indicates the ultimate interlock stress that was measured. The displacement that is recorded on the graph is the normal displacement, the crack width. This normal displacement is related to the shear displacement by the set-up of the rig; the ratio between them, Δ_N/Δ_S, is given in Table 6.2. The full set of results is shown in Table 6.3 where the material strength, f_{Su} and the normal ultimate stress f_{Nu}, are all recorded.

The shape of the shear stress-displacement curve was generally of the type shown in Figure 6.12 except where the upper block gripped

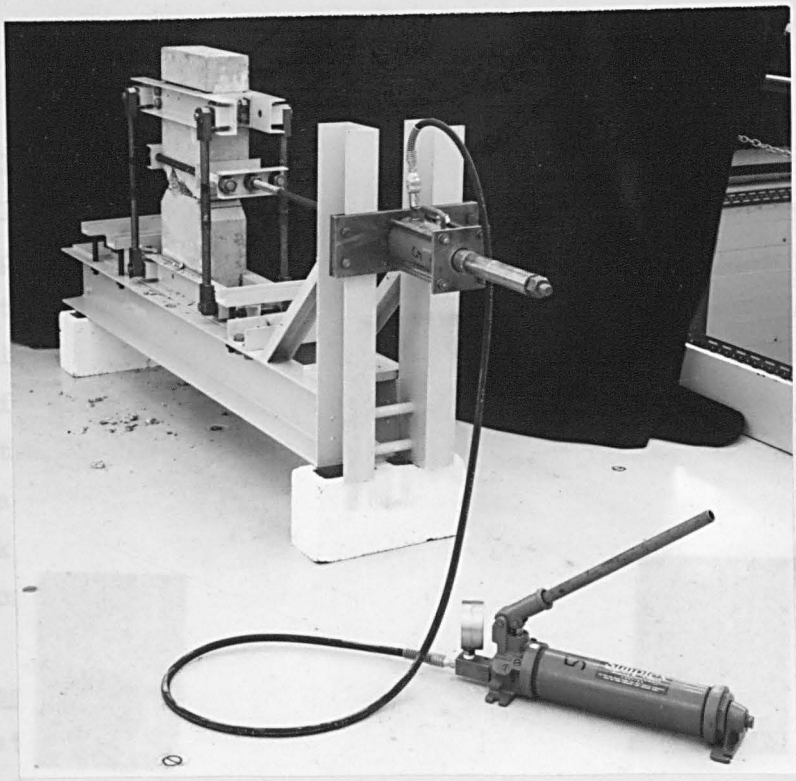

Fig. 6.10 Aggregate interlock test rig

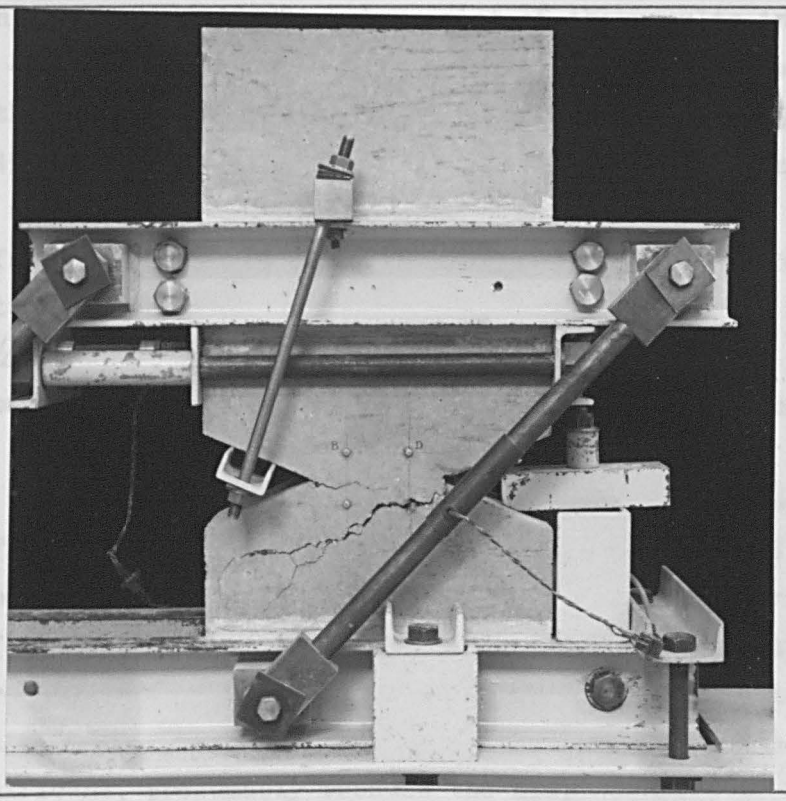

Fig. 6.11 Modification to test rig

the lower one. In these cases the curve was steeper until the block finally separated, when the slope changed abruptly. The cases where gripping occurred at the front of the block are marked in Table 6.3 together with the cases where one side of the crack opened significantly more than the other. In these cases the order of magnitude of the differential movement between one side of the crack and the other was about ten. The reason for this behaviour appears to have been a lack of symmetry of the crack: on one side of the block the crack was straight while on the other side, which gripped, the crack had undulations.

Series 1. The results of the tests on series 1 blocks show the variations that can occur with nominally identical specimens. It was after the first three blocks of this series were tested that the rig was modified as shown in Figure 6.11.

Series 2. The results of series 2 showed the effect of different displacement patterns on both the strength and ductility of interlock. Clearly there is a relationship between f_{Su} and Δ_N/Δ_S, as can be seen in Figure 6.15 which is a plot of the results in Table 6.3. The effect of Δ_N/Δ_S on the ductility of interlock was most marked. In the tests on blocks 4 and 8, which had high Δ_N/Δ_S values of 2.145 (i.e. the crack opened 2.145 times further than it sheared), the upper half of the block suddenly lifted clear of the lower half at failure. The curve of f_S/f_{Su} against Δ_N Figure 6.13) did not flatten appreciably. At the other extreme, blocks 7 and 11, with Δ_N/Δ_S values of 0.268, had considerable ductility; failure was accompanied by spalling of the concrete along the face of the crack.

The results of the tests on the series 2 blocks are plotted in Figure 6.13. Tests 4 and 8, 5 and 12, 6 and 10, 7 and 11 are comparable as far as the shape of the curve is concerned: the difference between each pair is that tests 4 to 7 used 19 mm gravel aggregate and tests 8 to 11 used 9 mm gravel aggregate. The effect of aggregate size variation in this range did not appear to be very significant, presumably because the displacements were small compared with the aggregate size. The 9 mm aggregate had interlock strengths between 61 and 100 percent of the 19 mm aggregate interlock strengths.

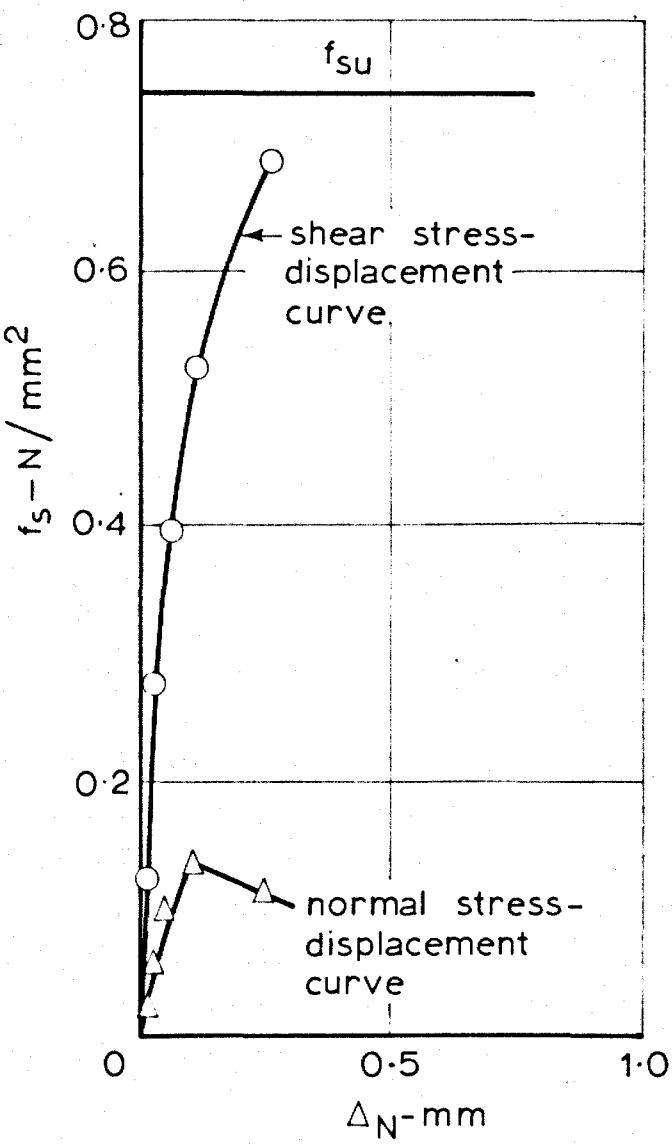

FIG. 6.12 TYPICAL TEST RESULTS

The test result on block 9 in which the sides of the crack gripped badly during the test has not been plotted with the result of the block 5 test in Figure 6.13; tests 9 and 12 are comparable and this latter result has therefore been substituted. The test results in Figure 6.13 have been plotted in terms of f_S/f_{Su} so that the shape of the curves may be compared. The trilinear curves that have been drawn represent a simple rationalization of the block behaviour. The co-ordinates of the turning points are:

f_S/f_{Su}	Δ_N(mm)
0·55	0·06
0·7	0·15
1·0	Δ_{Nu}

The ultimate value of Δ_N, Δ_{Nu}, varies with Δ_N/Δ_S and is plotted in Figure 6.14. For any value of Δ_N/Δ_S within the range tested, the value of Δ_{Nu} may be read from this Figure and the curve of f_S/f_{Su} against Δ_N may be reconstructed. Before these curves may be used quantitatively, a value of f_{Su} must be determined. This is subject to a considerable amount of scatter, but a plot of f_{Su} against Δ_N/Δ_S is shown in Figure 6.15. A straight-line relationship has been assumed to exist. The typical results already given in Figure 6.12 show a plot of the normal stress that existed across the crack as well as the shear stress; the full list of the ultimate normal stresses is given in Table 6.3. The test results from series 2 may also be studied to determine the relation between normal stress and displacement as well as that between shear stress and displacement.

Figure 6.16 shows plots of normal stress against displacement in a form similar to that of Figure 6.13. It may be seen that the peaks of the normal stress curves occur before the shear stress curves shown in Figure 6.13 reach their maximum values and that after this the stress reduces and sometimes becomes tensile. This result may be because the opposite sides of the crack are so rough that they produce frictional forces as they are moved away from each other for large displacements whereas, in the case of the initial small movements, these frictional forces do not develop. The fact that the falling branches of the curves on Figure 6.16 show an increase

TABLE 6.3

Block test results

Series	No.	150 mm cube strength (N/mm^2)	f_{Su} (N/mm^2)	f_{Nu} (N/mm^2)
1	1		0·688*	0·16
	1R	37·6	0·791	0·20
	2		0·950	0·30
	2R	37·6	0·812*	0·28
	3		0·899	0·26
	3R	40·6	0·623	0·14
2	4	32·2	0·309*	0·19
	5	32·2	1·214	0·13
	6	32·2	1·000	0·27
	7	32·2	1·109	0·27
	8	31·8	0·278*	0·19
	9	37·5	0·74*	0·26
	10	31·8	1·013	0·30
	11	31·8	0·814	0·30
3	12	40·7	1·058	0·16
	13	40·7	1·087	0·32
	14	48·5	1·251*	0·33
	15	48·5	1·381**	0·43
	16	30·0	0·973	0·34
	17	30·0	0·864*	0·22
4	18	51·5	0·691	0·15
	19	51·5	0·775	0·15
	20	51·5	0·735	0·15
	21	52·8	0·742	0·24
	22	52·8	0·496	0·10
	23	52·8	0·766	0·16
	24	32·2	0·571	0·15
	25	35·0	0·508**	0·11
	26	41·0	0·418	0·11
	27	29·4	0·561	0·23
	28	30·0	0·897*	0·25
	29	30·0	0·911**	0·35

Continued /....

TABLE 6.3 Continued /....

5	30	51•0	2•600	0•87
	31	51•0	2•840	0•87
	32	54•0	2•582	0•94

* block gripped at the front

** block gripped at the side

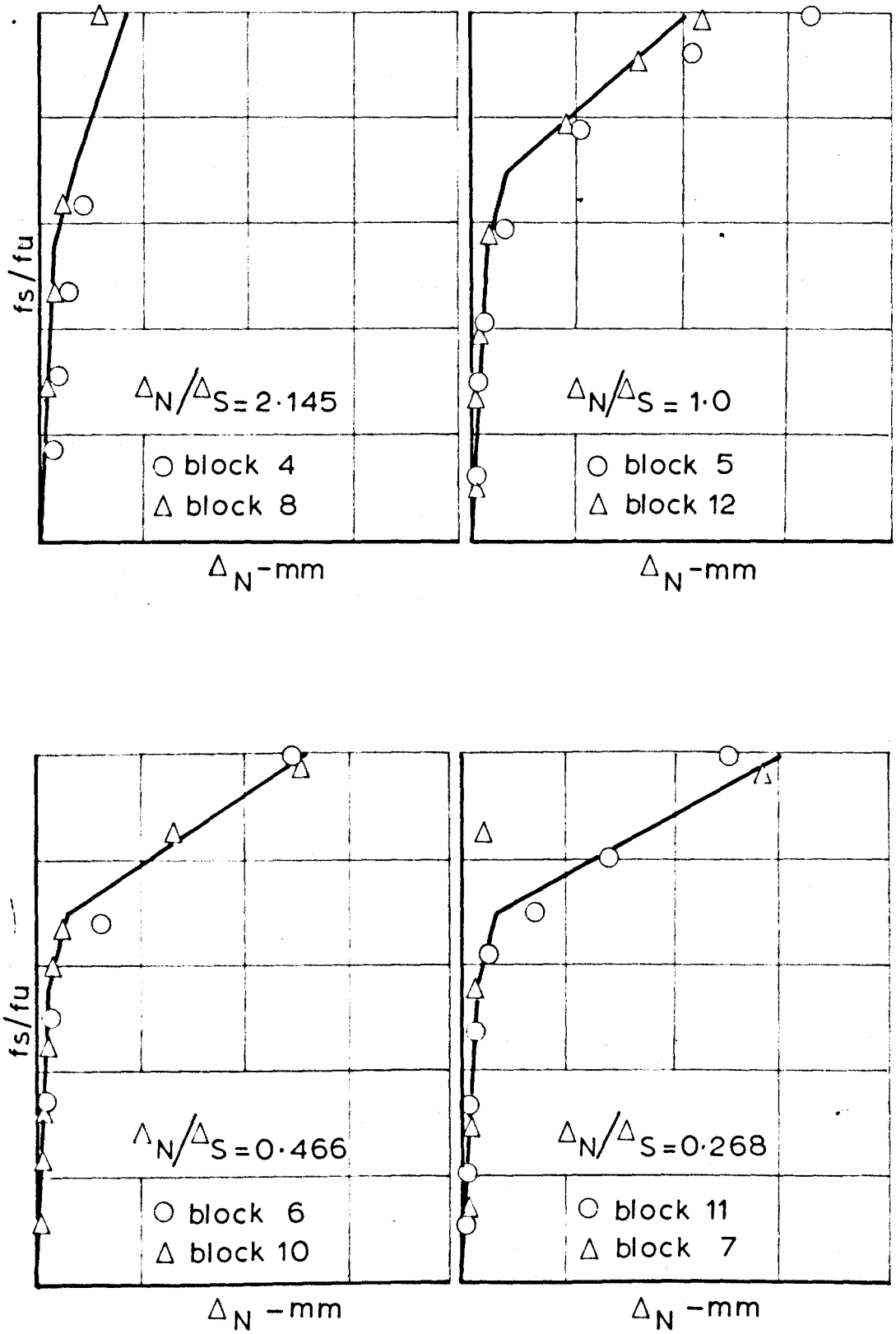

FIG. 6.13 TEST RESULTS, SERIES 3:
SHEAR STRESS - DISPLACEMENT PLOTS

of slope with an increase of Δ_N/Δ_S is evidence that this hypothesis is correct. It is nevertheless proper to treat this result with caution until more work is done on the subject.

Figure 6.17 shows the relationship between f_{Nu} and Δ_N/Δ_S. This Figure is plotted in a similar form to Figure 6.15. The fact that these normal forces exist is not unexpected and they may have to be assessed before the equilibrium equations 1 and 3 can be satisfied.

Series 3. Series 3 specimens were tested to see if there was a simple relationship between interlock strength and concrete strength. The results of Fenwick's tests, shown in Figure 6.6, indicate that concrete strength does affect interlock strength. The effect becomes less marked, however, as the concrete strength is increased. There is not a great variation of interlock strength for normal structural grades of concrete with cube strength between 33 and 45 N/mm^2.

The results of all the tests in this investigation are shown plotted in Figure 6.18. In this case, within the range of strength covered, a linear relationship has been assumed between f_{Su} and concrete strength with the exception of three of the tests from series 4, in which limestone aggregate was used.

Series 4. The results of the tests on series 4 blocks give more information on the effect of the concrete properties, including strength and aggregate type. Within limits, it can be estimated that aggregate interlock strength depends on concrete strength, but that the type of aggregate is also important.

The test results show that the type of aggregate is important and that the parameter is probably the relative strength of aggregate and matrix within the concrete. Although the highest stresses in concrete systems are in the matrix, because the aggregate produces stress concentrations, Swamy[32] has shown that the strength of the aggregate-matrix bond is low and that the failure of concretes of normal strength is probably caused by a breakdown of this bond.

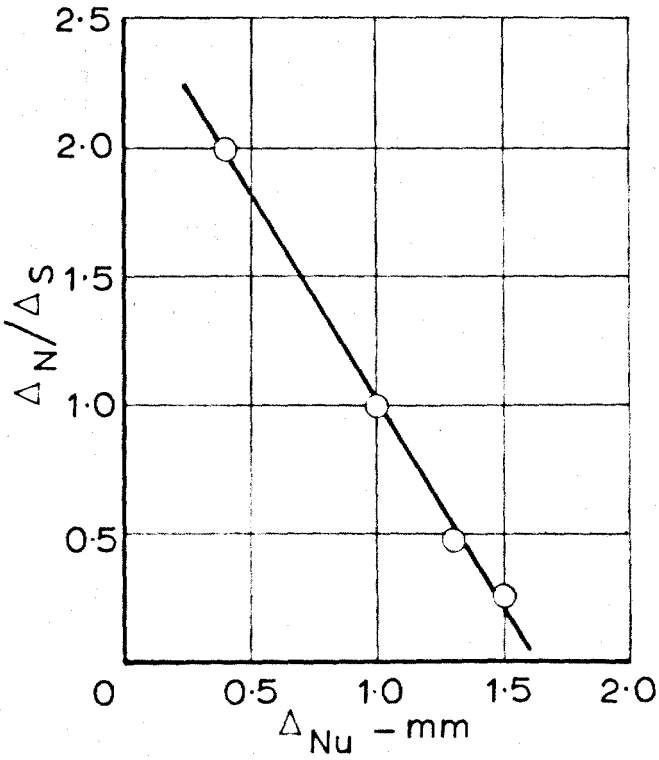

FIG. 6.14 ULTIMATE DISPLACEMENTS OF INTERLOCKING CRACK

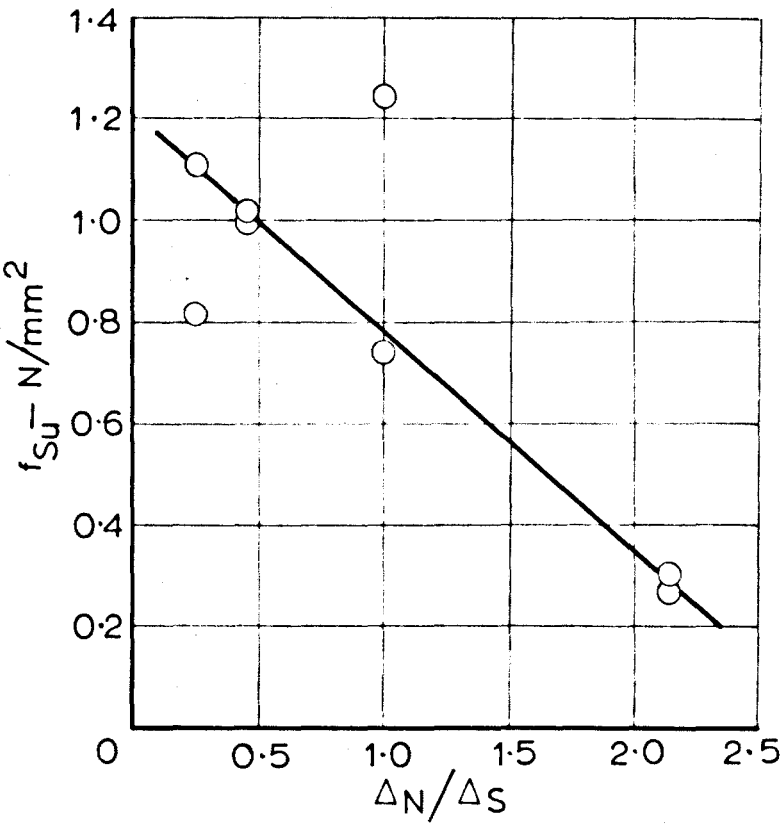

FIG. 6.15 ULTIMATE SHEAR STRESSES ACROSS INTERLOCKING CRACK

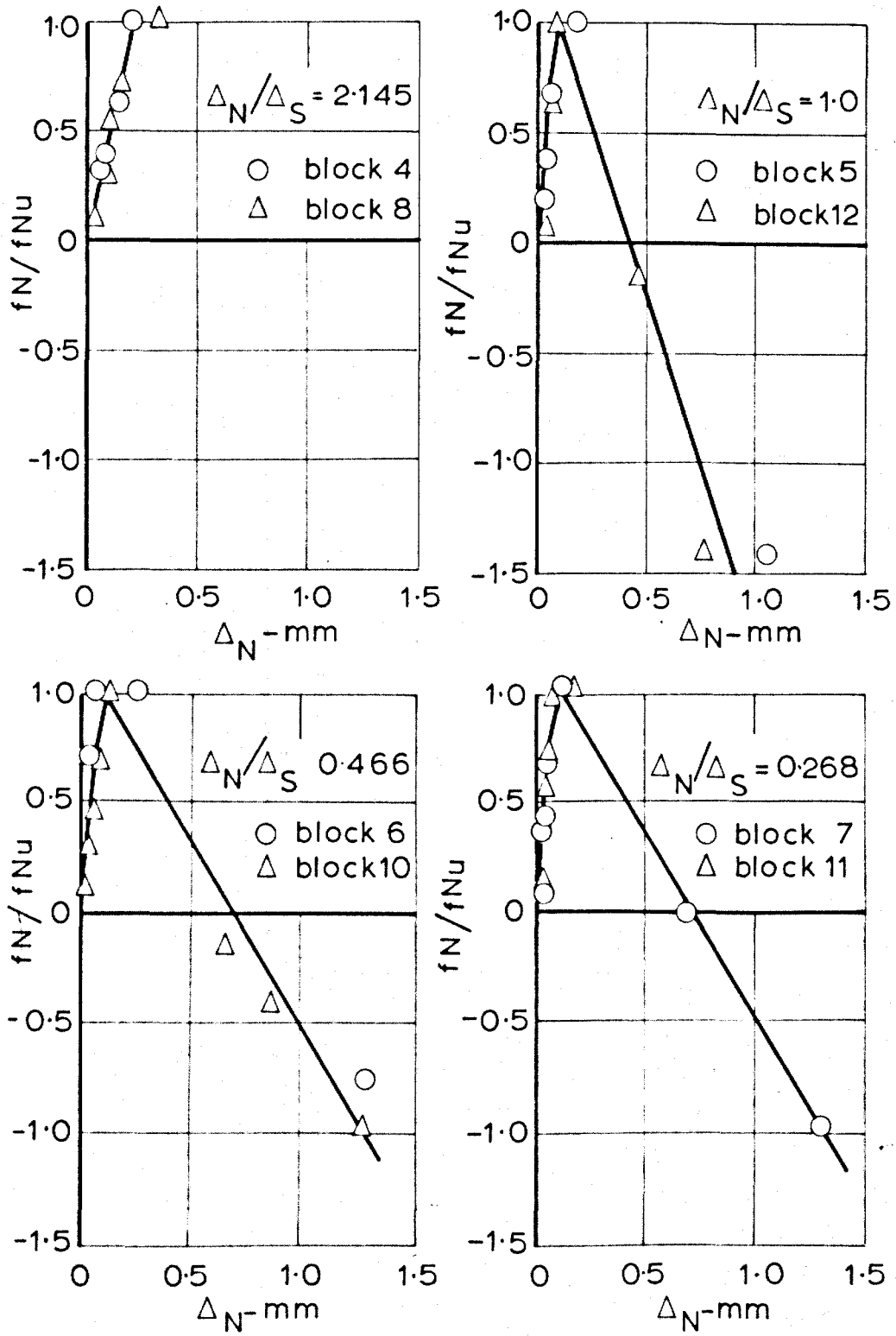

FIG. 6.16 TEST RESULTS, SERIES 3: NORMAL STRESS - DISPLACEMENT PLOTS

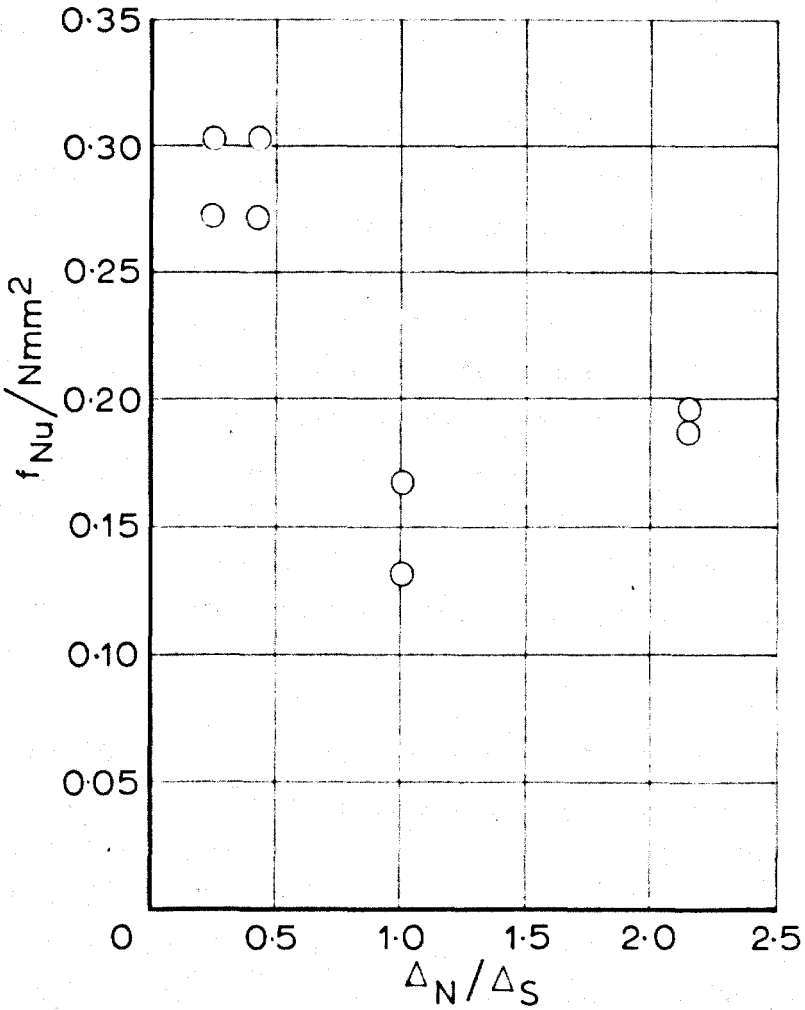

FIG. 6·17 ULTIMATE NORMAL STRESSES ACROSS INTERLOCKING CRACK

Figure 6.19(a and b) shows the cracked surfaces of typical blocks. The first illustration shows the surface of a block with 9 mm gravel aggregate and the second illustration shows the surface of a block with a rounded 19 mm gravel aggregate. In each case it is apparent that, whenever it was possible, the aggregate-matrix bond failed when the crack formed. These surfaces therefore have the maximum roughness that is possible.

Figure 6.19c shows the cracked surface of block 22, a block with limestone aggregate in the mix. The cracked surface here is much flatter than the previous ones as the concrete was stronger and the aggregate failed as the crack formed. In this case the interlock strength was also low. Because of this, the tests with limestone aggregate were repeated with a lower strength mix (tests 27-29) and this time the crack surface passed round the aggregate. The three blocks all had a higher interlock strength than block 22, and two of the values of interlock strength were higher than all three of the values from tests 21-23. Thus a decrease of concrete strength gave an increase of interlock strength. The results of tests 21-23 and 27-29 are included in Figure 6.18.

Figure 6.19d shows the cracked surface of a block containing Lytag. In this case, there is only a little aggregate failure and these blocks had interlock strengths between 0·4 and 0·57 N/mm^2. The cracked surfaces of lightweight concretes of other types have been studied and some of these are considerably smoother than the one shown. This is clearly an area where future research would be useful, not only to see whether these observations fit the reported results on tests on beams using lightweight aggregate but also to see if the effect of using very high-strength concrete for beams in shear may be explained in this way. In the latter case, for example, the new draft Code of Practice for structural concrete[10] does not allow any increase of shear strength in members where the concrete has a characteristic strength greater than 45 N/mm^2.

Series 5. The series 5 blocks contained two legs of a 6 mm diameter stirrup of plain reinforcing bar with a yield stress of 420 N/mm^2; the position of the stirrup is shown dotted in Figure 6.8. The stirrup

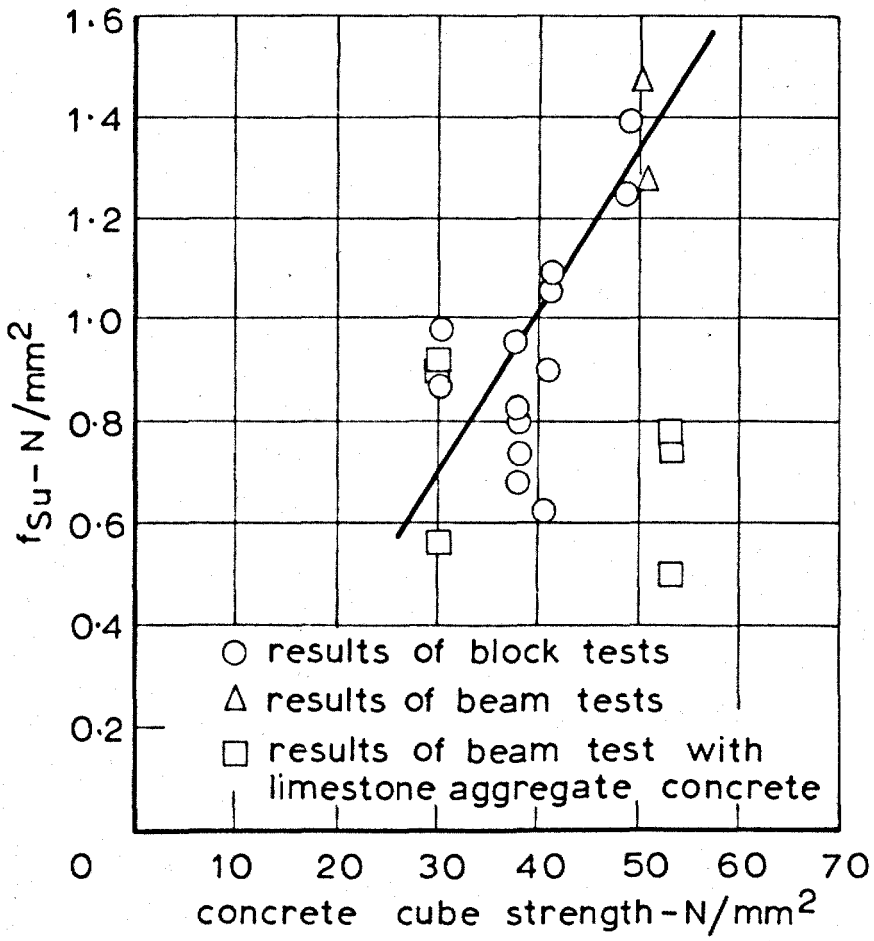

FIG. 6.18 RELATIONSHIP BETWEEN ULTIMATE SHEAR STRESS AND CONCRETE STRENGTH

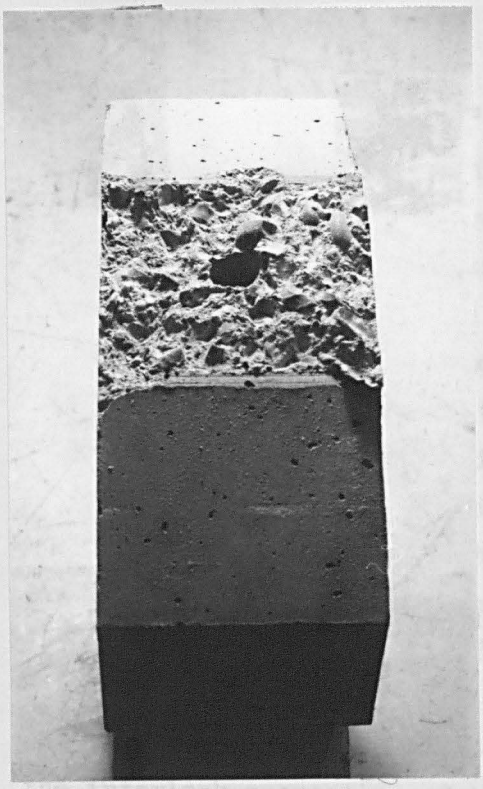

(a) block with 9mm gravel aggregate

(b) block with 19mm rounded gravel aggregate

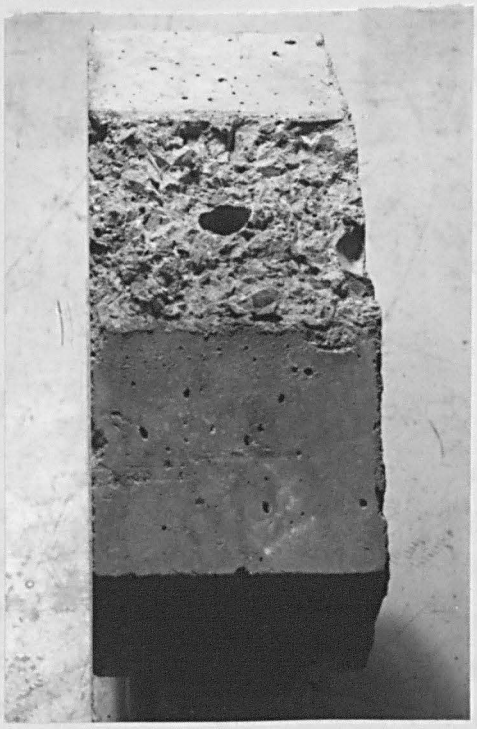

(c) block with limestone aggregate

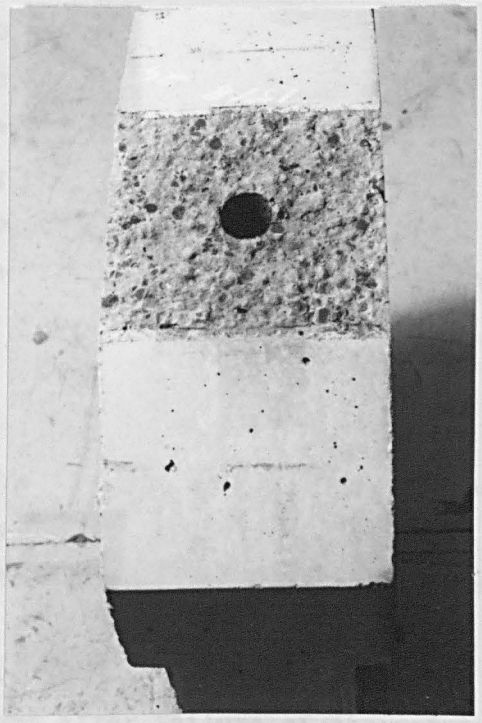

(d) block with Lytag lightweight aggregate

FIG. 6.19 Surfaces of cracks

was fixed at an angle of 45° to the crack and the block was oriented so that the stirrup was leaning towards the direction in which the crack was subsequently sheared. This simulated a crack in a beam, inclined at 45°, with a vertical stirrup passing across it. The strength of these blocks was considerably greater than that of the unreinforced blocks. The increase in shear strength of the block may easily be calculated on the assumption that the stirrup is yielding. This increase, written in terms of a stress across the crack, is 1·05 N/mm^2. If this figure is subtracted from the f_{Su} values given in Table 6.3, the resulting shear stress compares favourably with the f_{Su} values obtained from the unreinforced blocks. The relative contributions of the shear force carried by aggregate interlock and by the stirrup at other stages of the test are more difficult to determine as the presence of the stirrup may change the interlock properties of the crack. This is clearly an area where further study is needed. The design of the test rig was suitable for this study but the rig would have to be increased in scale before more work is carried out. The mode of failure of the blocks was different from that of the unreinforced blocks and is illustrated in Figure 6.11. The inclined crack at the lower half of the block is obviously a feature of the testing apparatus as the crack leads to the point where the block is clamped in the rig. This crack is analogous to the failure cracks produced by Fenwick, illustrated in Figure 6.4.

BEAM TESTS

In a series of frame tests by Cranston and Cracknell[33] one test was reported where a shear failure occurred in one column of a single-bay portal frame. In this case, because the rest of the frame had a reserve capacity of strength, a large rotation was able to occur at the point of the column failure before the frame test was completed. Figure 6.20 shows the column after failure of the complete frame. It is apparent from the photograph that most of the deformation of the column occurred across the inclined crack and that the upper part of the column rotated about the point where crushing of the concrete occurred. In the upper part of the crack, therefore, aggregate interlock was carrying shear force, although in this case stirrups were present in the section. It was considered that if a

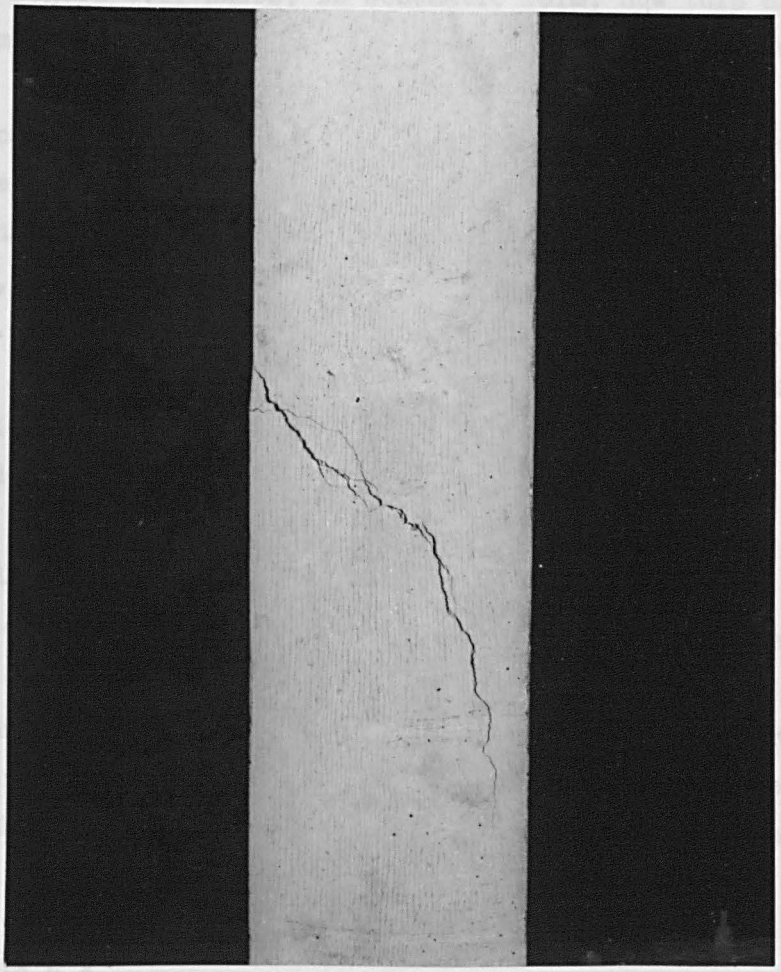

Fig. 6.20 Shear failure in reinforced concrete column reported by Cranston

crack of this kind could be induced in a beam, and if the dowel forces and the force in the compression zone could be either eliminated or measured, then this would be a good test for interlock.

Figure 6.21 shows, in schematic form, how this crack geometry was imposed on a beam and how the necessary force measurements were made. The compression zone was substituted by a steel packer, jack and load cell so that the load carried by it could be varied during the test. The dowel force was virtually eliminated in this case by casting a notch around the bars, and the compression zone direct force, C, and the shear force, V_1, were measured with the load cells shown. The strain in the steel was measured by means of a 50 mm Demec gauge with points stuck onto the bar. It was therefore possible to calculate the shear and normal forces acting across this crack by considering the equilibrium of the end of the beam.

Test specimens

Three beams of the type shown in Figure 6.22 were cast and six tests were then carried out. The beams were of 300 x 150 mm cross-section and were cast with the mix containing 9 mm aggregate described earlier. The beams were cured under damp sacking for one week and were then moved into the laboratory where they were instrumented and stored for three weeks before testing. Details of the beams and the strength of the beam concrete, measured on 150 mm cubes, are given in Table 6.4.

TABLE 6.4
Details of beam tests D1-6.

Beam	Dimension A (Figure 25) (mm)	150 mm cube strength (N/mm^2)
D1	100	57·0
D2	100	57·0
D3	100	42·5
D4	100	42·5
D5	150	50·0
D6	150	50·0

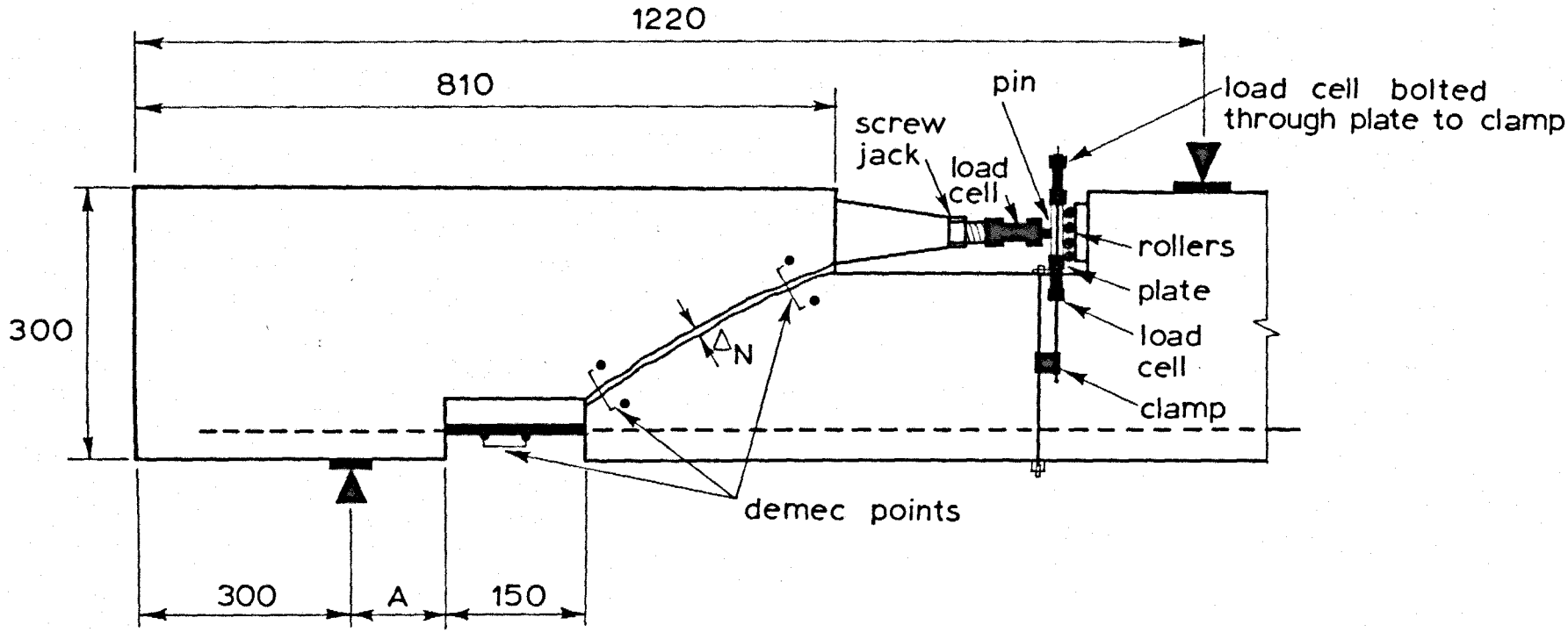

FIG. 6.21 LAYOUT OF TESTS D1 TO D6

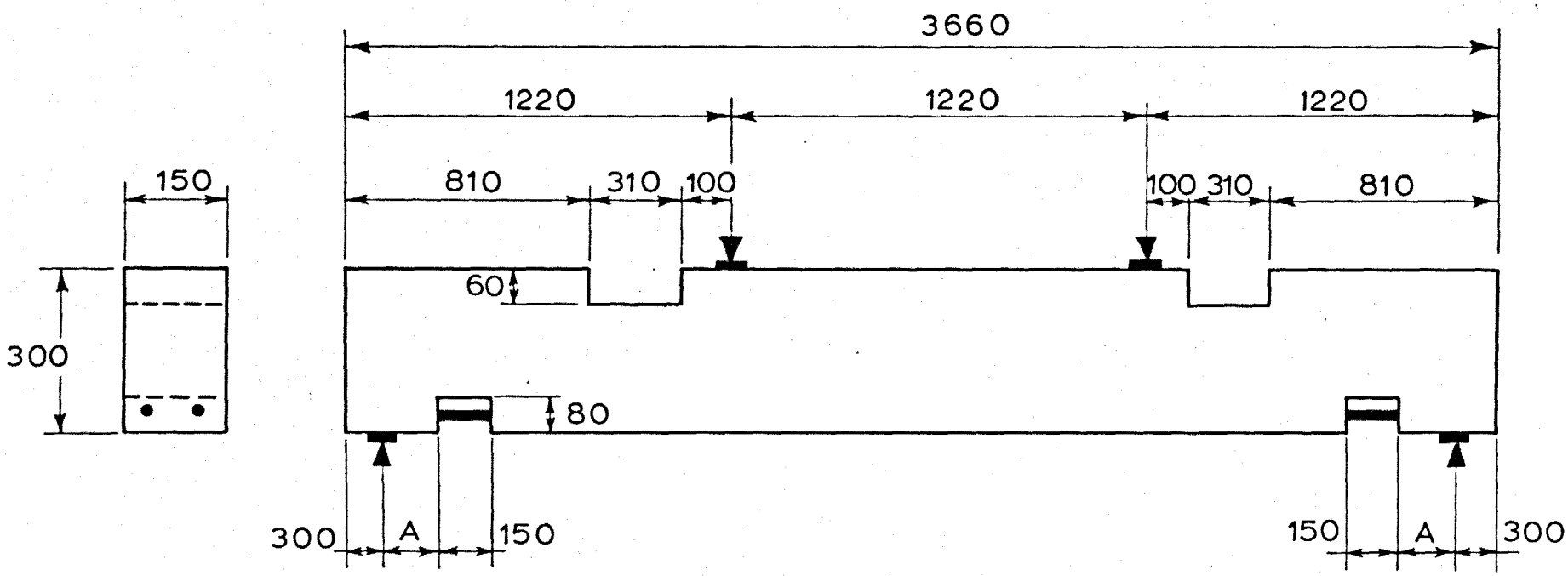

FIG. 6.22 LAYOUT OF BEAMS D1 TO D6

Details of tests

Test D1. This first test was carried out to see how the crack could be pre-formed. The crack was induced in this case by placing the beam on its side and supporting it on parallel line supports, 300 mm apart, with one on either side of the proposed crack location. A line load was then applied to the other side of the beam and this load was gradually increased until the crack formed. Because the supports were so close the crack was formed partly in flexure and partly in splitting. It was not possible to control the formation of the crack and therefore its width immediately after formation was approximately 0·4 mm. A further problem was that the crack was slightly S-shaped, which is not typical of shear cracks. The beam was still tested and carried a shear force of 22·5 kN before it failed. The beam did not have the two load cells to measure the shear force carried through the pin in the compression zone as this was assumed to be very small. It was found, however, that it was not possible to satisfy all the equilibrium equations with the forces that were measured. Either the pin was carrying a large shear force or there was a normal force acting across the crack that had not been eliminated.

Tests D2, 3 and 4. These were three tests in which the test method and rig were developed further until the final test rig was as shown in Figure 6.21. Firstly, a plate backed by horizontal rollers was put behind the pin and this plate was trapped between load cells which in turn were bolted to the main part of the beam through a clamp. Thus any shear transferred by the pin would result in the load cells altering their readings by the amount of the force. It is possible, though, that there was a significant amount of friction in the roller system and that the shear force may have been carried in this way, without affecting the load cells. However, if the coefficient of friction is assumed to be 0·1, then the percentage of the total shear carried by the rollers was less than 5% in all the tests. The greatest shear force measured by this apparatus in any of the subsequent tests was 100 N, indicating that no significant shear forces were carried by the pin. The compression block arrangement illustrated in Figure 6.21 was therefore considered to be satisfactory.

A second feature that was developed during these tests was the method of forming the crack. The method that was finally adopted involved forming the crack while the beam was being loaded in bending and shear in the correct way; this is explained in the description of the next two tests. The shape of the crack resembled the shape shown in Figure 6.20 during all the tests and the width of one end of the crack was never greater than 1·25 times the width of the other end.

Test D5. This test was the first one in which reliable quantitative results were obtained. The test procedure was as follows. The beam was set up in the test rig and the compression zone jack was adjusted until it was just finger-tight. The beam was then loaded until a flexural crack had formed at the notch above the dowel. The shear force on the beam at this point was 22·5 kN. The beam was then unloaded until the shear force was 6·5 kN and the compression zone jack was tightened until the crack formed right through the beam; this load stage is shown in Figure 6.23. The beam was then loaded to failure which occurred at a shear force of 24·8 kN; the beam at failure is shown in Figure 6.24. The new crack, which started at about the mid-point of the beam and travelled backwards towards the support side of the dowel notch, formed just as the beam failed. This form of crack, sometimes called a 'back-up' crack, is quite often seen in shear tests and is presumably caused by the concrete lamina between cracks failing because of the shears imposed on it by aggregate interlock and dowel action.

At each load stage, all the load cell readings were taken and Demec readings were taken across the crack. From these it was possible to calculate the normal and shear interlock forces across the crack and to produce a force-displacement graph. The ultimate interlock shear stress was 1·47 N/mm^2 and the normal stress was 0·49 N/mm^2, compressive.

The value of Δ_N/Δ_S measured during the test was similar to the Δ_N/Δ_S ratio imposed on the test blocks 6 and 10. The values of f_s/f_{Su} and Δ_N from this beam test should therefore compare with the curve for blocks 6 and 10 shown in Figure 6.13. Figure 6.25 shows

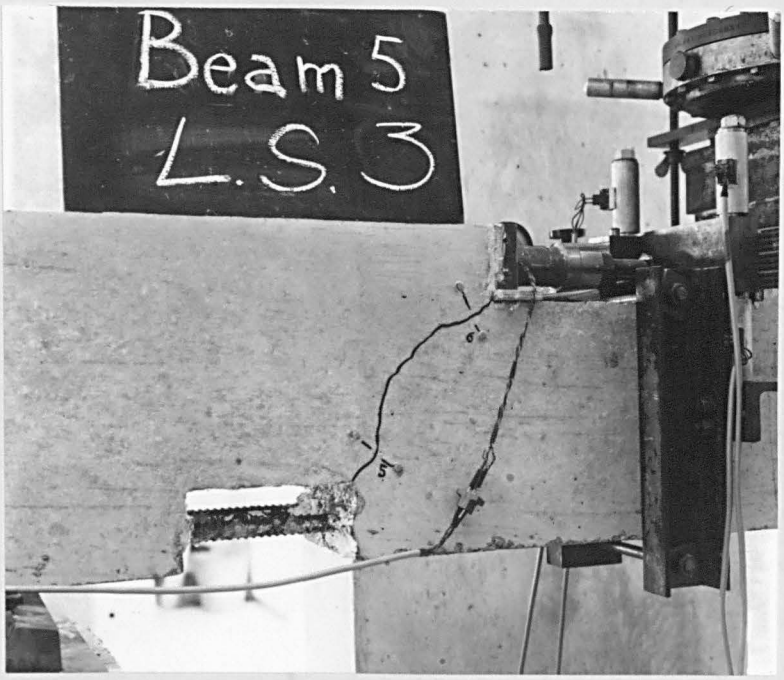

FIG. 6.23 Preformed crack on beam D5 at start of test

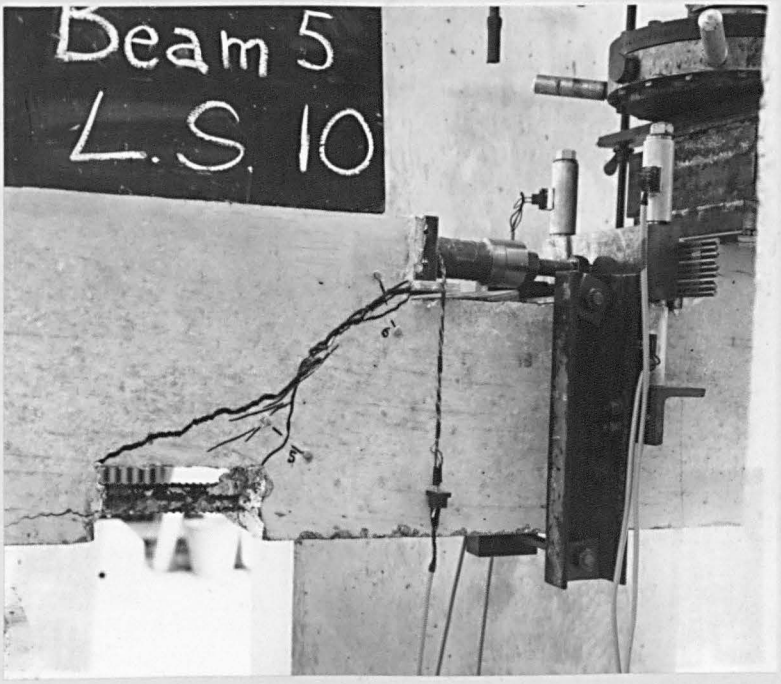

FIG. 6.24 Preformed crack on beam D5 at finish of test

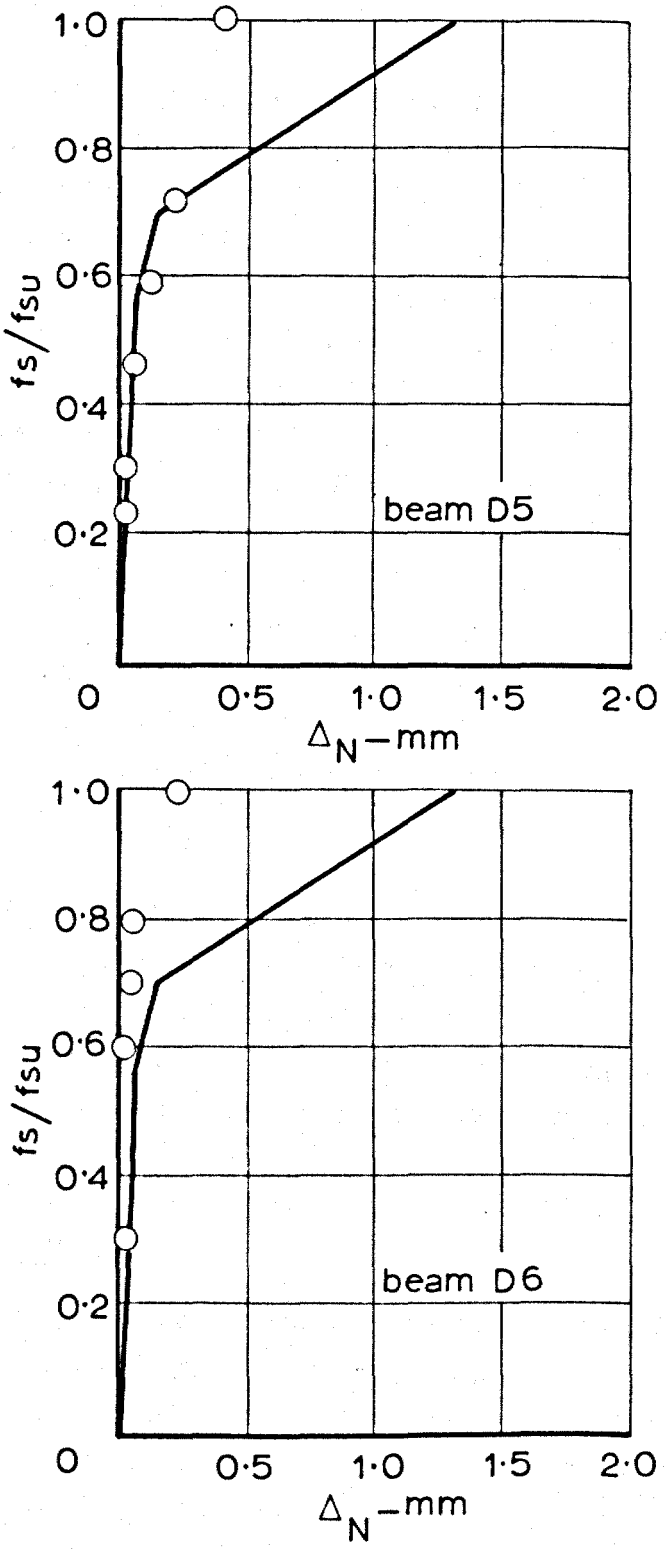

FIG. 6.25 TEST RESULTS FROM BEAMS D5 AND D6

the curve from Figure 6.13 with the values of f_s/f_{Su} and Δ_N from the test on beam D5 plotted in.

The difference between these lines and the test results at high load stages is probably due to the difference in the method of test and to different stiffnesses of the test rigs. In the block tests there was invariably some form of falling branch as the rig was fairly stiff and it was therefore possible to measure all the load cells at a load very near to f_{Su}, thus fixing the top of the curve accurately. In the beam tests, the beam failed immediately f_{Su} was reached, making it impossible to read the cells at that load stage. The f_{Su} values plotted in the Figures are calculated from the highest readings that were measured in the test and are, for both tests D5 and D6, slightly less than the true maximum values. This would have the effect of lowering the plotted points on Figure 6.25, the amount being greater for the higher values of f_s/f_{Su} than for the lower values. The value of the ultimate shear stress has been plotted on Figure 6.18; here, the effect would be to raise the points slightly.

Test D6. This test was similar to the previous one and was conducted in the same way. The shear force at failure was 23·6 kN, corresponding to an interlock stress of 1·27 N/mm^2 and a normal stress of 0·39 N/mm^2. This result is plotted in Figure 6.18 and the $f_s/f_{Su} - \Delta_N$ curve is shown in Figure 6.25. This result shows good agreement with the previous tests.

COMPARISON OF TEST METHODS

Each type of test has its advantages and disadvantages. The block test has the disadvantage of large scatter, but this could be improved if a much larger test rig were constructed, providing the forces in the rig could be measured accurately. This test, however, has the advantage that it can be carried out more rapidly than the beam test and that the test specimen is made more economically. The beam test has the advantage that it is a test of aggregate interlock in a beam environment but requires a considerable amount of skill from the experimenters before the crack formation can be controlled. On balance, the block test is the more satisfactory one and this test

provided most of the information for this chapter.

DISCUSSION OF RESULTS

It is useful at this stage to summarize the test results and show how interlock curves may be drawn for comparison with beam tests.

Firstly, the ultimate interlock strengths may be obtained by referring to Figure 6.18. This Figure has been drawn using the results of the tests in which $\Delta_N/\Delta_S = 1{\cdot}0$.

Secondly, knowledge of the Δ_N/Δ_S relation for any one crack allows values of f_{Su} and f_{Nu} to be read from Figures 6.15 and 6.17. These two Figures were drawn from the results of tests in which the concrete strength was 32 N/mm^2 and can therefore be modified, using the appropriate value of f_{Su} from Figure 6.18. Thus the value of f_{Su} for 32 N/mm^2 concrete, from Figure 6.18, is 0·78 N/mm^2 and this agrees with the value of f_{Su} from Figure 6.15 for $\Delta_N/\Delta_S = 1{\cdot}0$.

Thirdly, Δ_{Nu} may be found using the appropriate value of Δ_N/Δ_S in Figure 6.14. Using the following co-ordinates of the $f_S - \Delta_N$ curve, the interlock curve (Figure 6.13) may then be constructed:

$0{\cdot}55\ f_{Su}$,	0·06 mm
$0{\cdot}7\ f_{Su}$,	0·15 mm
f_{Su},	Δ_{Nu}

This curve applies to concretes with similar mix proportions to the ones used and with gravel aggregate, maximum size between 9 and 19 mm.

This representation of the test results may now be compared with Fenwick's tests and may be used to see if the vertical equilibrium conditions of the beam tests reported in Chapter 4 can be satisfied using the dowel forces and these interlock forces.

In general, the results of all the tests reported here were lower than those found by Fenwick. As mentioned previously, it seems

likely that his results were high due to the nature of his test.

The summation of the compression zone, dowel and interlock forces in tests that were conducted and reported earlier are now given. For this study the results from the beam tests reported in Chapter 4 were used.

In this chapter a series of graphs (Figures 6.26 - 6.29) have been produced in which, for all cases where the displacement measurements across cracks were adequate, the dowel shear force and interlock forces have been added. The graphs were drawn by first plotting the shear force in the compression zone against the shear force on the beam, using the values given in the Tables in Chapter 4. The diagonal line, which is the correlation line between the internal and external shears on the beam, was then drawn. The sum of all the methods of shear transfer in the beam should add up to this line. Two other straight lines are also drawn in. The vertical dotted line, drawn approximately half-way along the V axis, marks the point at which the section first cracked. The other vertical dotted line marks the point at which shear failure occurred. In the case of beam 9, however, this line does not appear as this beam failed in flexure by yielding of the steel.

The dowel force was added to the compression zone force using the test results from Chapter 5. In this case, the actual test results for the 200 mm beam tests were used. In the cases shown it may be seen that the dowel is carrying up to 25% of the total shear force in the beams without the pre-formed cracks, and is carrying nearly 30% of the total shear force in the other beam.

The aggregate interlock force was then calculated. The basic stress was taken as 1·0 N/mm^2 and this was modified using the Δ_N/Δ_S measurements taken on the beams, as described earlier. As the displacement rosettes were either 50 or 100 mm above the tension face of the beams, these values of interlock stress apply to the areas of the beam between the rosettes and the neutral axis. In most cases, the cracks were not significantly inclined and the same interlock stress was assumed to act throughout the depth of the beam up to the neutral axis. This is possibly a conservative assumption for the

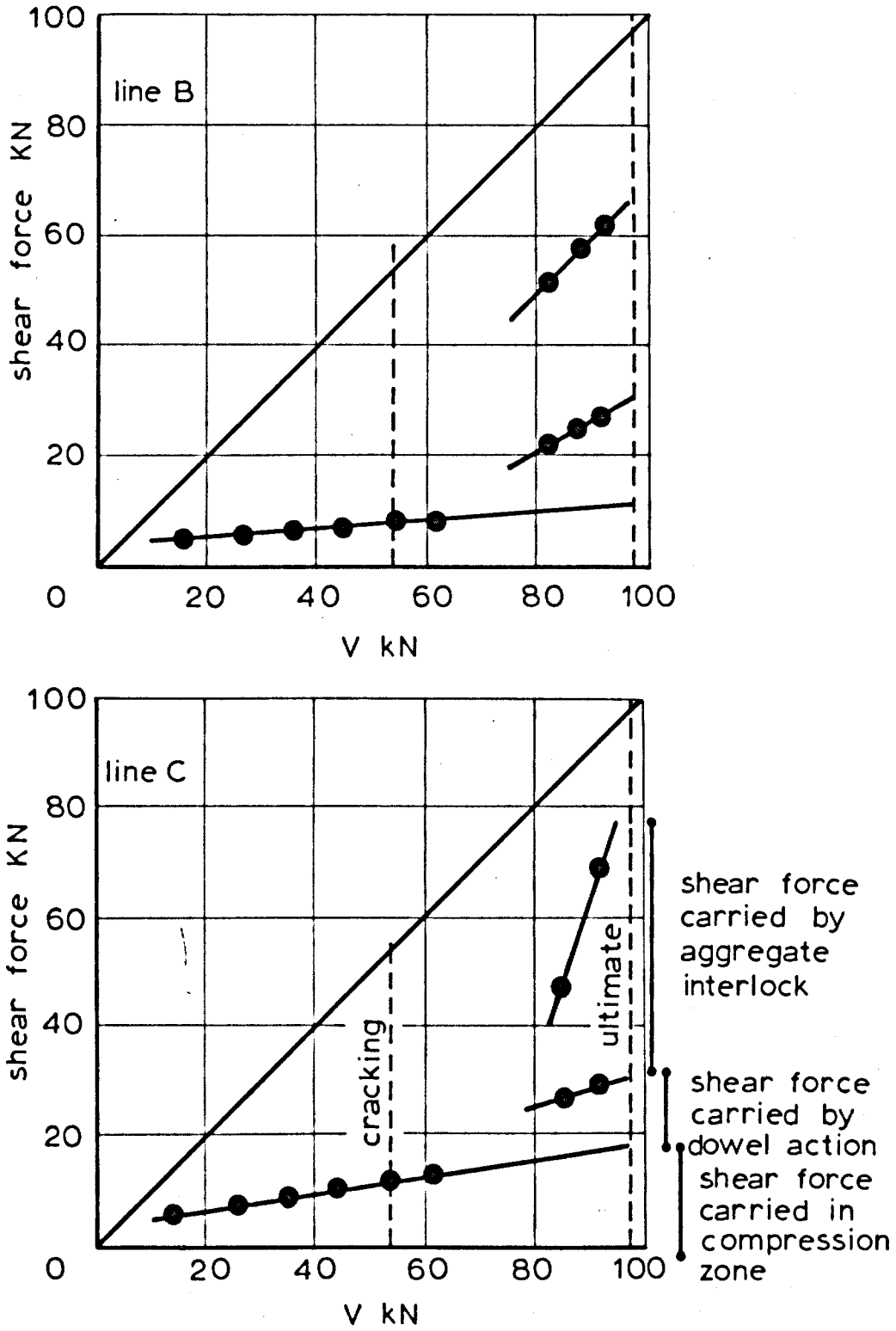

FIG. 6.26 DISTRIBUTION OF SHEAR FORCE IN BEAM 7

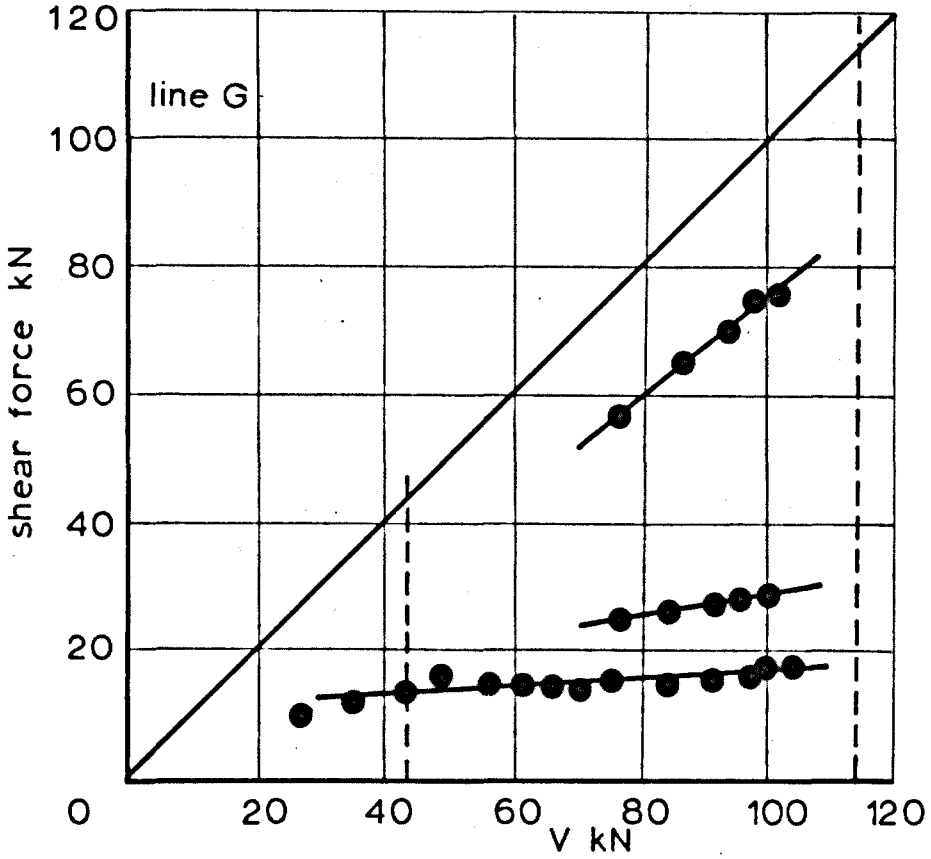

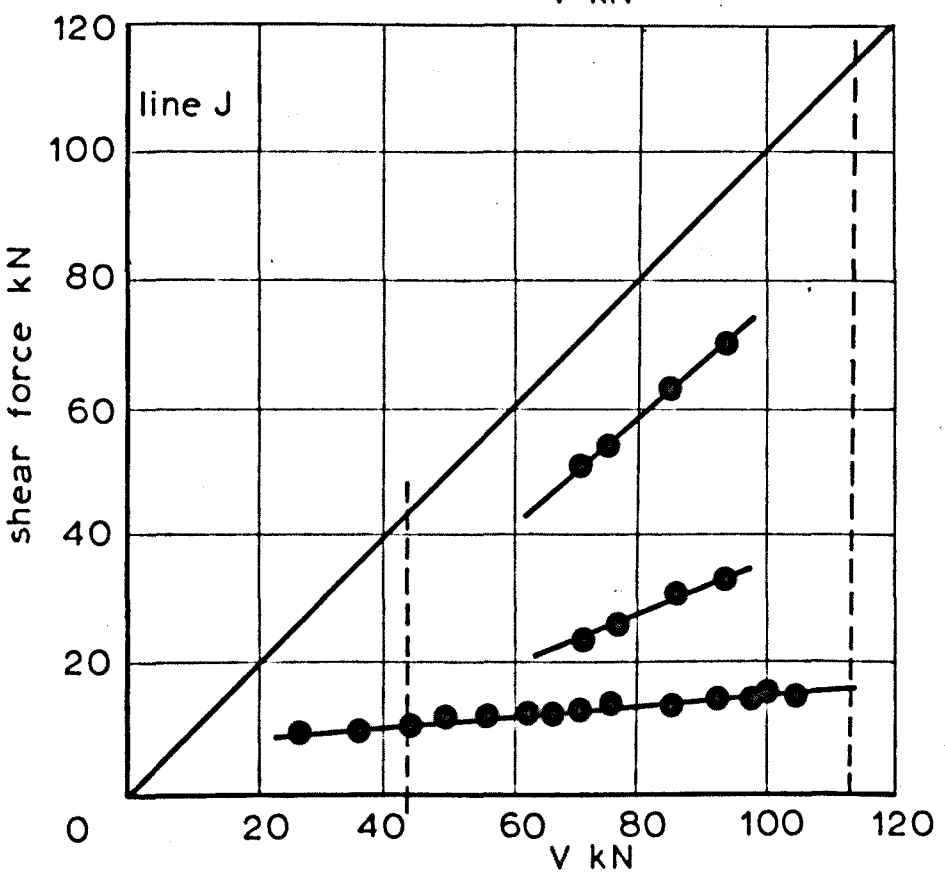

FIG. 6.27 DISTRIBUTION OF SHEAR FORCE IN BEAM 8

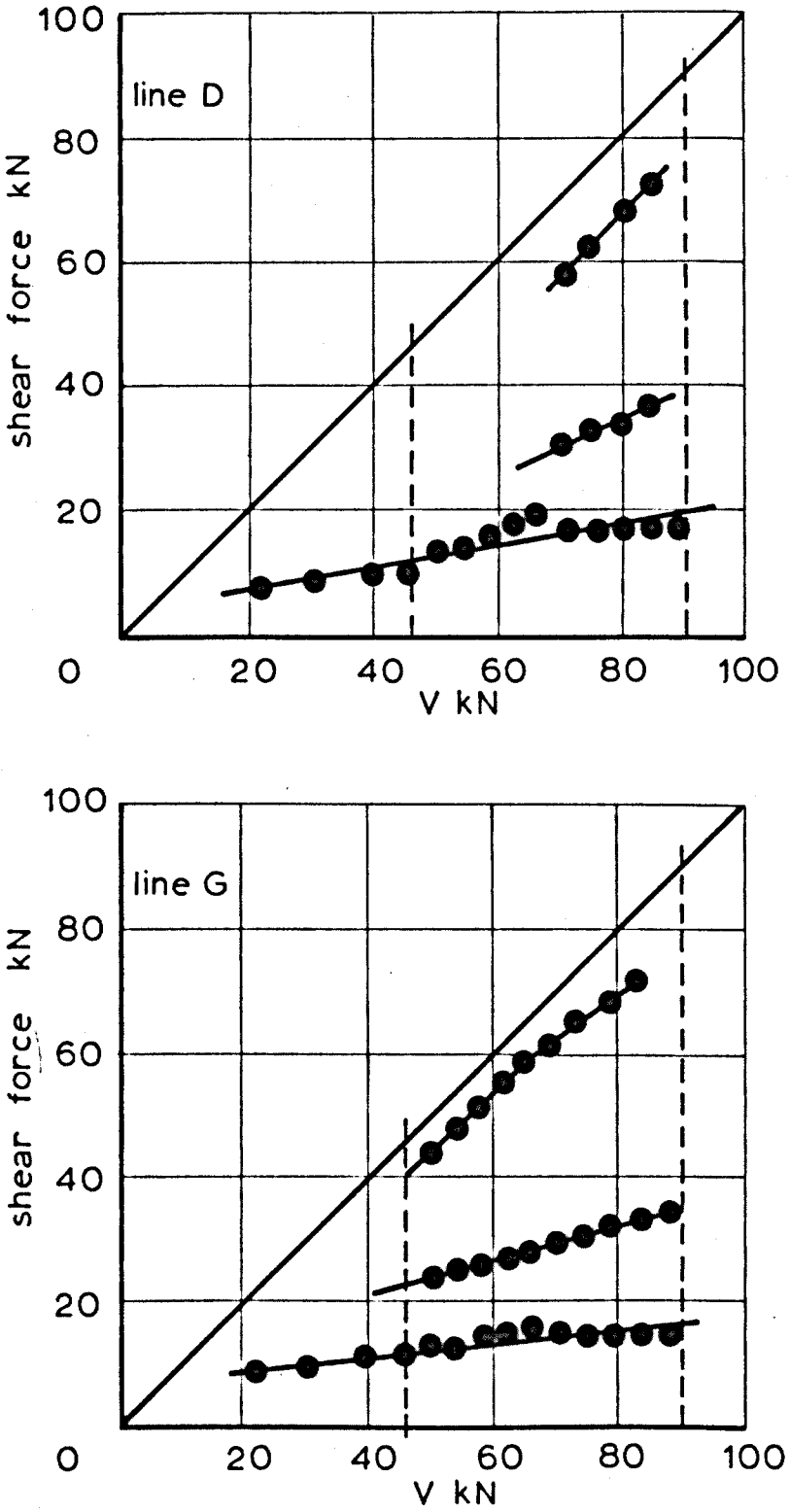

FIG. 6.28 DISTRIBUTION OF SHEAR FORCE IN BEAM 9

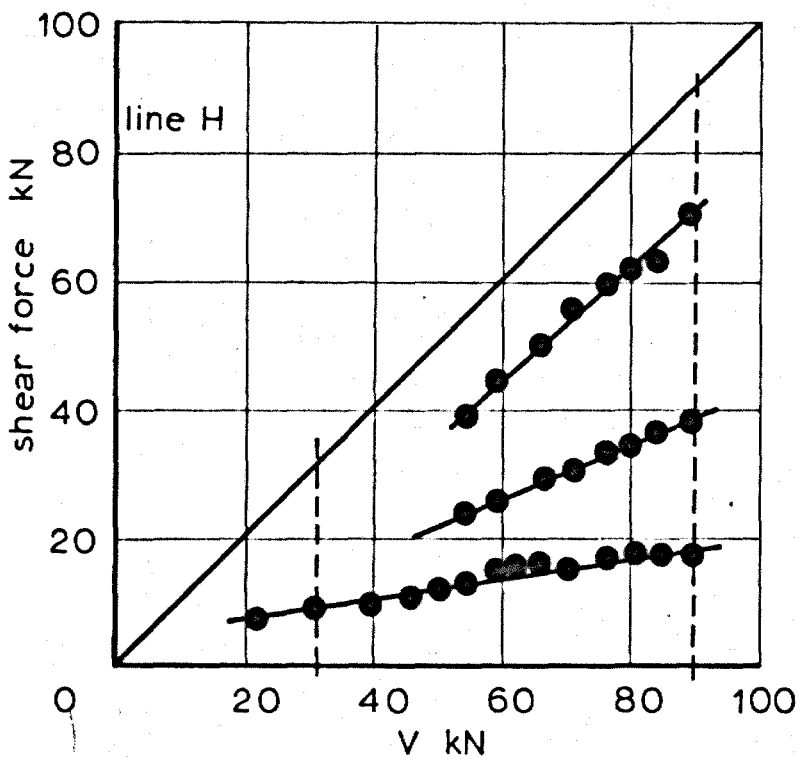

FIG. 6.28(cont.) DISTRIBUTION OF SHEAR FORCE IN BEAM 9

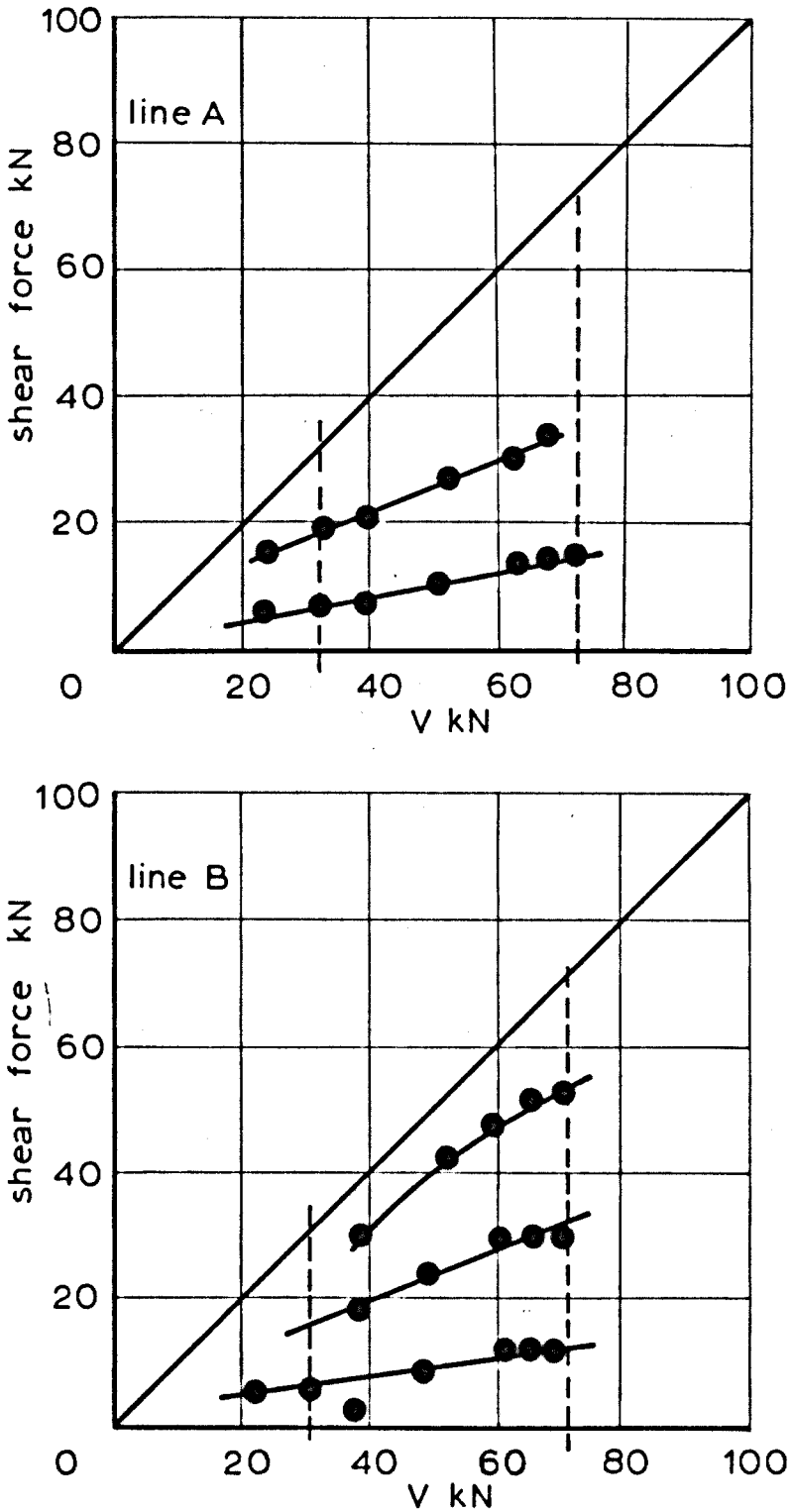

FIG. 6.29 DISTRIBUTION OF SHEAR FORCE IN BEAM 10

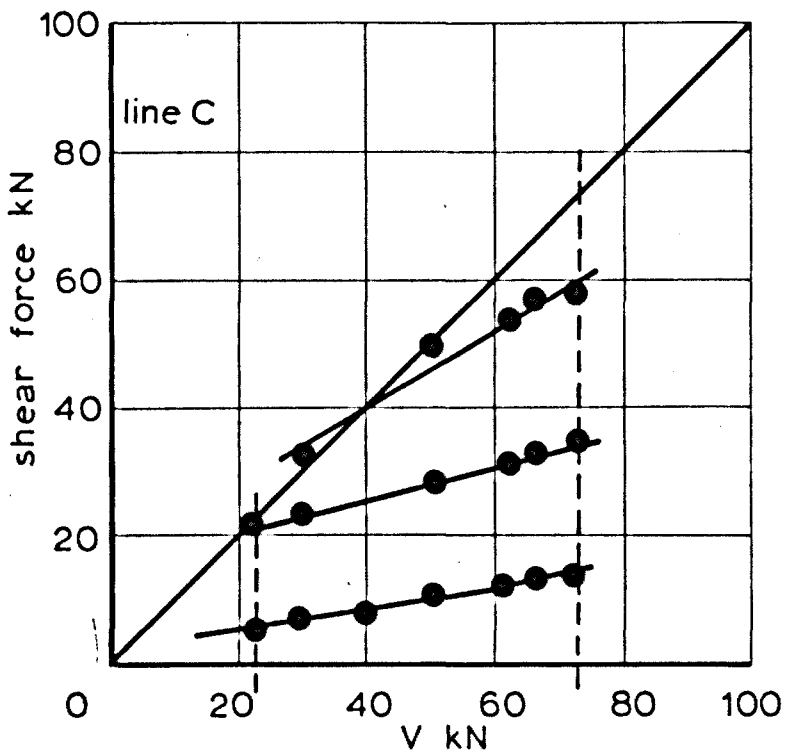

FIG. 6.29 (cont) DISTRIBUTION OF SHEAR FORCE IN BEAM 10

cases where the crack extends past the line where the shear forces in the compression zone were measured. If the crack ends at the point where the compression zone shear is measured, then, theoretically, as the cracking at its head is in a direction of principal tensile stress, there can be no shear displacement across the crack and therefore no interlock force. In this case, there must be a marked kink in the shear stress curve across the section as the shear stress becomes zero at the head of the crack and rises to the interlock strength below it.

Figure 6.30 shows a section of a beam with the neutral axis drawn in. Also shown is a shear stress diagram across the beam section, in this case for beam 9, line G, load stage 14. The three contributions to the shear strength of the beam are drawn to scale, showing their relative magnitude. This diagram is typical of a series of diagrams that may be drawn, one for each load stage of the tests on beams 7, 8, 9 and 10.

The shear stress distribution is very like the classical Mörsch one shown in Figure 2.1 in that the stress is distributed through the section. It is now possible to see how shear forces are carried across cracks and now that this mechanism has been isolated it is possible to study the implications of it in beams of widely differing types.

The results of the summation of the three effects in Figures 6.26 to 6.29 are interesting. It was only possible to put the displacement rosettes onto the beam after it had cracked and to then start to measure the movement of the cracks. It was naturally not possible to measure the displacements from the point at which the section just cracked as this would require the rosettes to be stuck on before the crack appeared. In practice, there were at least two load stages between the stage at which the section cracked and the stage when the interlock and dowel stresses are first given, one for the crack to rise sufficiently for the rosette to be positioned and one for a set of zero rosette readings to be taken. All the dowel and interlock readings are therefore conservative, which probably explains why the sum of the contributions to the shear capacity of the beams does not add up to the total shear force on the beams.

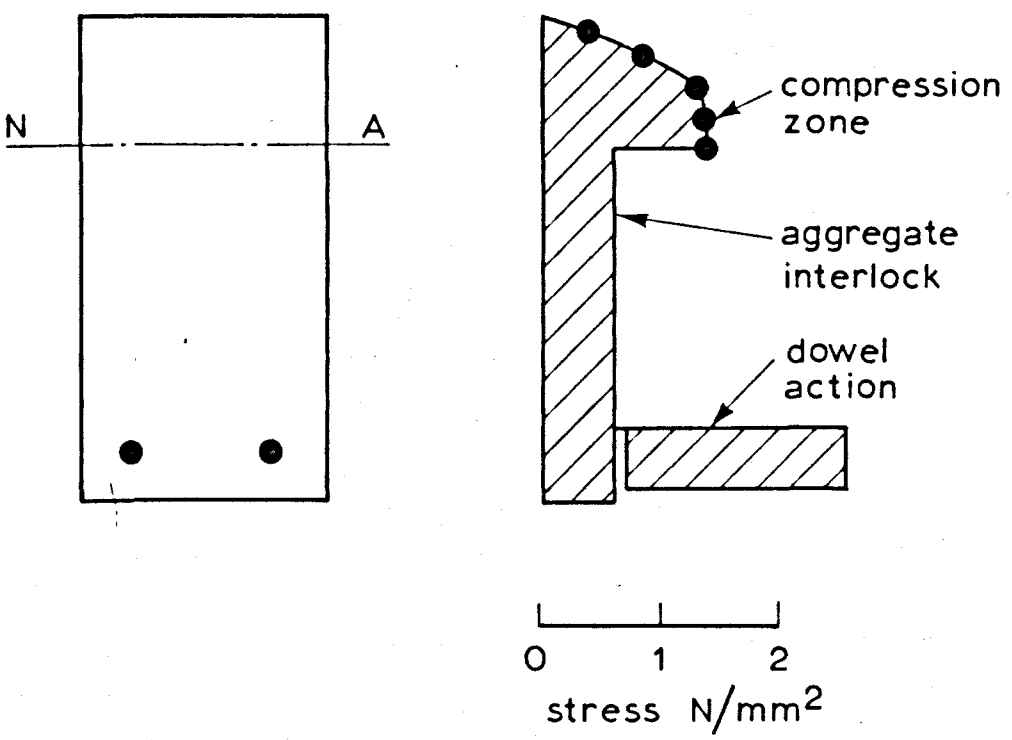

FIG 6.30 DISTRIBUTION OF SHEAR STRESS IN BEAM 9, LINE G, LOAD STAGE 14

The results of the test on beam 7, shown in Figure 6.26, indicate that the three contributions are short of the total shear force on the beam, particularly for line C. This is presumably because the ratio between shear span and effective depth for this beam is very small and the beam is carrying shear also by acting as a tied arch. The threshold between tied arch action and beam action for beams with the steel percentage of beam 7 is at $a/d_1 = 3$. The tied arch behaviour of beams with a/d_1 ratios less than this are not within the terms of reference of this Thesis. The results of the tests on beams 8 and 9 are much more satisfactory. The proportions of the total shear force carried by aggregate interlock, by the compression zone and by dowel action respectively are 50%, 20% and 20%. The exact proportions vary in each case, depending on the inclination of the crack, the roughness of the crack and the depth of the compression zone.

The results of the test on beam 10 are also satisfactory. In this case, the aggregate interlock forces shown are for the section of the crack that formed above the pre-formed crack. In the case of line A, the one nearest to the support, the displacement reading showed that no interlocking was occurring. The shear forces elsewhere are shown in Figure 6.29. Clearly there must have been some shear force transfer across the crack unless the compression zone shear forces were underestimated. The other two lines on beam 10 show better agreement and all the shear force is accounted for.

In Chapter 3, the work by Kani and Leonhardt was mentioned in which, when the size of a member was increased, a loss was found in the ultimate strength. The aggregate interlock work reported in this Chapter points to the fact that providing the crack spacings increased in scale, the cracks will be wider and the interlock strength less in a large beam than in a small one. If the aggregate size is kept the same, a large beam could thus fail at a lower shear stress than a smaller beam.

If increasing the size of a specimen and keeping the aggregate size constant is likely to reduce the strength then increasing the size and the aggregate size to scale could cause the strength to remain the same. A further complication is that in general, large

concrete specimens are weaker than small ones, a point which may be explained by the theory that failure may be likened to being caused by the weak link of a chain and that a weak link has a higher probability of being found in a long chain than in a short one.

A series of tests on beams of different scale was carried out to see if these predictions were true; to see if the effect of scale reported by Kani was sufficiently serious to be considered in design; and to see whether increasing the aggregate size could be a design solution for very large members.

Three beam sizes were used, one to a normal scale and two others, twice and four times the original scale. The basic beam was 100 x 250 mm in section, with 1·5% of GK60 reinforcement and was tested with an $^{a}/_{d_1}$ ratio of 3·5. Details of the test beams are given in Table 6.5. Five beams of the type 15 were tested so that the standard deviation could be found and one of each of the other beams were cast. Beam 15 had 4 No. 10 mm reinforcing bars with 12·5 mm side and bottom cover. The distance between the outer bars was 50 mm and between the inner bars was 40 mm. All the dimensions in Beams 16 and 17 were scaled exactly. After a series of trial mixes was made, the following mix designs were found to give equivalent strengths. The 9 mm aggregate mix was tested in 70 mm cubes, the 19 mm mix in 100 mm cubes and the 38 mm mix in 150 mm cubes.

Mix with 9 mm aggregate

9 - 5 mm	aggregate	40%
5 - down		50% by weight
aggregate/cement ratio	7·0	
water/cement ratio	0·76	

Mix with 19 mm aggregate

19 - 9 mm	aggregate	45%
9 - 5 mm	aggregate	14%
5 - down		41% by weight
aggregate/cement ratio	7·2	
water/cement ratio	0·72	

TABLE 6.5

Details of beams 15 - 17

Beam	Beam width mm	Beam effective depth mm	a/d_1	Aggregate size	Scale
15•1-5	100	232•5	3•5	9	1
16•1	200	465	3•5	9	2
16•2	200	465	3•5	19	2
16•3	200	465	3•5	38	2
17•1	400	930	3•5	19	4
17•2	400	930	3•5	38	4

TABLE 6.6

Shear force at failure of beams 15 - 17

Beam	Shear force kN	Standard deviation kN	Strength to scale %	Concrete strength N/mm²
15•1-5	24•2	2•20	100	32•4
16•1	80•0	-	82•8	31•0
16•2	83•0	-	85•9	39•5
16•3	99	-	102	
17•1	328•4	-	84•9	34•5
17•2	358•4	-	92•5	36•6

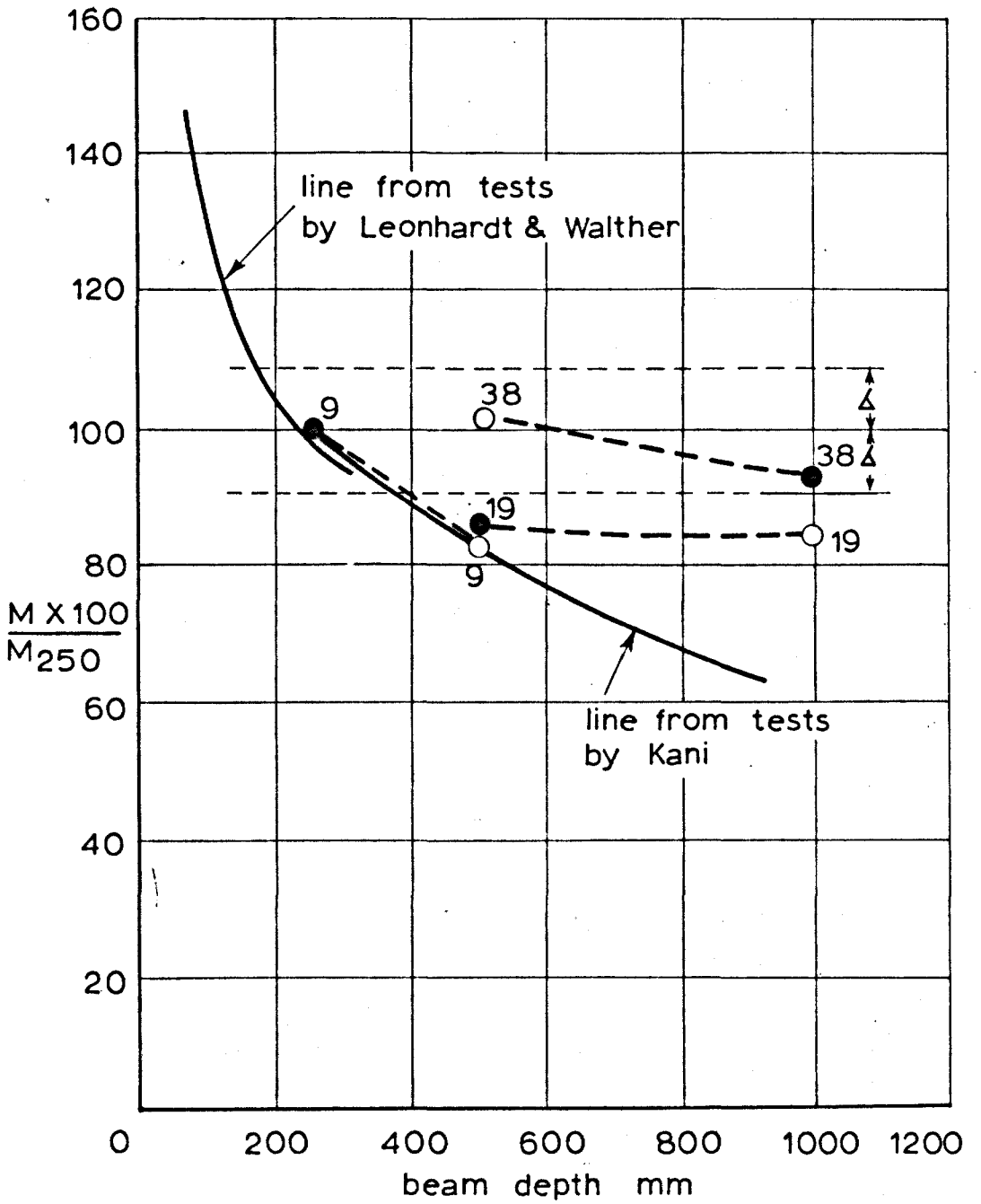

• aggregate size true to scale

FIG. 6.32 EFFECT OF BEAM DEPTH ON SHEAR STRENGTH

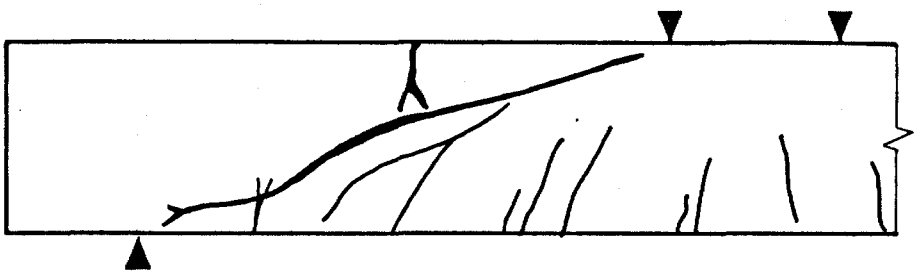

beam 15

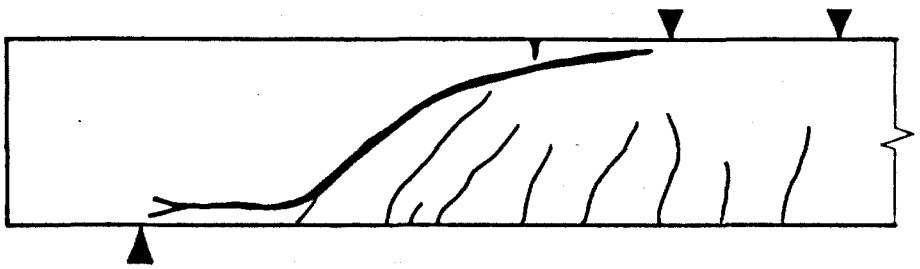

beam 16

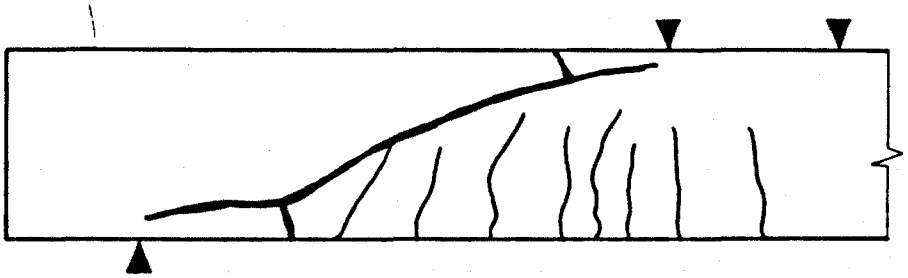

beam 17

FIG. 6·31 CRACK PATTERNS OF BEAMS 15 TO 17

Mix with 38 mm aggregate

38 - 19 mm	aggregate	40%
19 - 9 mm	aggregate	16%
9 - 5 mm	aggregate	12%
5 - down		32% by weight

aggregate/cement ratio 7·8
water/cement ratio 0·72

The crack patterns from a typical beam 15, 16 and 17 are shown in Figure 6.31 shown to the same scale. There was no significant difference between the crack patterns of beams using different aggregate sizes and it can be seen from the Figure that the difference between crack patterns of different scaled beams is negligible. As the spacing of the cracks scaled then so did their widths.

The results of the tests are shown in Table 6.6 and Figure 6.32. In Table 6.6 the actual shear force carried by the beams is given taking the difference in dead weight of the beams into account and the strength of the beams is also given reduced to the smallest scale size. The coefficient of variation of the Beam 15 tests is 9·1. The results, to the beam 15 scale are shown in Figure 6.36. In this Figure the ultimate moment of the beams, to the 250 mm scale, is given as a ratio of the ultimate moment from the 250 mm beams and is plotted against the actual beam depths. The lines on the Figure come from the tests by Kani on beams with 2·88 percent of steel and from tests by Leonhardt and Walther on beams with 1·6 percent of steel. The Leonhardt beams were true scale models without the aggregate size being scaled but the Kani beams were all the same width and were not scaled exactly.

It can be seen from the Figure that at the steel percentage level used in these tests, 1·5%, which is reasonable for such structural members, the effect of scale, regardless of aggregate size is not serious. In each case shown, increasing the scale and leaving the aggregate size constant reduced the strength and increasing the scale and increasing the aggregate size increased the strength. The beams with the aggregate size kept in proportion to the scale did not

have significant reduction in strength. These results are only just significant when the scatter of the lowest scale results are considered, 68% of the results of an infinitely large series of type 15 beams would be within the range marked on the Figure, assuming them to be normally distributed. These results do not confirm Kani's tests and show that in this range of member size, there is no design problem. The design clauses in all Structural Concrete Codes are based on tests of beams which were generally between 200 and 400 mm in depth and are sufficiently accurate for large scale beams.

Two effects contributed to the loss of strength reported by Kani. Firstly, all his beams had a constant width of 150 mm and the dowel effect could not therefore scale. The dowel strength of the large beams, which had a number of bars in the 150 mm width was very low. Secondly, the crack spacings did not scale in Kani's tests. The large beams had many more cracks at the steel level than the small beams because of the influence of the large amount of steel in the narrow section. Thus for small vertical displacements, a large shear force was transmitted across the closely spaced narrow cracks at the steel level and only a little shear force was transmitted across the wider shear cracks. For large vertical displacements, the concrete at the steel level could only carry small shear forces because of the dowel breakdown but the main shear cracks were then capable of carrying large interlock forces. The two effects were therefore never additive. The loss of strength effect reported by Kani is only a design problem for beams with large depth to width ratios (the largest beam tested by Kani had a depth to width ratio of six) and with a/d_1 ratios greater than 2·5.

Where the compression zone shear forces were estimated in Chapter 4, they were compared with a failure criterion for the concrete to see if they were capable of being carried by the concrete. In the same way, it should be possible to apply the dowel and aggregate interlock forces isolated in this and the last Chapter, to a section of a beam tensile zone between two cracks to see if the section of the beam is capable of carrying the forces. Secondly, the deformations of the tensile zone under the action of the forces should agree with the measured displacements in beams. This analysis has been carried out and is presented in the Appendix to this Thesis.

CHAPTER 7

MATHEMATICAL MODEL OF A BEAM WITHOUT STIRRUPS

The next step in this work is to see if the information found from the detailed study of a few beams can be used to build up a mathematical model of the behaviour of beams in shear. This model would have two immediate uses. Firstly it would confirm that the breakdown of the shear force in the members is correct if the behaviour of the original beams is predicted and secondly the model could be used to study the effect of some of the other parameters of the shear problem mentioned in Chapter 2. If the effect of the parameters is predicted then this further confirms that this description of beam behaviour is correct. If the model is very successful it could be used to study the effect of some parameters for which there is as yet no experimental evidence.

The problem of analysing a beam in bending and shear has been shown to be a complex statically indeterminate one. The horizontal, vertical and rotational equilibrium of any section of a beam must be ensured, with the compatibility of displacements on either side of the section.

The equilibrium of a section of a beam bounded by an inclined crack and a vertical section through the compressive zone has already been studied experimentally and the general equilibrium equations have been given in Chapter 3. The equations are repeated here for convenience and are derived from Figure 3.1.

$$C - T + H_I = 0 \qquad 7.1$$

$$V - V_1 - V_2 - V_3 = 0 \qquad 7.2$$

$$Vh - V_2 s - V_3 n - H_I t - Tl_a = 0 \qquad 7.3$$

The mathematical model, in the form of a computer program is designed to predict the shape of the inclined crack shown in Figure 7.1 and to solve the equilibrium equations. The compatibility condition used was based on the measurements taken on the test beams that were described in Chapter 3. Compatibility will be discussed later in this Chapter. A final basic feature in such a model is that a set of

failure criterion must be included which predict the failure of the various parts of the member under the combined actions of the shear and longitudinal forces that are proposed. It is only necessary here to accurately predict the failure of those parts of the force system that do fail in practice for if it can be shown that the rest of the member can never be stressed to failure then its strength is irrelevant.

The mathematical model considers the section of a beam shown in Figure 7.1. A basic step in the program is to extend the crack from point a where all the equilibrium and compatibility conditions have already been satisfied to a new location b which also marks a possible stable location for the head of the crack. At point a the curvature on the beam is ϕ_a and a new curvature ϕ_b which is slightly more than ϕ_a is proposed by the program. The basic step of the program is therefore defined by increments of curvature, the curvature increment being part of the initial data. All possible locations between a and b are studied to see if the equilibrium equation and compatibility conditions may be solved until a stable point is found. This process is then repeated continuously until one of the failure criteria is reached.

The content of the program will now be described in more detail.

Equilibrium Equations

The equilibrium equations 7.1 - 7.3 have been simplified in the program as the horizontal component of the interlock force has been neglected. This is not essential as some data have been given in Chapter 6 but its addition would add considerably to the complexity of the program and in Chapter 6 some doubts were cast on the reliability of the normal forces. The implication of missing out the horizontal interlock force is that the equilibrium equation 7.1 would not be solved at the correct neutral axis position. The order of magnitude of the ultimate normal interlock force is 0·25 N/mm^2 and this, particularly near to the failure of the beams, is much less than the average force in the compression zone so that the error in neutral axis position would not be great.

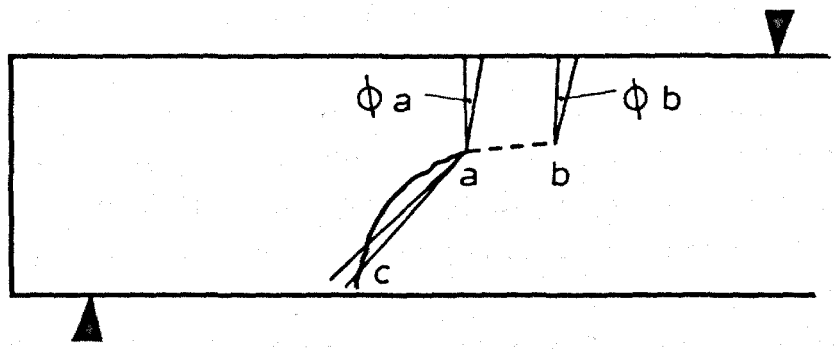

FIG. 7.1 CRACK ANALYSED BY MATHEMATICAL MODEL

The equations that were solved by the program in the simplified form are

$$C - T = 0 \qquad 7.4$$

$$V - V_1 - V_2 - V_3 = 0 \qquad 7.5$$

$$Vh - V_2 s - V_3 n - Tl_a = 0 \qquad 7.6$$

As has already been explained the curvature in the compression zone is used in the program and the increment of curvature is used as a basic step in the analysis. The assumption is made that plane sections remain plane in the compression zone and that the head of the crack is at the neutral axis. This assumption is reasonable and has been justified by the strain readings taken in beam compression zones described in Chapter 4. From this it is a simple matter to find the strain at any point in the compression zone and by substituting this into a stress-strain curve for the concrete to find the concrete compressive force. The stress-strain curve assumed for the concrete is shown in Figure 7.2. The compression part of the curve is initially parabolic, joining a straight line at a strain of $\sqrt{u_w}/5000$. The straight line was used rather than a falling branch as this then avoided the possibility of trouble in the program which may not find a solution as the outer compressive face of the beam went onto the falling branch. This possibility was very remote however and the shape of this part of the stress-strain curve was largely irrelevant as shear failures usually occur before large strains occur in the concrete compressive zone.

The concrete was assumed to have the tensile stress-strain properties shown in the Figure and the tensile force was subtracted from the force C in equation 7.4. The tensile stress strain curve for the concrete was added to the program at a late stage as it was found that without it, the crack tended to rise very rapidly up the beam to the depth that comes from normal elastic cracked section analysis. In practice the crack moves up the beam more slowly due to the loss of tensile stress in the concrete. The tensile stress-strain curve that was used simulated the vertical movement of the crack reasonably well. The work of Evans and Marathe[34] suggests that in pure tension, tensile stress is possible for small strains. At some

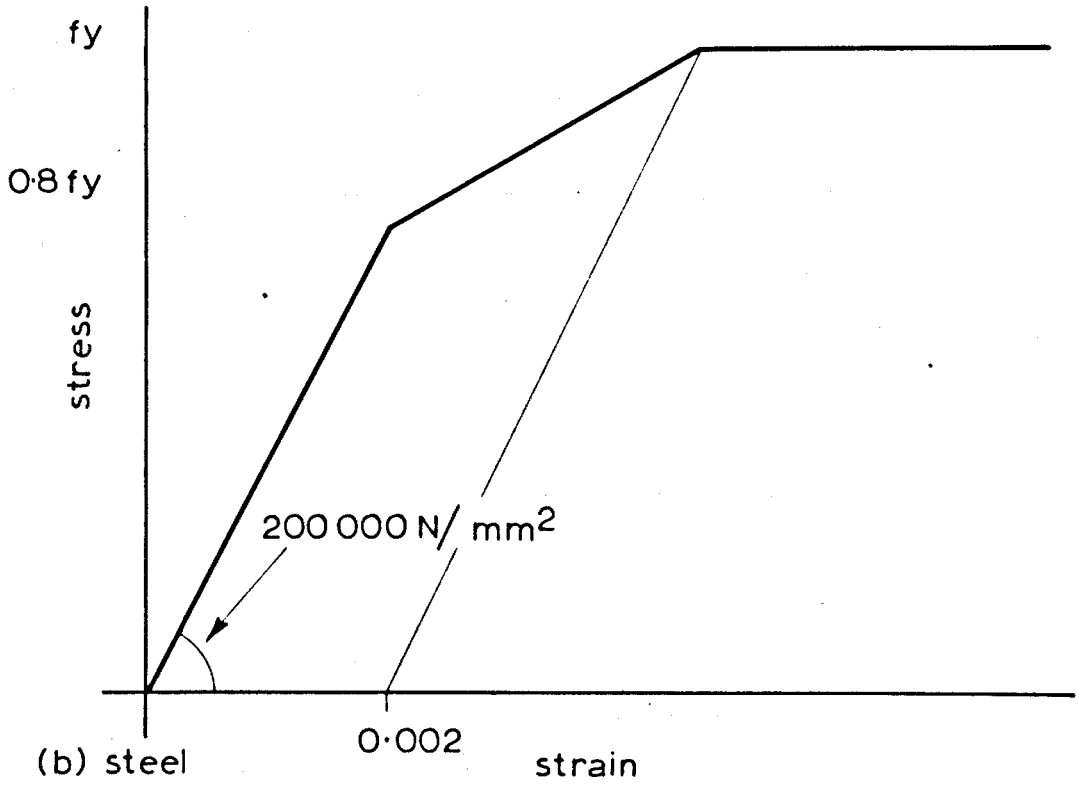

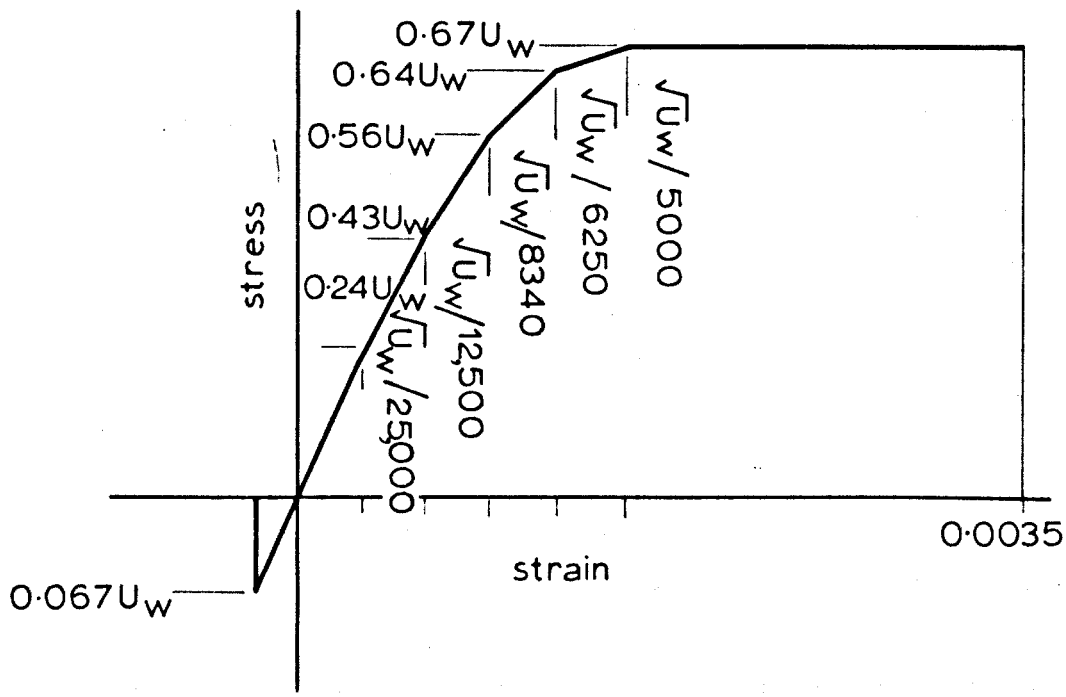

FIG. 7.2 STRESS STRAIN CURVES USED IN MATHEMATICAL MODEL

stage, when shear displacements are present across the crack, the stress across the crack becomes compressive and the work in Chapter 6 shows that at even larger displacements this stress may once again become tensile. As the normal stress across the crack was neglected, the tensile stress-strain curve that was used in the model had a cut off at a strain corresponding to a stress of 0·067 u_w.

The steel force T was found from the steel-strain curve shown in Figure 7.2(b) and the assumption shown in Figure 7.1 that the point c rotates about a.

The vertical equilibrium equation may only be solved by calculating the values of the three contributions to the shear force, V_1, V_2 and V_3.

The work described in Chapter 4 showed that shear force in the beam compression zone is distributed parabolically in a way similar to that from the classical distribution proposed by Mörsch. Because of the great similarity between the classical Mörsch analysis and the results of the tests the classical approach was used in the model to find the shear capacity of the compression zone. The shear force V_1 was therefore calculated from

$$V_1 = \frac{2 V d_n}{(3d_1 - d_n)} \qquad 7.7$$

The only other way to calculate V_1 is to assume a direct strain distribution about the section of the compression zone being considered and analyse this with the method used in Chapter 4. As no experimental strain readings are available, the results would be the same as those from equation 7.7. The dowel force V_2 and the aggregate interlock force V_3 both require the use of a compatibility condition as the basic data required to calculate dowel or aggregate interlock forces across the crack is a displacement. The displacements will be considered in detail later in this Chapter.

Once the vertical displacement across the dowel is known the dowel force is calculated by the method proposed in Chapter 5 from equations 5.1 and 5.2. The steel percentage of the beam being analysed was a part of the initial data and in all cases apart from

some large scale beams, this steel was assumed to be in two bars with 25 mm cover, regardless of their size. This means that the model is likely to under-estimate the dowel strength of beams with high steel percentages as these in practice would tend to have steel in more than one layer, giving a very high dowel strength.

The aggregate interlock force was calculated by dividing the crack into four sections and working out the interlock stresses at each section separately. These stresses were then integrated up the crack by Simpson's Rule to give the aggregate interlock force. The interlock stress was calculated using the information given in Chapter 6 to calculate the appropriate interlock stress - normal displacement curve. The way that the interlock was calculated is shown in Figure 7.3, the head of the crack is at point s and the horizontal displacement was then calculated at points 1, 2, 3 and 4. Using the compatibility condition the vertical displacement was then found at the same points. These displacements were then resolved into the normal and shear displacements across the crack and this data was used to construct the interlock curves.

A further refinement of the calculations for the interlock strength was that the concrete near to the reinforcing bars was assumed to have different displacements from the rest of the concrete and therefore to have more interlock strength. Work on cracking on reinforced concrete members[35] has shown that the cracking phenomenon can be successfully explained by the theory that the width of a crack at the steel-concrete interface is very low and the crack tapers outwards in width as it travels to the surface. This was later confirmed by basic research and analysis on bond by Lutz[36]. The crack in the area around the bars equal to the full width of the beam, multiplied by twice the difference between the depth and effective depth of the beam was therefore assumed to have the full vertical displacement from the displacement condition and half the horizontal displacement, when calculating the interlock strength.

Compatibility Condition

The results of the rosette measurements given in Chapter 4 indicate that a compatibility condition may be developed from

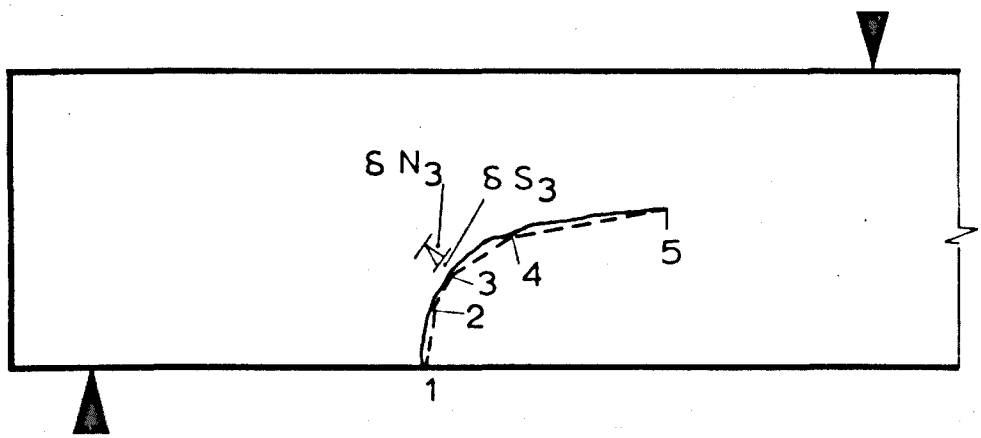

FIG. 7.3 METHOD OF INTEGRATING FORCES ACROSS A CRACK

knowledge of the shape of the crack and of the horizontal displacement across the crack.

The simple displacement condition shown in Figure 7.1 can be used to calculate the horizontal displacement across the crack by assuming an average crack width and that the curvature shown in the Figure is in fact the average curvature for that spacing. The curvature may then be used to calculate a rotation between consecutive cracks and hence to find the displacement between cracks.

In the last few years a lot of work has been carried out on the prediction of crack widths and crack spacings. This has led to the general conclusion that the spacing of cracks in reinforced concrete beams is dependent on the layout of the bars in the beams and more particularly the distance from the surface of the member to the nearest reinforcing bar. Recent work by Beeby[37] has shown that the spacing of flexural cracks in a member is not only dependent on the layout of the reinforcing bars but also on the initial height of the cracks when they are first formed. This latter conclusion agrees reasonably well with the observed crack spacing in the shear span of beams. The spacing of the main cracks which become inclined and reach the beam compression zone is governed by the initial crack height and the cracks which form later between the main cracks are governed by the layout of the reinforcement. The final crack pattern is therefore dependent on the layout of the reinforcing bars. As the spacing of the initial cracks is governed by the crack height, this was the value used to calculate the horizontal displacement between cracks. The photographs of the beams shown in Chapter 4 indicate that at the time that beams fail in shear the major cracks had formed and only a few secondary cracks were present. The assumption that the displacement in the tension zone is concentrated in the major cracks is therefore reasonable.

The initial crack height may be calculated from elastic theory, taking into account the tensile strength of the concrete. From Figure 7.4 the following equations may be obtained.

From the equilibrium of forces

$$a = n + \sqrt{n^2 - 2mp\ (1 - n)}$$

where p is A_{st}/bd_1

m is the modular ratio

or

$$n = \frac{a^2 + 2mp}{2(a + mp)}$$

From the equilibrium of moments

$$\frac{n^3 + (a + n)^3 + 3mp\ (1 - n)^2}{3(a - n)} = \frac{M}{bd_1^2\ ft}$$

Using these equations it is possible to compute the crack depth at any load.

When M = Mc (the cracking moment) there are two solutions:

(a) a = c

(b) a = a_o (the initial crack depth)

Using (a) to compute $M_c/bd_1^2\ ft$, (b) may then be computed for any value of m and p. As this is an iterative process, a simplified fit to plotted curves of $\frac{h_o}{d_1} - \frac{m\ Ast}{bd_1}$ was made and this was used in the program to calculate the initial crack height and the crack spacing. The simplified formula fits the curves to within five percent and is

$$\frac{h_o}{d} = \left[0{\cdot}955 - (mp + 0{\cdot}01)\ (4{\cdot}87\ (\frac{d}{d_1})^2 - 17\ \frac{d}{d_1} + 15{\cdot}8)\right]^2$$

where h_o is the initial crack height.

Once the horizontal displacement across the crack is determined the next step is to calculate the vertical displacement. One way to calculate the vertical displacement across a crack is to work out the vertical displacement from Figure 7.1. This gives a small displacement, much smaller than that found experimentally as it ignores the

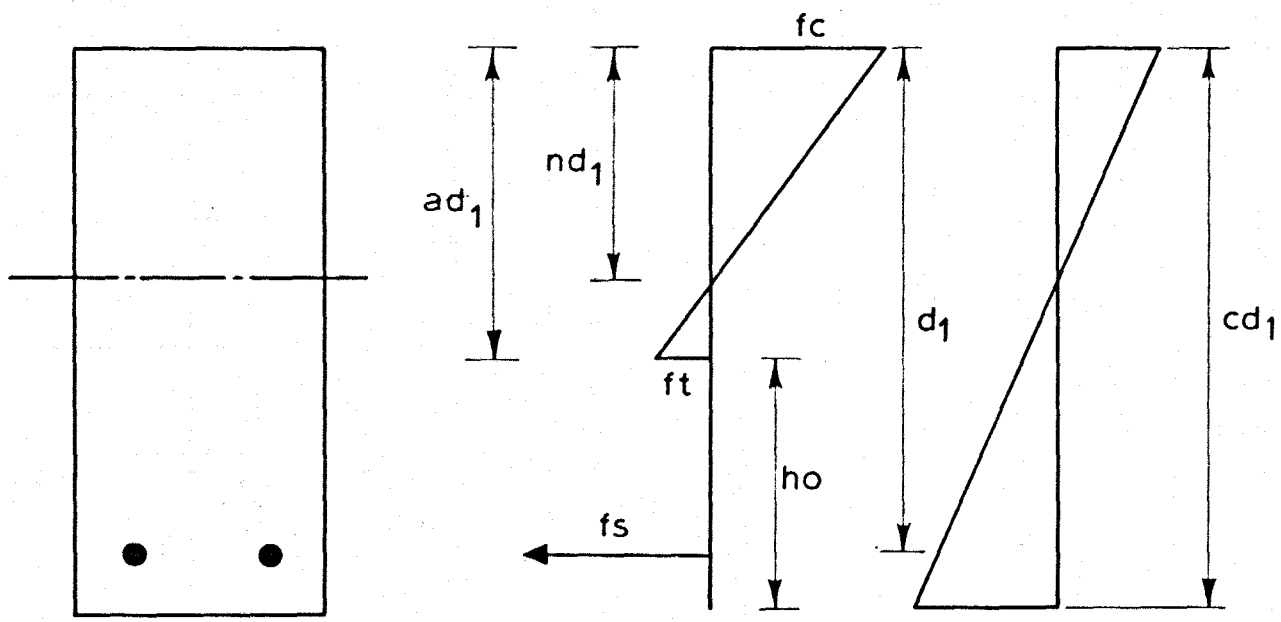

FIG. 7.4 DERIVATION OF FORMULA FOR THE INITIAL CRACK HEIGHT

movements of the beam tension and compression zones under the action of the shear and longitudinal forces imposed on them. The analysis described in the appendix shows that considering the forces on the concrete 'teeth' between cracks, the displacements are in the direction that are found in practice.

The displacement measurements taken across the cracks in the beam tests described in Chapter 4 are summarised in Figure 4.38. This Figure relates the shape of the crack, in terms of $\delta V / \delta H$ (where δV is the vertical projection of the distance from a point on the crack to its tip and δH is the horizontal projection) and $\Delta H / \Delta V$ (where ΔH is the horizontal displacement of the crack at the point considered and ΔV is the vertical displacement. The points on Figure 4.38 fit roughly on a straight line with the equation

$$\frac{\Delta H}{\Delta V} = 0{\cdot}55 \frac{\delta V}{\delta H} \qquad 7.8$$

and are confirmed by the finite element analysis described in the appendix.

Fenwick tested three beams in which he measured the displacements across the cracks. The displacements have been taken from his Thesis and have been plotted in the style of Figure 4.38 in Figures 7.5 and 7.6. Details of the beams are given in Table 7.1.

TABLE 7.1 Details of displacement test beams - Fenwick

	b_{mm}	d_{1mm}	a/d_1	$\frac{Ast}{bd_1} \times 100$	u_w N/mm²	f_y N/mm²
FA 4	152	356	4	1·43	41	480
SC 3	152	305	3	2·18	39	303
CA 1	152	356	4	1·87	41	296

The beams also had the following peculiarities. Beam FA 4 had preformed cracks with smooth crack formers 25 mm wide in the side of the specimen. The bars were wrapped with foam plastic and were only connected to the concrete teeth halfway between the cracks. Beam CA 1 had studs welded onto the bars in holes cast into the side of the beam, thus the dowel stiffness was very low as the cracks formed

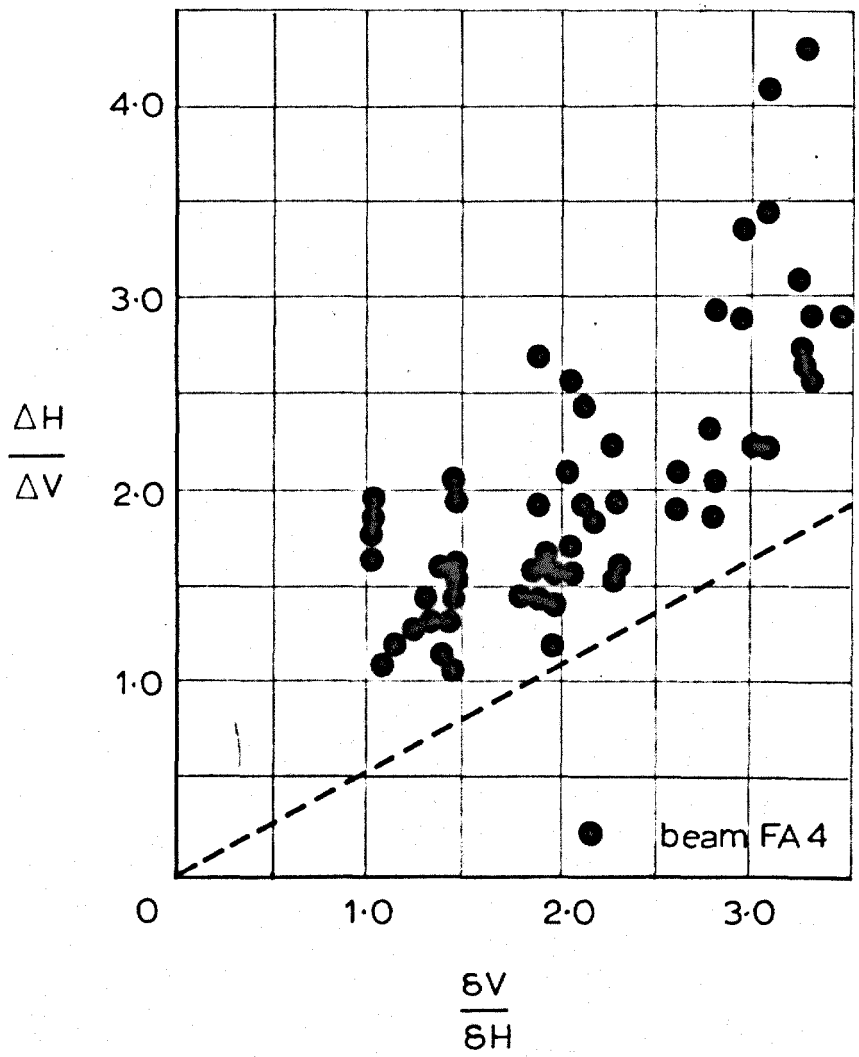

FIG 7.5 DEFORMATIONS FROM TESTS BY FENWICK

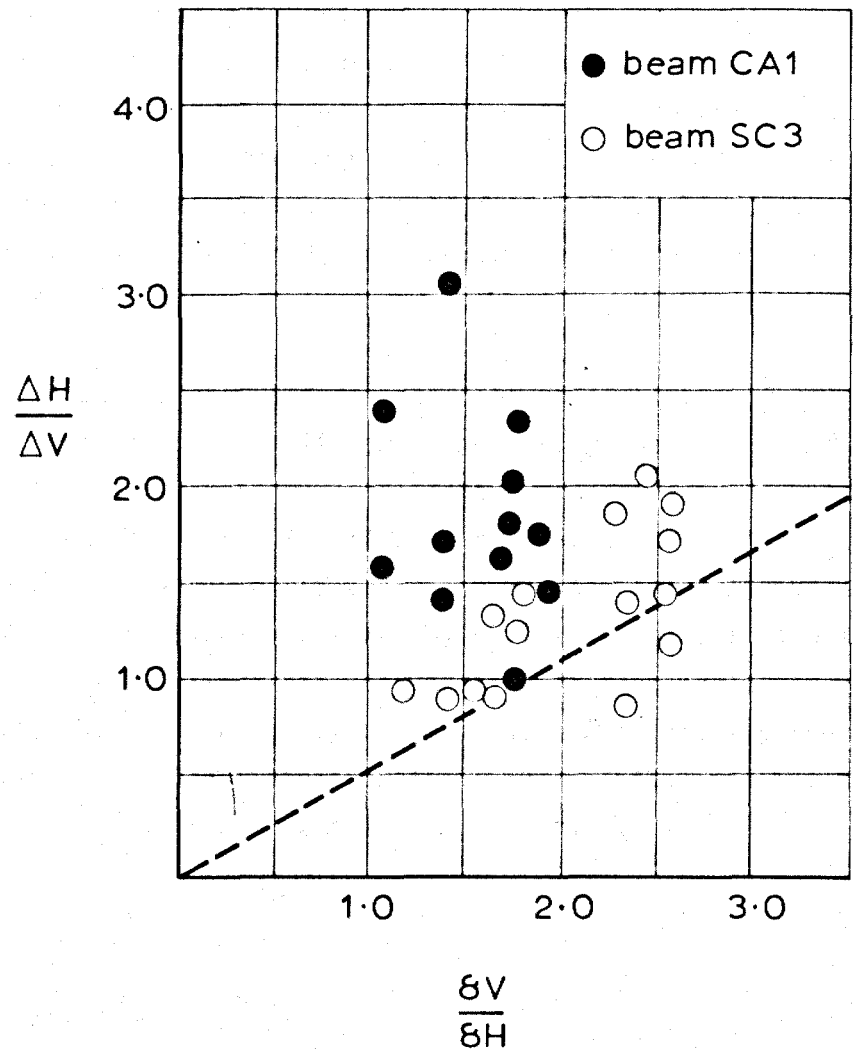

FIG. 7.6 DEFORMATIONS FROM TESTS BY FENWICK

through the holes. Beam SC 3 had 20 mm crack formers cast into its side touching the main steel so that the only concrete holding the dowel was between the bars. In each case therefore the vertical stiffness of the beams was much less than that found in normal beams. The lines shown on Figures 7.5 and 7.6 come from the equation 7.8 which fits the test data in Chapter 4.

This leads to the apparent paradox that the vertical stiffness of the beam decreases with decrease of steel percentage. This can only be explained by the fact that the cracks are more inclined in beams of low steel percentage so that steel percentage interacts with $\frac{\delta V}{\delta H}$ in the Figures. The beams tested by Fenwick had cracks that were considerably more inclined than the cracks on the beams described in Chapter 4.

This is the only information that is available on the displacements and before it can be generally used it should ideally be extended to cover beams of different stiffness. The main factors which affect the vertical stiffness of the beam are the steel percentage which governs the height of the crack and the dowel layout. In the model the dowel layout was fixed by having two bars in the tension zone, a simplification that, as has already been explained, underestimates the dowel capacity of beams with high steel percentages. The way that a generalised compatibility condition was built up was to use a version of equation 7.8 in the form

$$\frac{\Delta H}{\Delta V} = n \frac{\delta V}{\delta H}$$

where $n = e^{-ap}$

100p is the steel percentage

Thus when

$n = 0{\cdot}55 \qquad p = 1{\cdot}0$

$n = 1{\cdot}0 \qquad p = 0$

The first relation comes from the tests described in Chapter 4 and the next comes from considering the possible displacements at an extreme. When there is no steel, the cantilevers between the cracks

would simply rotate around the compression zone so that $\frac{\Delta H}{\Delta V}$ would equal $\frac{\delta V}{\delta H}$ and thus corresponds to the results of Fenwick's Tests.

Equation 7.8 in its final generalised form is

$$\frac{\Delta H}{\Delta V} = e^{-0\cdot6p} \frac{\delta V}{\delta H} \qquad 7.9$$

The value of $n = e^{-0\cdot6p}$ is shown plotted for a sensible range of steel percentage in Figure 7.7. This equation has no practical base, apart from at the 1·0% steel level and the rest of the curve is only derived using the logic mentioned above.

A very useful area of further study would be to find experimental displacement conditions for beams of widely differing steel percentages to modify the equation 7.9.

Failure Criterion

Flexural tensile or compressive failure was never found at the section considered but in some cases, the flexural moment at the load point, calculated by multiplying the shear capacity of the crack being considered by the length of the shear span was greater than the flexural capacity of the beam. These cases were recognised from the data by comparing each set of results with a flexural design chart that was prepared from another program.

The compression zone was never stressed in flexure and shear beyond the failure criterion mentioned in Chapter 4 and this was therefore not checked in the program.

The aggregate interlock and dowel forces were both capable of being lost causing the failure of the beam. The dowel force was usually on the falling branch mentioned in Chapter 5 before the beam failed.

If the vertical equilibrium equation was not capable of being solved because of the loss of their forces, the program was halted as soon as the crack reached the load point at the centre of the beam.

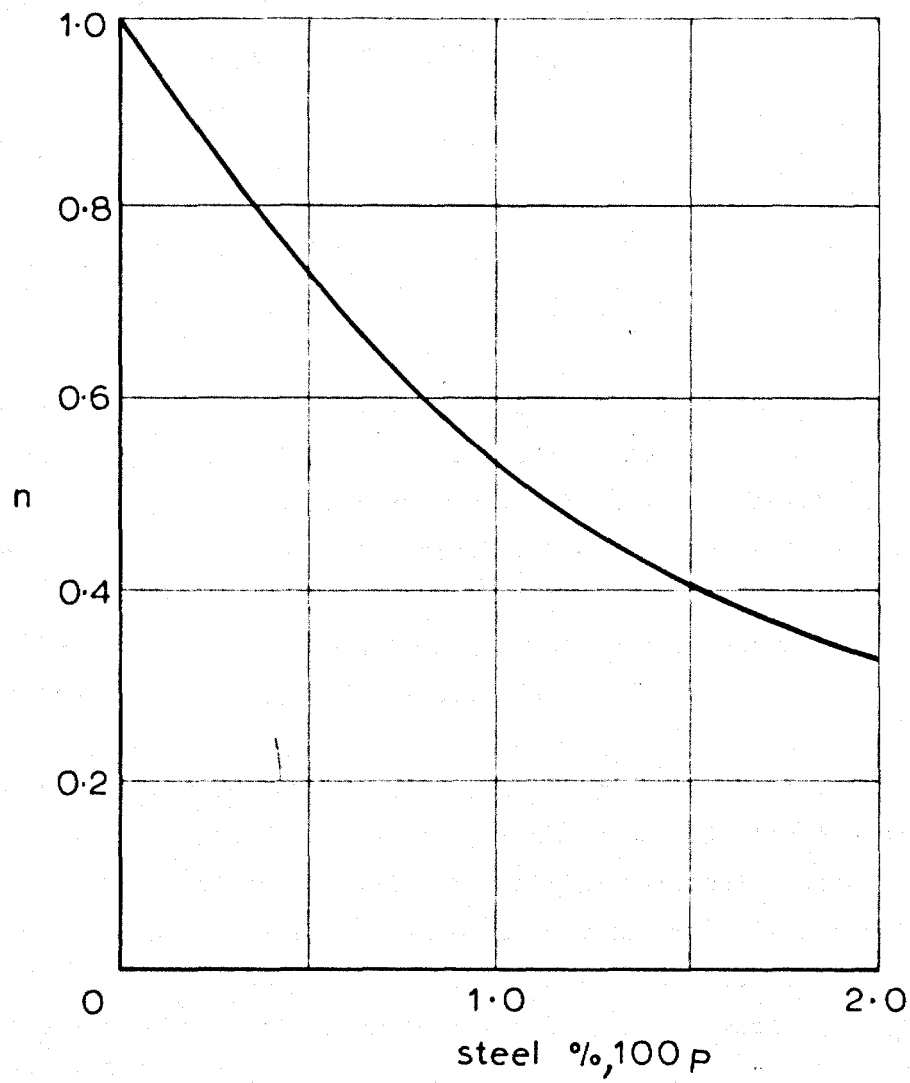

FIG. 7·7 VARIABLE n USED IN THE FAILURE CRITERION

Program Description

The flow chart of the program is shown in Figure 7.8. The program can be divided into a number of small sections which are described in detail below.

a. The initial data for the program consists of defining the basic beam properties,

Beam Width
Beam Depth and Effective Depth
Bar Layout
Bar size
Steel Strength
Concrete Strength
Shear Span
Crack Positions

These are all self explanatory apart from the last item. The starting point of the crack that is to be considered has to be defined and the program develops a crack for each given location. The shear strength of the beam corresponds to the crack which reaches failure first.

b. The initial crack height and curvature are calculated using the method that has already been described.

c. Four iterations are carried out in which the horizontal equilibrium equation 7.4 is solved, without considering the other equations, in order to simulate the initial vertical movement of the crack. This is the part of beam behaviour in which it has not been possible to find exactly how the shear force is distributed, as has been shown in the conclusions to the experimental work in Chapter 6, in Figures 6.26 to 6.29.

d. In this section of the program, the horizontal equilibrium equation 7.4 is solved, just as in section (c) apart for the fact that the program now goes on to satisfy the two other equilibrium equations.

e. A solution of the vertical equilibrium equation 7.5 is now attempted and if it is not satisfied the crack is moved horizontally

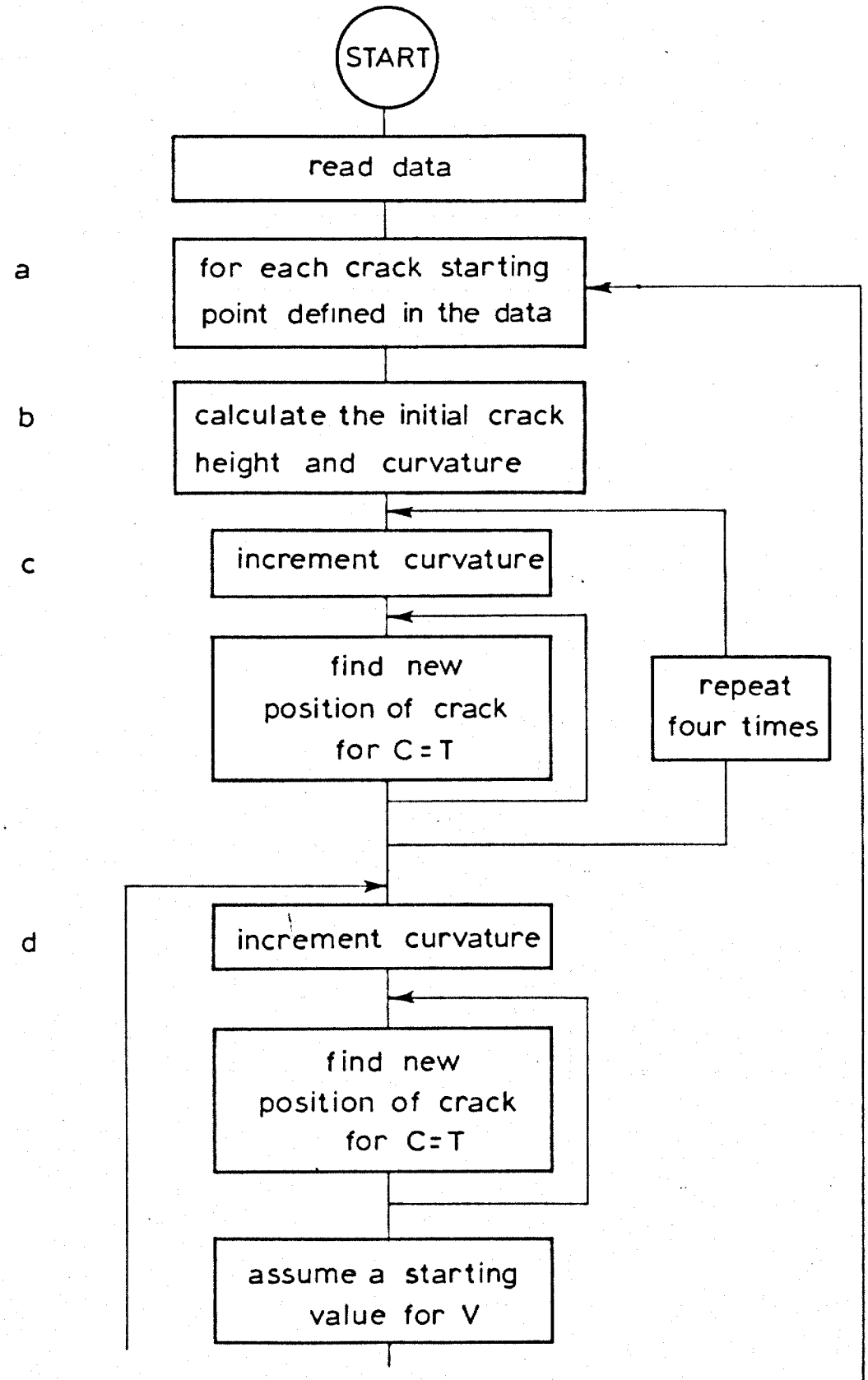

FIG. 7.8 FLOW CHART OF MATHEMATICAL MODEL COMPUTER PROGRAM

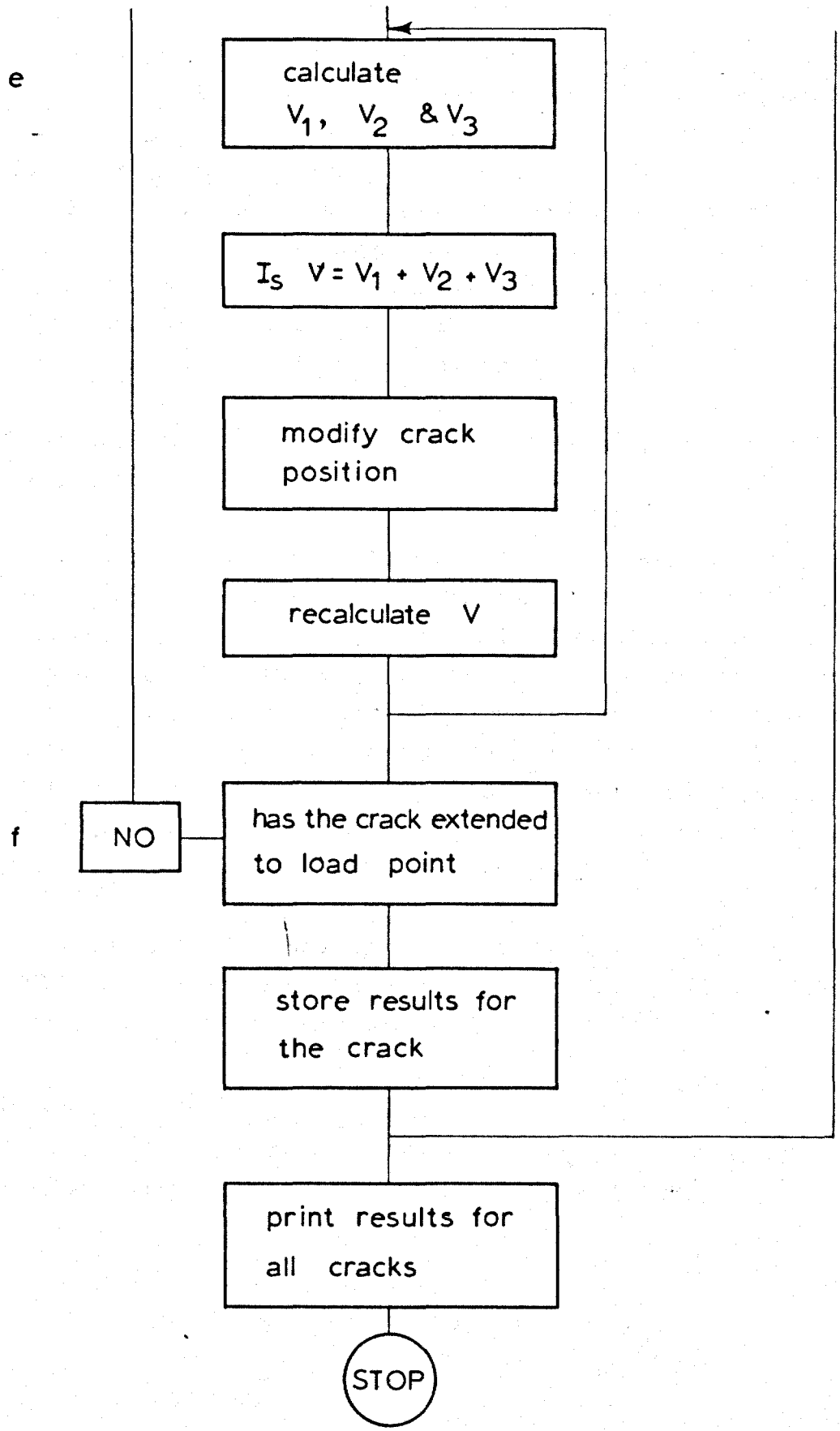

FIG. 7.8 FLOW CHART OF MATHEMATICAL MODEL COMPUTER PROGRAM

and a new value of V from the rotational equilibrium equation, equation 7.6, is re-calculated and then this section is repeated.

f. Finally the curvature is incremented and steps c and d are repeated until a solution of one of the equations is impossible or the crack extends to the support. When this happens, the output is produced in which the crack position, the curvature, all the forces in the equilibrium equations and the bending moment at the centre of the beam is punched out, for all curvature stages.

The computer time taken for each crack is approximately 3 minutes.

It can be seen from this description that equation 7.4 is solved separately from equations 7.5 and 7.6 which are solved simultaneously. This naturally leads to an error as all the equations should be solved simultaneously but, providing the curvature increment was low, the error was found to be not large and the error between the true and computed values of both C and T was less than five percent. A version of the program was written which did solve the equations simultaneously and this took more than ten times the computer time than the simple version of the program.

Future versions of programs of this type must have very efficient "hill climbing techniques" in order to solve the equations quickly and not use too much computer time.

Results

A typical set of results from the analysis of a beam with the following properties is shown in Figures 7.9 and 7.10.

Beam width 185 mm
Beam depth 370 mm
Beam effective depth 335 mm
Steel percentage 1·00
Shear span 1665 mm
Distance of crack from support 500 mm

The extent of the crack at various stages of the analysis is shown in Figure 7.9 and in Figure 7.10 the relative contributions of the compression zone, aggregate interlock and dowel forces are shown. It can be seen in Figure 7.9 that the crack does not incline gradually as in practice and this difference between the true and predicted behaviour is probably due, as has previously been stated, to inaccuracies in simulating the normal forces across the crack. The dotted parts of the crack have been added to show when the crack runs to the support and the beam fails and when the reversed inclined crack occurs.

The distribution of shear force predicted by the model shown in Figure 7.10 is very similar to that found in the experiments described in Chapter 6. On this Figure, the dotted lines are extrapolations into the sections of the program where the crack initially formed and became inclined. This part of beam behaviour is particularly difficult to explore experimentally as very sudden changes in the internal force distributions in the beam are possible just as it cracks. Figure 7.10 however points to the possibility that, as the crack forms, the dowel force builds up quickly and then as this is lost, the aggregate interlock force builds up.

A number of runs of the program was made in order to study its predictions of the effect of the various parameters in the shear problem. These were to study the effect of the following parameters; steel percentage, concrete strength, steel strength and scale.

Steel Percentage and Concrete Strength

These two parameters are now considered in the Draft Unified Code[10] in a table of nominal shear stresses from the equation $q = \frac{Q}{bd_1}$, for use at the Ultimate Limit State.

The stresses were established from a study of all the available experimental data and therefore give a good picture of the effect of the parameters. Table 7.2 shows some of the stresses in the Draft Code, with the material partial safety factor removed.

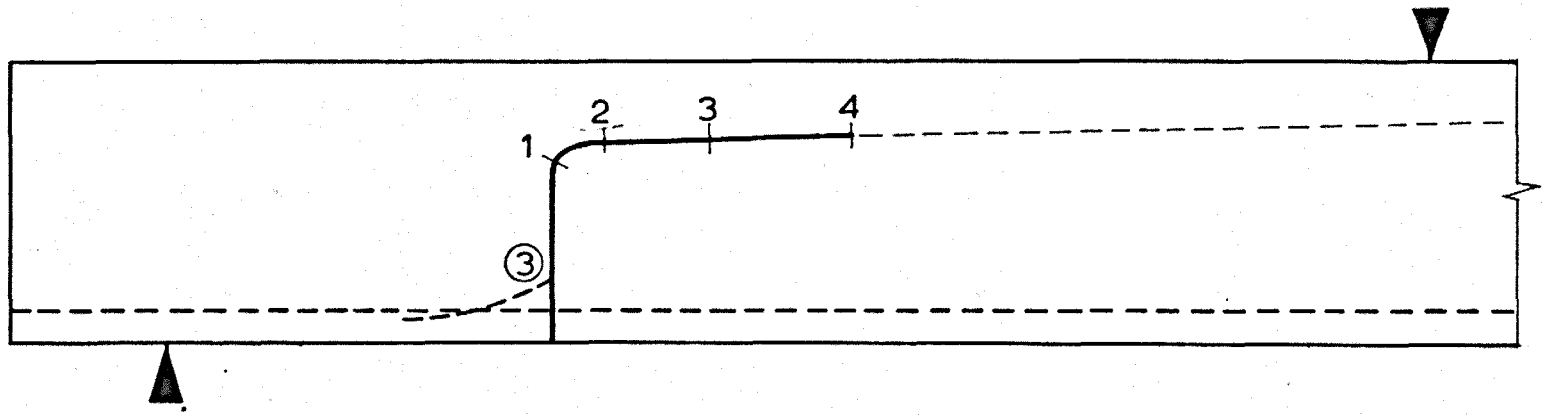

FIG 7.9 CRACK SHAPE PREDICTED BY MATHEMATICAL MODEL

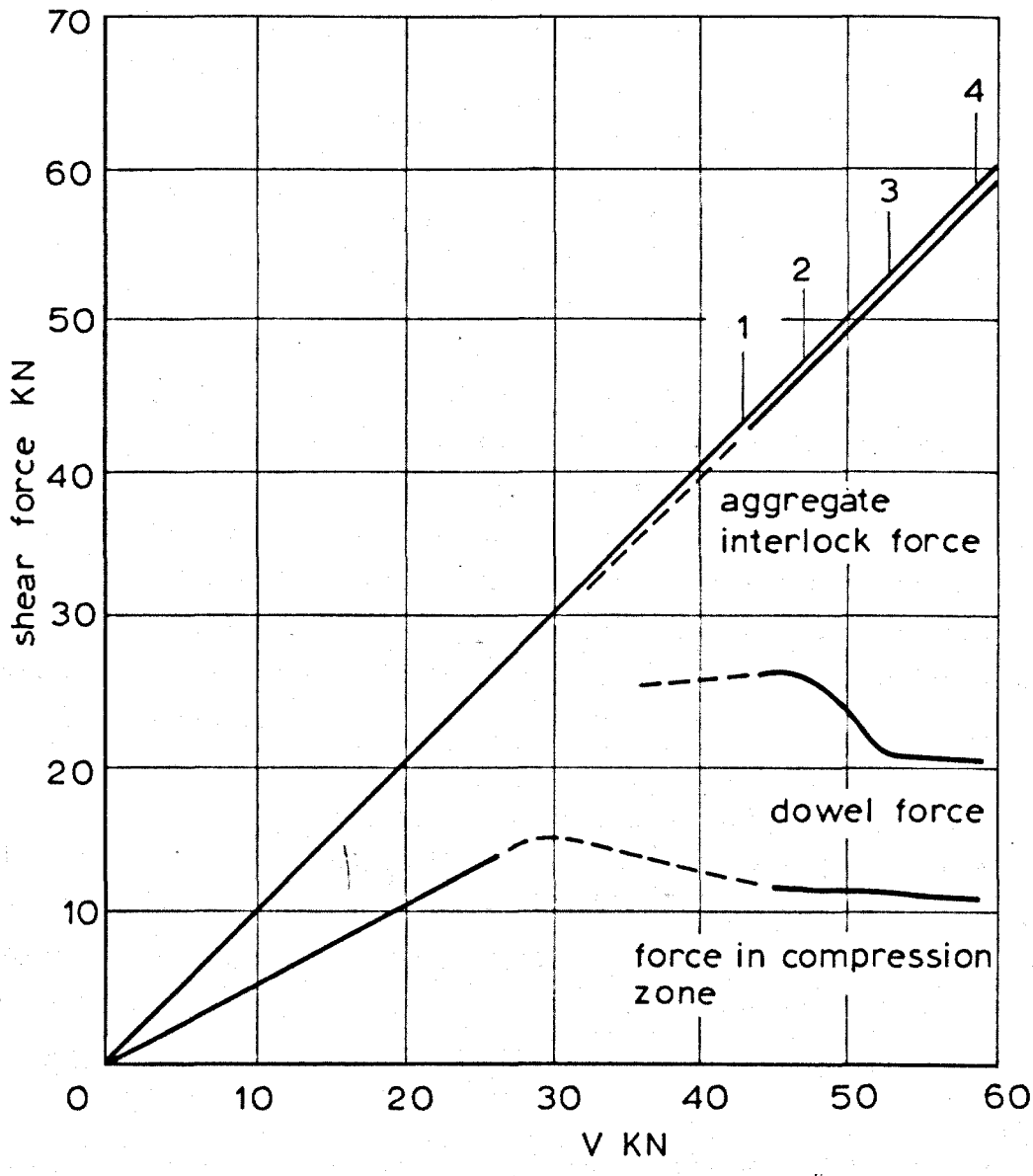

FIG. 7.10 DISTRIBUTION OF SHEAR FORCE IN A BEAM PREDICTED BY THE MATHEMATICAL MODEL

Table 7.2 Shear stress from Draft Unified Code N/mm^2

Steel percentage	Characteristic Concrete Strength N/mm^2 22·5	30	37·5	45 and more
0·5	0·40	0·50	0·60	0·65
1·0	0·50	0·60	0·70	0·80
1·5	0·60	0·70	0·80	0·90
2·0	0·65	0·75	0·85	1·00
2·5	0·70	0·80	0·90	1·05
3·0 and more	0·75	0·85	0·95	1·10

The partial safety factor of 1·5 was removed by copying the stresses in each column of Table 7.2 from a column in the Draft Code corresponding to a concrete characteristic strength 1·5 times that in the Table 7.2 column. Thus the stresses in the 30 N/mm^2 column in Table 7.2 come from the 45 N/mm^2 column in the Code. Even then, the stresses all form a lower bound to test results and the mean stresses from tests are likely to be about 1·3 times higher than the ones in the table.

A series of beams with various steel percentages and concrete strengths of 22·5 and 45 N/mm^2 was analysed by the model program and the shear stresses at the failure of the beams were calculated. The stresses are shown in Table 7.3.

Table 7.3 Shear stresses from Mathematical Model N/mm^2

Steel percentage	Concrete characteristic strength N/mm^2 22·5	45
0·5	0·590	-
1·0	0·769	0·832
1·5	0·772	0·902
2·0	0·780	0·880
2·5	0·885	1·052
3·0	0·905	1·090

There is a reasonable agreement between the model and the test results but the model does not predict shear stresses as low as those found in tests when the steel percentage is reduced. This is presumably because the compatibility condition is inaccurate, although there is very little experimental evidence to justify the stresses for beams with steel percentages less than 1·0.

The inaccuracies in predicting the dowel strength of the high steel percentage beams would also make the stresses in the high steel percentage beams from the model too low.

Another way of presenting the information is in a plot of moment capacity against shear span. Such a plot for point loaded beams with a concrete strength of 45 N/mm^2 is shown in Figure 7.11 and it can be seen that this is very similar to the experimental curve, Figure 2.5.

Effect of scale

A series of beams of full, one and a half and twice full scale models of a beam with 1·0% of steel, a/d_1 of 3 and a full scale depth of 370 mm was analysed to see if the mathematical model confirmed the loss of strength with increasing size of beam that was reported at the end of the last Chapter.

The results of this analysis are given in Table 7.4.

Table 7.4 Effect of scale on strength of beams

	Scale		
	1	1½	2
Failure moment/scale kNm	57·5	51·0	52·0

The beam with a depth of 740 mm has a strength to scale that is 90% of the strength of the smallest beam, a result that is in good agreement with the experimental results shown in Figure 6.32.

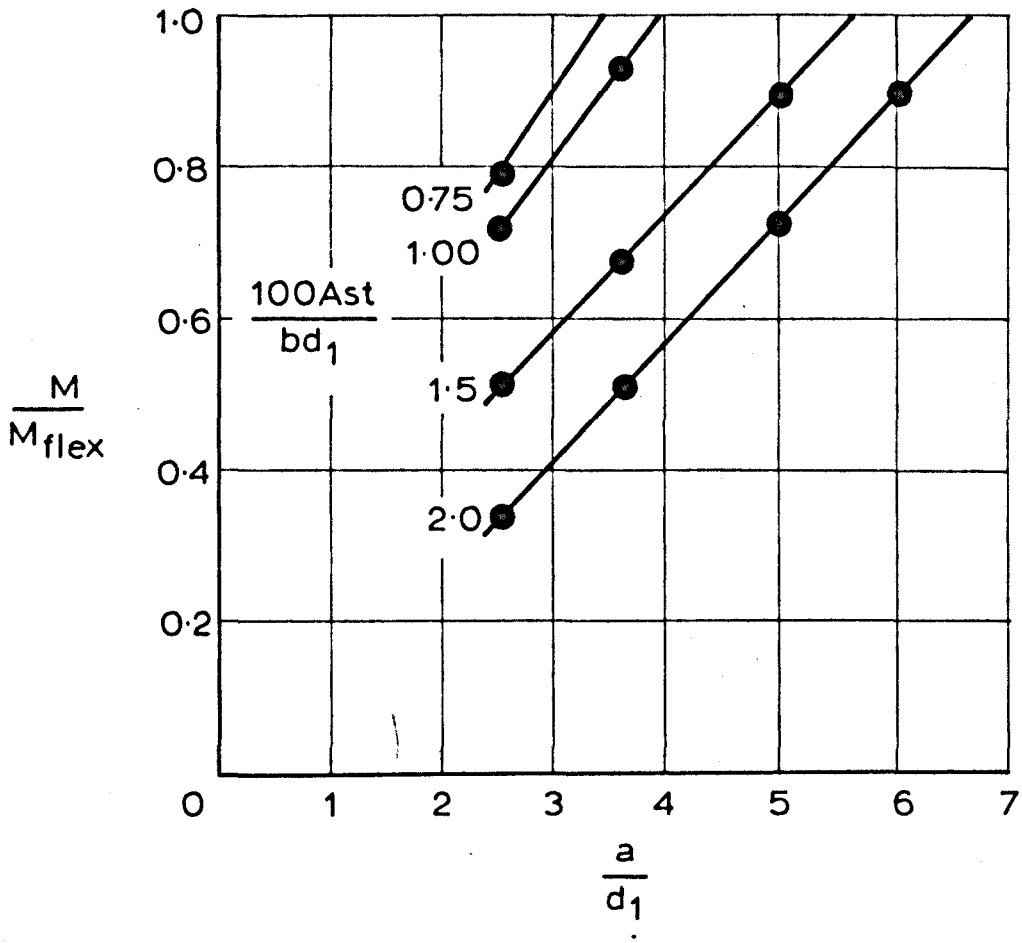

FIG. 7.11 RELATION BETWEEN BEAM FAILURE MOMENT AND SHEAR SPAN PREDICTED BY MATHEMATICAL MODEL

So far the model has only been used to predict the behaviour of beams with point loads but it should be capable an analysing beams with uniformly distributed load after a few modifications. The chief problem would be to predict the position of the failure crack and a number of runs of the program would have to be made for each beam before the critical crack could be located.

The work with the model has shown that it is possible to simulate the behaviour of beams in shear using the experimental results from the previous chapters and despite the simple compatibility condition used this simulation correctly predicts the trends of some of the important parameters in the problem although the degree of the effect of the parameters is not always correct.

CHAPTER 8

DISTRIBUTION OF SHEAR FORCES IN BEAMS WITH STIRRUPS

In this chapter, previous research in which test evidence is given of the internal distribution of forces in beams with stirrups is discussed and a limited series of tests is described in which aggregate interlock and dowel forces in beams with stirrups were measured.

In Chapter 2 the truss analogy for beams with stirrups introduced by Mörsch was described. It was soon recognised that the analogy, in which the stirrups and tension steel were considered to act as tension members of a pin jointed statically determinate truss, was conservative and was wasteful when used in design. Because of this, design Codes allowed the shear force carried by an equivalent beam without stirrups to be added to the shear capacity of the truss. This proved to be a very successful method and is in use to this day. One way of visualising this approach is to assume that until the main shear cracks are formed in a beam, the stirrups are not effective and after this point is reached they begin to carry force in the way that the truss analogy suggests. The shear force to cause cracking is never lost.

Since the truss analogy was first proposed, workers have suggested that its conservatism may be due to a variety of reasons. Firstly the truss is statically determinate, implying pin joints between stirrups and compression zone, compression zone and inclined struts and stirrups and main reinforcing steel. Secondly, the designer rarely uses the true slope of the compression struts between the lower tensile and upper compressive booms of the truss. When close spacings of stirrups are used it is often very difficult to rationalise the crack pattern and stirrup positions to a truss at all. Thirdly, the forces carried by dowel action are ignored and, in a previous chapter, these have been shown to be quite considerable, particularly if the crack is close to a stirrup.

The effect of dowel action has been considered in a proposed design method by R. Taylor[38]. Taylor said that as the cracks in

beams not only penetrate upwards and then incline towards the point of application of load they also propagate backwards towards the support point. He therefore suggested that the inclined crack across which all the shear force should be carried by stirrups should be lengthened to account for the reversed cracking. This meant that for a given spacing at least one extra stirrup was considered to carry shear forces across the crack. This design approach had the effect of considerably reducing the number of stirrups in a beam compared with the current British Code, which says that all shear forces must be carried by stirrups when the shear cracking load of a section is exceeded. The new approach predicted strengths that agreed well with tests. Leonhardt[39] has developed a method of shear design from a study of extensive tests that he has carried out. This method, which he calls the method of reduced reinforcement for shear, gives a way of reducing the shear reinforcement from the truss analogy amount so that the conservatism may be allowed for in design. Figure 8.1 shows a typical curve which gives the factor of shear coverage to be applied to the shear requirements of the truss analogy to reduce it to a design value, in this case, for working stress design. Different curves are proposed for simply supported and continuous beams.

The vertical axis of the Figure has the nominal shear stress on the section plotted as a ratio of the concrete strength and the factor η which is dimensionless, plotted horizontally. It is possible to take values of η from the Figure and plot $\frac{V}{fc'} - \frac{\eta V}{fc'}$ which is the contribution of the concrete to the shear capacity (i.e. the shear stress not carried by truss analogy).

This is shown in Figure 8.2 and has nearly a constant value indicating that the method is simply another way of stating the truss analogy.

A very different concept as to how stirrups carry shear forces was described in a paper by Kani[40]. Kani said that the stress trajectories in a beam in shear follow the shape of a series of arches which support the compression zone. This concept is illustrated in Figure 8.3. In the Figure the arches can be seen with the stirrup

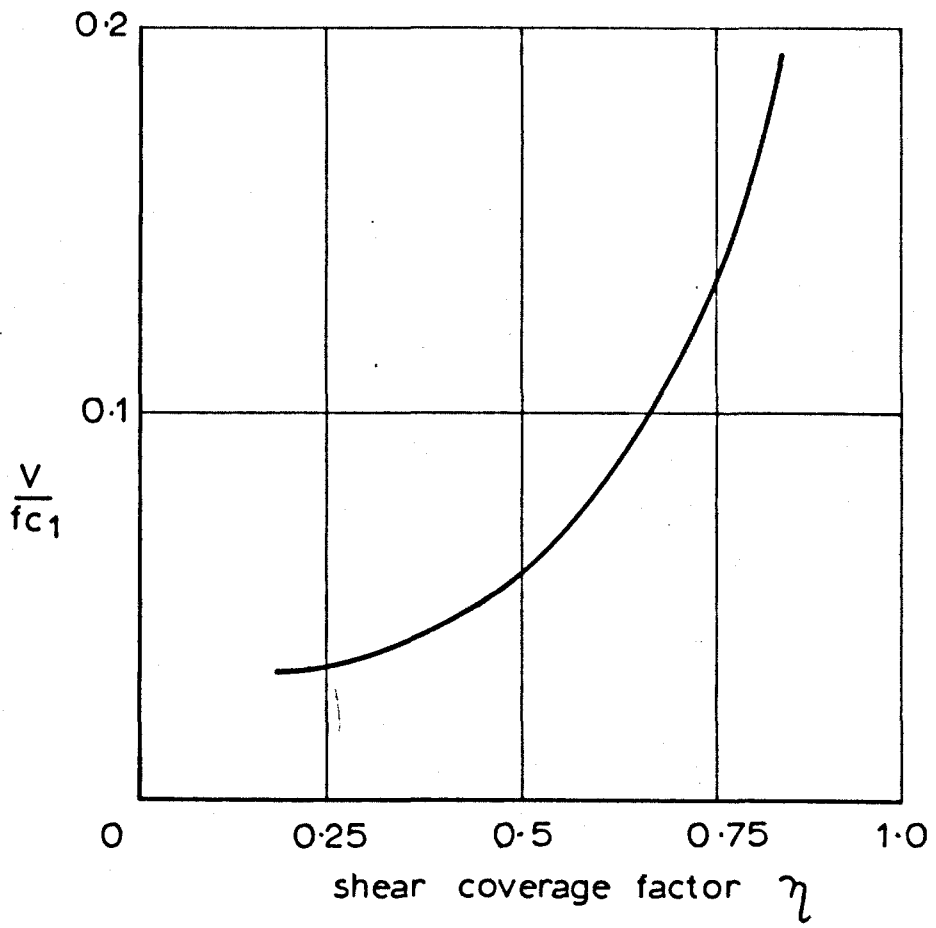

FIG. 8.1 FACTOR FOR SHEAR COVERAGE - LEONHARDT

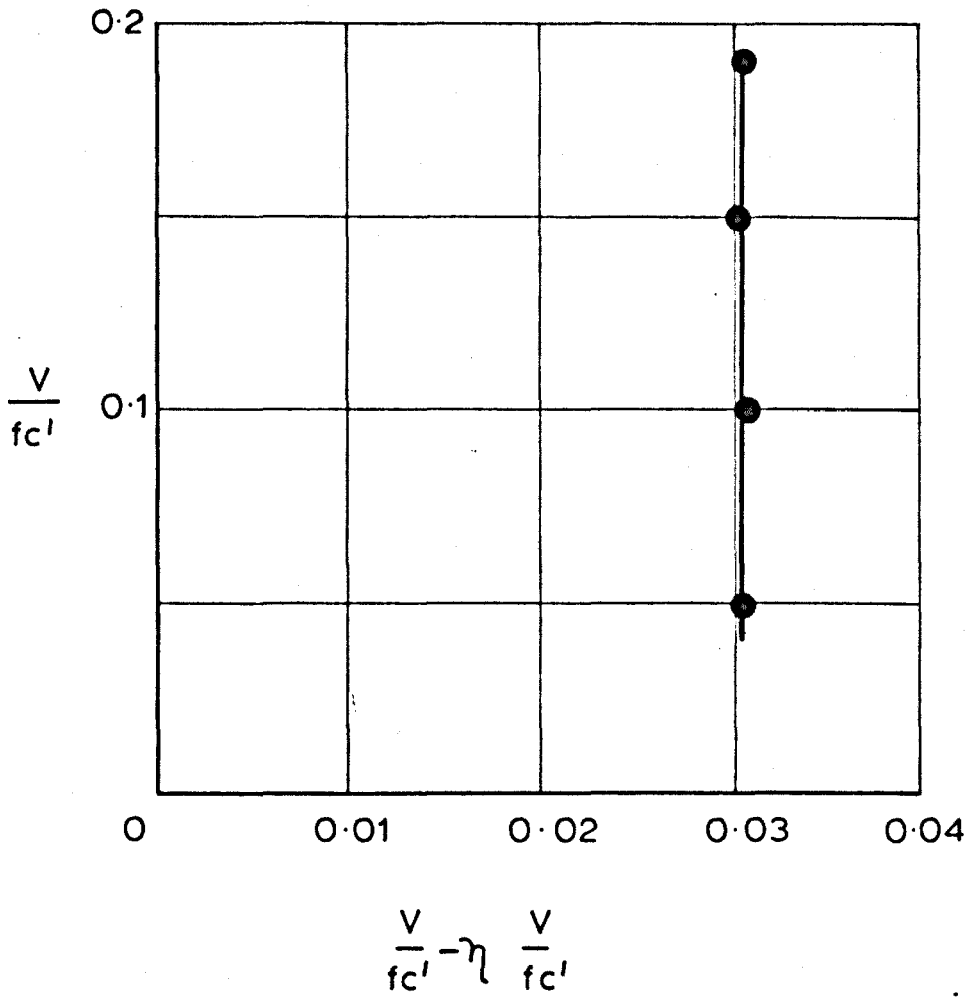

FIG.8.2 SHEAR STRESS NOT CARRIED BY SHEAR COVERAGE FACTOR – LEONHARDT

reinforcement proposed by Kani. The reinforcement should ideally be inclined to converge at the point where the support and compression zone thrusts meet although vertical stirrups, shown dotted, may also be used but are slightly less effective. Kani said that only the stirrups shown are necessary and the other areas of the beam do not need shear reinforcement. This has been recognised before by a number of workers who have pointed out that the provision of an area of concentrated stirrups at the mid point of the shear span of a beam merely turns it into two shorter beams with a/d_1 ratios half that of the original. Kani's description of the behaviour of stirrups illustrates that a number of analogies of how stirrups carry forces are possible and each such equilibrium solution should produce a safe lower bound to the strength of the beams.

A good experimental study of the forces carried by stirrups was carried out by Rüsch and Mayer[41]. The tests are summarised in Table 8.1 and Figure 8.4. In the tests, the main steel and stirrups were instrumented so that it was possible to measure the strains in them. Small studs were welded onto the steel with a small hole drilled in the top of each stud to take a mechanical strain gauge of the demec type. The beams were cast with sleeves over the studs and when the concrete had set the sleeves were removed leaving the studs free standing in holes in the sides of the beams. By providing studs on the bars at regular spacings and reading the strains from one stud to another it was possible to draw a histogram of strain down the beam in the form shown in Figure 8.5. A smooth curve may then be drawn over the histogram with the same area underneath it as the area under the histogram. The maximum point of the curve usually coincides with the point where an inclined crack crossed the stirrup and from this peak strain given in the report it has been possible to estimate the force carried by the stirrups in the beams. The force carried by the stirrups is plotted against the total shear force on the beams in Figures 8.6 to 8.9. The letters on the curves correspond to the end of the beam and the numbers to the number of the stirrup as shown in Figure 8.4. In the case of Figures 8.6 and 8.7, the truss system was assumed to consist of two trusses superimposed on each other, the inclined concrete compressive struts have been assumed to go from the bottom of one stirrup to the

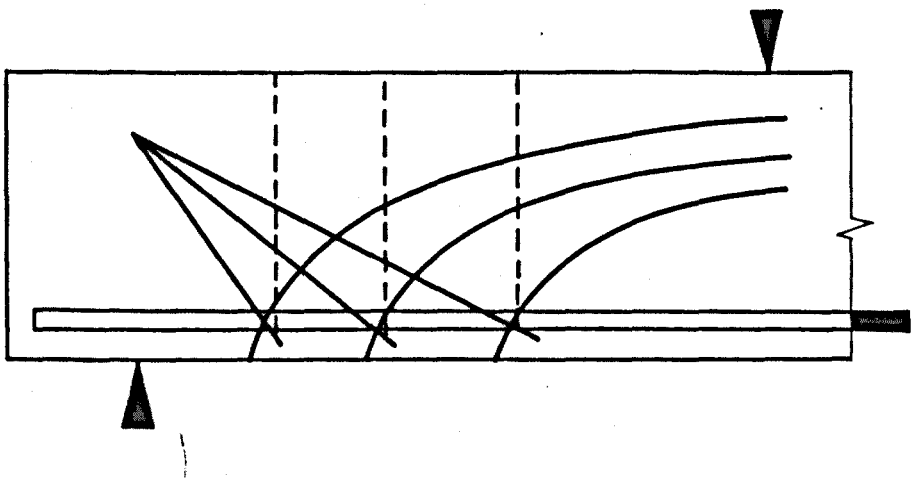

FIG.8.3 ACTION OF STIRRUPS PROPOSED BY KANI

TABLE 8.1

Test	Rüsch and Mayer Details of Tests										
	beam properties						steel properties				Concrete strength N/mm²
							Yield stress N/mm²		Diameter mm		
	d_1 mm	b mm	a mm	a/d_1	$\bar{t}$ mm	$\frac{A_{st}}{bd_1}$ %	Main	Stirrup	Main	Stirrup	
62/1	319	107	1100	3·82	139	3·6	410	450	2 No.26·6	9·9	57·8
62/4	321	110	1100	3·91	360	3·6	425	475	2 No.26·6	11·8	58·4
62/3	319	108	1100	3·84	550	3·6	440	465	2 No.26·6	11·9	57·8
62/2	323	110	1100	3·90	790	3·6	420	460	2 No.26·6	11·9	66·5
62/5	322	111	1100	3·86	360	3·6	470	490	2 No.25·2	11·4	63·6

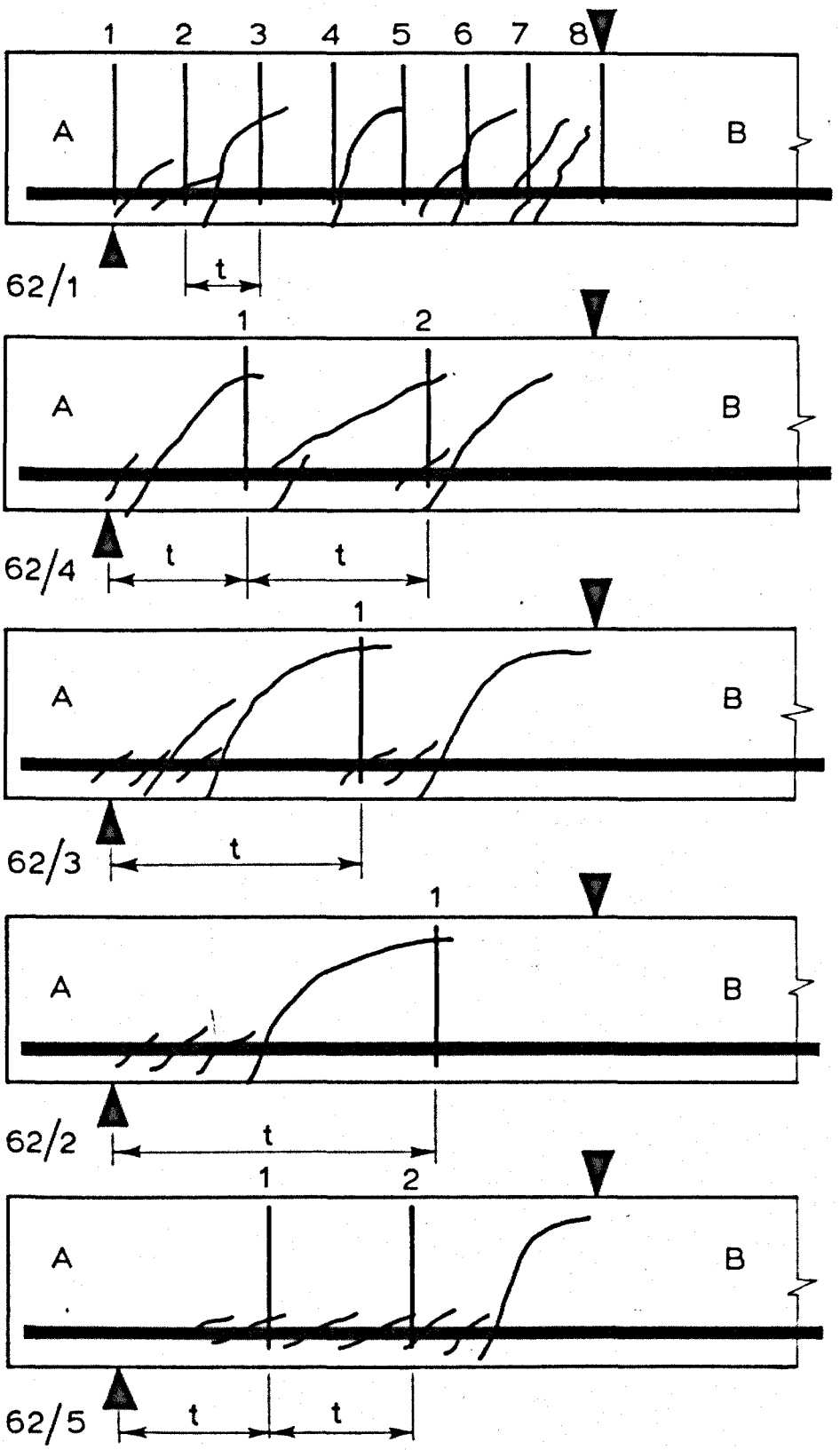

FIG. 8.4 LAYOUT OF TEST BEAMS-RÜSCH AND MAYER

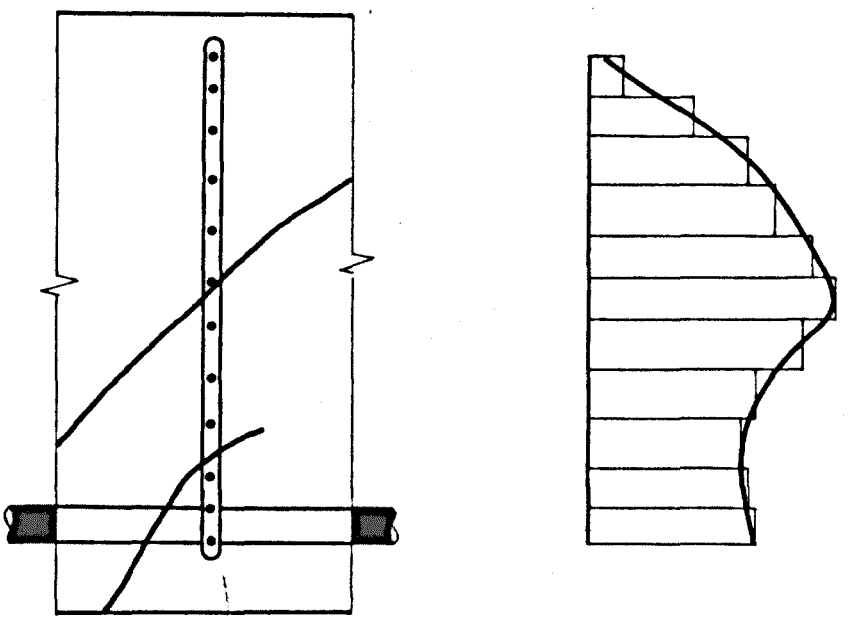

FIG.8.5 METHOD OF DETERMINING STRAIN IN STIRRUPS -RÜSCH AND MAYER

top of the next stirrup but one, from stirrup n to n + 2. Each stirrup, according to the truss theory should therefore carry half the shear force on the beam. The lines on Figures 8.6 and 8.7 show this theoretical truss theory line. In the other beams, the system was assumed not to overlap and each stirrup must therefore carry the whole of the shear force on the beam.

The failure loads of the beams are shown in the Figures and are given more accurately in Table 8.2 below.

Table 8.2 Failure loads of beams tested by Rüsch and Mayer (kN)

	Beam 62/1	62/4	62/3	62/2	62/5
Load kN	95	95	81	52	72

If the shear strength of the beams is compared with the shear capacity from the truss analogy it will be seen that none of the beams reached the truss analogy shear strength. This is because beam 62/1 failed in flexural compression in the zone of constant moment between the points of load application and the other beams failed because the stirrups were too widely spaced to stop the small sections of beam between them failing in shear. The first beam was therefore over-reinforced in shear and the rest had too wide a stirrup spacing for the stirrups to be effective.

This does not mean that the stirrup forces that were measured are not useful as they show how the stirrups effect the shear capacity of the beams.

The Figures show that the line of force carried by the stirrups is very variable, it is not always parallel to the truss theory line but tends, in some cases, to incline towards it. The variability is mainly explained by the difference in cracking over each stirrup and partly by the fact that the plots of strain given in Rusch's report from which the Figures in this Chapter have been derived are to a very small scale, making precision of calculation difficult.

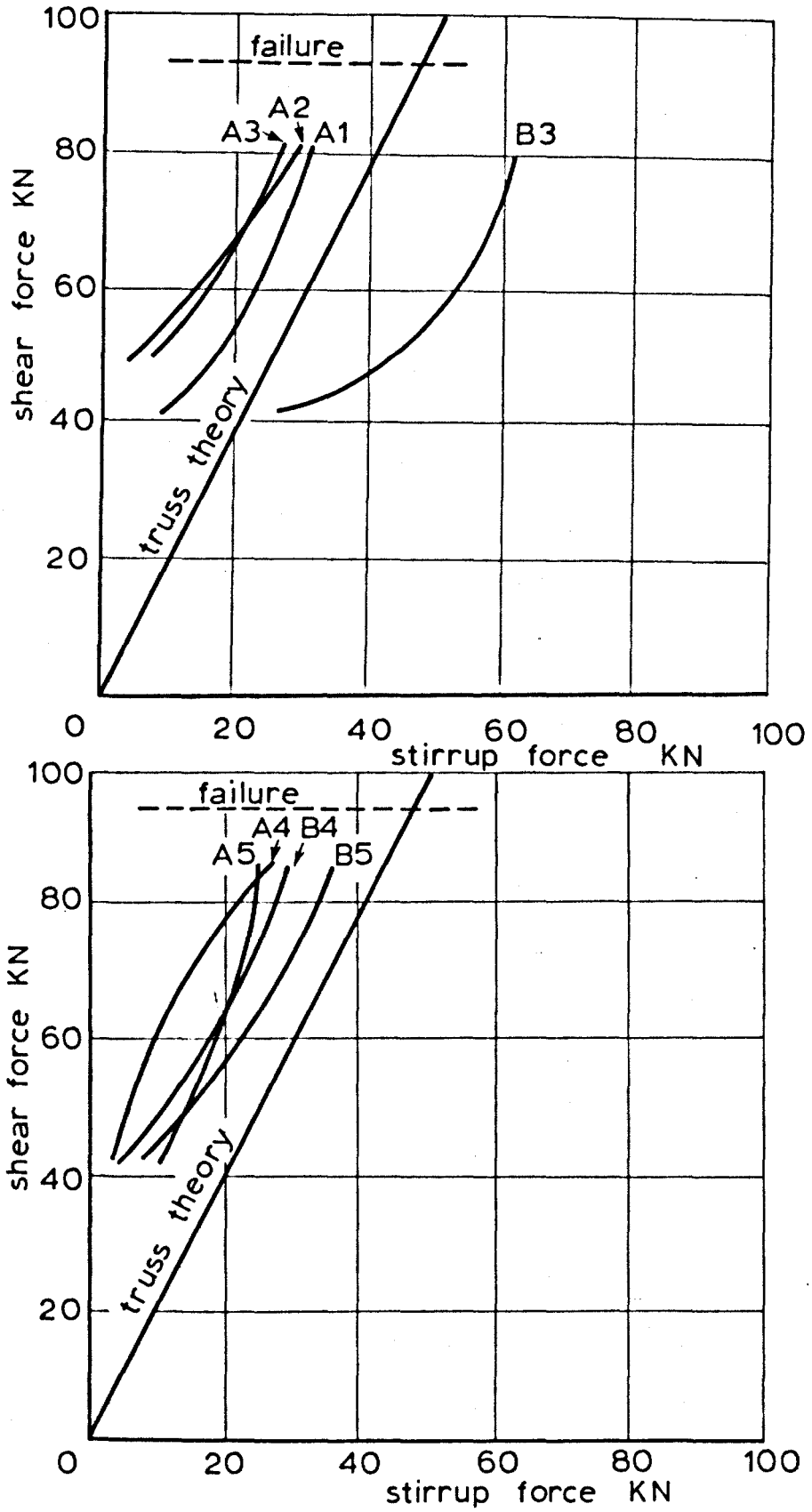

FIG.8.6 STIRRUP FORCE CARRIED IN BEAM 62/1

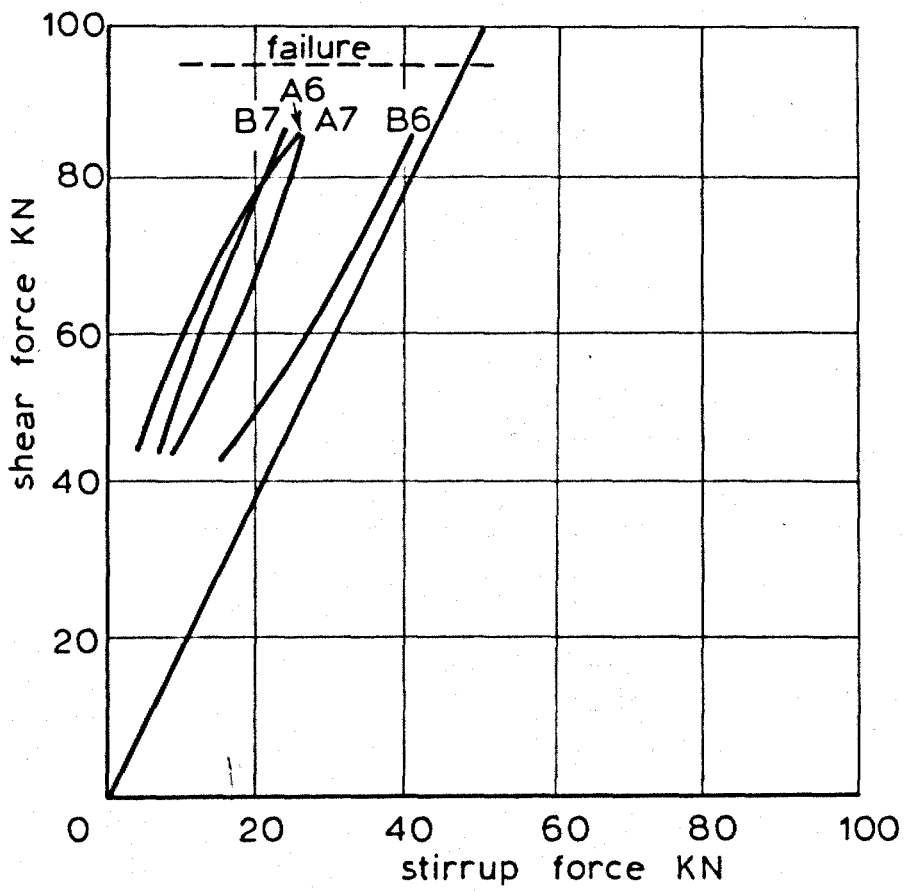

FIG.8.7 STIRRUP FORCE CARRIED IN BEAM 62/1

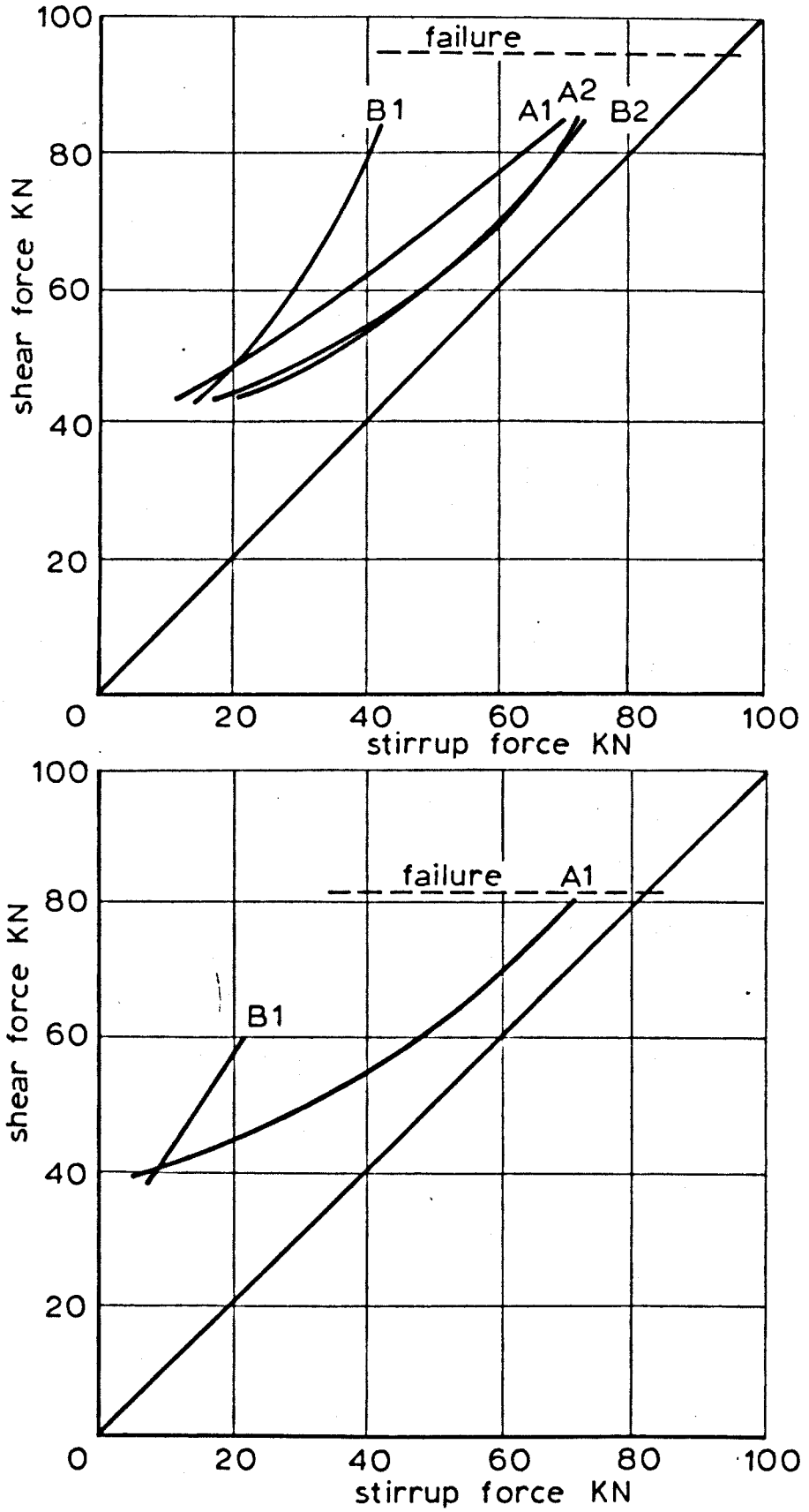

FIG.8.8 STIRRUP FORCE CARRIED IN BEAMS 62/4 & 62/3

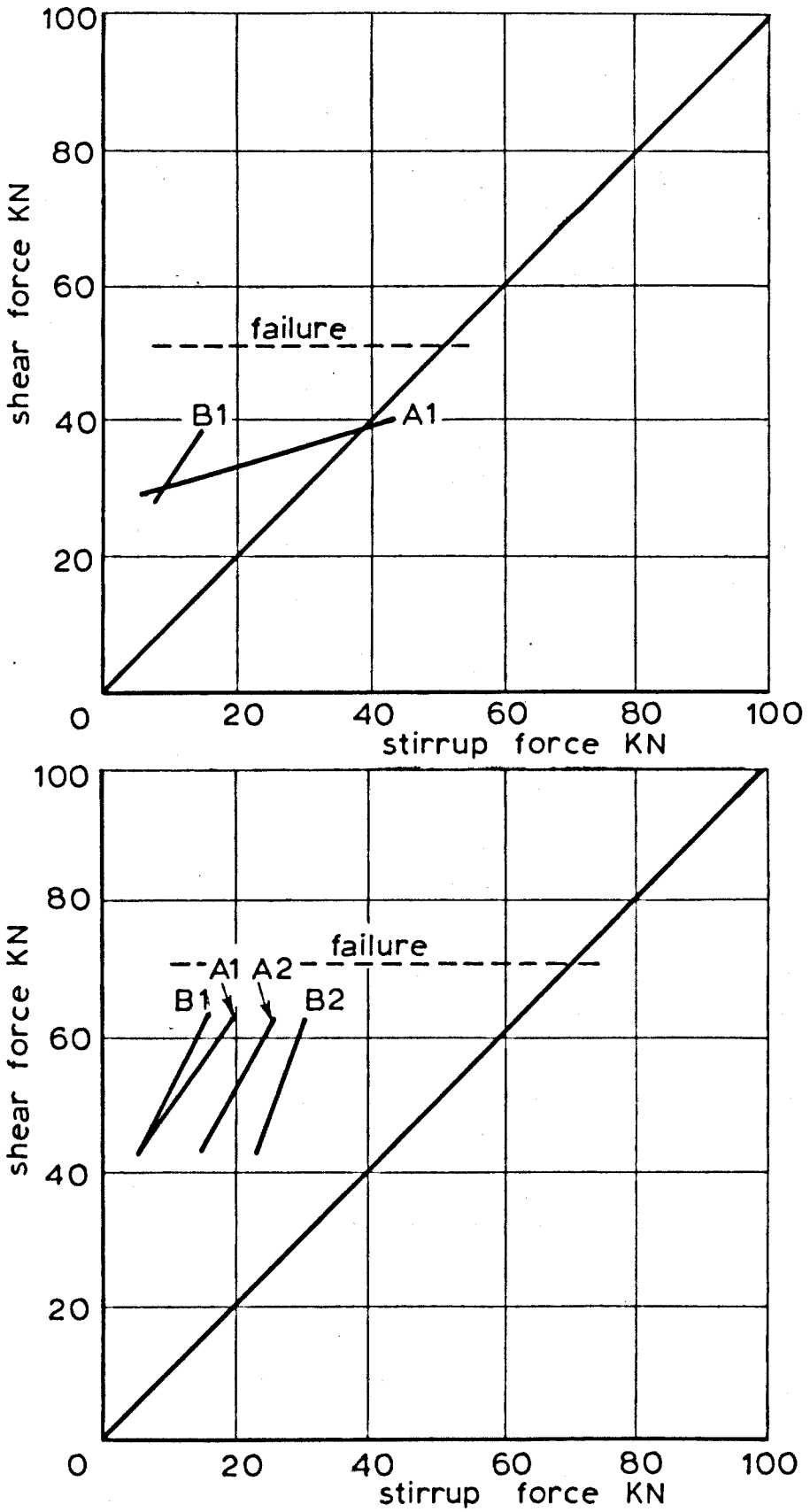

FIG.8.9 STIRRUP FORCE CARRIED IN BEAMS 62/2 & 62/5

The next section of this Chapter describes four tests on beams with stirrups in which measurements were taken on the beam compression and tension zones in a manner similar to that used in the tests on beams without stirrups. In this case, the same analysis of compression zone strains was made but this time with less success than before.

Details of the test beams are given in Table 8.3.

Table 8.3

Details of beams 11-14							
Beam No.	Shear Span (mm)	a/d_1	Steel percentage	Stirrup diameter mm	Stirrup spacing mm	Stirrup yield stress N/mm^2	Concrete cube strength N/mm^2
11	1470	3·99	1·03	6	180	410	43
12	1170	3·16	1·03	6	180	410	41
13	864	2·32	1·03	6	180	410	49
14	864	2·32	1·03	6	288	250	54

The first three beams had high strength stirrups at a close spacing and failed in flexure as they were over-reinforced in shear but inclined cracking had advanced to an extreme stage, especially in the case of beam 13, before the beams failed. Beam 14 was provided with mild steel stirrups at a wider spacing and this did reach a stage where the inclined crack was almost at failure before the beam failed. It is particularly difficult to design a rectangular beam with a low tensile steel percentage and a close stirrup spacing to fail in shear, although if the test beams were of T section this would be possible. These tests were carried out on rectangular beams as the methods of estimating the shear force are all much simpler to apply, particularly in the case of the compression zone forces.

The layout of the crack patterns at the final load stages of the beams are shown in Figure 8.10 and the details of the shear forces for each load stage are shown in Table 8.4. The crack patterns can be compared with the patterns of beams 7, 8 and 9 shown in Figure 4.20. Beam 11, apart from the addition of stirrups was identical in layout to beam 9. Both beams failed in flexure at a

similar load, the shear force was 89·0 kN for beam 9 and 82·0 kN for beam 11. Beam 12 was comparable with beam 8 and both of them failed in flexure. The shear forces were 114·0 kN for beam 8 and 105·0 kN for beam 12. Beams 13 and 14, of which beam 13 failed in flexure and beam 14 was at the point of shear failure, compare with beam 7 which failed in shear. The shear force at the failure of beam 7 was 99·0 kN and at the failure of beams 13 and 14 was 130·2 and 107·2 kN. The failure of beam 14 was therefore a shear failure, intermediate between the behaviour of beams 7 and 13.

Longitudinal strains were measured in the compression zone of all the beams in vertical sections at the positions shown in Figure 8.10 and these strains were used in the program described in Chapter 4 to compute the compression zone shear stresses and shear forces. Not all the computations were successful as it was found that when the large inclined crack formed and did not, in the case of the beams with stirrups, cause failure, it did produce large discontinuities in the strain readings which made further calculations impossible. Because of this only the shear forces before the discontinuities occurred are given in Table 8.5 - 8.7. No compression zone shears are given for Beam 13 as the only shear forces that were calculated were at very low loads and were of little use in defining the shear stress distributions in the beam at high load stages.

When the inclined cracks formed, the strain in the compression zone at the outer fibre of the beam at the head of the crack decreased, the strain just above the crack increased and the beam behaved as an arch, much as in the way found by Watstein and Mathey in short beams unreinforced in shear. Another possible contributary effect to the change in the stress conditions in the compression zone was that as the crack formed there was some shear displacement across the crack which enabled the stirrups to act as dowels and produced some interlock shear force which, as the cracks were inclined at less than 45 degrees to the horizontal, produced a longitudinal compressive force at the level of the crack.

Delta rosettes for the 50 mm demec gauge were fixed over the cracks in the way described in Chapter 4 so that the normal and

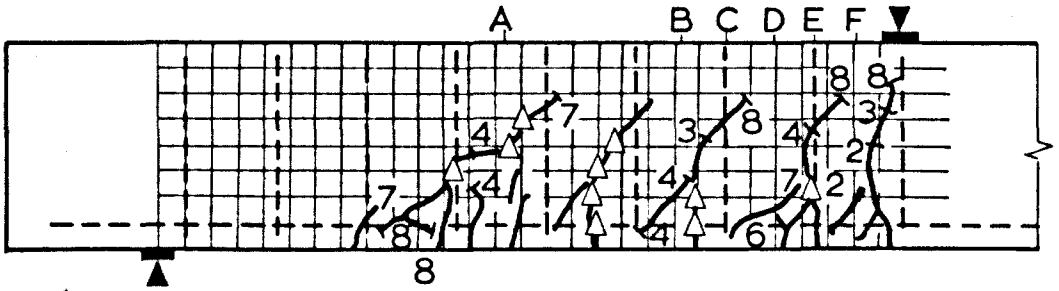

beam 11

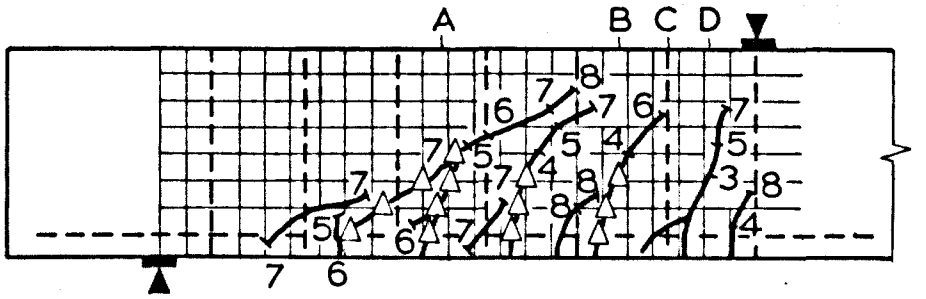

beam 12

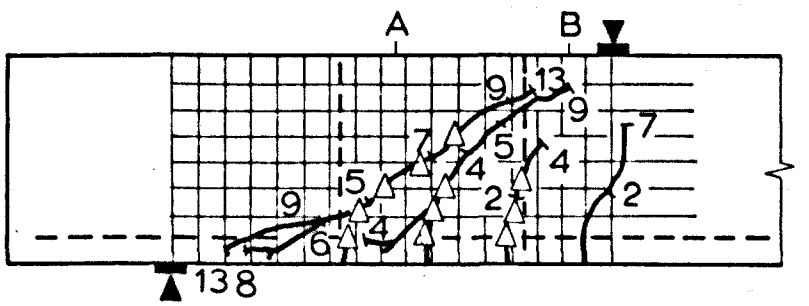

beam 13

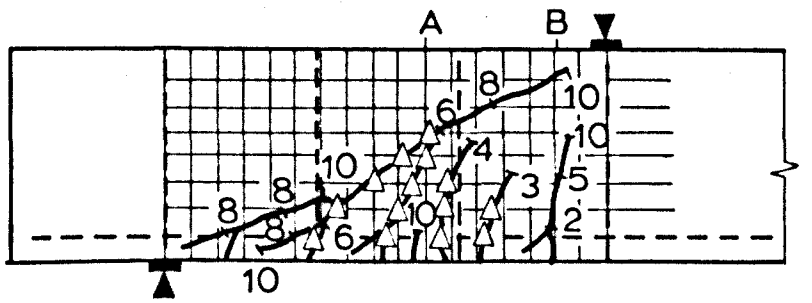

beam 14

FIG.8.10 LAYOUT OF BEAMS 11 TO 14

TABLE 8.4

Test results from beams 11 - 14

Shear force kN				
Load stage	11	12	13	14
1	0	0	0	0
2	26•0	31•0	45•8	45•8
3	39•0	43•5	53•5	53•6
4	52•0	55•9	61•1	61•2
5	58•5	68•4	68•8	68•8
6	65•0	80•6	76•5	76•5
7	71•5	93•1	84•0	84•3
8	78•0	99•5	91•9	91•9
9	82•0	105•0	99•5	99•6
10			107•1	107•2
11			114•8	
12			112•4	
13			130•2	

TABLE 8.5

Beam #1 - shear force, V_1 in the compression zone kN							
Load Stage	V_{kN}	Gauge Line					
		A	B	C	D	E	F
2	26·0	6·7	7·6	6·5	3·8	9·2	6·3
3	39·0	8·9	9·6	8·9	5·2	10·9	7·9
4	52·0	9·6	11·4	11·2	6·9	10·9	9·3
5	58·5	12·2	12·5	11·9	7·5	12·0	10·3
6	65·0	12·6	14·2	16·4	8·3	13·2	11·3
7	71·5	13·8	15·6	17·8	9·1	14·0	12·3
8	78·0	14·7	16·3	18·0	9·8	14·0	12·3
9	82·0	15·3	17·2	18·2	10·3	13·7	12·5

TABLE 8.6

Beam 12 Shear force V_1 in the compression zone kN				
Load stage	V_{kN}	Gauge Line		
		A	B	D
2	31·0	5·0	8·6	6·7
3	43·5	6·1	9·7	8·2
4	55·9	6·8	12·1	10·1
5	68·4	9·7	15·5	9·4
6	80·6	12·7	19·7	-
7	93·1	18·2	22·6	-
8	99·5	29·8	23·8	-
9	105·5	37·5	25·6	-

TABLE 8.7

Beam 14 Shear force V_1 in the compression zone kN		
Load Stage	V_{kN}	Gauge Line B
2	45·8	5·2
3	53·6	6·4
4	61·2	8·1
5	68·8	9·1
6	76·5	10·0
7	84·3	10·0
8	91·9	-
9	99·6	-
10	107·2	-

shear displacements across the cracks could be measured. The position of the rosettes are shown in Figure 8.10.

The aggregate interlock and dowel forces across the cracks were calculated using the measured displacements and the methods described in Chapters 5 and 6. In the case of the dowel forces, the presence of the nearest stirrup to the dowel was considered and taken account of in the manner shown in Figure 5.20.

The relative amounts of the shear force carried by the compression zone, aggregate interlock and dowel action are shown in Figures 8.11 - 8.14. The compression zone force is shown, whenever it was calculated and in the case of beam 13 is ignored. In the other Figures, the compression zone shear line is extrapolated whenever necessary.

Inclined cracking was never extensive in beams 11 and 12 so that the beams behaved in a way very similar to beams 8 and 9 although not as much of the total shear force on the beams was accounted for. The rest of the force is presumably carried by the stirrups. The large increase of aggregate interlock force in beam 13, line B, corresponds to the time when the inclined crack formed and a large area of crack was suddenly available to carry shear forces. Assuming that the compression zone is only carrying a low shear force, the shear force carried by the stirrup is quite considerable. The same situation arises as the aggregate interlock force suddenly increases in beam 14 at a shear force of 91·9 kN when the large diagonal crack formed.

Assuming that the shear force unaccounted for is carried by the stirrups it should be possible to plot a series of Figures similar to 8.6 - 8.9 but, as the same inaccuracies in Figures 6.26 - 6.29 apply in Figures 8.11 - 8.14, the plots would be very unreliable. The general conclusion that the stirrup forces are low until the large inclined cracks form and open is still admissible. An important area of future work would be to carry out experiments similar to the ones just described, including the measuring of stirrup strains by Rüsch's methods on a number of beams, preferably T beams, to tie these two pieces of work together.

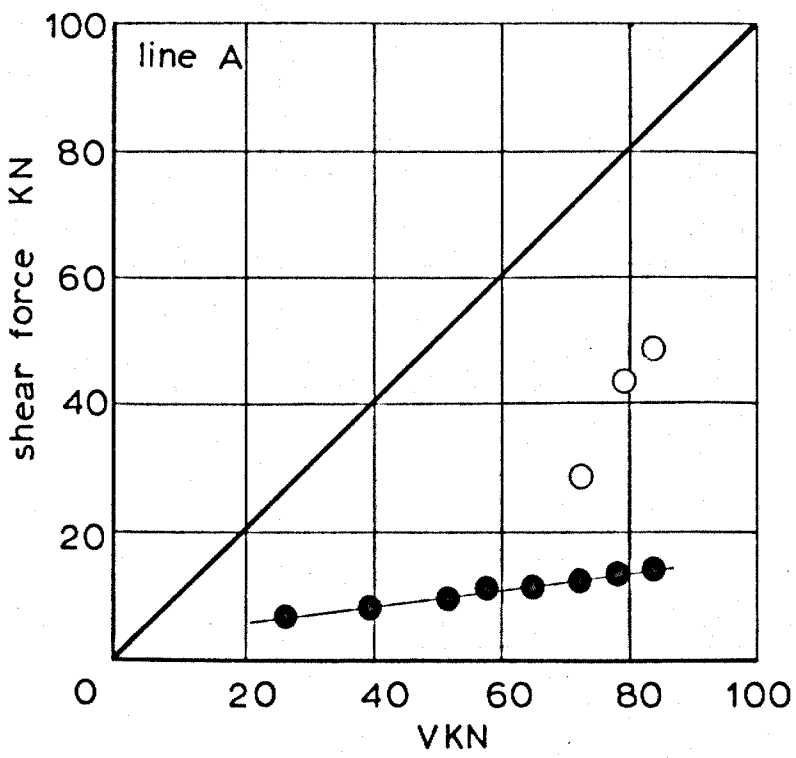

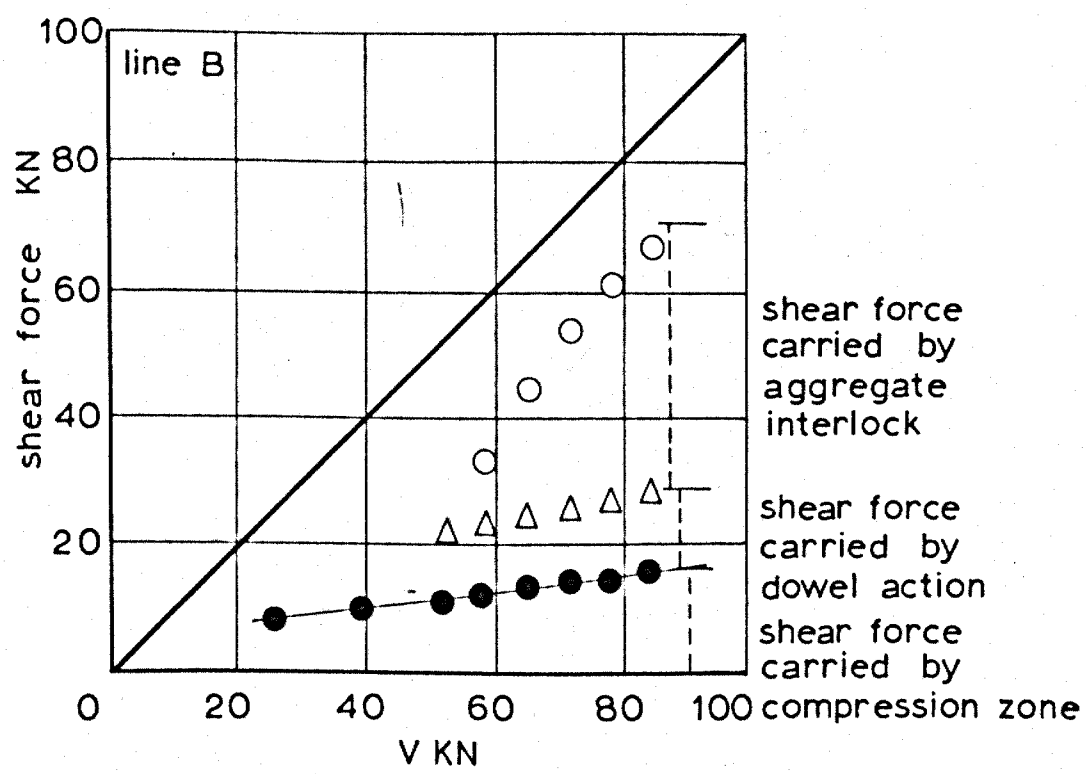

FIG.8.11 DISTRIBUTION OF SHEAR FORCE IN BEAM 11

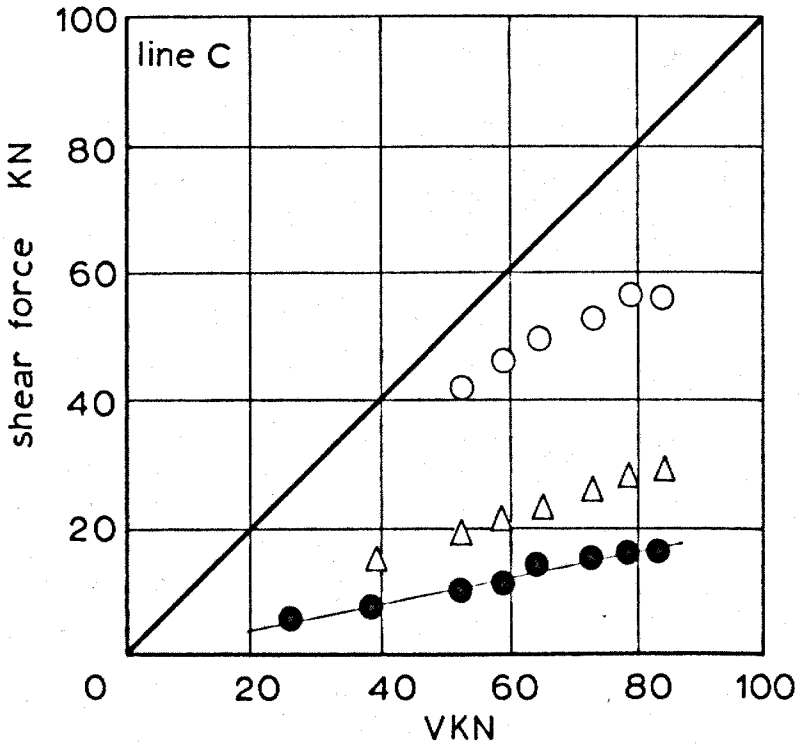

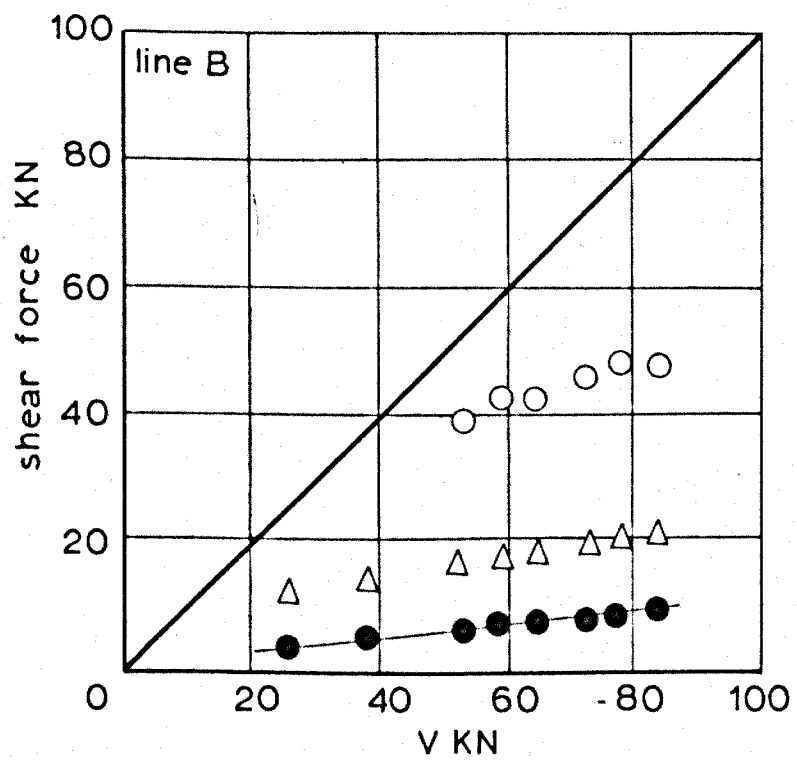

FIG. 8.11 DISTRIBUTION OF SHEAR FORCE IN BEAM 11

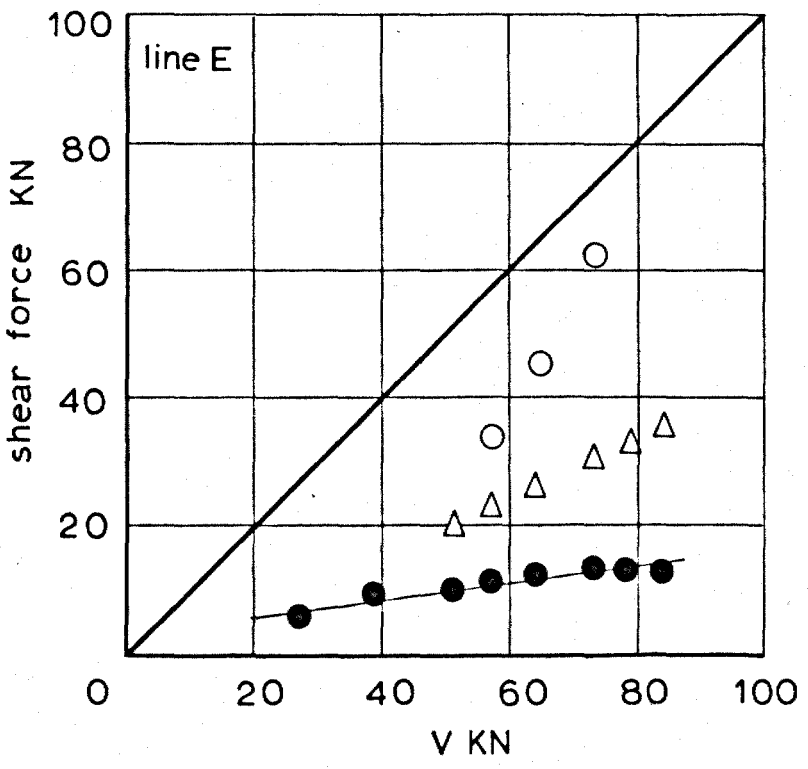

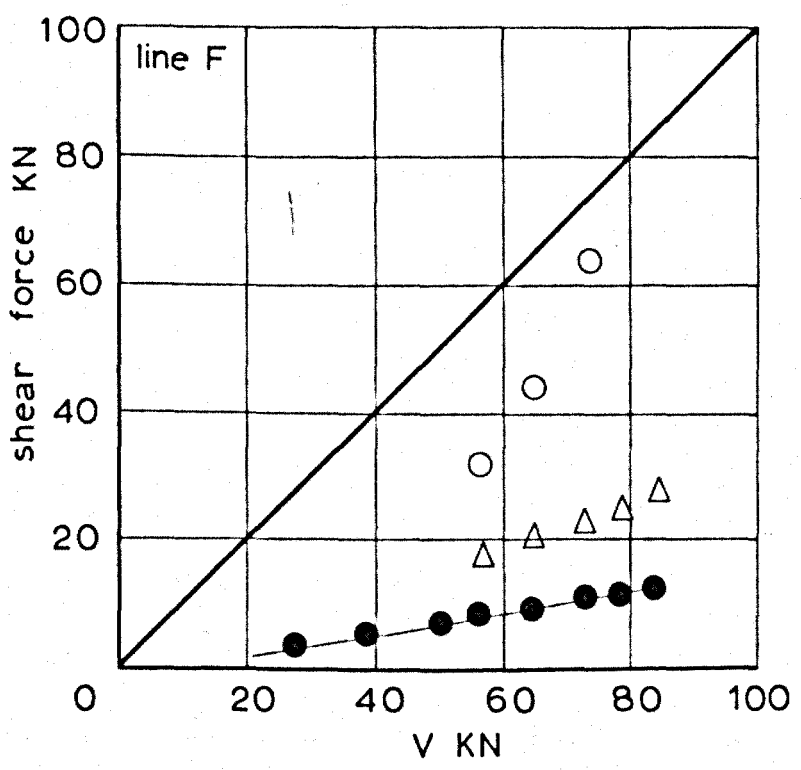

FIG. 8.11 DISTRIBUTION OF SHEAR FORCE IN BEAM 11

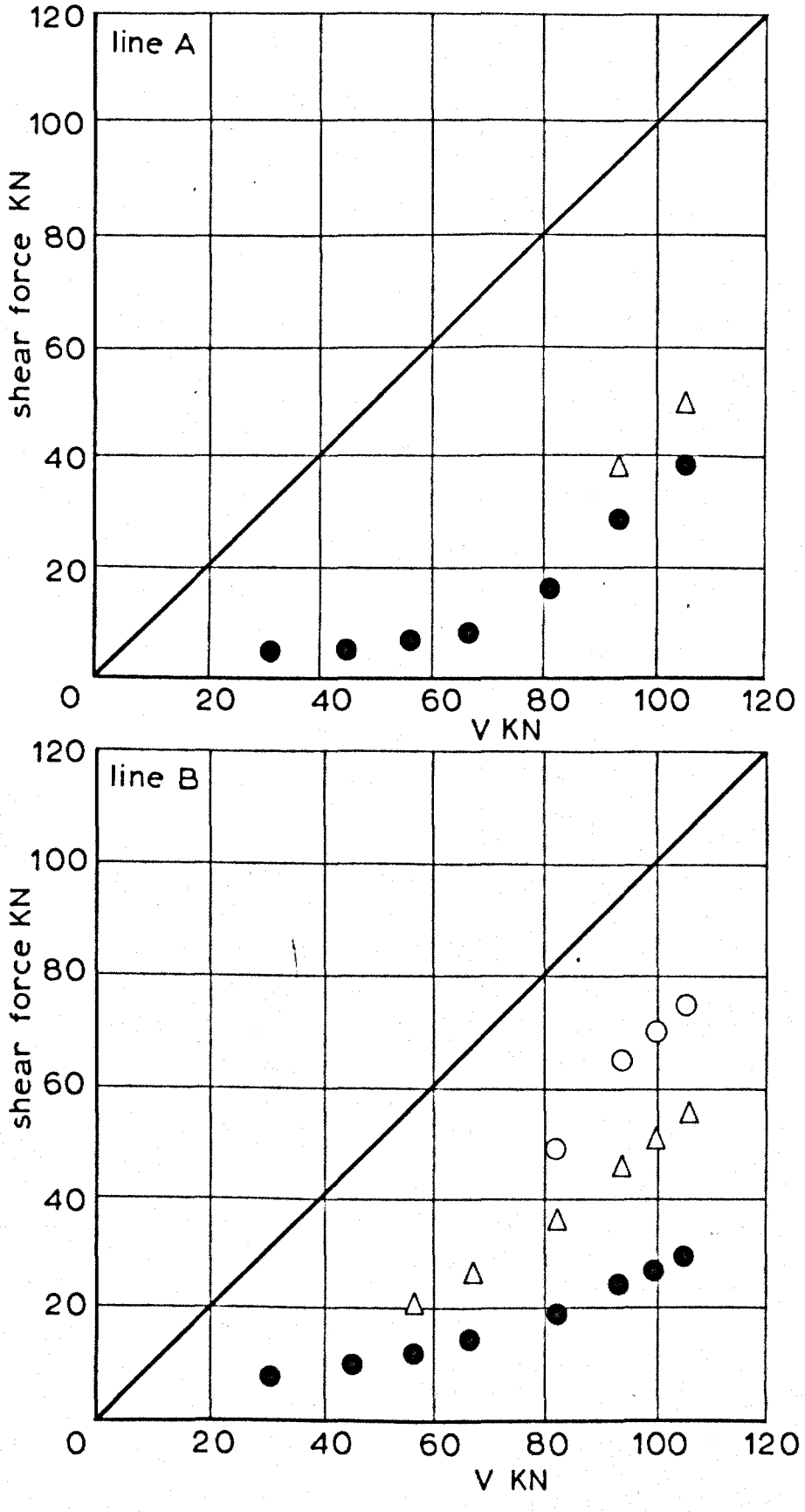

FIG. 8.12 DISTRIBUTION OF SHEAR FORCE IN BEAM 12

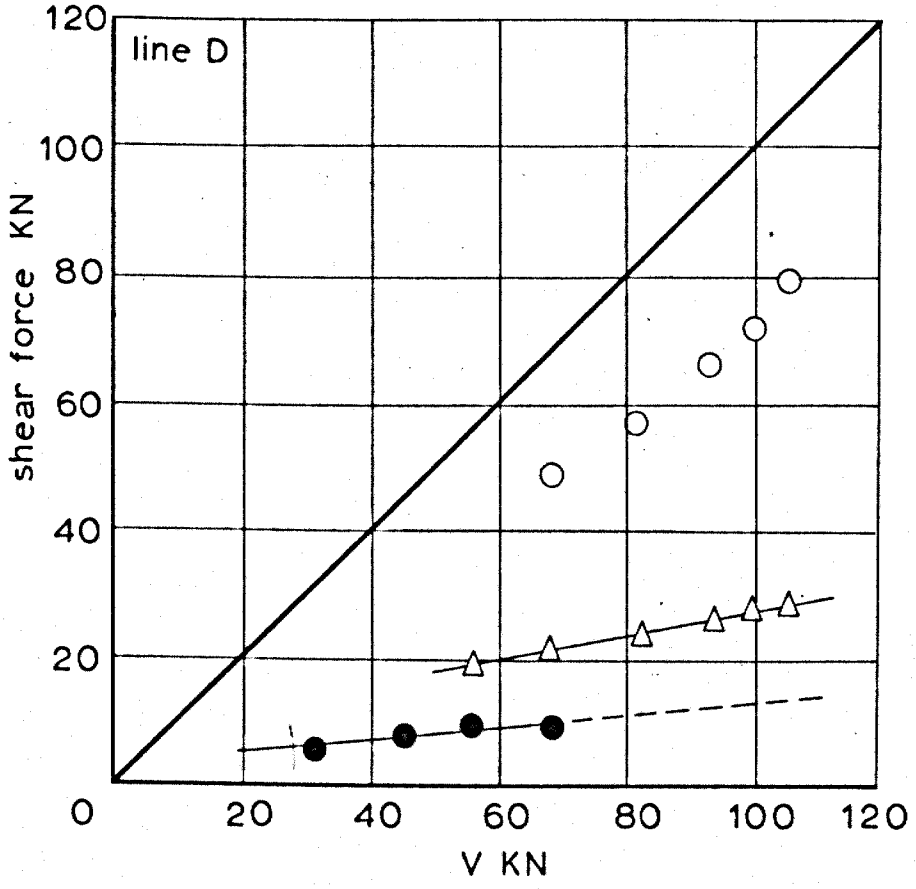

FIG. 8.12 DISTRIBUTION OF SHEAR FORCE IN BEAM 12

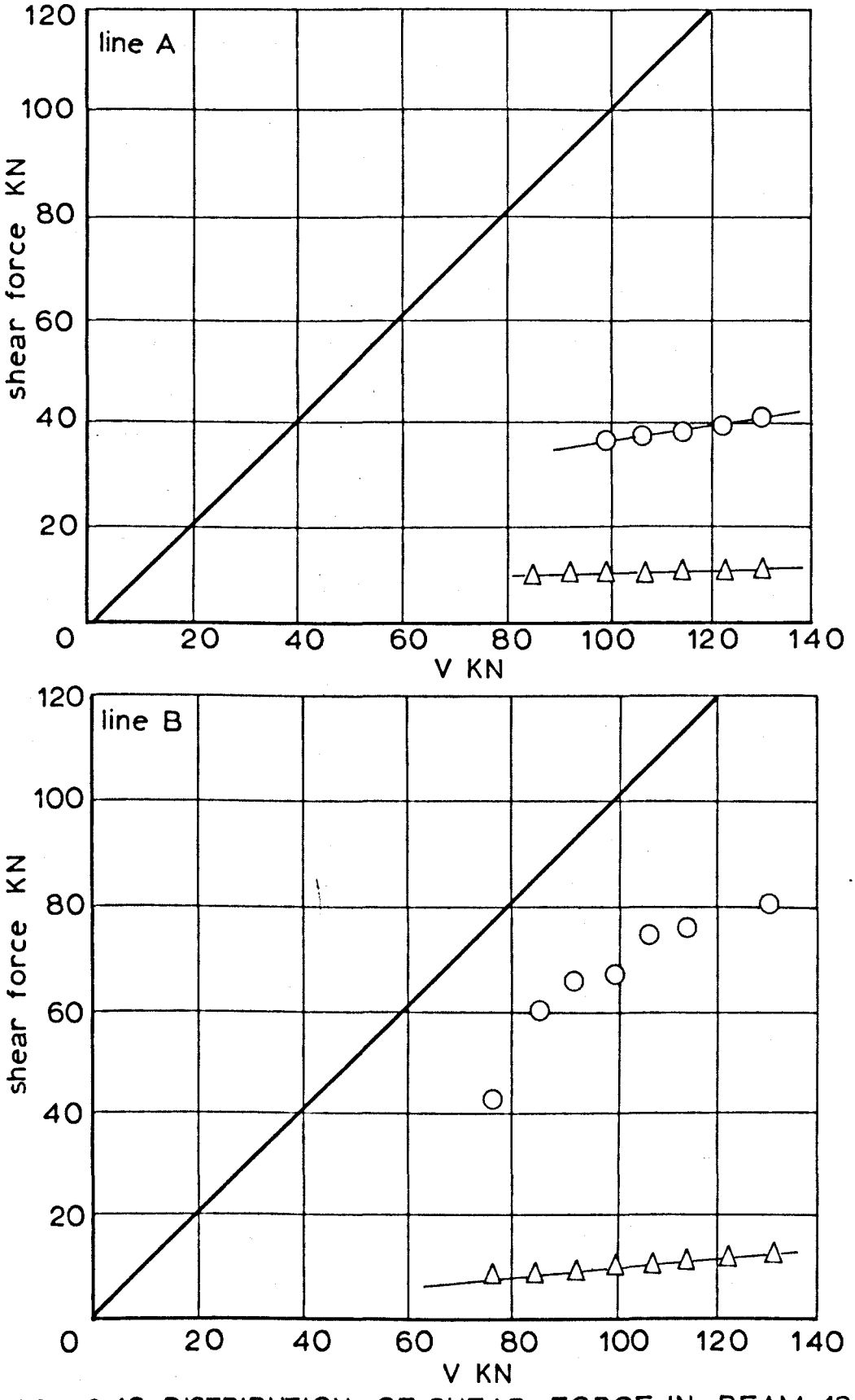

FIG. 8.13 DISTRIBUTION OF SHEAR FORCE IN BEAM 13

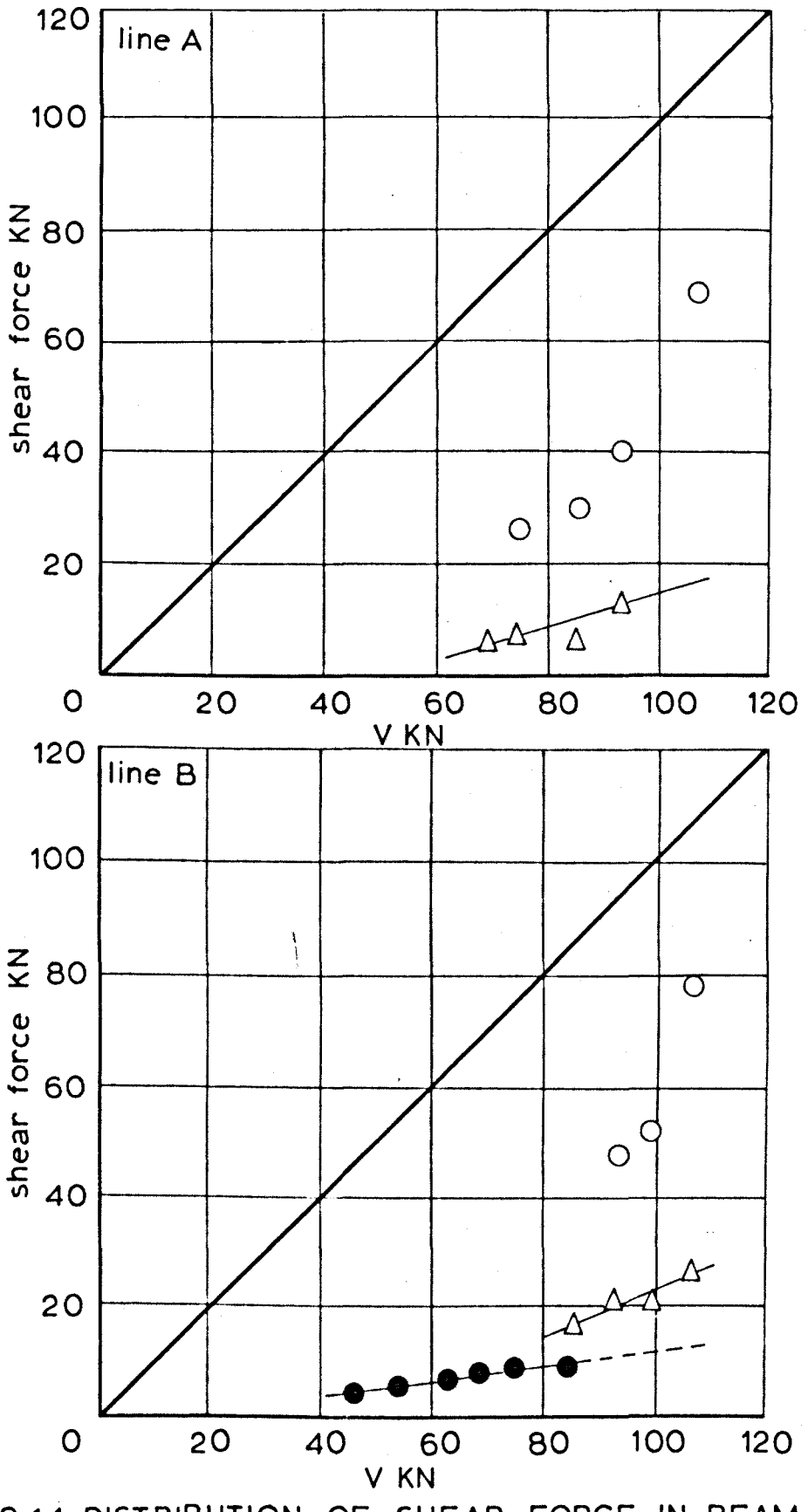

FIG. 8.14 DISTRIBUTION OF SHEAR FORCE IN BEAM 14

A number of theories for the behaviour of beams with stirrups, assuming that the stirrups are yielding at failure and considering the shear capacity of the compression zone using a failure criterion for the concrete, exist and give good results. The theories by Walther[43] and Regan[44] are examples of this work. The fact that these theories are reliable, points to the conclusions above being reasonable and hence, possibly, that the consideration of the dowel shears in such theories would add considerably to this accuracy. Another way of carrying out this work would be to extend the mathematical model described in the last Chapter to deal with stirrups and then the whole of the behaviour of beams with stirrups could be predicted. This is possible but some more very careful tests to determine the falling branch characteristics of dowel and aggregate interlock action would have to be carried out first of all.

The work described so far in this chapter indicates that a beam with stirrups acts in much the same way as a beam without stirrups until the large diagonal crack forms. At this stage, as the crack opens, the aggregate interlock force is gradually lost and the stirrups carry more and more shear force. It is reasonable to assume that the stirrups in such a beam will yield when the beam fails in shear and that the conservatism of the truss approach is due to the shear capacity of the compression zone, the dowel capacity of the main steel and any residual aggregate interlock forces across the crack. More experimental work is necessary to confirm this description of beam behaviour.

CHAPTER 9

CONCLUSIONS

Content of the work

(1) The primary object of this work was to investigate the behaviour of reinforced concrete beams without stirrups in shear and to measure the internal distribution of forces in them.

(2) Tests were carried out on a series of specimens that were designed to isolate the effect of the forces that can be carried across cracks and to obtain a quantitive assessment of their magnitude.

(3) A mathematical model of a beam in shear was developed to see if the measured force distributions and observed crack shapes could be predicted and to study the implications of the theory throughout the range of the major parameters to the shear problem.

(4) A limited number of tests was carried out on beams with stirrups to see if the behaviour of the beams could be explained in terms of the internal forces that were measured in the earlier tests.

Conclusions

(1) The tests to measure the shear forces carried in beam compression zones showed that 10 to 25 percent of the shear force on a beam was carried in this way. This shear force produced shear stresses in the compression zone that were consistent with a simple failure criterion.

(2) The tests to measure the forces carried across cracks by dowel action of the reinforcement showed that 15-25 percent of the shear force on a beam without stirrups was carried in this way. A small series of tests of dowel specimens with stirrups showed the effect stirrups have on restraining dowel splitting and showed that close stirrup spacings are required if the first stirrup restraining the dowel is to yield when a beam fails.

(3) The tests to measure the forces carried across cracks by interlocking of the aggregate showed that between 33 and 60 percent of the total shear force on a beam was carried in this way. The aggregate interlock tests were carried out on unreinforced concrete blocks and in order to confirm the results a limited series of tests was carried out on beams which were specially designed to carry shear only by interlocking of the aggregate. Good agreement was found between the tests.

(4) A series of tests on beams of different scales using three aggregate sizes showed that some of the previously reported scale effect was due to the aggregate not being properly scaled. When scaled aggregate was used, the strength of the beam was always greater than the strength of a similar beam made with smaller aggregate. The scale effect, for normally shaped beams was not serious but deep beams, with a large steel percentage concentrated in a narrow web width had a dowel capacity that was so low as to demand extra stirrups in design.

(5) In the aggregate interlock work, three tests were carried out with a Lytag mix with a strength between 32 and 41 N/mm^2 and these gave interlock strengths that were 62% of the strength of the dense concrete specimens. Thus, for this aggregate type which has a fairly rough crack, and assuming that the same internal force distributions apply as in dense concrete beams, the ultimate shear strength should be 1 - 0·38 x 0·6 times the strength from Table 7.2. Although not all lightweight aggregates give cracks of the same roughness as Lytag, it should be possible to put the current lightweight aggregates into two grades and allow shear strengths of say 0·8 times the Code values in Table 8.2 for the first grade, and the current design values of 0·5 times the values in Table 8.2 for the lower grade.

(6) The mathematical model that was developed predicted the shape of shear cracks and simultaneously produced a distribution of internal forces in beams that agreed with the experimental results. The ultimate shear strengths of a series of beams with a variety of steel percentages and concrete strengths were computed and, despite the limitations of the compatibility condition in the mathematical model,

the results compared well with the results of tests.

(7) It has not been possible to find the relative proportions of the internal forces in beams for the full range of the important parameters of steel percentage and concrete strength as this would require a considerable amount of new test work to be carried out but the following basic points apply.

(a) The compression zone shear forces are likely to be high when the compression zone is large, as in the case of beams with high steel percentages and at the same time the aggregate interlock force, because the crack is shorter, is likely to be low.

(b) The dowel force is dependent on the amount of steel present in the beam and a beam with two layers of well separated steel is likely to have a very high dowel force. The test described in Chapter 5 showed that this dowel force could be 50% greater than the force carried in a beam of the same width with a two bar dowel.

(8) A study of the beam tension zone, described in an appendix to this Thesis, has shown that the dowel and interlock forces restrain the concrete cantilevers between cracks and stop the bond force moment at the root of the cantilevers from becoming excessively high. Theories of beam behaviour which neglect interlock forces have been shown to predict that the cantilevers break off prematurely and give very low shear capacities to the beams.

(9) The behaviour of beams with stirrups has been shown to be explained by the internal force distributions described in this Thesis although very little test evidence is available to confirm this conclusion.

Future Work

(1) Detailed tests in which the distribution of shear force in beams with stirrups is measured are needed to provide basic data for extensions of the methods of analysis described in this Thesis.

(2) Although the description of beam behaviour presented in this Thesis explains the results of many shear tests and confirms the known interactions between the basic parameters, much more experimental work of the type described in this Thesis should still be carried out. The effect of many common dowel arrangements has not yet been investigated and more interlock tests, with a variety of test arrangements, are needed.

(3) The compatibility condition used in the mathematical model needs refinement and, in order to do this, displacement measurements should be carried out across cracks on beams with a wide range of steel percentages to provide the basic data.

(4) It is possible to extend the mathematical model to include beams with stirrups and in conjunction with this, more detailed studies of the falling branch behaviour of the interlock and dowel mechanisms are necessary.

REFERENCES

1. BROCK G. Effect of shear on ultimate strength of rectangular beams with tensile reinforcement. Journal of the American Concrete Institute, January 1960. pp 619 - 637.

2. KANI G.N.J. Basic facts concerning shear failure. Journal of the American Concrete Institute. June 1966. pp 675 - 691.

3. ZIPKES S. Die Scher-und Schubfestigkeit des Eisenbetons. Beton und Eisen (Berlin) Vol. 5, Nos 1-4, January-April 1906.

4. RITTER W. Die Bauwise Hennebigue. Schweigerische Bauzeitung (Zurich) Vol. 33, No. 7, February 1899. pp 59 - 61.

5. MÖRSCH E. Die Scher-und Schubfestigkeit des Eisenbetons. Beton und Eisen (Berlin) Vol. 5, No. 11, November 1906. pp 289 - 290.

6. TALBOT A.N. Tests of reinforced concrete beams. University of Illinois, Engineering Experiment Station Bulletins 4, 8, 12, 14, 28 & 29. 1906 - 1909.

7. RICHART F.E. An investigation of web stresses in Reinforced Concrete Beams. Bulletin No. 166. University of Illinois Engineering Experiment Station. June 1927. 103 pp.

8. MORETTO O. An investigation of welded stirrups in reinforced concrete beams. Journal of the American Concrete Institute. Vol. 17, No. 2, November 1945. pp 141 - 162.

9. CLARK A.P. Diagonal tension in reinforced concrete beams. Journal of the American Concrete Institute. October 1951. pp 145 - 156.

10. DRAFT BRITISH STANDARD CODE OF PRACTICE FOR STRUCTURAL USE OF REINFORCED CONCRETE. British Standards Institution, London, 1970.

11. LAUPA A, SEISS C.P. and NEWMARK N.M. Strength in shear of reinforced concrete beams. Bulletin 428. University of Illinois Engineering Experiment Station. March 1955.

12. MOODY K.G., VIEST I.M., ELSTNER R.C. and HOGNESTAD E. Shear strength of reinforced concrete beams. Journal of the American Concrete Institute. Part 1. Vol. 51, December 1954 Part 2. Vol. 51, January 1955 Part 3. Vol. 51, February 1955 Part 4. Vol. 51, March 1955

13. LEONHARDT F. & WALTHER R. The Stuttgart shear tests 1961. Library Translation No. 111. Cement and Concrete Association, London.

14. KANI G.N.J. How safe are our large Reinforced Concrete Beams? Journal of the American Concrete Institute. March 1967.

15. FABER O. Reinforced concrete beams in bending and shear. Concrete Publications Ltd., London 1924.

16. WATSTEIN D. and MATHEY R.G. Strains in beams having diagonal cracks. Journal of the American Concrete Institute. December 1958.

17. JONES R. The ultimate strength of reinforced concrete beams in shear.
Magazine of Concrete Research. August 1956. pp 69 - 84.

18. ACHARYA D.N. and KEMP K.O. Significance of dowel forces on the shear failure of rectangular reinforced concrete beams without web reinforcement.
Journal of the American Concrete Institute. October 1965. pp 1265 - 1279.

19. HOGNESTAD E., HANSON N.W. and McHENRY D. Concrete stress distribution in ultimate strength design.
Journal of the American Concrete Institute. December 1955. pp 455 - 479.

20. GOPALAKRISHNAN K.S. Discussion of paper by ACHARYA and KEMP.
Journal of the American Concrete Institute, Part 2, June 1966. pp 1777 - 1780.

21. KREFELD W.J. and THURSTON C.W. Contribution of longitudinal steel to shear resistance of reinforced concrete beams.
Journal of the American Concrete Institute. March 1966. pp 325 - 344.

22. LORENTSEN M. Shear and bond in prestressed concrete beams without shear reinforcement.
Handlingar Nr 47 Translations
Utgirara : Statens Råd för Byggnadsforsking
Håkan Ohlssons Boktrgckeri, Lund 1964.

23. KANI G.N.J. The riddle of shear failure and its solution.
Journal of the American Concrete Institute. April 1964. pp 441 - 467.

24. FENWICK R.C. The shear strength of reinforced concrete beams.
Thesis for the degree of Doctor of Philosophy in Engineering. University of Canterbury, Christchurch, New Zealand 1966.

25. BRESLER B. and PISTER K.S. Strength of concrete under combined stress.
Journal of the American Concrete Institute. Vol. 30, September 1958. pp 69 - 84.

26. REEVES J.S. The strength of concrete under combined direct and shear stress.
London, Cement and Concrete Association. November 1962. TRA/365 pp 11.

27. BAUMANN T. Versuche zum studium der verdubelungswirkung der biegezugbewehrung eines stahlbetonbalken Technischen Hochschule München Bericht 77, 1968.

28. ARROYO J. Study of dowel action of the main reinforcement of reinforced concrete beams.
Thesis for Diploma for Membership of Imperial College, London 1969.

29. PARMELEE, R. A study of the ultimate shear strength of reinforced concrete beams.
University of California, Berkeley, January 1961. Graduate Student Report No. 11.

30. JOHNSON R.P. Strength tests on scaled models suitable for models, with a note on mix design.
Magazine of Concrete Research. Vol. 14, No. 40, March 1962. pp 47 - 53.

31. GERGELY P. Splitting cracks along the main reinforcement in concrete members.
Department of Structural Engineering, Cornell University, Ithaca. N.Y. April 1969. pp 51.

32. SWAMY N. Aggregate-matrix interaction in concrete systems. Paper presented at an international conference on structure, solid mechanics and engineering design in civil engineering materials. Southampton 1969. pp 15. Paper 31.

33. CRANSTON W.B. and CRACKNELL J.A. Tests on reinforced concrete frames. 2 Portal frames with fixed feet. London, Cement and Concrete Association. September 1969. pp 35. Technical Report TRA/420.

34. EVANS R.H. and MARATHE M.S. Microcracking and stress-strain curves of concrete in tension. Materiaux et Constructions No. 1. Janvier-Fevrier 1968. pp 61 - 64.

35. BASE G.D., READ J.B., BEEBY A.W. and TAYLOR H.P.J. An investigation of the crack control characteristics of various types of bar in reinforced concrete beams. Research Report 18, Cement and Concrete Association, London.

36. LUTZ L.A. The mechanics of bond and slip of deformed reinforcing bars in concrete. Department of Structural Engineering, School of Civil Engineering, Cornell University.

37. BEEBY A.W. An investigation of cracking in slabs spanning one way. TRA 433, Cement and Concrete Association, London, April 1970.

38. TAYLOR R. A new method of proportioning stirrups in reinforced concrete beams. Magazine of Concrete Research, Volume 15, Number 45, pp 177 - 181.

39. LEONHARDT F. Reducing the shear reinforcement in reinforced concrete beams and slabs. Magazine of Concrete Research, Volume 17, Number 53, December 1965.

40. KANI G.N.J. A rational theory for the function of rib reinforcement. Proceedings of the American Concrete Institute. March 1969.

41. RÜSCH H. and MAYER H. Funf versuche zum stutium der verformungen in quertraftbereich eines stahl-betonbalkens. Teil I, Teil II. Technische Hochschule Munchen 1964.

42. BUILDING CODE REQUIREMENTS FOR REINFORCED CONCRETE ACI 318-63 American Concrete Institute Detroit, Michigan.

43. WALTHER R. Calculation of the shear strength of reinforced and prestressed concrete beams by the shear failure theory. C.&C.A. Library Translation No. 110 from Beton und Stahlbetonbau, Vol. 57, No. 11, November 1962, pp 261 - 271.

44. REGEN P.E. Combined shear and bending of reinforced concrete members. Thesis for degree of Ph.D. University of London 1967.

APPENDIX

THE BEAM TENSION ZONE

In Chapter 4, when the shear force carried by the beam compression zone was estimated, a comparison of the stresses was made with a failure criterion to show that the compression zone was capable of carrying the measured shear forces without distress. Now that the shear forces in the beam tension zone are known, it is possible to carry out a similar check to see that the stresses in the tension zone are consistent with the observed cracking and to see if the displacements are similar to those that were measured in the tests.

In this Appendix, the results of a series of finite element analyses of a section of a beam tension zone are presented to illustrate that the stress conditions and deformations are consistent with observations of test beams.

The equilibrium of a section of a beam tension zone between two cracks has already been mentioned in Chapter 3 and Kani's theory, which assumes no aggregate interlock forces across cracks, was described. Figure A.1 shows such a section between two cracks drawn on a beam the shape of beams 9 and 10. The cantilever shown in the Figure is connected to a section of the beam compression zone and it was on this section of the beam that the analysis described in this Chapter was carried out.

This particular beam was used as it was possible to select a cantilever that fits the crack pattern of Beam 9 and at the same time has the shape of the partially smooth cracks of beam 10. Three analyses are therefore possible. Firstly the cantilever may be analysed with the forces found from the tests on Beam 9 and this would simulate the conditions in a complete beam. Secondly the cantilever can be loaded with the forces found in the tests on Beam 10, which was not a true beam as the cracks were partly smooth sided, and this would be a halfway case between the first and third load cases. The third loading system could be for a 'Kani' cantilever with smooth sides.

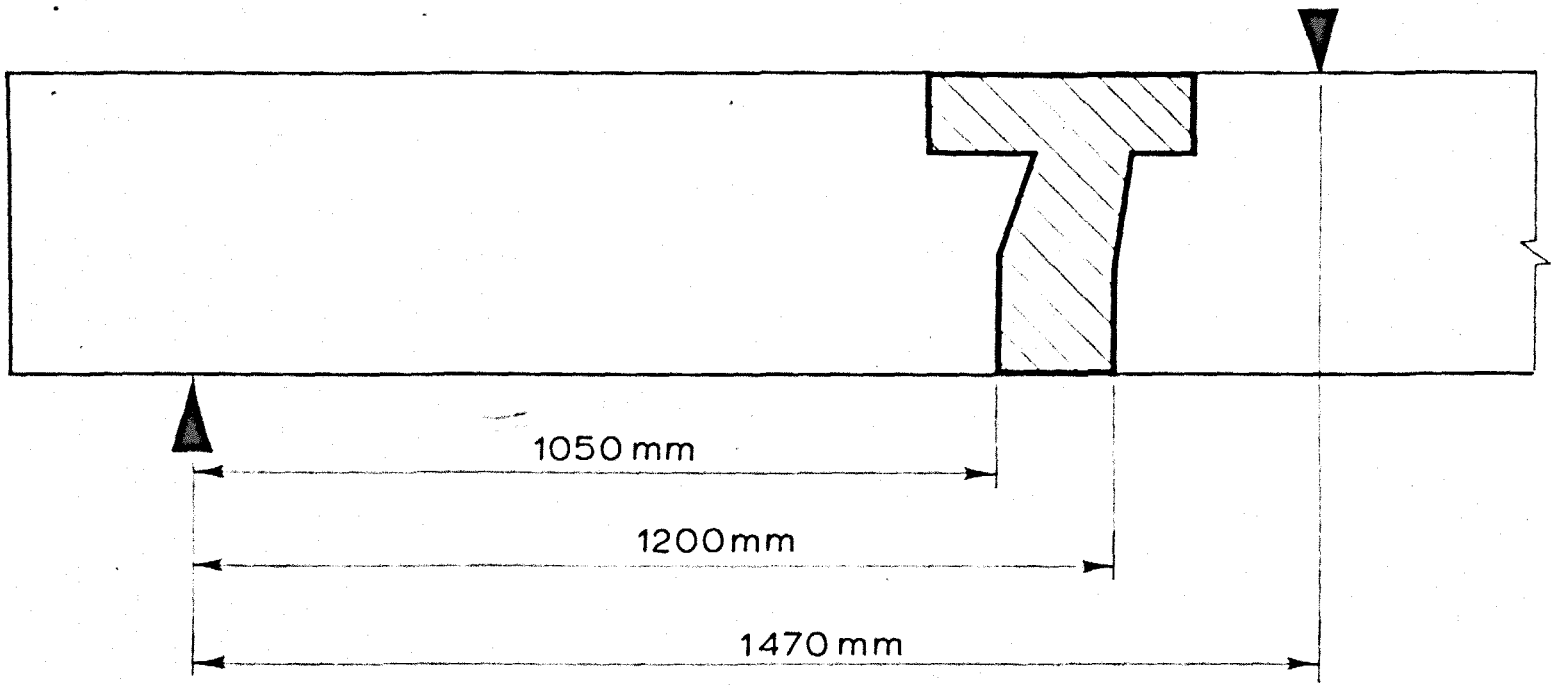

FIG.A.1 CONCRETE CANTILEVER IN BEAM 9 USED IN FINITE ELEMENT ANALYSIS

The magnitude of the loading that was selected was derived from the last load stage on Beam 10 and the corresponding equal load stage on Beam 9.

Details of the distributions of the shear force on the cantilevers are given below.

Case I Beam 9 Load Stage 11

V 71 kN
$V_1 = 0{\cdot}25\ V$
$V_2 = 0{\cdot}22\ V$
$V_3 = 0{\cdot}53\ V$

Case II Beam 10 Load Stage 9

V 71 kN
$V_1 = 0{\cdot}36\ V$
$V_2 = 0{\cdot}22\ V$
$V_3 = 0{\cdot}42\ V$

Case III

V 71 kN
$V_1 = 0{\cdot}78\ V$
$V_2 = 0{\cdot}22\ V$
$V_3 = 0$

In each case, the dowel force was assumed to be the same and interlock force came either from tests or was zero.

From these shear forces and assuming that the main tensile steel stress increases uniformly from support to load point it was possible to derive the compressive and tensile force, C and T, necessary to hold the tooth in equilibrium. The final systems of forces were then applied to the cantilever in the analysis. The compression zone shear force was not included as the analysis was primarily carried out to study the stresses and deformations in the beam tension zone where compression shears would not have a significant effect.

The layout of the finite element grid, boundary conditions and the loads that were applied in the three load cases are shown in Figure A.2. The finite element program was an elastic plane stress program using six noded triangular elements. These elements have nodes at their corners and at the centre of each side and are more accurate than three noded triangular and four noded rectangular elements in plane stress problems. A total of 80 nodes were used in the grid and the lower four elements of the grid all had a higher stiffness than the other elements to simulate the presence of the reinforcement. This was the maximum complexity allowed by the program and computer although ideally more elements should be used at the steel level.

The compression zone force was applied to the beam in a triangular distribution and the steel force from the previously described calculations was applied to the nearest node to the steel position. The dowel forces were applied to the same node and the aggregate interlock forces, where appropriate, were distributed uniformly along the crack.

The results of the analysis are in the form of displacements and principal stresses at each node point. Both sets of results are presented in Figures A.3 to A.5. The deformations and principal stresses are not shown to any particular scale but the same scale was used throughout the Figures so that comparisons can be made.

Looking at the deformations it may be seen in Figure A.5 that the cantilever is deformed most with the loads from load case III applied, and the deformations from the other two load cases were very similar to each other.

This situation is also shown by the principal stresses at the bottom of each Figure. As there were so many stresses produced by the program, only the tensile stresses relevant to the cantilever are shown.

In the case of load case I, the moment on the cantilever from the shears almost balances the bond force moment and the principal

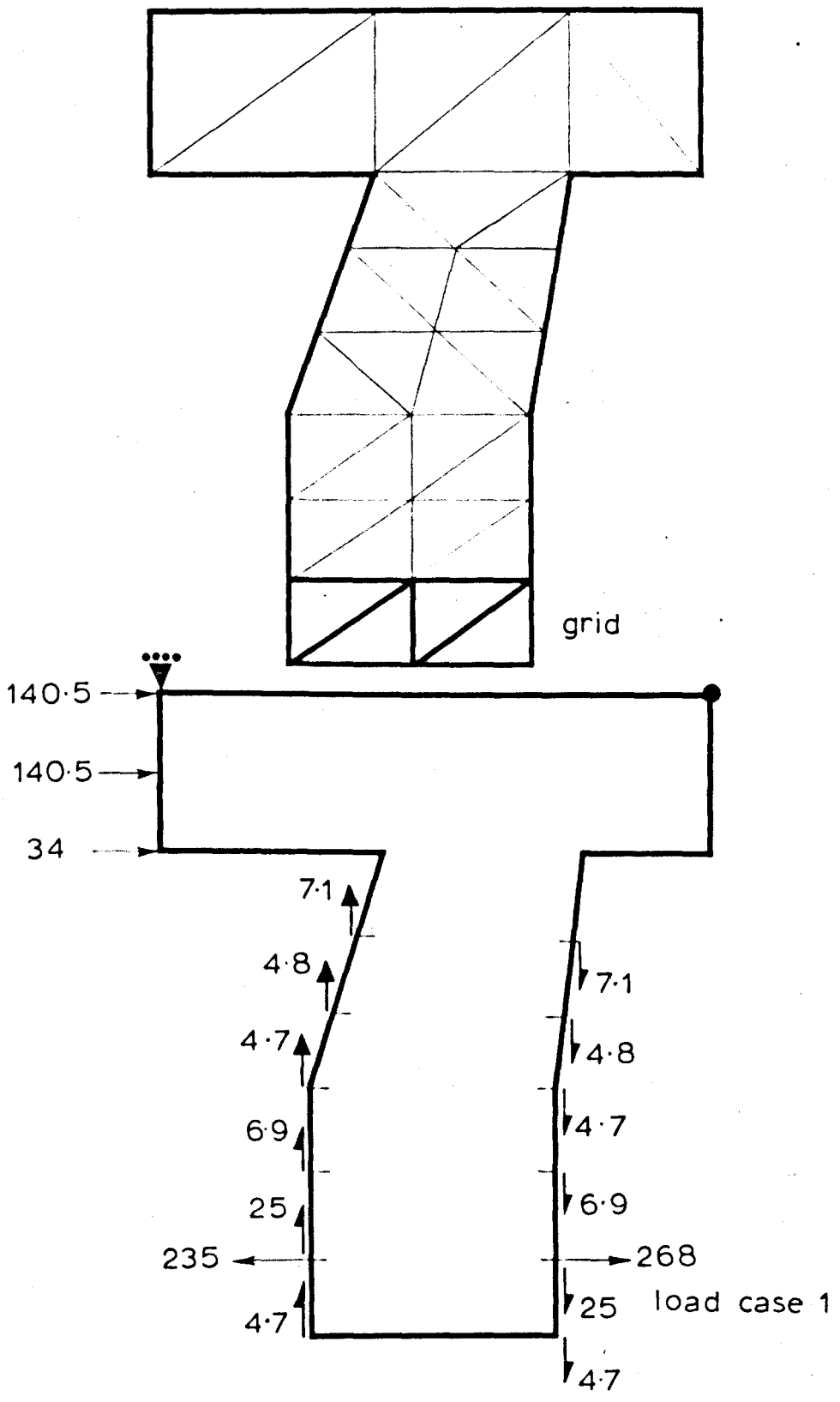

FIG. A. 2 LAYOUT OF FINITE ELEMENT GRID, BOUNDARY CONDITIONS AND LOADING OF SINGLE CANTILEVER

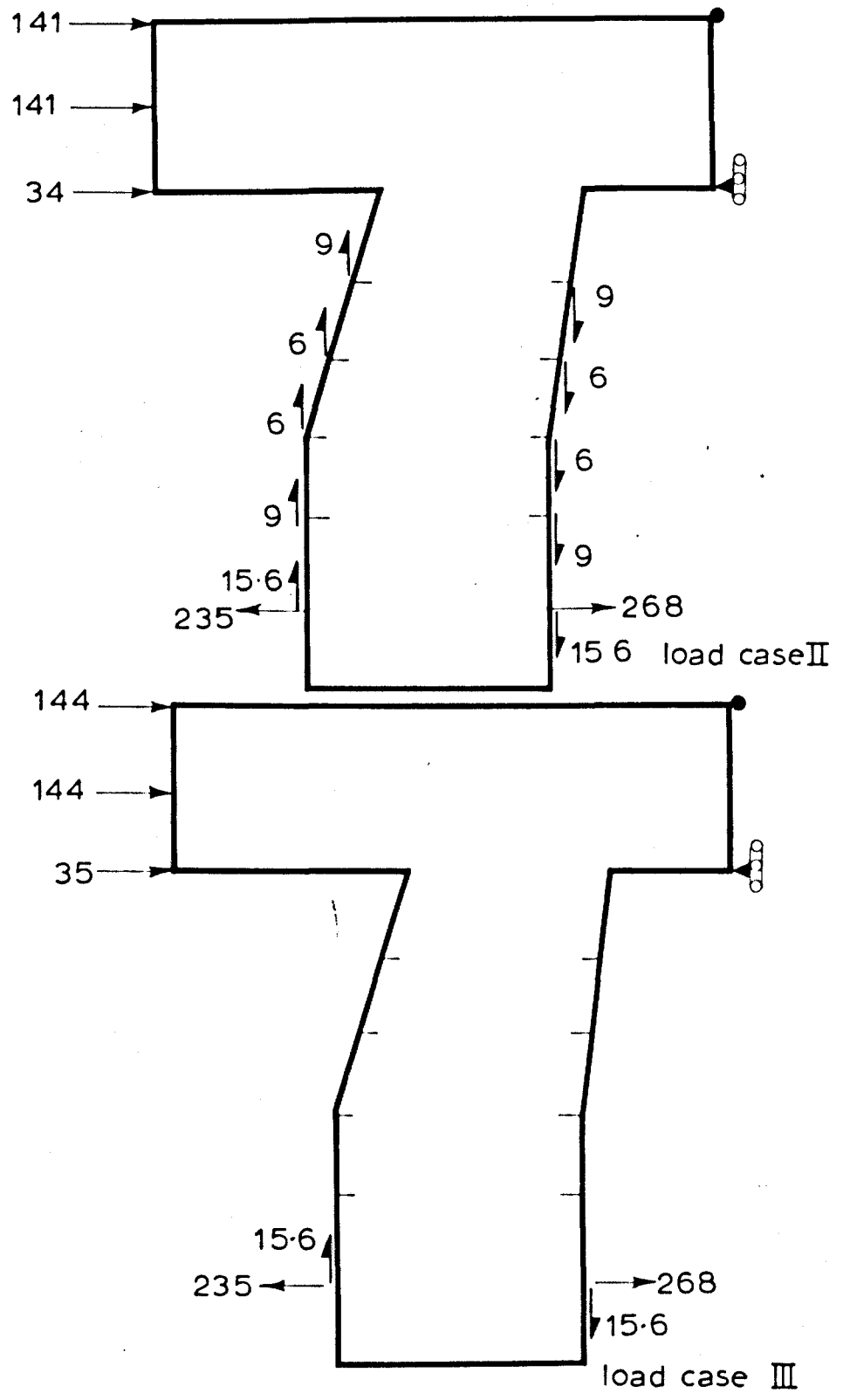

FIGA.2 LAYOUT OF FINITE ELEMENT GRID BOUNDARY CONDITIONS AND LOADING OF SINGLE CANTILEVER

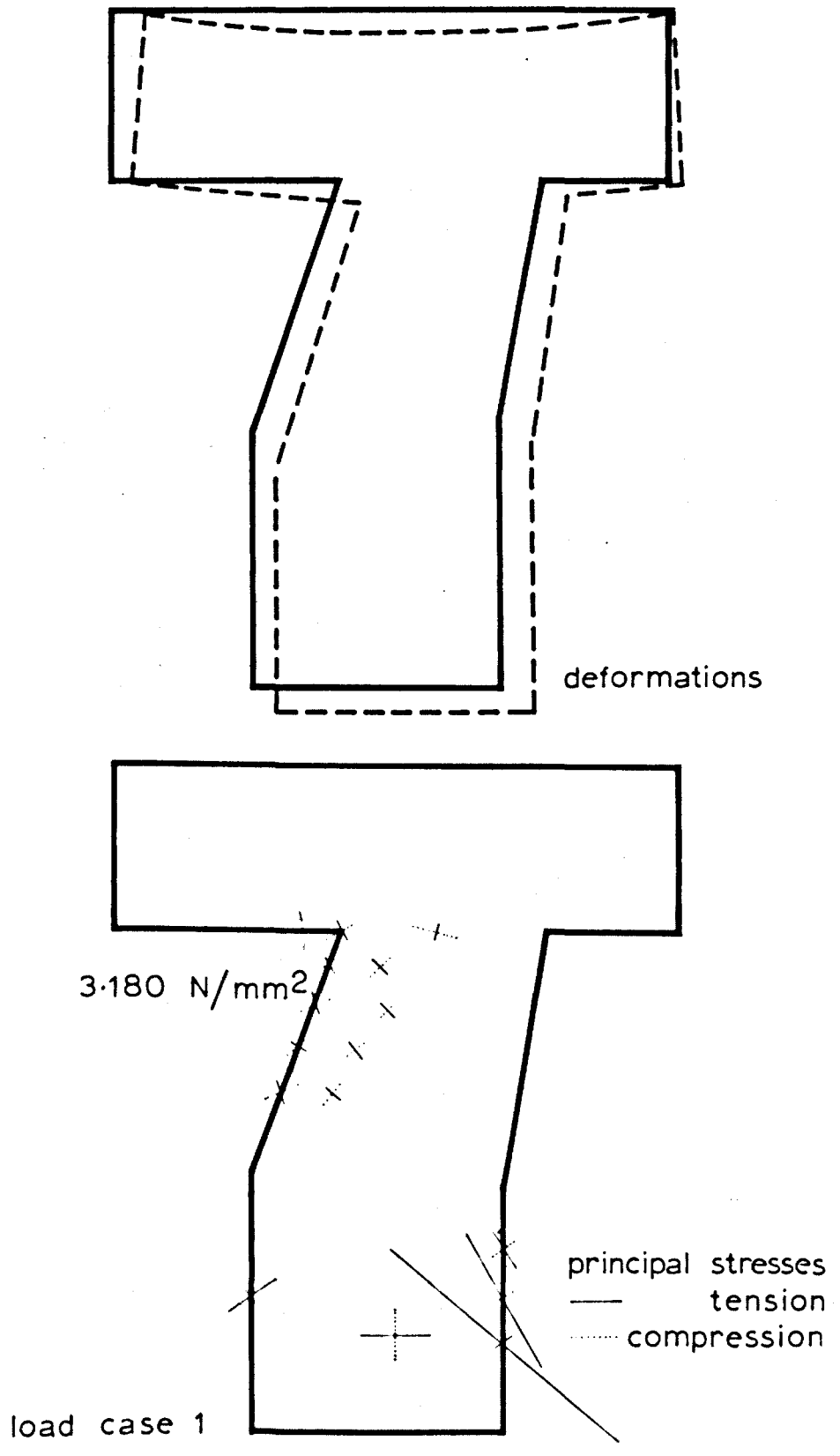

FIG.A. 3 RESULTS OF SINGLE CANTILEVER ANALYSIS
LOAD CASE 1

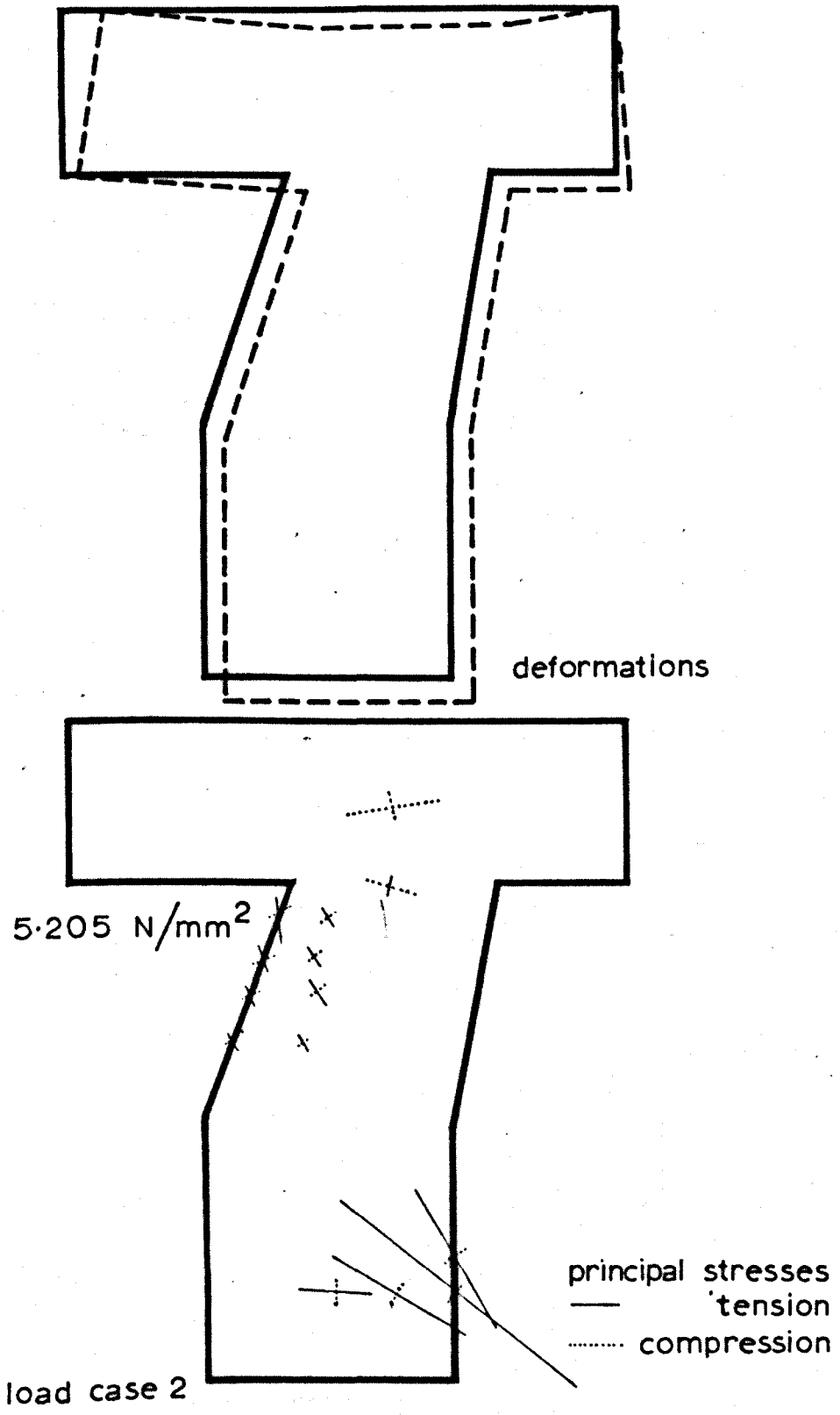

FIG.A.4 RESULTS OF SINGLE CANTILEVER ANALYSIS, LOAD CASE 2

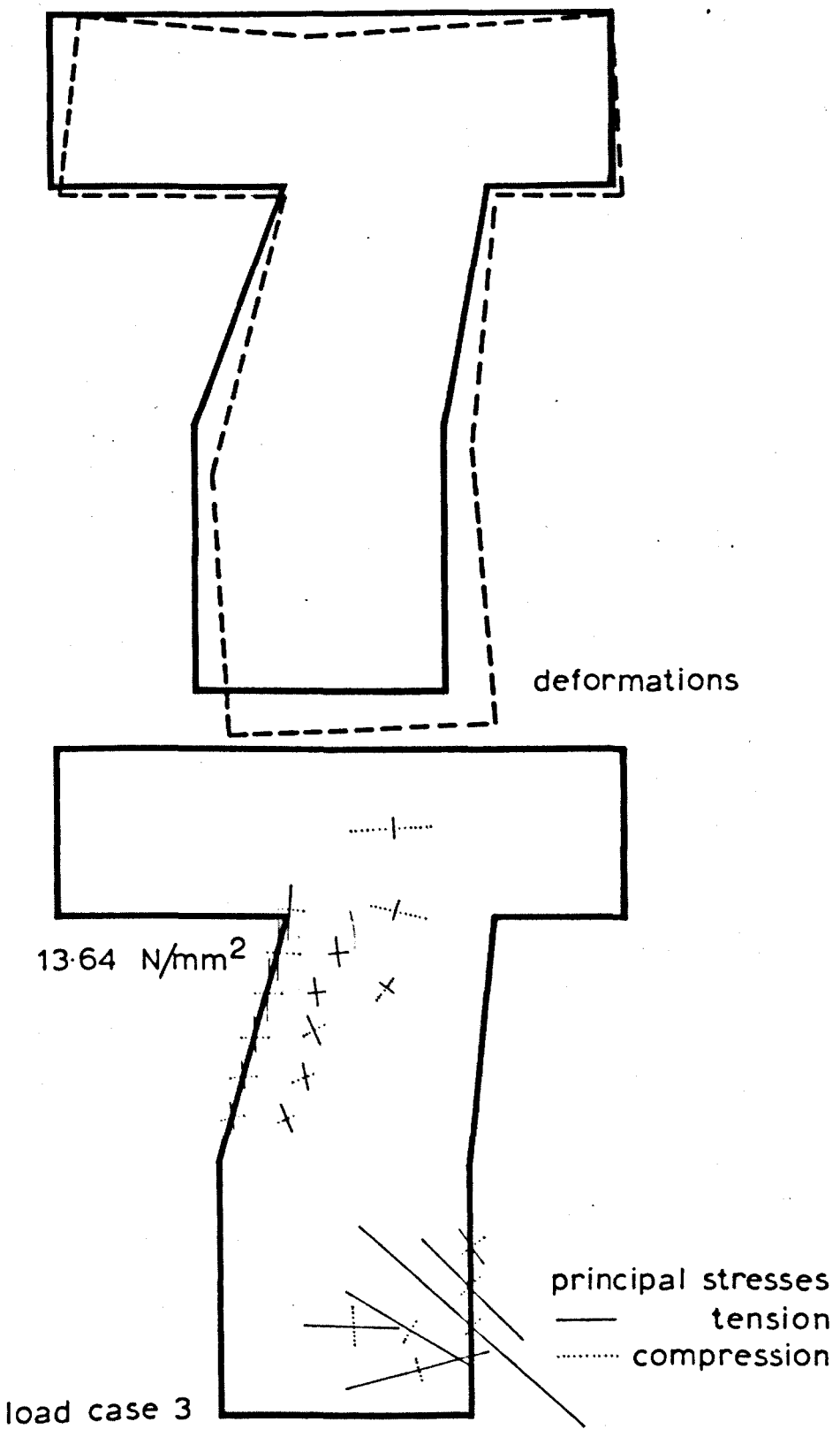

FIG.A.5 RESULTS OF SINGLE CANTILEVER ANALYSIS LOAD CASE 3

tensile stresses at the cantilever root are low. This shows that the tooth is stable with that load configuration and is unlikely in practice to have broken off. The second Figure shows a higher stress just at the level at which cracking would be expected and the Kani, third tooth, has a very high tensile stress at the root, much higher than that which can be carried by the concrete.

A very simple check that these stresses are correct may be obtained by working out the net moment on the cantilever and then assuming a linear stress distribution at the root. In the case of the Kani tooth, this gives a vertical stress of 10·05 N/mm^2. This compares well with the finite element result of 13·64 N/mm^2 which is a principal stress and is at a slightly different angle.

High tensile stresses are predicted at the outer face of the cantilever where the higher steel force is applied. These stresses are caused by the dowel and interlock forces at the foot of the crack and, although the finite element simulation of the dowel behaviour is crude, these stresses indicate that dowel cracking would occur. The stresses at the foot of the crack would also cause cracking in the cantilever above the dowel, when the inclined part of the crack travelled downwards. This form of cracking is found in practice and in this Thesis is called reversed inclined cracking. A beam with a number of these cracks may be seen in Figure 4.6.

The analyses of the single tooth cantilevers have shown that the stresses produced by the aggregate interlock and dowel loading are not high and are easily capable of being sustained by the concrete teeth. Next a series of three double tooth cantilevers were analysed to see if the displacements from the three loading patterns were reasonable and agreed with the measurements that were taken on the beams described in Chapter 4.

The layout of the finite element grid, boundary conditions and the loadings for the three load cases with full, partial and no aggregate interlock, are shown in Figure A.6. The two cantilevers were separated by a crack of zero width and the interlock, dowel and tensile steel force were applied to each side of the crack in the

appropriate directions. As before, the lower four elements were stiffened to take account of the stiffness of the steel and concrete in the section. It was not possible to have a finer grid of elements than the one shown owing to space limitations in the computer.

The deformed shape of the cantilevers from the analysis are shown in Figures A.7 - A.8. The scale to which the displacements are plotted is common throughout the three Figures. The displacements from load cases I and II are similar and this is because the aggregate interlock forces are distributed in a similar way in the two load cases. Because of the relatively coarse grid used in the analysis, it was not possible to distribute the aggregate interlock forces correctly. The displacements from load case II however do show less shear distortion as less interlock forces are applied. The displacements from load case III are much different from the other two load cases and the crack does not open but closes so that the cantilevers interfere. This is quite possible in the analysis as the analytical model can be likened to two separate cantilevers which may slide over each other.

It is possible to obtain the ratio of horizontal to vertical movement of opposite sides of the crack from the analysis, Δ_H/Δ_V, and plot this against the parameter defining the shape of the crack, δ_V/δ_H, in the same way that the experimental results are plotted in Figure 4.35. This has been done in Figure A.10. In the Figure the displacements from the analyses on load cases I and II are plotted together with a line that passes through the experimental results in Figure 4.35. It can be seen that both load cases give good results, the displacements from load case I gave more vertical movement for a given crack slope than the displacements from load case II, in accordance with the additional shear distortions.

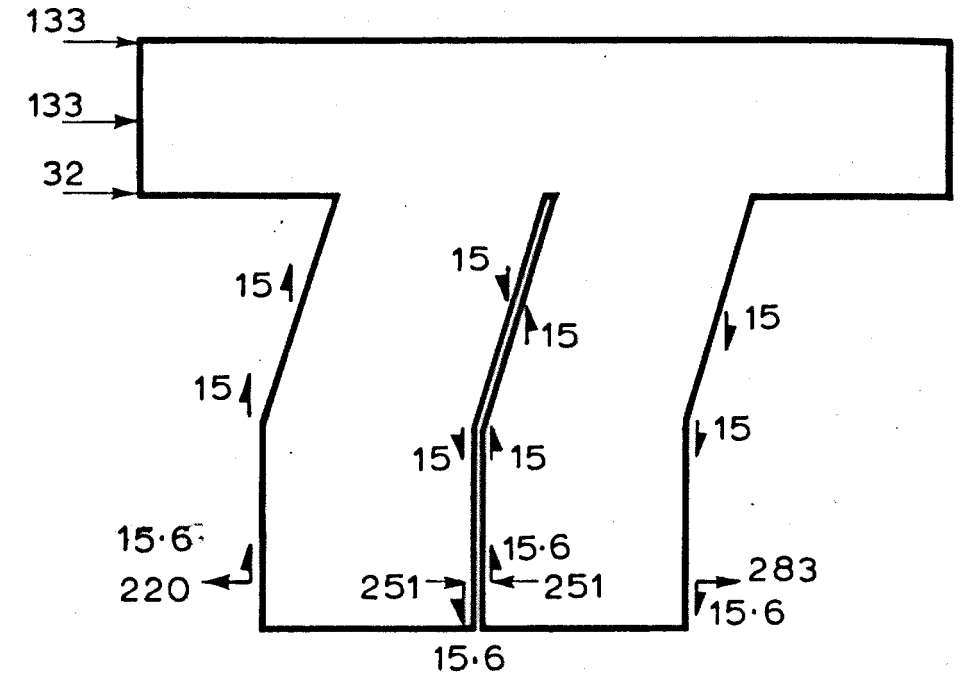

load case 2

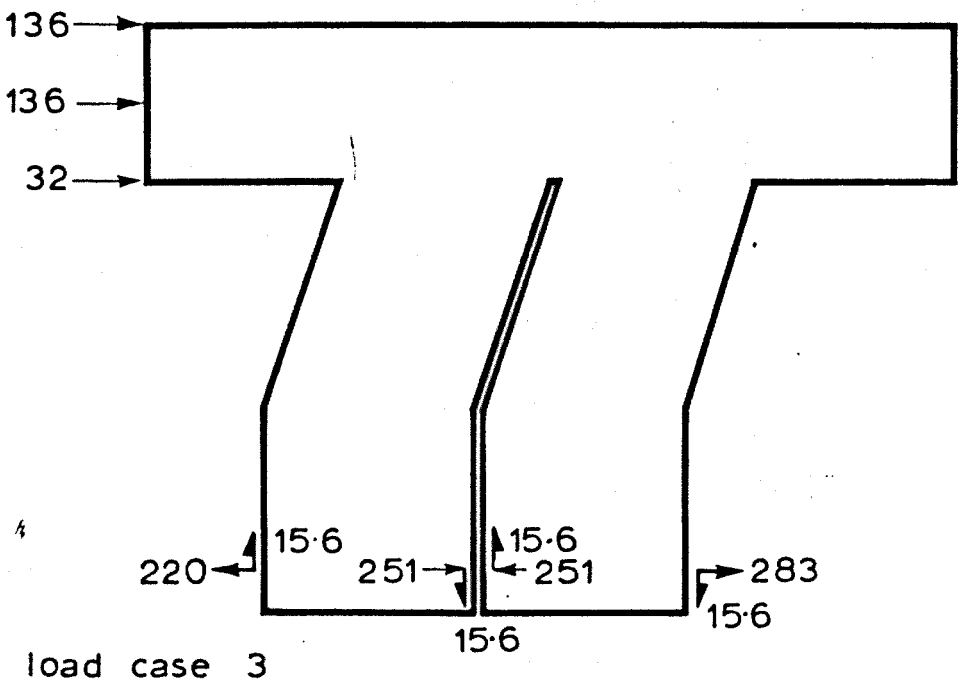

load case 3

FIG.A.6 LAYOUT OF FINITE ELEMENT GRID BOUNDARY CONDITIONS AND LOADING OF DOUBLE CANTILEVER

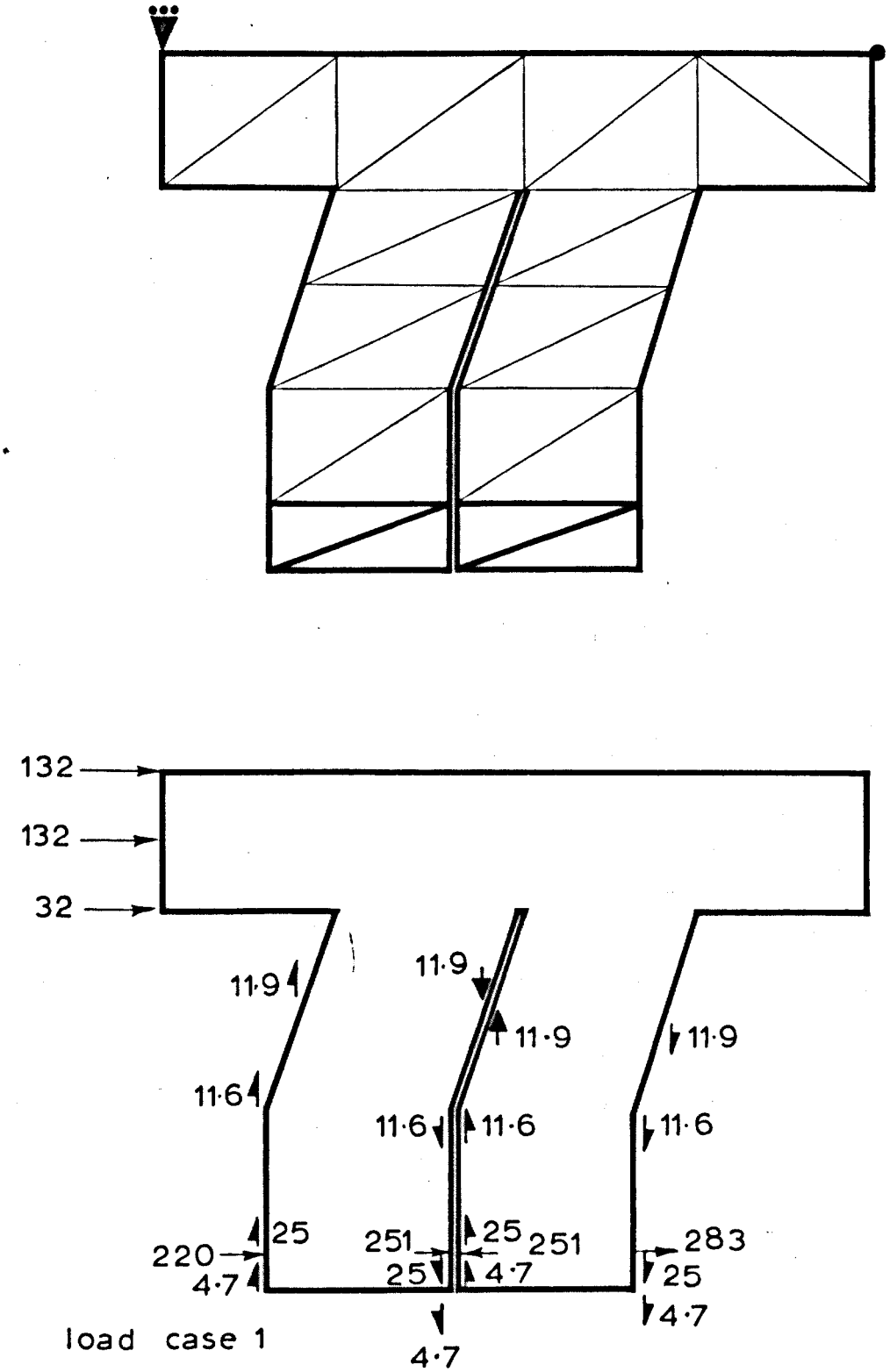

FIG.A·6 LAYOUT OF FINITE ELEMENT GRID, BOUNDARY CONDITIONS AND LOADING OF DOUBLE CANTILEVER

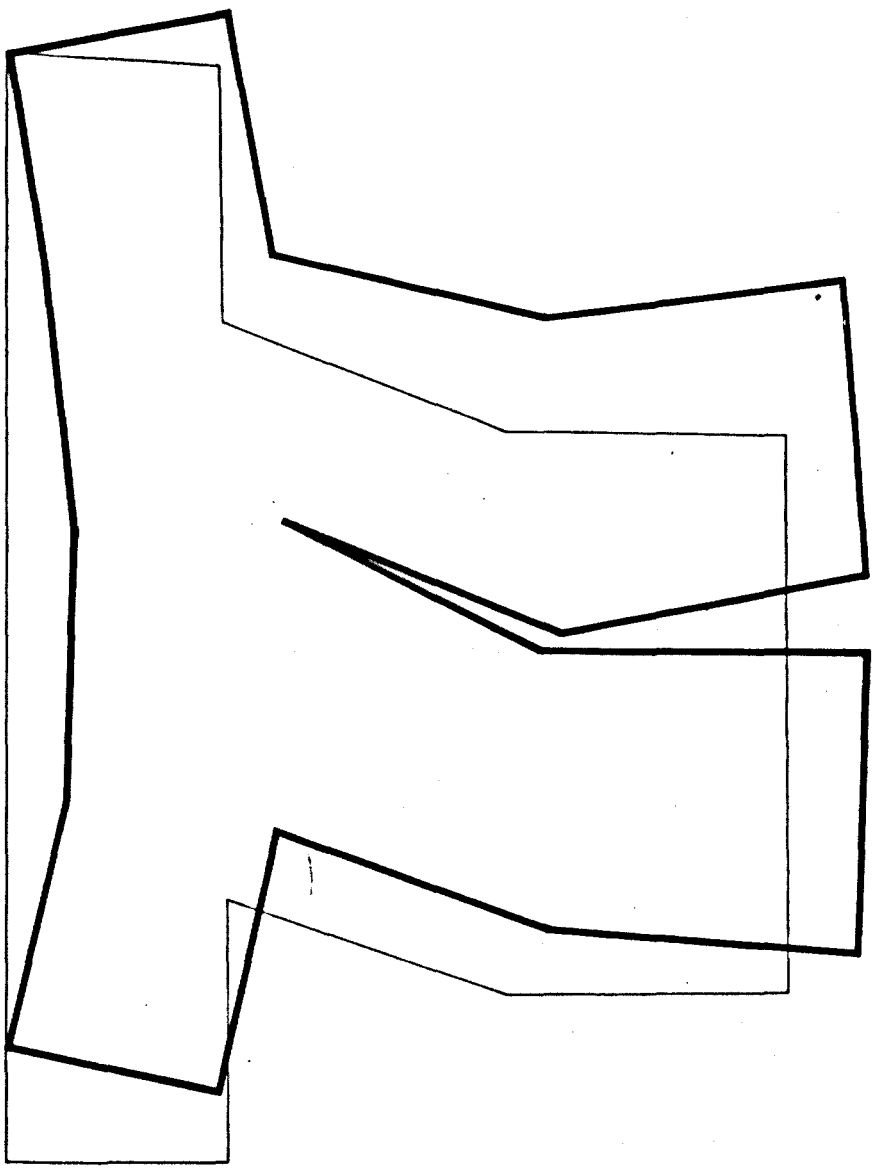

load case 1.

FIG.A.7 RESULTS OF DOUBLE CANTILEVER ANALYSIS, LOAD CASE 1

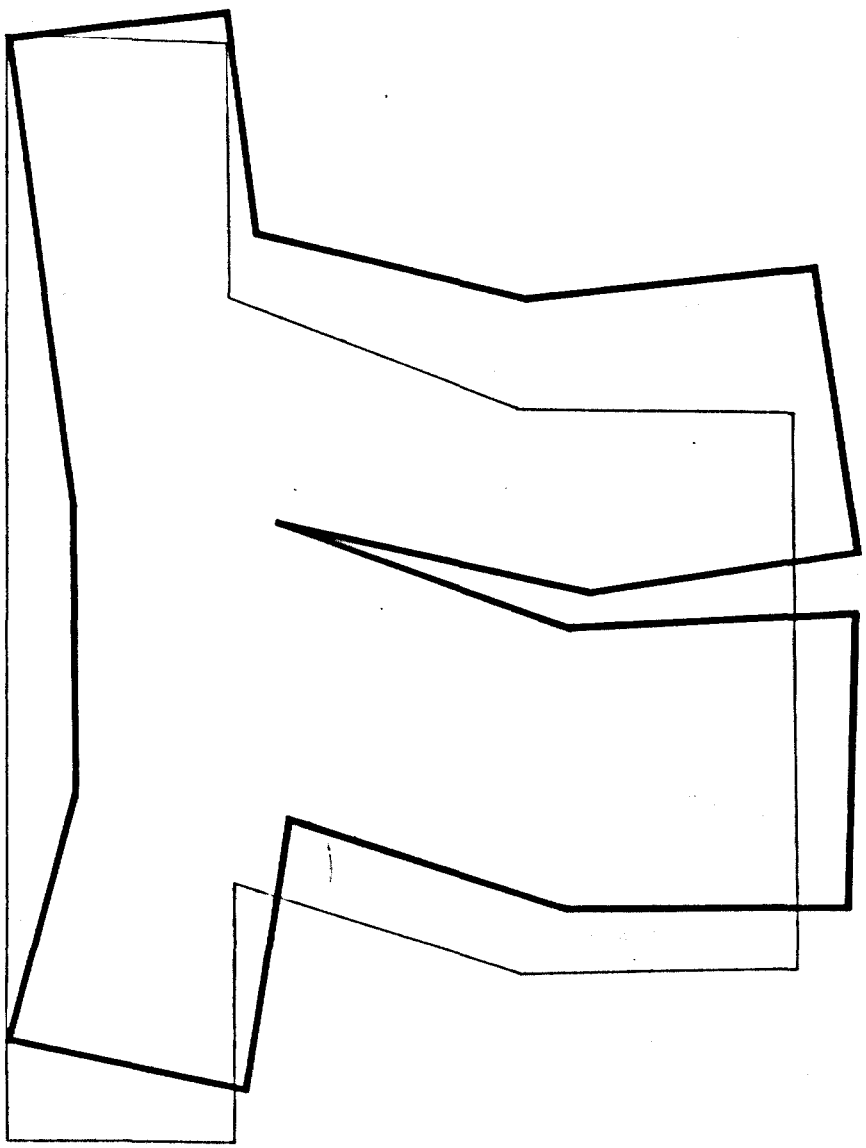

load case 2 .

FIG.A.8 RESULTS OF DOUBLE CANTILEVER ANALYSIS
LOAD CASE 2

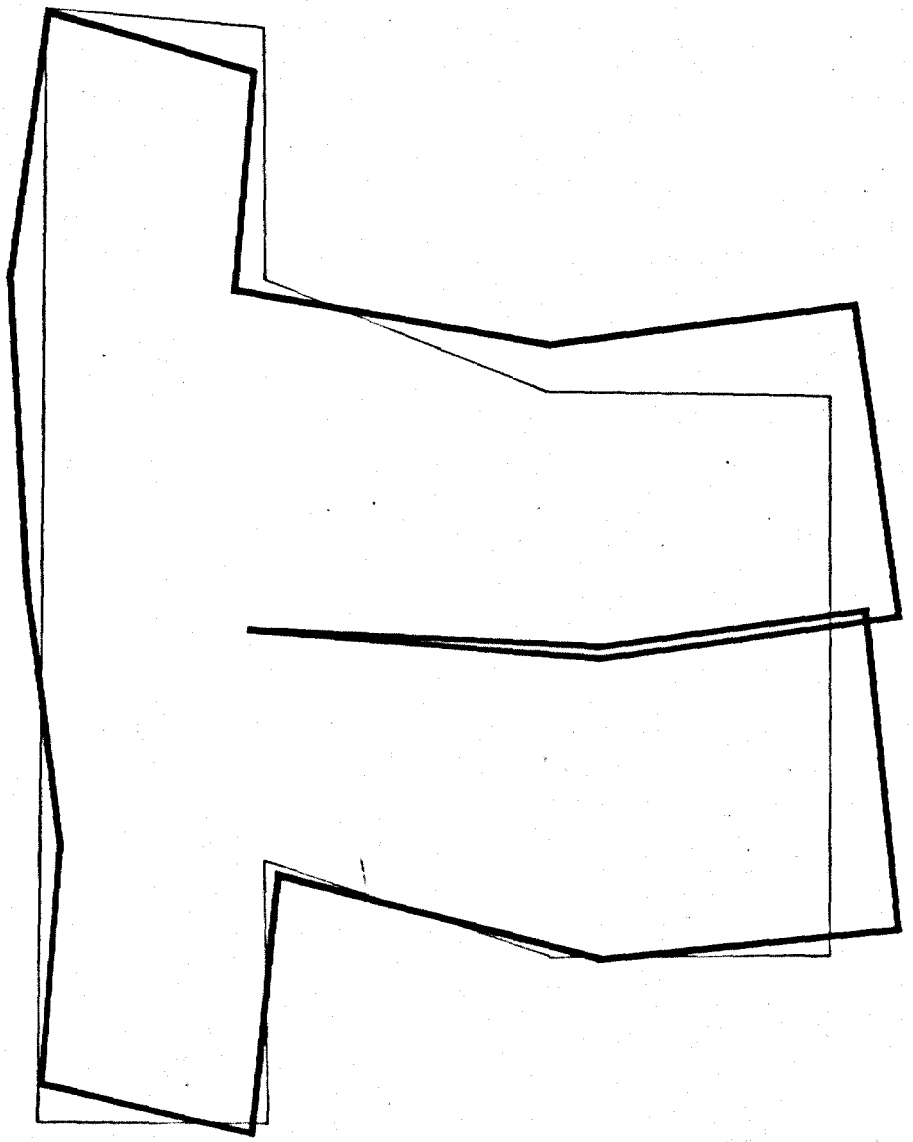

load case 3

FIG.A.9 RESULTS OF DOUBLE CANTILEVER ANALYSIS
LOAD CASE 3